Universitat Autònoma de Barcelona

Functional and structural studies of AKR1B15 and AKR1B16: Two novel additions to human and mouse aldo-keto reductase superfamily

JOAN GIMÉNEZ DEJOZ

Universitat Autònoma de Barcelona

Functional and structural studies of AKR1B15 and AKR1B16:

Two novel additions to human and mouse aldo-keto reductase superfamily

Memòria presentada per

JOAN GIMÉNEZ DEJOZ

per optar al Grau de Doctor en Bioquímica i Biologia Molecular

Treball realitzat al departament de Bioquímica i Biologia Molecular de la Universitat Autònoma de Barcelona, sota la direcció dels Doctors **SERGIO PORTÉ ORDUNA, JAUME FARRÉS VICÉN** i **XAVIER PARÉS CASASAMPERA**

Sergio Porté Orduna **Jaume Farrés Vicén**

Xavier Parés Casasampera **Joan Giménez Dejoz**

Bellaterra, 17 de juny de 2016

Agraïments

En primer lloc vull agrair als caps del grup, el Dr. Jaume Farrés i el Dr. Xavier Parés l'oportunitat de posar un peu a la ciència, iniciar-me en la carrera científica, els seus bons consells i l'obtenció final d'aquesta tesi. També voldria agrair especialment a tots els ADHs amb qui he compartit laboratori, sense vosaltres això no hauria estat possible. Gràcies per aguantar tants dies a les fosques!

Al Sergio-せんせい, per tot el que m'has ensenyat durant aquests anys, la bona guia, direcció, les inacabables correccions, per ensenyar-me a ser crític amb la meva pròpia feina i intentar sempre ser rigorós i auto exigent tant amb els experiments com amb la redacció i preparació de les figures (repassar cada figura mil cops buscant defectes abans de donar-la per bona ja s'ha convertit en costum) i tots i cada un dels inacabables "*Podries...*"que tant hem trobat a faltar en la època final. Raquel, gràcies per tantes i tantes estones de feina compartida amb el llum apagat a l'HPLC (la meva companya del costat fosc), l'inigualable moment del canvi de la bombona de nitrogen, mai m'he rigut tant al lab com aquell dia xD, per aguantar la meva música i no posar-me sempre la teva, tota la xocolata i cafès compartits i tot el suport d'aquest últim any en el que hem estat més sols per aquí. Per ser una persona tan incansable i pel teu bon humor i optimisme. Ànims, que encara que no ho vegis ara mateix sé que faràs una gran tesi! (només t'hi has de posar) Al Julio, per la seva constància i treball, els infortunis de l'HPLC i les seves les reparacions màgiques de l'HPLC (només t'estima a tu aquest trasto!) i ensenyar-me a bussejar. El crack de l'Isidro, tu si que tens pasta per ser un bon científic! Estic segur que te'n sortiràs de tot el que et proposis. Gràcies per totes les millores informàtiques i trucs que m'has ensenyat! A la Cristina, pel teu somriure i caràcter que alegraven el laboratori, per la estrella ✰ feta amb post-its decorant el laboratori, per fer les comandes quan a la pissarra ja no hi cabia ninguna més, a tots ens hauria agradat que haguessis pogut continuar al lab amb nosaltres però segur que allà on vagis t'anirà bé. Xavi-せんぱい el primer en ensenyar-me el món del laboratori, la recerca i les AKRs. Jo vaig començar just quan tu acabaves, però t'estic agraït per tots els protocols ensenyats, i a mirar a ojimetro la OD dels cultius. Espero haver estat un relleu a l'alçada, encara que ha estat difícil això. I també a tots els padawans, màsters, gent de pràctiques, màsters i lacais que han passat pel lab durant aquets anys, especialment els "mariquites" de l'Àlvaro i el Javi per les cervesetes compartides, la bona feina i encara més bon humor. La nostra amiga hongaresa Esther, l'Alba i

la seva manera curiosa de fer, l'Agrin, i també a en Roger, la Marina, la Natasha i l'Ignacio.

També vull agrair a tota la gent del departament amb qui més ho menys he compartit temps i feina a la torre. A tota la gent de la planta 3, les meves disculpes per apagar les llums del passadís i sala de cultius! El grup germà dels llevats, amb el Biosca i la Chari, gràcies per tots els consells i el bon humor, sempre disposats a ajudar en el que calguès. Als kinasics Fani i Jordi, especialment pels consells amb els westerns (el protocol que utilitzem és basicament *Made in kinasics*) i les estones a la sala de cultius. No voldria deixar-me ningú del departament amb qui he viscut bones experiències; Mohammed, Javi, Lu, Guillem, Salva, Magda, Santi, Laia, Jofre, Gisela, Andrea, Eva, Jordi, Valentín, Carla, Laura, Lucia, Irantzu, Inma, Alicia, Ana Paula, Edu... I a l'Helena per ser sempre tan alegre i positiva, pels consells donats, tooooooots els tampons i medis preparats, puntes posades i autoclavades, vialets netejats i per aguantar també uns quants dies a les fosques. A l'Albert Suades, per les seves visites des de biofísica, els seus consells i el bon rollo. Iago, gran amic, ja company d'infortunis en el màster amb les puteines i company de pesars durant la tesi, estic segur que acabaràs trobant el que busques. Tenim pendents unes quantes idees de negoci per fer plegats, per quan el forn de pa/pastisseria a Tokyo o el nou producte revolucionari, la *gayasa*? Sento no haver-te visitat a Santander (potser en la defensa de la tesi?), però vas ser un magnific guia a Londres. Hem de fer una altre viatge a Japó plegats! ありがとうございます。

A les meves "*Zorras*", gràcies per les sessions frikis i les nits de vici, la glòria obtinguda d'haver petat el Minecraft (tu no Andreu) per totes les birres gaudides en la vostra companyia, i les que ens queden! El businessman de l'Andreu, canviant el fosforito pel traje i ara el business casual, que arribarà allà on es proposi i tantes estones i aventures passades junts des de l'institut (i abans) (Mendoooosaaaaaaaaaaa). Marc, com han canviat les coses des de que et vaig tornar a conèixer a la granja... i mira't ara, casat amb l'Alba i amb un fill. Per sort tu segueixes sent el mateix, no canviïs mai! Moi, per obrir-me a un món encara més friki, per ser com ets d'entusiasta, la nostra princesa friki del pèsol, gran persona i amic (*Metaaaaaal GeeeaaAAAAAAAAAAAaaaar!!*). Humbert, per ser tan bona persona, bon amic, per estar sempre de bon humor, les lliçons i morts al CoD (tot i haver perdut el mojo) i pel teu riure màgic (*Mmwwhhhoohhhhooohhooo, ya ves*). Al David, per la teva amistat, i per totes les frikades, birres, i juergues passades, molta sort amb aquesta nova etapa que encetes! A tota la resta de la colla: l'Anna (pàdelteam!), la Mireia, l'Aza, el Vicente (moltes gràcies per aquesta gran portada!), el Sergi, l'Hugo, l'Alba, l'Alba i el Jordi, la Cris i el Ricard, l'Angel, el Carlos, l'Irene i el Martí. Sou uns grans amics tots i m'alegro molt de ser part d'aquest magnífic grup! A la Jenny, que tot i que estàs voltant pel món sempre hi ets present.

I per descomptat a la meva família i especialment als meus pares, gràcies per haver-me aguantat tant de temps entendre ben bé feia. Gràcies per confiar sempre en mi, això no hauria estat possible sense vosaltres.

七転び八起き。

“Fall seven times, stand up eight.”

Proverbi japonès

Functional and structural studies of AKR1B15 and AKR1B16:

Two novel additions to human and mouse aldo-keto reductase superfamily

Joan Giménez Dejoz

Abstract

The aldo-keto reductase (AKR) superfamily comprises a large number of monomeric proteins with cytosolic localization and a molecular weight of about 36 kDa. AKRs have a common evolutionarily conserved protein fold which consists of a $(\alpha/\beta)_8$ barrel. Most AKRs act by reducing aldehydes and ketones to their respective alcohols in a NADPH-dependent reaction, with a broad spectrum of substrates ranging from simple sugars to potentially toxic aldehydes.

This Thesis dissertation is a part of the structural and functional studies performed by our group on the characterization of AKRs, especially on their contribution in the biosynthesis pathway of retinoic acid (RA). Our group identified retinaldehyde reductase activity in the AKR family, and since then it has been involved in the deep functional and structural study of the human AKR proteins in relation to this important physiological role. We obtained the crystallographic structure of the highly efficient retinaldehyde reductase AKR1B10, a human enzyme overexpressed in cancer. A relationship was proposed between high retinaldehyde reductase activity and cancer development.

The first part of the Thesis is based on the purification and characterization of a novel human AKR enzyme, AKR1B15, an enzyme sharing 92% sequence identity with AKR1B10. The recombinant protein was expressed mostly in the insoluble fraction, showing limited activity when it was solubilized with detergents. We developed a novel approach in AKRs, using a coexpressing system with chaperones that was successful in increasing the amount of protein in the soluble fraction, in monomeric active form. Enzymatic activity was characterized with a broad range of typical AKR substrates. AKR1B15 shows lower k_{cat} and K_m values than those of AKR1B10 with most substrates, with the exception of ketones and α-carbonyls substrates, which resulted in higher catalytic efficiency. Moreover, AKR1B15 showed superior catalytic efficiency towards the 9-*cis*-retinaldehyde than AKR1B10, being one of the best 9-*cis*-retinaldehyde reductases within the AKR superfamily. Inhibition studies showed that AKR1B15 has a narrower inhibitor selectivity than AKR1B10 and 1B1, and several known aldose reductase inhibitors (ARI) do not inhibit this new enzyme. A structural model was build to analyse the distinct substrate-binding site features of AKR1B15. The residue changes localised in loops A and C, resulting in a smaller, more

hydrophobic and more rigid active site in AKR1B15 as compared to the AKR1B10 pocket, which explains the distinct substrate specificity and narrower inhibitor selectivity of AKR1B15. In addition, a cellular study on the retinaldehyde reductase activity of the AKR1B15 and 1B10 enzymes was carried out. Using HEK293T cells as a model and transient transfection, it was observed that AKR1B10, but not AKR1B15, participates in the reduction of retinaldehyde, which results in changes in the amount of RA in the cells.

The second part of this work is centered on the study of the relationship between the structural differences of the binding pockets of AKR1B15 and 1B10 and the distinct function of the two enzymes. Mutants of AKR1B10 were prepared to mimic the catalytic pocket of AKR1B15, with the aim of converting one enzyme into the other, and trying to understand the factors that determine their distinct substrate specificity and inhibitor selectivity. The mutant proteins displayed higher k_{cat} and K_m values than the wild-type enzymes, with features resembling AKR1B15, such as the activity with ketones, and the ability to efficiently reduce the 9-*cis*-retinaldehdye isomer.

Finally, the characterization of AKR1B16, a novel mouse enzyme, was performed. Previous studies determined that AKR1B16 was an active protein expressed in murine tissues. In this Thesis, we have performed a phylogenetic analysis, and a wide kinetic characterization with a variety of substrates, including retinaldehyde isomers. The enzyme displayed moderate activity with all the assayed substrates being poorly active with retinaldehyde. These results indicate that AKR1B16 is not an orthologous protein of AKR1B10.

Contents

Table list

Figure list

Abbreviations

ACCA	acetyl-CoA carboxilase-α
ADH	alcohol dehydrogenase
AGE	advanced glycosilation end-product
AKR	aldo-keto reductase
ALDH/RALDH	aldehyde dehydrogenases
AR	aldose reductase
ARE	antioxidant response element
ARI	aldose reductase inhibitor
BCO1	β-carotene-15,15'-monooxygenase
BCO2	β-carotene-9,10'-dioxygenase
BSA	bovine serum albumine
COX	cyclooxygenases
CRABP	cellular retinoic acid binding protein
CRBP1	cellular retinol-binding protein type-1
CRBP2	cellular retinol-binding protein type-2
CYP26	cytochrome P450 family 26
DMEM	Dulbecco's modified Eagle's medium
DMSO	dimethyl sulfoxide
DR	vitamin D receptor
DTT	1,4-dithiothreitol
EDTA	ethylenediaminetetraacetic acid

FBS	fetal bovine serum
FPLC	fast protein liquid chromatography
GST	glutathione-s-transferases
HCC	hepatocellular carcinoma
hCG	human chorionic gonadotropin
HNE	4-hydroxy-2-nonenal
HPLC	high pressure liquid chromatography
HSD	hydroxysteroid dehydrogenase
IC_{50}	half maximal (50%) inhibitory concentration
IPTG	isopropyl β-D-1-thiogalactopyranoside
K_D	dissociation constant
K_i	inhibition constant
K_m	Michaelis constant
k_{cat}	catalytic constant
LH	luteinizing hormone
LRAT	lecithin:retinol acyltransferase
MDR	medium-chain dehydrogenase/reductase
mRNA	messenger RNA
MVDP	mouse vas deferens protein or AKR1B7
NAD^+	nicotinamide adenine dinucleotide (oxidised)
NADH	nicotinamide adenine dinucleotide (reduced)
$NADP^+$	nicotinamide adenine dinucleotide phosphate (oxidised)
NADPH	nicotinamide adenine dinucleotide phosphate (reduced)
NR	nuclear receptor
NSAID	nonsteroidal anti-inflammatory drug
NSCLC	non-small cell lung cancer
ORE	osmotic response element

P450	cytochrome p450
PAH	polycyclic aromatic hydrocarbons
PBS	phosphate-buffered saline
PDB	protein data bank
$PGF_{2\alpha}$	prostaglandin $F_{2\alpha}$
PGFS	prostaglandin $F_{2\alpha}$ synthase
PMSF	phenylmethanesulfonyl fluoride
PPAR	peroxisome proliferator-activated receptor
PUFA	polyunsaturated fatty acids
RA	retinoic acid
RAL	retinaldehyde
RAR	retinoic acid receptor
RARE	retinoic acid response elements
RBP	retinol binding protein
RDH	retinol dehydrogenase
REH	retinol ester hydrolase
ROL	retinol
ROS	reactive oxygen species
RXR	retinoid X receptor
RXRE	retinoid X response element
SAR	structure-activity relationship
SDH	sorbitol dehydrogenase
SDR	short-chain dehydrogenases/reductases
siRNA	small interference RNA
STRA6	stimulated by retinoic acid gene 6
TR	thyroid hormone receptor
TTR	transthyretin

VSMC	vascular smooth muscle cell
WAT	white adipose tissue

Chapter 1

General introduction

1.1 Oxidoreductases

The reversible conversion of alcohols to their respective aldehyde/ketones is performed in nature mainly by the action of medium-chain dehydrogenase/reductases (MDR), short-chain dehydrogenase/reductases (SDR) and the enzymes of study in this Thesis, the aldo-keto reductases (AKR). These three enzyme superfamilies group a large number of structurally related proteins (*1*).

The members of the MDR superfamily are enzymes formed generally by two or four subunits of approximately 350 residues. The members of this superfamily can be divided into two large groups: Zn^{2+}-containing MDRs (including vertebrate alcohol dehydrogenases (ADH), the most largely investigated); and the Zn^{2+}-lacking MDRs (including quinone oxidoreductases). Each subunit of these enzymes has two domains, a catalytic domain that binds the Zn atom in the zinc dependent MDR, and the cofactor binding domain known as Rossmann fold (*2*).

The enzymes of the SDR superfamily constitute one of the largest protein superfamilies known, with more than 100,000 proteins. They have typically around 250 amino acid residues and can be monomers, dimers, or tetramers. The typical SDR fold consists in a β-sheet sandwiched between three α-helices on each side, forming a Rossmann fold. This family is formed by distant enzymatic groups and includes the alcohol dehydrogenases of Drosophila and the human retinol dehydrogenases/reductases (*3*).

Table 1.1: General characteristics of the three oxidoreductases superfamilies

	MDR	**SDR**	**AKR**
Primary structure	350 aa	250 aa	320 aa
Typical fold	Rossmann	Rossmann	$(\alpha/\beta)_8$ barrel
Quartenary structure	dimer/tetramer	monomer/dimer/tetramer	monomer
Active site	Zn/No Zn	Tyr, Lys, Ser, Asn	Tyr, Asp, Lys, His
Coenzyme preference	NAD	NAD(P)	NADP

1.2 Aldo-keto reductases: general perspective

Aldo-keto reductases (AKRs) constitute an enzyme superfamily that form a structurally related group with a common origin, and have been described in all phyla, ranging from vertebrates, invertebrates, plants, protozoa, fungi and bacteria (*4*). In fact, it was not until 1989 that the term AKR was first used to define the superfamily (*5*).

The AKRs are monomers with approximately 320 amino acid residues and a molecular weight of approx. 36 kDa with cytosolic localitzation. Their three dimensional structure consists of a $(\alpha/\beta)_8$ barrel, and they are NAD(P)H dependent. Although they have a significant degree of sequence identity (the members of each family share at least 40% of sequence identity, and the members of a subfamily share 60% or more sequence identity (*1*)), small variations in the loops

near the C-terminal end and point substitutions in their active-site center confer to these proteins a great variability in their substrate specificity, being able to reduce carbonyl groups of a high variety of chemical compounds including aromatic and aliphatic compounds (*6*, *7*).

$$Aldehyde/Ketone + NAD(P)H + H^+ \overset{AKR}{\leftrightarrows} Alcohol + NAD(P)^+$$

These substrates can be endogenous compounds (carbohydrates, steroids, retinoids, prostaglandins, lipid peroxidation products), some of them with hormone properties and therefore the aldo-keto reductases can regulate the amount of ligand that may be available for nuclear receptors, indirectly regulate gene transcription (*8*). AKRs also can use xenobiotic compounds, like several drugs, pharmaceuticals, foods, carcinogens and pollutants with reactive carbonyl groups, that yield carbonyl compounds from their *in vivo* metabolism. For this reason AKRs can be considered as enzymes of *Phase I drug metabolism*, because they can inactivate or bioactivate these compounds. Accordingly, AKRs are implicated in the resistance to chemotherapeutic drugs with a carbonyl group in their structure. Moreover, most of the *AKR* genes are regulated by stress (osmotic, electrophilic or oxidative) and consequently they play a role in the cellular response to stress (*9*).

The AKRs comprise about 120 proteins distributed in 15 enzymatic families (AKR1 - AKR15), clustered following phylogenetic and sequence identity criteria. Delineation of families occurs at the 40% amino acid identity level. Members of an AKR family should have $\leq$40% amino acid identity with members of any other family. Within a given family, subfamilies may be defined by a $\geq$60% identity in amino acid sequence between subfamily members (*1*, *4*). AKR1 is the most numerous and studied family, which comprises the subfamilies of aldehyde reductase (AKR1A), aldose reductase (AR; AKR1B), hydroxysteroid reductase (AKR1C) and ketosteroid reductase (AKR1D). Although the majority of the AKRs are monomeric enzymes, the members of the AKR2, AKR6 and AKR7 families are able to form multimers (*6*, *7*). Information on the nomenclature and the existing and potential members of the AKR superfamily can be obtained in: http://www.med.upenn.edu/akr/.

1.3 Genetic structure of AKR

1.3.1 Genetic structure of the human *AKRs*

The AKRs are an enzymatic ancient superfamily, already present in procaryotes. They are believed to be originated from a multifunctional ancestor (now extinct) by divergent evolution, involving gene duplication and subsequent evolutionary variations in substrate binding and preferences (*1*, *10*). In general, the *AKR* genes consist of an average of 10 exons and have an average length of $\sim$ 17 kb. AKR members belonging to the same family form gene clusters on the same chromosome and have similar gene structures (*6*). For example, Figure 1.1a, shows the chromosome localization

of the human *AKR1B* genes, and in figure 1.1b the position of the human and mouse *AKR1B* genes is displayed in their clusters.

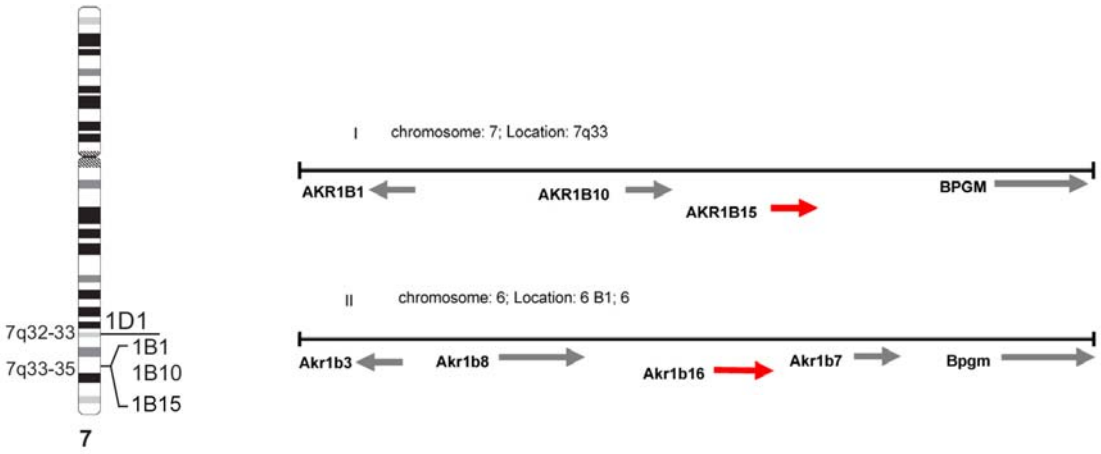

(a) *AKR1B* genes in chromosome 7.

(b) Locus map of human and mouse *AKR1B* genes.

Figure 1.1: Position of *AKR1B* genes in human chromosome and mouse genome. The AKR1B family forms a cluster on the same chromosome. (a) Localization of human *AKR1B* genes in chromosome 7. Modified from (*6*) (b) Loci maps for human chromosome 7q33–35 and mouse chromosome 6B1 showing the positions of human *AKR1B15* and mouse *Akr1b16* genes (in red), which code for the novel enzymes described in this Thesis. Taken from (*11*).

The human genes *AKR1B1*, *AKR1B10* and *AKR1B15* are located one near the other in the chromosome 7q33-35. The *AKR1B15* gene makes an alternative use of the first exons of the gene, leading to two different transcripts and giving rise to two splice variants (*12*).

1.3.2 Homology between human and murine *AKR1B* genes

The *AKR* families of rodents differ from those of humans. Although some rodent *AKR* genes are directly correlated to human genes, this is not the case for many others. The only unambiguous orthology in the AKR1B subfamily is between the AKR1B3 (mouse) and 1B4 (rat) and human aldose reductase (AKR1B1), based on their expression pattern and catalytic activity with glucose as a substrate. However, neither mouse AKR1B7 or AKR1B8 (or their rats orthologs) are clearly orthologous to human AKR1B10, according to their tissue distribution and catalytic properties. Thus, a total of four AKR1B enzymes for mouse and three for human, with distinct tissue distribution and kinetic properties, have been found. Accordingly, the *Akr1b* cluster on mouse chromosome 6B1 contains four genes: three previously described and the recently discovered *Akr1b16*, which shares 82.9% amino acid identity with AKR1B10. This imposes a limitation on the use of the *knockout* technology for studying the physiological function of AKRs. Even in cases where the orthologous protein has been established and clearly identified in mouse (as with aldose reductase),

the presence of different family members that can partly compensate for the loss of function limits our ability to fully understand their corresponding function in humans (*6*).

1.4 Structural and catalytic properties of AKRs

1.4.1 Structural properties

As mentioned previously, AKRs share a common three dimensional structure with a $(\alpha/\beta)_8$ barrel fold, a conserved and compact motive including a pyridine nucleotide binding site. Substrate binding is mainly achieved through the loops localised in one of the sides of the $(\alpha/\beta)_8$ barrel. It is in these loops where most of the variations occur between the different AKRs. Modifications of the loops alter the binding properties and catalysis without affecting the basic protein structure. Mainly 3 loops can be distinguished conferring the structurally distinct identity to the different families and subfamilies of AKR: loop A, residues 112 to 136; loop B, residues 216 to 227; and loop C, residues 299 to 310 (AKR1B10 numeration).

The substrate-binding pocket is located on the top of the barrel and it is formed by the loops A, B and C together with residues from the center of the barrel. The cofactor enters from a lateral side and constitutes the base of the active center. The majority of the AKR enzymes share a high sequence identity in their cofactor-binding site and in the catalytic center. Structurally, most AKRs retain a conserved characteristic catalytic tetrad, which consists of Asp44, Tyr49, Lys78 and His111 (AKR1B10 numbering). Regarding the substrate binding site, it is in the loops A and C where most variations occur between the various AKRs (Figure 1.2). Therefore, the rational design of selective inhibitors for these enzymes has to take advantage of the differences found in the sequence of the loops. This feature has been studied in some enzymes of the family, but it still requires a more extensive study, to avoid cross inhibition because of the high number of AKRs present in an organism (*6*).

The NADPH binding site is determined mainly by loop B. This loop is larger in the members of AKR1B than in those of the AKR1C subfamily. In the AKR1B enzymes the larger loop has more mobility, allowing a series of opened and closed shift movements of the loop over the bound cofactor (acting as a "safety belt" over the pyrophosphate bridge). These interactions are not possible in the AKR1C subfamily due to their shorter loop B. This feature, the binding and release of the cofactor implying a conformational change in loop B with an opening movement, is responsible in the AKR1B subfamily of the rate-limiting step of the reaction, cofactor dissociation, while in AKR1C, with a shorter loop B, the chemical step and the release of the reaction product are more limiting than cofactor dissociation (*14*).

Regarding the cofactor type, AKR enzymes prefer NADPH over NADH as a reduced cofactor, as it can be seen from the values of the binding and kinetic constants for the two cofactors (*15*, *16*). The AKRs, like other oxidoreductases, are capable to discriminate between oxidised and reduced

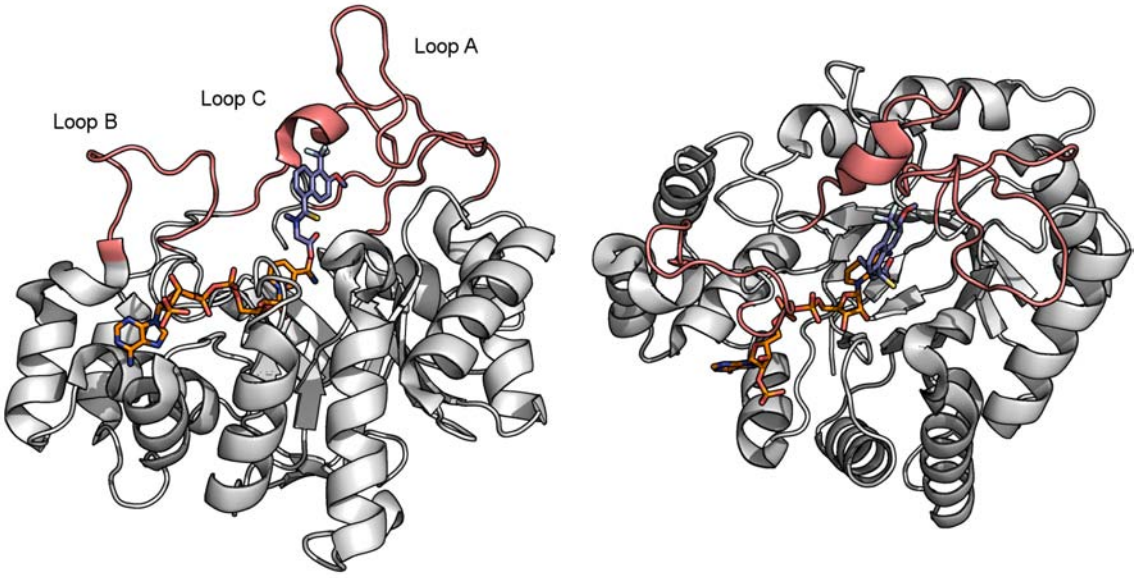

(a) Lateral view of the $(\alpha/\beta)_8$ barrel. (b) Top view of the $(\alpha/\beta)_8$ barrel after rotating 90°.

Figure 1.2: Crystal structure of AKR1B10 complexed with $NADP^+$ and tolrestat inhibitor. (a) Lateral view of the $(\alpha/\beta)_8$ barrel. Cofactor approaches the catalytic site from one side of the barrel, and inhibitor tolrestat enters the barrel from the upper face. (b) View from the top of the barrel after rotating 90°. The catalytic site is located in the center of the barrel. $NADP^+$ is represented in orange and tolrestat in blue. PDB code: 1ZUA (*13*). Structural images were created using the program PyMOL (www.pymol.org).

cofactor, binding the reduced one with higher affinity (Table 1.2). Some AKRs are able to use NADH as coenzyme and they even have a k_{cat} value higher for NADH over NADPH. However, as the cofactor binding is weaker, its K_m value for NADH is also increased compared with NADPH, resulting in a lower catalytic efficiency than for NADPH. This is the case for AKR1C12 and AKR1B7 (*17*, *18*). The structural determinants for the cofactor preference are linked to charged residues (lysines and arginines) that bind the 2'-phosphate group of NADPH (*16*, *19*, *20*).

In the metabolically active cells, $NADP^+$ is predominantly found in its reduced form, as NADPH, whereas its dephosphorylated counterpart, NAD^+, is largely present in its oxidized state (*25*). Therefore most AKR prefer reductive reactions, and reduction is favored over oxidation. The NADPH/$NADP^+$ ratio is an indication of the synthetic capacity of the cell and is kinetically and thermodynamically dissociated from the NAD^+/NADH ratio, which is mostly regulated by rates of glycolysis and respiration. The higher NADPH levels, provide a strong driving force for AKRs to catalyze reduction under a wide range of energetic states of the cell associated with different levels of respiration, growth, or starvation (*6*).

Until now, it has not been possible to obtain a crystal structure of an AKR1B enzyme bound to a substrate or a substrate analogous. This has been possible for some AKR1C. The reported studies are based on the utilization of slow substrates with the oxidized cofactor, facilitating the formation

Table 1.2: Dissociation constant values for cofactor binding to various AKRs

AKR	Buffer	K_d NADPH (μM)	K_d $NADP^+$ (μM)	Reference
AKR1A1	5 mM KPi, pH 7.5	0.13	0.36	(*21*)
AKR1B1	5 mM KPi, pH 7.0	0.01	0.006	(*22*)
AKR1C2	10 mM KPi, pH 7.0	0.12	0.21	(*23*)
AKR6A3	100 mM KPi, pH 7.4	1.8	5.6	(*16*)
AKR6A2	200 mM KPi, pH 7.4	0.12	0.36	(*24*)

KPi: potassium phosphate buffer

of an abortive ternary complex (complex AKR1C3-NADP prostaglandin D2, PDB 1RY0). In contrast, many AKR1B-inhibitor structures could be obtained. Hence, the wide research to obtain new and selective inhibitors for AKR1B1 (known as ARIs, Aldose Reductase Inhibitors) has always entailed the structural study of AKRs (*26*).

1.4.2 Catalytic properties

The vast majority of AKRs are catalytically active proteins. However, there are some AKR members that have a structural function: *i)* AKR1C10 (or *ρ-crystalline*), which only has an important structural function in the bullfrog lens (*27*); *ii)* Kvβ, member of the AKR6 family, which has little catalytic activity, is a cytosolic protein that forms a permanent complex with a Kv1 voltage-dependent potassium channel, being its β-subunit (*28*, *29*); and *iii)* AKR1B10, apart from being a monomeric and active catalytic enzyme, can be found associated with the acetyl-CoA carboxylase-α (ACCA) and mediates its ubiquitin-dependent degradation by the proteasome. Thereby, AKR1B10 is critical to cell proliferation and survival through its regulation of ACCA, a rate-limiting enzyme of *de novo* fatty acid synthesis (*30*, *31*). Other catalytically active AKRs have variable kinetic features. The members of the AKR1A and AKR1B subfamilies are more efficient acting as reductases. In contrast, the members of the AKR1C subfamily have similar catalytic efficiency acting either as reductases or dehydrogenases *in vitro* (*32*). However, the kinetic mechanism seems to be similar in all AKRs. In general, AKRs exhibit an ordered bi-bi sequential mechanism, in which the reduced cofactor first binds to the enzyme, and the limiting step is the release of the oxidized cofactor (Fig. 1.3) (*7*, *20*).

The catalytic mechanism of AKRs involves stereospecific reduction or oxidation reactions that utilize pyridine nucleotides. The process of reduction by AKRs proceeds in two steps: *1)* A hydride ion is transferred from the pro-*R* hydrogen of the NADPH nicotinamide ring to the carbonyl carbon of the substrate, and *2)* a proton is added from the solvent to reduce the carbonyl to an alcohol (Fig. 1.4). Oxidation-reduction reactions of AKRs involve general acid-base catalysis, although under some conditions AKRs can catalyze the oxidation or reduction entirely by an effect of proximity

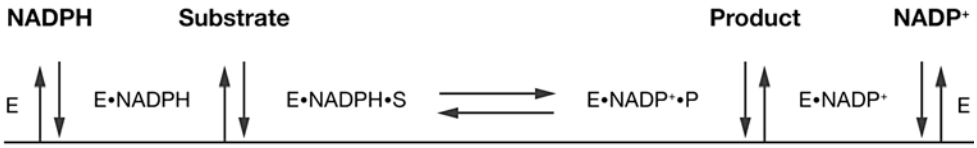

Figure 1.3: Sequential ordered bi-bi mechanism to the reversible reaction catalyzed by AKRs. Reproduced from (*9*).

and orientation (i.e. rat liver AKR1C9) (*33*).

Structurally, most AKRs retain a conserved catalytic tetrad, which consists of Asp44, Tyr49, His111 and Lys78 (AKR1B10 numbering) (*7*). The pK value of the group involved in acid-base catalysis was determined and reported to be 6.5 - 7.0 for AKR1B1 and AKR1C (*33*, *34*). His111 was first proposed to be the acid-base catalytic group due to the low pK value observed (*34*). However, later studies by site-directed mutagenesis showed that the mutation of the Tyr49 (or equivalent residue) to Phe, resulted in the generation of a completely inactive protein (*35*, *36*), whereas the mutation of His111 led to a partial inactive enzyme. Hence, it was suggested that the acid-base catalytic group in AKRs was Tyr49. Another evidence that supports this hypothesis is that the Tyr is universally conserved among the AKRs, while His111 is not conserved in all the families (for example, the AKR6 family). This His seems to have an important role in the orientation of substrates in the catalytic center. The low pK value of the Tyr49 will be given by a hydrogen bond net generated by the residues Asp44 and Lys78 (*35*). However, the fact that mutants with residues other than Tyr (His or Ser) have also some activity (*35*), or that mutants of the Tyr to Phe still retain some activity with 9,10-phenantrenequinone (*36*) suggests that other catalytic acid-base mechanisms may be possible, and that a contribution of His111 could not be discarded.

1.5 Human AKR functions

Until now 14 human AKR have been identified, distributed in the AKR1, AKR6 and AKR7 families. As previously mentioned, they have a broad substrate specificity. However, there are some features in the human AKRs worth to mention: *i)* Not all proteins are enzymes, some of them such as the AKR6 family members, are a structural part of a K^+ channel; *ii)* not all enzymes have carbonyl reductase activity; for example AKR1D1, reduces a double bond in steroids, and has the catalytic tetrad altered, with the histidine changed to a glutamic acid; *iii)* not all the proteins are monomeric, the AKR6 subfamily forms tetramers and the AKR7 members can be found as homo or heterodimers (*8*). However, the AKR functionality in general is based on its capacity to reduce carbonyl groups.

Regarding physiologic functions, first of all AKRs participate in the detoxification of lypidic

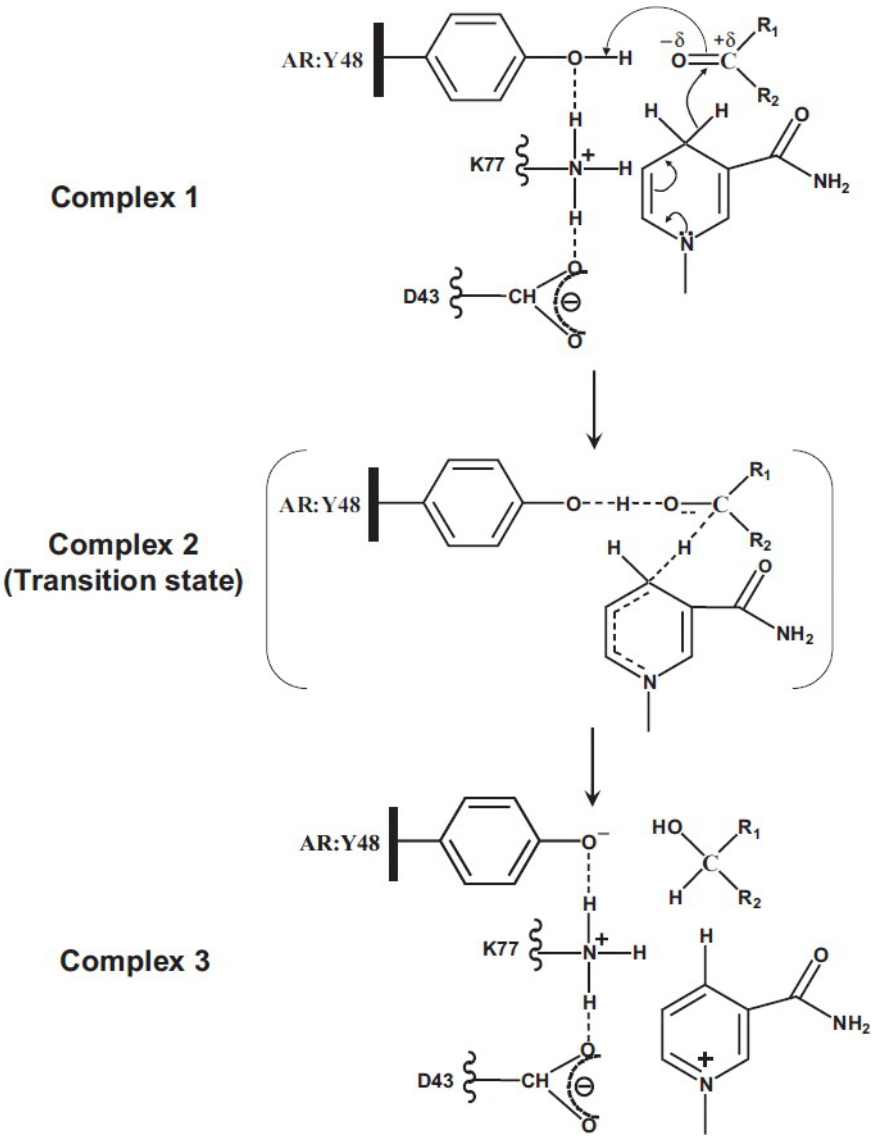

Figure 1.4: Catalytic mechanism of aldo-keto reductases. In complex 1, active-site Tyr-48 (AKR1B1 numbering) is shown to form a hydrogen bond with the substrate carbonyl, resulting in the carbonyl polarization and acceleration of the hydride transfer of the pro-R hydrogen from the nicotinamide ring of NADPH to the substrate carbonyl carbon. The hydrogen-bonding network provided by Lys-77 and Asp-43 serves to lower the pK_a of tyrosine, making the proton transfer easier. Complex 2 shows a transition state in which the polarization at the carbonyl is quenched by the proton transferred from the protein tyrosine and a concerted hydride transfer to the carbonyl carbon. The reduced carbonyl then dissociates from the acid-base catalyst, and a net charge on the tyrosinate anion is stabilized by the hydrogen bonding network (complex 3). Reproduced from (*6*).

aldehydes. Reactive oxygen species (ROS: superoxide anion, hydrogen peroxide and hydroxyl radical), produced under conditions of oxidative stress, attack polyunsaturated fatty acids (PUFA, i.e., arachidonic acid and linoleic acid) to form a series of lipid peroxides that breakdown to yield reactive bifunctional electrophiles, like 4-hydroxy-2-nonenal (HNE). These electrophiles are implicated in the pathogenesis of atherosclerotic plaques and neurodegenerative disease (Parkinson's disease and Alzheimer's disease) since they can form protein cross-links. HNE and 4-oxo-2-nonenal can also form highly mutagenic DNA adducts. To limit their potential toxicity, a number of enzyme systems exist, like alcohol dehydrogenases (ADHs), aldehyde dehydrogenases (ALDHs), glutathion-S-transferases (GSTs) and AKRs (*8*, *37*) (Figure 1.5).

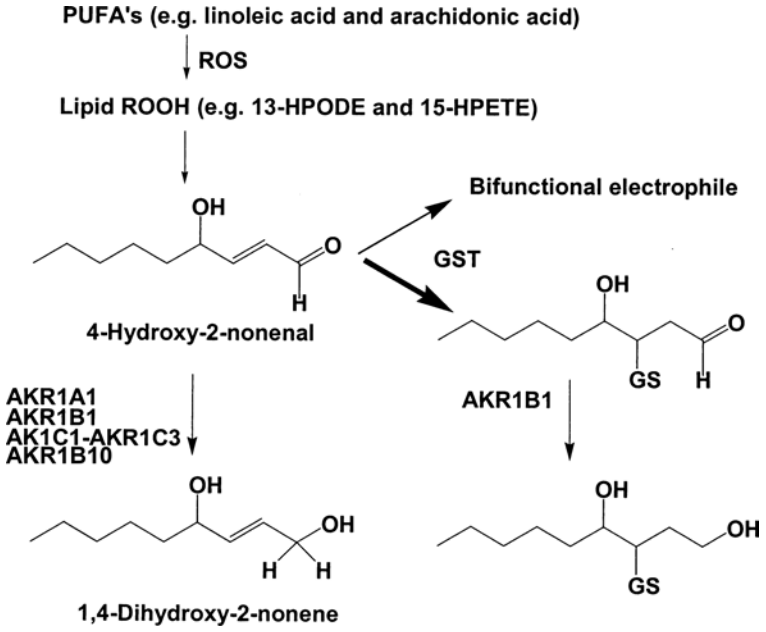

Figure 1.5: AKR isoforms and the detoxification of lipid aldehydes. 13-HPODE: 13-hydroperoxy octadecadienoic acid. 15-HPETE: 15-hydroperoxyeicosatetraenoic acid. Adapted from (*8*).

Another physiological function of AKRs is the regulation of the ligand availability at the pre-receptor level for some nuclear receptors. In consequence, they can affect gene transcription. Thus, human AKRs reduce a large variety of important lipophilic effectors, e.g., ketosteroids, ketoprostaglandins and retinals, and can thereby regulate the biological response generated by the interaction between ligand and receptor. In some cases they favor the formation of ligand, and in others they prevent it, resulting in activation or inhibition of the hormonal response (Table 1.3) (*8*).

One last relevant function of AKRs as enzymes of *phase I drug metabolism* is on the metabolism of xenobiotic compounds, among them some environmental pollutants, pharmaceutical drugs, carcinogens and reactive aldehydes (Figure 1.6). Basically, AKRs are implicated in the metabolism of three classes of chemical carcinogens: activation of polycyclic aromatic hydrocarbons (PAH), and deactivation of aflatoxin and nicotine derived nitrosamino-ketones, mainly 4-(methylnitrosamino)-

Table 1.3: Regulation of nuclear receptors (NR) by human AKRs (*8*).

Aldo-keto reductase	**Reduction reaction**	**Nuclear receptor**
AKR1A1	BP-7,8-diol → BP-7,8-dione	AhR[a]
AKR1B10	all-*trans*-retinal → all-*trans*-retinol	RAR[a]
AKR1C1	Progesterone → 20α-OH-progesterone	PR[a]
AKR1C1	5α-DHT → 3β-androstanediol	ERβ
AKR1C2	5α-DHT → 3α-androstanediol	AR[a]
AKR1C3	Adione → testosterone	AR
AKR1C3	Estrone → 17β-estradiol	ERα
AKR1C3	Progesterone → 20α-OH-progesterone	PR
AKR1C3	9-*cis*-retinal → 9-*cis*-retinol	RXR
AKR1C3	DOC → 20α-DOC	MR[a], OR
AKR1C3	PGD_2 → 9α,11β-PGF_2	PPARγ
AKR1C1-4	BP-7,8-diol → BP-7,8-dione	AhR[a]
AKR1D1	Progesterone → 5β-pregnane-3,20-dione	hPXR, hCAR

[a]Positive in *trans*-activation assays

Abreviatures: AhR, aryl hydrocarbon receptor; AR, androgen receptor; BP, benzo[*a*] pyrene; CAR, constitutive androstane receptor; DHT, dihydrotestosterone; ER, estrogen response element; MR, mineralocorticoid receptor; NR, nuclear receptors; OR, orphan receptors; PPARγ, peroxisome proliferator-activated receptors γ; PR, progesterone receptor; PXR, pregnane X-activated receptor. Modified from (*8*).

1-(3-pyridyl)-1-butanone (NNK). Aflatoxin is a hepatocarcinogen, while PAH and NNK are compounds found in the tobacco smoke that are involved in lung cancer (*8*, *9*).

1.6 Human AKR1B subfamily

1.6.1 AKR1B1

The biological function of AKR1B1, also named as human aldose reductase (AR), is still poorly known nowadays. However, its potential role on the development of secondary complications in diabetic patients has made it so far the most studied member among all the AKRs (*38*). Along with sorbitol dehydrogenase (SDH), it is responsible for the polyol pathway. This name is given to the metabolic pathway that generates fructose from glucose. Under normal glycemic conditions, only a small fraction of glucose is metabolized through the polyol pathway, as the majority is phosphorylated by hexokinase, and the resulting product, glucose-6-phosphate, is utilized as a substrate for glycolysis or pentose phosphate metabolism. However, in response to chronic hyperglycemia,

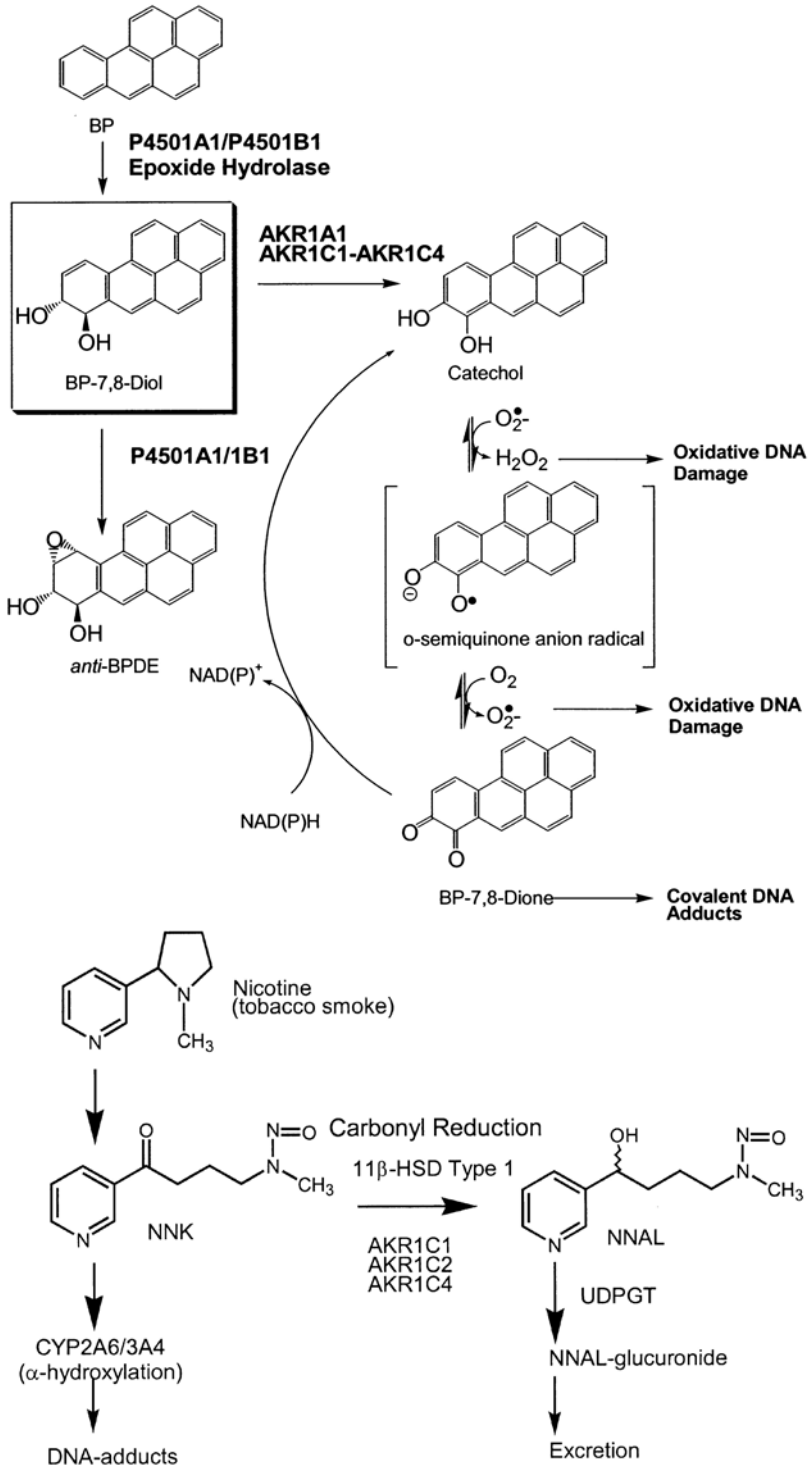

Figure 1.6: Role of human AKR in the metabolim of xenobiotic compounds, in the PAH-activation and NNK metabolism. BP, benzo[*a*]pyrene; NNAL, 4-(methylnitrosamino)-1-(3-pyridyl)-1-butanol. Adapted from (*8*).

glucose flux through the polyol pathway is markedly increased (*39*). AKR1B1 enzymatically transforms cytosolic glucose into sorbitol, a molecule that poorly penetrates cell membranes and is slowly metabolized, by SDH to fructose, as the rate-limiting step. Both sorbitol and fructose, the final product of this pathway, are highly osmotic compounds that generate an increase in the osmotic pressure, which subsequently induces the expression of AKR1B1. Transcriptional regulation of *AKR1B1* gene expression appears to involve complex mechanisms that use multiple *cis*-acting elements and *trans*-acting factors. Importantly, in its promoter region three osmotic response elements (ORE) can be found. Also, AKR1B1 expression is enhanced by oxidative substances such as hydrogen peroxide, nitric oxide (NO), oxidized low-density lipoprotein, and advanced glycation end-products (AGEs). Thus, AKR1B1 can be designated as an oxidative stress-inducible protein (*40*, *41*). Therefore, the induction of AKR1B1 expression increases the flux through the polyol pathway in a positive feedback leading to osmotic stress in the cell (in the kidney the osmoregulation is a critical feature, and the enzyme is implicated in the urine concentration (*39*)), and results in secondary complications of diabetes such as eye diseases, including cataract and retinopathy, increased risk of painful neuropathy, heart disease, nephropathy and kidney failure (*6*, *42*). All these data and the success of preclinical studies with ARI led to the named "Osmothic Hypothesis"(Fig. 1.7).

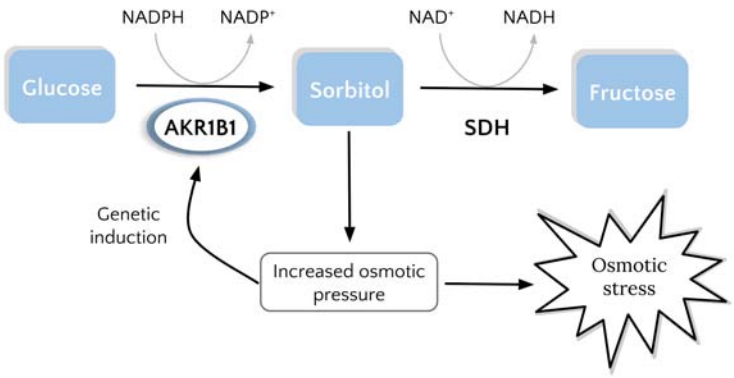

Figure 1.7: Role of AKR1B1 in the osmotic hyphotesis. AKR1B1 expression is regulated by an osmotic response element, and both sorbitol and fructose contribute to increase osmotic pressure in the cell. This creates a positive feedback where the osmotic pressure increases and might cause secondary complications. Modified from (*43*).

The participation of AKR1B1 in the polyol pathway is widely accepted under hyperglycemic conditions. However, due its catalytic constants with glucose (K_m = 76 mM and k_{cat} = 97 min^{-1} (*44*)), it is thought that under normal glycemic conditions the flux of this pathway its very limited. Also, AKR1B1 has a broad expression pattern and can be found in many tissues like heart, blood vessels, skeletal muscle, brain, and mainly in adrenal gland. This suggests that can it be implicated in other processes as well.

The highly hydrophobic character of the AKR1B1 substrate-binding pocket does not seem very suitable for the reduction of sugars. Indeed, AKR1B1 has a broad substrate specificity and can reduce a wide range of substrates. The enzyme catalyzes the reduction of many substrates of physiological significance, including AGE precursors, isocorticosteroids, lipid peroxidation products, such as HNE and oxidized phospholipids, and glutathione conjugates of unsaturated aldehydes and environmental pollutants (e.g., acrolein and its glutathione conjugate) (*6*, *9*).

A unique feature of AKR1B1 is its sensitivity to oxidation. Cys298 is a residue localised in the active-site pocket. The oxidation of this residue accelerates catalysis and prevents binding of ARIs. This is due to a decrease in the affinity of the enzyme for NADPH, facilitating the dissociation of the $NADP^+$. Because $NADP^+$ release is rate limiting in AKR1B1 catalysis, an increase in the $NADP^+$ releasing rate elevates the k_{cat} value. Several studies suggest that oxidation of Cys298 is a physiological process, and that represents a mode of redox regulation. These studies also show that Cys298 could be glutathiolated and nitrosylated (*6*).

Different works have demonstrated that AKR1B1 may participate in cellular signaling pathways by regulation of several factors like PKC, NFκB and others (in the promoter region of the *AKR1B1* gene, phorbol ester responsive element (AP-1) and an antioxidant response element, ARE, have been found), through a protein kinase cascade (PLC/PKC/PI3K/MAPK) activation. These activated factors result in the transcription of various inflammation-related genes, which cause cell proliferation, dysplasia and cancer. The mechanism is still unknown, but it has been suggested that it could be through the product of a reaction catalyzed by the enzyme. Other studies have proposed other roles for the enzyme, especially functions related to the control of cellular proliferation (*45*). AKR1B1 is also related to atherosclerosis and restenosis because it is involved in abnormal vascular smooth muscle cell (VSMC) proliferation (*46*).

Recently, *in vivo* studies showed that administration of AKR1B1 small interfering RNA (siRNA) to nude mice bearing SW480 human colon adenocarcinoma cells completely arrested tumor progression (*47*), therefore ARIs would have an antitumoral effect. This new pathological implication, the relationship of AKR1B1 with cancer, had been shown previously in hepatoma (*48*) and it would be performed through its detoxification capacity of cytotoxic carbonyls, hence helping the tumoral cells to achieve an immortal state. Also, it has been observed that in the ischemic heart, stimulation of endogenous NO production increased AKR1B1 activity, whereas inhibition of NO synthesis prevented its activation. Taken together, these observations support that AKR1B1 activation during ischemia is due to NO-mediated oxidation of AR cysteines to sulfenic acid. Therefore, this regulation could have an important role in cell proliferation, inflammation and apoptosis (*49*). Recently, a study found a novel role for AKR1B1 as a specific derepressor of nuclear receptors. They point that AKR1B1 interacts with nuclear corepressors that specifically regulate hystone deacetylase 3 (HDAC3), a chromatine-modifying enzyme, decreasing its ability to regulate HDAC3 levels. The consequence is the induction of PPARγ target genes that mediate accumulation of lipids, and the derepression of RAR (retinoic acid receptor) target genes, altering retinoid metabolism (*50*).

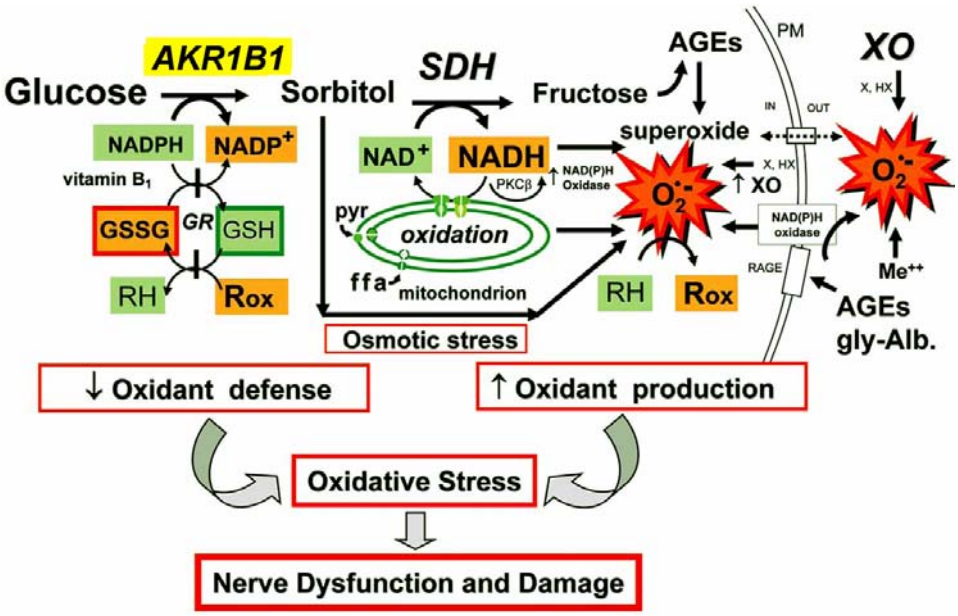

Figure 1.8: The metabolic flux hypothesis emphasizes the pathogenic importance in diabetic tissue of the rate of substrate flux through the AKR1B1 polyol pathway. The rate of substrate flux is directly linked to the turnover of the respective coenzyme systems that provide key links with the generation of oxidative stress. If oxidant production exceeds oxidant defense capacity, oxidative stress results. Abbreviations: GSH, reduced glutathione; GSSG, oxidized glutathione; RH, reduced cellular molecule; Rox, oxidized form of RH; GR, glutathione reductase; pyr, pyruvate; ffa, fatty acid; PKCβ, protein kinase C beta; X, xanthine; HX, hypoxanthine; XO, xanthine oxidase; PM, plasma membrane; Me^{++}, metal ion; AGEs, advanced glycation endproducts; RAGE, receptor for AGEs; gly-Alb., glycated albumin. Reproduced from (*38*).

Driven by the osmotic hypothesis, and with positive preclinical results on prototype ARIs, researchers worldwide have targeted diabetic neuropathy with ARIs for four decades. However, most double-blind placebo-controlled ARI diabetic neuropathy trial outcomes have been disappointing. These results and the knowledge of new functions and substrates of AKR1B1 have led to reconsider this hypothesis (*38*). An alternative mechanism appeared, related to the oxidative stress linked to the redox imbalance on cofactor regeneration, the "metabolic flux hypothesis"(Fig. 1.8) (*51*, *52*). This is especially relevant in the nervous cells of retina where the cellular damage produced by oxidative stress, in conjunction with neovascularization, could lead to diabetic retinopathy and, eventually, cause blindness. Cell damage could also affect other types of neurons, thus sorbitol accumulation could be one of the causes of sensitivity loss in the limbs of diabetic patients.

AKR1B1 inhibitors

The role of AKR1B1 in pathological conditions (diabetes, atherosclerosis, cancer, etc.) has undoubtedly raised a great interest. Therefore many compounds had been developed as inhibitors of AKR1B1 (ARIs; Aldose Reductase Inhibitors) with the purpose to use them to treat the patholo-

gies in which AKR1B1 is involved. Currently, three types of ARIs can be distinguished (Figure 1.9):

- Cyclic imides, such as fidarestat (Figure 1.9a)
- Derivates from cyclic imides with a carboxylic acid, like tolrestat (Figure 1.9b)
- Piridazinones, a new class of inhibitors, represented by the ARI-809 (Figure 1.9c), that includes the compounds without either a ciclic imide nor a carboxylic acid in their structure.

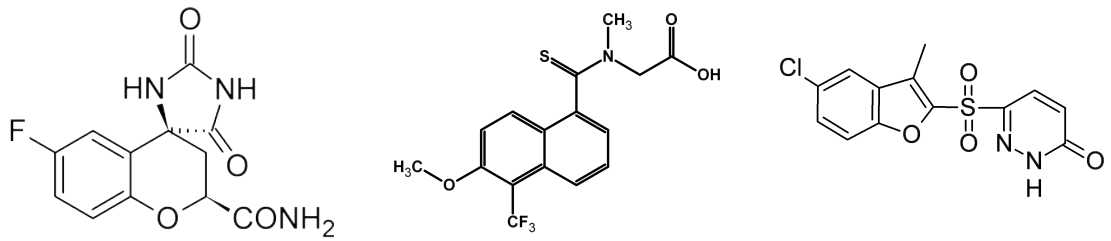

(a) Fidarestat (b) Tolrestat (c) ARI-809

Figure 1.9: Molecular structure of the three ARIs types.

A large number of AKR1B1 inhibitors have been developed in the recent years, but very few of them showed sufficient therapeutic efficacy in clinical trials. However, some inhibitors like tolrestat were commercialized for some time (epalrestat has been approved for pharmaceutical use in Japan, and is the only ARI commercially available to date). Most of the drug candidates failed because of their poor pharmacokinetic properties and/or unacceptable side effects, mainly due to their toxicity and unspecific *in vivo* action (*53*, *54*). Nonetheless, it is still common the use of tolrestat as a classic representative of ARI in the study of AKRB1. A recent study suggests the implication of AKR1B1, through its ability to synthesise $PGF_{2\alpha}$, during adipocyte differentiation (AKR1B1 steadily increases during adipogenesis) and for the regulation of white adipose tissue (WAT) metabolism, suggesting that ARI could have an obesogenic potential (*55*).

At the time of intensive development of ARIs, AKR1B1 was the only AKR1B member known in humans. Therefore, ARI selectivity *in vitro* was determined comparing their inhibitory potency towards AKR1B1 and AKR1A1. However, as we now know, there are other AKR1B enzymes, such AKR1B10 and AKR1B15. With the discovery of AKR1B10, a possibility arises that many ARIs designed to inhibit AKR1B1 could also cross inhibit AKR1B10 (and AKR1B15). It is thought that the inhibition of AKR1B10 is the origin of some the off-target and undesirable side effects of ARIs observed in clinical trials *in vivo* (*6*). Our group has pioneered this approach, performing comparative studies of tolrestat inhibition between AKR1B1 and AKR1B10 (*13*, *44*, *56*).

1.6.2 AKR1B10

This enzyme, initially named aldose reductase-*like* (AR-L) or *human small intestine reductase* (HSI-reductase), was first identified simultaneously by two groups in 1998 (*57*, *58*). Whereas AKR1B1 has a ubiquitous tissue distribution, AKR1B10 is manly expressed in the small intestine, colon, liver, thymus (*57*) and adrenal gland (*58*).

AKR1B1 and AKR1B10 share 71% of sequence identity, and its substrate specificity and sensitivity to inhibitors are similar. However they present some kinetic differences, thus glucose can be reduced by AKR1B1, but not by AKR1B10 (*44*). In addition, AKR1B10 exhibits a higher optimal pH, and k_{cat} values for some substrates between 3- and 6-fold higher (methylglyoxal, 2-,3-, and 4-nitrobenzaldehydes and diacetyl) (*57*). This suggests that cofactor dissociation (therefore the opening and closing of the loop B) is faster than in AKR1B1. The enzyme displayed values of catalytic efficiency 100-fold greater than those of AKR1B1 for all-*trans*-retinaldehyde (*56*) and for some ketones, including pharmaceutical drugs like daunorubicin and dolasetron (*59*). Moreover, it has been observed that AKR1B10 also presents a high catalytic activity for long-chain aliphatic alcohols, specially farnesal and geranylgeranial (*60*). The first three dimensional crystal structure, the ternary complex AKR1B10-NADP-tolrestat, was obtained by our group (PDB: 1ZUA), and published in 2007 (*13*). At present, there are 13 available structures in the protein data bank.

Recently, it has been reported that AKR1B10 may have a no-catalytic function. It seems that it can bind ACCA and block its ubiquitination and further proteasomal degradation. In fact, in breast tumor epithelial cells, the use of siRNA depletes AKR1B10 protein levels, leading to an increase in ACCA degradation. As a consequence, there is 50% reduction in the synthesis of lipids and fatty acids (*30*). In further studies this new function was confirmed in cell lines of colon and lung cancer. Moreover, the decrease of the lipid synthesis due to the treatment with AKR1B10 siRNA leads to apoptosis mediated by caspases and to elevation of the oxidative stress. This elevation also results from an increase of lipid peroxides since AKR1B10 is able to reduce them *in vitro* (*37*) and *in vivo* (*31*). Therefore, AKR1B10 could indirectly promote the synthesis of lipids, stimulating the cell survival and proliferation (*31*) (Fig. 1.10).

AKR1B10 and cancer

Since its early identification, AKR1B10 has been associated with various tumors, mainly human hepatocellular carcinoma (HCC) (*57*). Cao *et al.* (*57*) confirmed that about 54% of HCCs contained high levels of AKR1B10 mRNA, indicating that many HCCs over-express the *AKR1B10* gene. Other authors have corroborated these results (*61*, *62*). The data of a recent study (*63*) suggested the involvement of AKR1B10 up-regulation in the early stages of hepatitis B virus (HBV) related hepatocarcinogenesis. The study showed that HBV infected patients with <15% expression of AKR1B10 have low risk of developing HCC, and its up-regulation is a significant risk factor for HCC development, being a novel predictive marker for this cancer. Moreover, upregulated 1B10

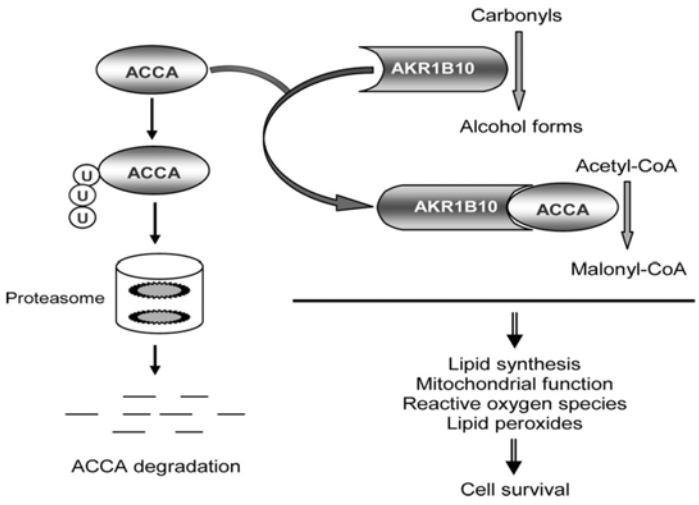

Figure 1.10: Role of AKR1B10 in lipid metabolism and cell survival. ACCA is degraded through the ubiquitination/proteasome pathway. AKR1B10 blocks ubiquitin-dependent degradation of the ACCA and thus regulates lipid synthesis, mitochondrial function, oxidative status and lipid peroxidation; AKR1B10 also reduces carbonyls to less toxic alcohol forms, blocking their cytotoxicity. Through these two independent pathways, AKR1B10 promotes cell survival (*31*).

has been detected in patients with chronic hepatitis C and steatohepatitis (*63*). AKR1B10 was linked with colon, liver, pancreatic cancers, among others (*64–67*). Additionally, AKR1B10 levels were found to be over-expressed in patients with non-small cell lung carcinoma (NSCLC), especially in case of tobacco consumption, even in pre-cancerous states (*68*). Particularly, it has been found elevated in 84% of the NSCLC cases and in the 29% of adenocarcinoma cases. This suggests the participation of AKR1B10 in the carcinogenesis process of NSCLC. It has been proposed that the increase of the retinaldehyde reductase activity by AKR1B10 over expression could be behind, the development of NSCLC by depleting the retinoic acid (RA) levels, a well-known differentiating and antiproliferating agent (*69*) (Fig. 1.11). An alteration of the retinol/retinaldehyde interconversion, by changing the AKR1B10 enzymatic levels, may result in disturbances in gene control and cell proliferation. Thus, the up-regulation of retinaldehyde reductase activity of AKR1B10 found in cancer could be linked to the depletion of RA levels and subsequent loss of cell differentiation and cancer development. In addition, cell dedifferentiation produced by RA depletion could lead to cancer stem cell formation (*70*). As stem cells have a low replication rate, traditional chemotherapeutics will not affect these cells significantly, therefore this tumor will remain in a latent state. This could produce a tumor recurrence because after tumor cells are killed by chemotherapy, cancer stem cells could still regenerate them, and thus the elimination of stem cells is a priority. A possible way is restoring RA signaling by suppressing AKR1B10 activity.

This hypothesis has been reinforced by the appearance of new data. It has been observed that the expression of AKR1B10 is induced by tobacco smoke toxic compounds, such as benzo[a]pyrenes,

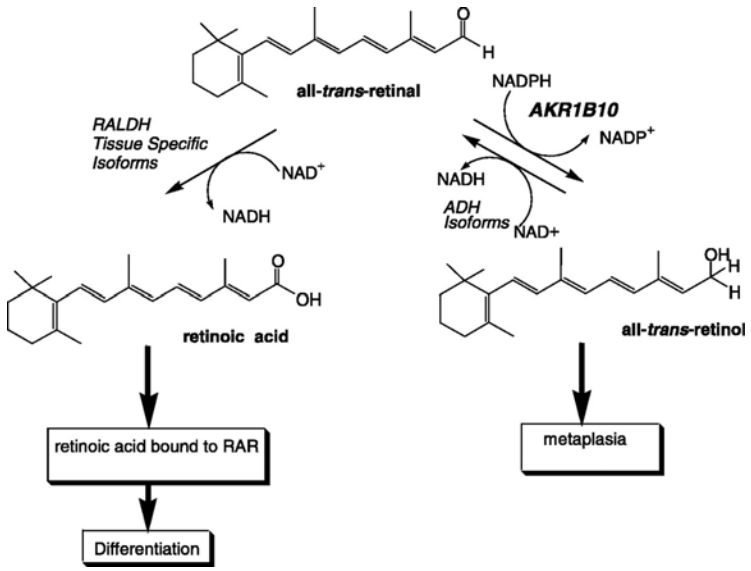

Figure 1.11: Potencial role of AKR1B10 in the cellular signaling of retinoic acid and its relation with cancer. An overexpression of AKR1B10 would decrease the amount of retinoic acid that could be formed, promoting metaplasia. RALDH: retinaldehyde deshidrogenase. Reproduced from (*71*).

that act through antioxidant response elements, like Nrf2, and response elements to dioxins localized in the *AKR1B10* promoter (*72*). An independent study found that the *AKR1B10* promoter has different response elements, putatively oncogenic related to tumor suppression, including binding sites for c-Ets-1, C/EBP, AP-1 and p53 (in contrast with AKR1B1, no ORE has been found) (*73*).

The previous work is in accordance with another study, in which AKR1B10 expression was knocked down through siRNA, producing a decrease in cell growth rate and a suppression of DNA synthesis in colorectal cancer cells (HCT8), and supporting a critical role of the enzyme in cancer (*74*). Additionally, it has been observed that AKR1B10 catalyzes the reduction of compounds present in the tobacco smoke, such as acrolein, cronotonaldehyde (*74*), NNK (*59*), PAHs (*75*), thus protecting cells from oxidative stress. Moreover, the higher catalytic efficiency of AKR1B10 *in vitro* for all-*trans*-retinaldehyde reduction compared to PAH *trans*-dihydrodiol metabolism suggests that AKR1B10 may play a greater role in lung carcinogenesis through dysregulation of RA homeostasis than through oxidation of PAH *trans*-dihydrodiol (*75*). Another role of AKR1B10 could be the detoxification of products derived from ROS action. It is well known that the high metabolic rate in tumor cells produces large amounts of ROS that could not be detoxified by normal methods, such as glutathione. Accumulation of ROS and their products covalently modify cellular structures of cells, such as DNA, proteins and lipids, that could lead to cell death. Overexpression of AKR1B10 could help detoxifying these derivatives, helping cells to survive (Figure 1.12).

AKRs can metabolize xenobiotic compounds as *phase I-drug metabolizing enzymes*. Substrate specificity differs between each member of the superfamily, thus a great amount of environmental

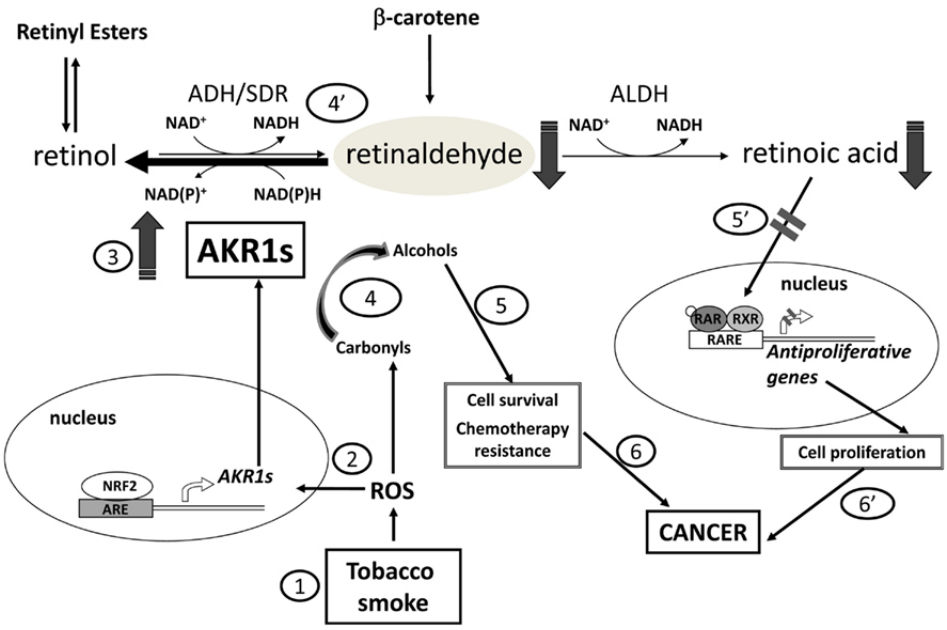

Figure 1.12: Relationship of AKR1 enzymes with carcinogenesis at different levels. Reactive oxygen species (ROS), generated by tobacco smoke, trigger the expression of some AKR1 enzymes (steps 1, 2, 3). Subsequently, activity of AKR1 enzymes with retinaldehyde provokes retinoic acid (RA) deprivation blocking its differentiating effect (steps 4' and 5'), and favoring cell proliferation. Besides, AKR1 enzymes participate in the detoxification of lipid peroxidation aldehydes and can also metabolize various antitumoral agents bearing a carbonyl group (step 4). Through these activities, the enzymes promote cell survival and chemotherapeutic drug resistance (step 5). Overall, induction of AKR1 enzymes fosters tumorigenesis (steps 6 and 6'). Reproduced from (*76*).

pollutants, drugs, carcinogens and other molecules can be bioactivated or detoxified by the AKR superfamily (*9*, *54*, *77*). AKR1B10 has been related with chemoresistance against daunorrubicin, doxorubicin and their derivatives, and it is known to be overexpressed in cell lines with resistance to some chemoterapheutic agents such trichostatin, cyclophosphamide and methrotrexate (all of them without carbonyl groups) (*78–80*), and mitomycine and doxorubicin (with a carbonyl group) (*81*). For example, the product of the reduction of doxorubicin, doxorubicinol, is a million fold less toxic than its precursor but it is more cardiotoxic. Thus, the overexpression of AKR1B10 in some tissues could lead to tumor resistance and adverse effects, while AKR1B10 non-overexpressing tissues will suffer the toxic effects of chemotherapy (*82*, *83*). Combined therapy using AKR1B10 inhibitors along with anticancer agents could be a new therapeutic option.

As mentioned above, AKR1B10 participates in regulating cellular fatty acid synthesis, lipid and isoprenoid metabolism. All these metabolic processes contribute to carcinogenesis as they are involved in protein prenylation, cell proliferation and apoptosis. Farnesol, the reduced product of AKR1B10 from farnesal, is phosphorylated into farnesyl pyrophosphate, which is the intermediate of cholesterol synthesis involved in protein prenylation. Some proteins, like G proteins, have to

be prenylated in order to perform their function. Higher prenylation levels could lead to higher activity of these proteins, which most of them are involved in cell proliferation. On the other hand, we already mentioned that AKR1B10 was found to be involved in acetyl-CoA metabolism, interacting with ACCA and protecting it from degradation. This could enhance lipid synthesis and promote cell survival (Fig. 1.13) (*31*, *66*).

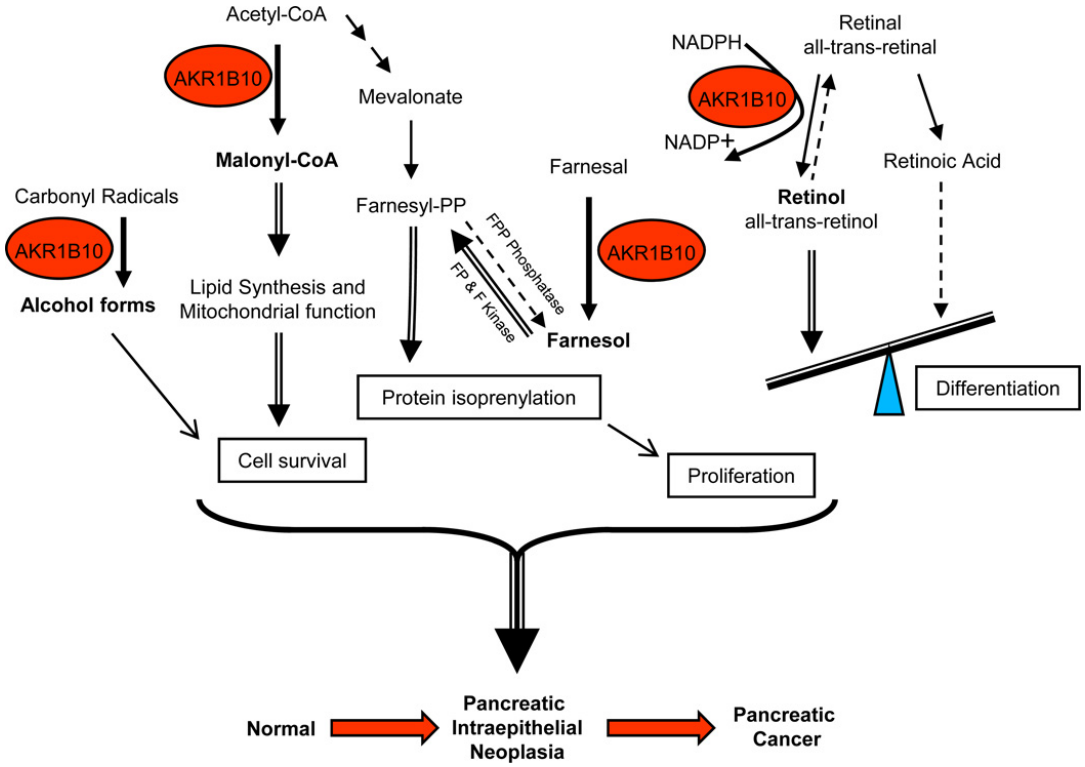

Figure 1.13: The proposed interactive role of AKR1B10 in carbonyl, farnesyl and lipid metabolism as in maintaining the homeostasis of retinol to retinaldehyde that is involved in cellular apoptosis, protein prenylation, cell proliferation and differentiation and cell survival. The overexpression of AKR1B10 could imbalance many metabolic pathways and lead to neoplasia. Reproduced from (*66*).

AKR1B10 inhibitors

The important functions described for AKR1B10 and its similar structure with AKR1B1 have made necessary to perform a comparative study of the ARI effects. As mentioned in the section "AKR1B1 inhibitors" it is possible that some of the ARIs off-target and undesired actions, in the diabetes treatment, would be due to its lack of selectivity and its cross interaction/inhibition with AKR1B10 (and maybe with AKR1B15). A large amount of studies have been published recently regarding this aspect (*52*, *54*, *60*, *84–94*). Interesting results are the identification of selective steroid-type inhibitors for AKR1B10 (*60*), and the identification of the most potent inhibitor so far for AKR1B10, bisdesmethoxycurcumin, 85-fold more specific for AKR1B10 than for AKR1B1

(*86*). Other representative potent inhibitors are a caffeic acid phenethyl ester (CAPE) derivative (IC_{50} = 80 nM), present in the honeybee propolis products, and the novel designed CAPE-based inhibitors, the best one with an IC_{50} value of 2.6 nM (*93*). Moreover, compounds derivated from chromene-3-carboxamide have a high inhibitory potency for AKR1B10 (IC_{50} = 40 nM), but with a low selectivity (AKR1B1 is also strongly inhibited) (*84*), and natural substance derivatives, such as butein isolated from the total extract of the tree bark of *Rhus verniciflua*, showed an IC_{50} value of 1.5 μM (*95*). Inhibitor screening using *in silico* techniques and computer-aided ligand docking, identified the ligand 9-methyl-2,3,7-trihydroxy-6-fluorone, that showed an IC_{50} value of 0.4 μM with a 4-fold selectivity towards AKR1B10 relative to AKR1B1 (*96*). Non-steroidal antiinflammatory drugs such N-phenylanthranilic acids, diclofenac and glycyrrhetic acid inhibit AKR1B10 in a competitive mode, with high selectivity towards AKR1B10 as compared to AKR1B1 (*85*). However, it has to be mentioned that some of the inhibitors mentioned before, although being selective towards AKR1B10 as compared to AKR1B1, they are not too selective regarding the AKR1C enzymes (*6*, *97*). Finally, some of these publications report the inhibition of AKR1B10 with ARIs designed for AKR1B1. In general, ARIs have lower inhibitory potency with AKR1B10, although its selectivity is rather diverse (*60*, *84*, *85*, *98*).

1.6.3 AKR1B15

Recently, a novel gene was identified in the human AKR1B genetic cluster, along with *AKR1B1* and *AKR1B10* in chromosome 7. This third cluster gene, *AKR1B15*, has been predicted in the last decade as a result of high-throughput sequencing and annotation projects. Weber *et al.* (*12*) predicted by *in silico* and then confirmed by PCR that the *AKR1B15* gene undergoes alternative splicing, giving rise to two protein isoforms *in vivo*, designated as AKR1B15.1 and AKR1B15.2. The former, AKR1B15.1 (henceforth referred as AKR1B15 for brevity), is a 316 amino acid enzyme that displays 92% and 67% sequence identity with AKR1B10 and AKR1B1, respectively. In the other hand, AKR1B15.2 is a 344 amino-acid protein that has a longer N-terminus. This isoform does not exhibit enzymatic activity or nucleotide binding. Its high homology with AKR1B10 suggests that AKR1B15 is a result of a recent duplication event (*11*, *12*). AKR1B15 has been demonstrated to be a functional gene with low expression restricted to adipose tissue, skeletal muscle, thymus, thyroid gland, and reproductive tissues (ovary, placenta, prostate, and testis). Interestingly, it has been localised in the mitochondrial fraction, however AKR1B15.2 isoform has a cytosolic localization. This is surprising feature, since most of the other human AKRs are cytosolic enzymes. Similarly to *AKR1B10*, the *AKR1B15* gene was found to be up-regulated in the airway epithelium by smoking (*99*) and by exposure to sulforaphane, a known activator of the antioxidant response (*100*). Interest in the *AKR1B15* gene has risen lately because some allelic variants have been linked to a mitochondrial oxidative phosphorylation disease (*101*), somatic missense mutations in serous ovarian carcinoma (*102*), upregulated in a result of *T. cruzi* infection, the etiological agent of Chagas disease, in the absence of thromboxane signaling (*103*) and increased

longevity (*104*) .

1.6.4 AKR1B enzymes from other species

Some murine AKR1B enzymes had been studied in the search of enzyme homologous to the human AKR1B members. Thus, in mouse, besides AKR1B3 (aldose reductase, active with glucose) (*105*), mouse vas deferens protein (MVDP or AKR1B7 (*106*)) and the fibroblast-growth factor 1-regulated protein (FR-1 or AKR1B8 (*107*)) had been characterized. AKR1B8 shows the highest sequence identity to AKR1B10 (82%), is mainly expressed in the colon and small bowel with a low level in the stomach, liver, and brain, similar to the human AKR1B10 expression. AKR1B8 also displayed a similar enzymatic activity and kinetics to AKR1B10, but with low catalytic efficiency towards all-*trans*-retinaldehyde (*108*), a higher K_m value for D,L-glyceraldehyde and a null activity with glucose (*109*). Importantly, similar to human AKR1B10, mouse AKR1B8 associates with murine ACCA and mediates fatty acid synthesis in colon cancer cells. Taken together, the data suggest that murine AKR1B8 could be the true ortholog of human AKR1B10, but this is still controversial. AKR1B7 has a low enzymatic activity and a limited tissue distribution, mainly localised in the adrenal gland, the only tissue where it is abundant (*18*), while other organs, including kidney, show poor expression of this enzyme. AKR1B7 is selectively expressed in renin-producing cells, but AKR1B7 appears not to be important for the regulation of renin secretion *in vivo* both at organ and cellular levels (*110*), and seems to be regulated by cAMP within the renin cells (*111*). Although AKR1B1 is the most structurally related human AKR to AKR1B7, AKR1B7 is unable to catalyze the conversion of glucose to sorbitol (*18*). Another study suggests a possible role of AKR1B7 in the detoxification of acrolein in the sperm surface (*112*).

According to *in silico* studies, a new murine *Akr1b* gene, *2310005E10Rik*, hereafter referred as *Akr1b16*, has been found. It has an open reading frame sharing 82-84% amino acid identity with AKR1B10, and it has been suggested to be its mouse ortholog (*11*). The tandem arrangement of the murine gens suggests that these genes arose from an ancestral genetic duplication event.

There are also four different AKR1B members in rat, identified through proteomic studies (*113*). AKR1B4, active with glucose (*114*), is the orthologous protein of AKR1B1. On other hand, AKR1B13 and AKR1B14 are orthologs to the mouse enzymes AKR1B8 and AKR1B7, respectively, with almost identical catalytic properties (*115*). The last AKR1B member is AKR1B17, which shows more than 88% overall amino acid sequence identity with AKR1B13, 1B14 and 1B16. It presents the peculiarity that is activated by hydrophobic carboxylic acids (*116*).

There are other AKR1B proteins of interest. In the CHO hamster cell line, the CHO reductase (AKR1B9) has been characterized, with kinetic characteristics similar to AKR1B10, but with the distinct feature that can use ketones as substrates (*117*); chicken AKR1B12 is an enzyme with a unique capacity for oxidation ethanol and to reduce retinoids, discovered and characterized by our group (*118*).

The lack of uniformity in the AKR forms present in the different species, despite their se-

quence similarity, imposes a limitation on the use of the knockout technology for the study of the physiological function of the AKRs. Even in cases where the orthologous protein has been clearly established and described (e.g. mouse aldose reductase AKR1B3), the presence of different family members may partially compensate the loss of function and that could limit the ability to fully understand the corresponding function in humans. This issue explains why, only four knockout models had been described so far for AKRs, and only one for the AKR1B subfamily (*119*). The study of the three-dimensional structure of this protein group has been focused mostly as a model to examine how subtle changes in the amino acid sequence could have effects on the catalysis and the binding of ARIs (*120*).

1.7 Retinoids

The term "retinoid" is used to refer to a wide range of compounds derived from vitamin A (retinol), were they natural or synthetic, with or without biological activity. However, the vitamin A designation refers only to the compounds that have the biological activity of retinol. Thus, vitamin A participate in many essential biological processes such as development of fetal and adult tissues, cell proliferation and differentiation or the visual cycle (acting as a chromophore).

1.7.1 Chemical structure of retinoids

All-*trans*-retinol, a primary alcohol of *Mr* 286, is the compound from which other retinoids originate. Their basic structure is divided into three domains: an end with a cyclohexene ring or β-ionone, an aliphatic chain with four conjugated double bonds, and a polar group which may show different oxidation states: alcohol, aldehyde or acid (resulting in retinol, retinaldehyde or RA, respectively, Fig. 1.14). The different configuration of the double bonds of the aliphatic chain leads to the formation of isomers, being the all-*trans*, 9-*cis*, 11-*cis* and 13-*cis*-retinoids the most frequent (*121*). Retinoids are hydrophobic and unstable compounds, that are easily oxidised in the presence of oxygen, and are degraded by light, which yields to isomerization of double bonds. For this reason they have to be manipulated under inert atmosphere and red or dim light.

Tween-80 (polyethylene glycol sorbitan monooleate) is a non-ionic, non-denaturalizing detergent. It has been used during much time in preparing retinoid solutions, with the aim to facilitate their solubilisation and increase their stability. This detergent has been widely employed in the enzymatic activity assay with retinoids. However, it has been demonstrated that the presence of this compound has a strong influence on the kinetic constants of ADH with retinoids. Tween-80 produces an inhibitory effect, displaying a competitive pattern (*122*).

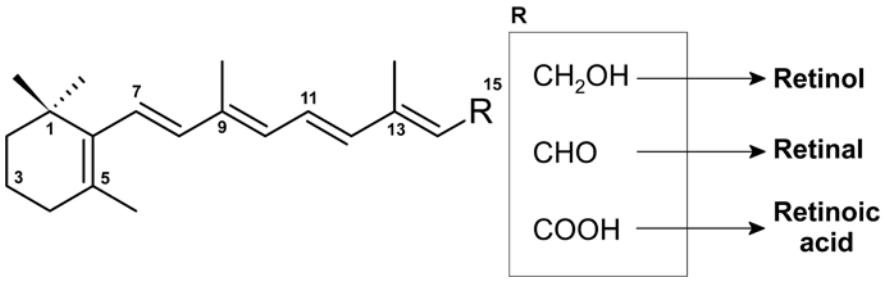

Figure 1.14: Chemical structure of retinoids, showing the carbon numbering, and the nature of its polar group (R), that leads to different retinoids.

1.7.2 Vitamin A absorption, transport and metabolism

Vitamin A needs to the incorporated through the diet, either as retinyl esters or retinol from animal sources, or as provitamin A carotenoids from fruits and vegetables, mainly as β-carotene. Retinol is taken up directly by mucosa endothelial cells. However, retinyl esters are unable to enter the intestinal mucosa and have to be hydrolysed by a luminal retinyl ester hydrolase to yield free retinol. Retinyl esters can be also hydrolysed in the intestinal lumen by non specific pancreatic enzymes. Regarding β-carotene, it can be directly absorbed by passive diffusion or through facilitated transport into the cells. In the enterocyte, β-carotene can be cleaved into two molecules of all-*trans*-retinaldehyde by the enzyme β-carotene-15,15'-monooxygenase 1 (BCO1) (Fig. 1.16). In addition, intact β-carotene can accumulate in blood and tissues. Inside the enterocyte, all-*trans*-retinaldehyde is then reduced by one or more retinaldehyde reductases to retinol, which can bind to cellular retinol-binding protein type-2 (CRBP2) (Fig. 1.15). Then it undergoes sterification with long-chain fatty acids through the action of lecithin:retinol acyltransferase (LRAT). CRBP2 plays a primary role in the regulation of retinol absorption in the enterocytes and its intracellular metabolism, preventing its free access to cytosol oxidoreductases (*123*). Retinyl esters are then incorporated into chylomicrons and transported to the liver parenchymal cells where are captured by specific receptors and transferred to stellate cells for storage, which constitutes 50-80% of the body retinol in the form of retinyl esters.

When required in the peripheral tissues, retinyl esters are hydrolyzed to retinol by retinyl ester hydrolase (REH). Retinol associates with the retinol binding protein (RBP) in hepatocytes and then it is secreted from the liver into the lymphatic system for uptake into general circulation and to be transported in the blood. Previous to its secretion, the retinol-RBP complex is in turn complexed with the thyroxine-binding protein transthyretin (TTR) to reduce its glomerular filtration (Fig. 1.15). The retinol bound to RBP enters the cell through a multidomain membrane protein, the cell-surface receptor *stimulated by retinoic acid 6* (STRA6), which mediates the cellular vitamin A uptake and facilitates its transport across cell membrane. There is no high resolution structure for STRA6, but simulations predict that it contains nine transmembrane segments, with a short N-terminal tail that faces the extracellular space and a long C-termirnal tail in the cytosol.

STRA6 is a cellular receptor for RBP, and their interaction is highly specific (*124–126*). STRA6 mechanism for retinol uptake is different from all other cellulars uptake mechanisms. It is not a primary active transport, since STRA6 has no ATP binding domain. A remaining possibility is a channel/facilitated transport, which depends on the electrochemical gradient of free ligand. However, the substrate for STRA6 is not free but bound to RBP. LRAT stimulates STRA6 activity, and CRBP1, but no CRBP2, is loaded with retinol by STRA6, and it affects its function. There are numerous hypotheses on the mechanism of STRA6-mediated cellular vitamin A uptake from RBP (*125*, *127*, *128*). Almost all the retinol that enters the cells is recycled to the plasma (over 90%), thus, only a small fraction is sterified for its storage, or it is activated to RA, or catabolised to inactive compounds (Fig. 1.16) (*76*, *121*, *129–132*)).

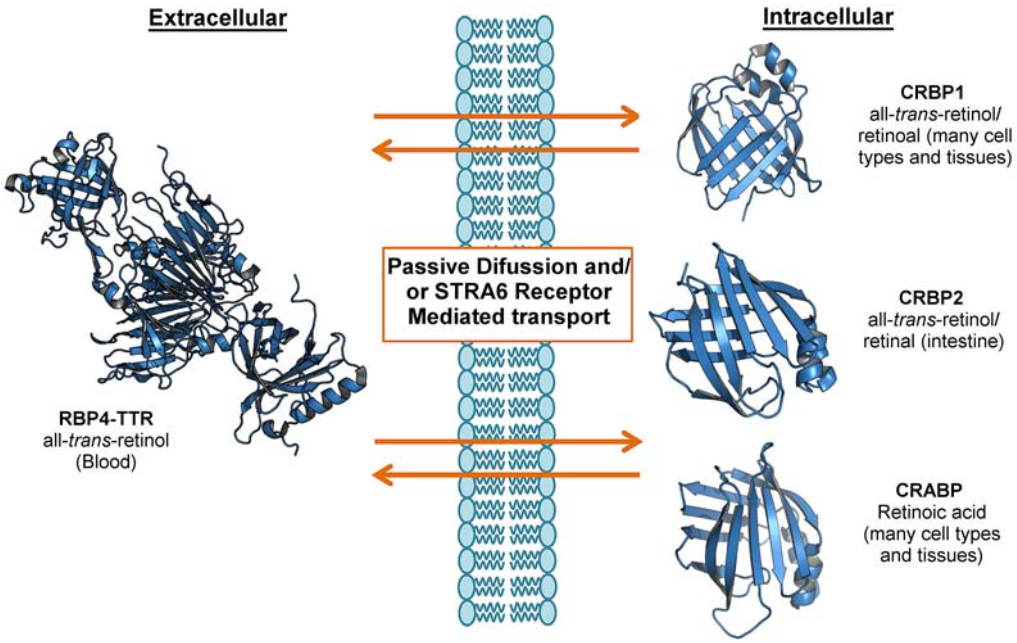

Figure 1.15: Structures and functions of different mammalian extra and intracellular retinol-binding proteins. RBP4, also known as RBP, binds all-*trans*-retinol, and is the major binding protein in the circulation. RBP-4 is found complexed with transthyretin (TTR) to reduce its glomerular filtration (RBP4-TTR). The STRA6 receptor mediates the uptake of retinol and its transport through the membrane. CRBP1 and 2 are major cellular retinol binding proteins, and bind all-*trans*-retinol and all-*trans*-retinaldehyde in cells. Synthesized retinoic acid binds to cellular retinoic acid binding protein (CRABP) and is transported to the cell nucleus. Modified from (*124*), protein structures were obtained from the Protein Data Bank.

1.7.3 Biosynthesis of all-*trans*-retinoic acid from retinol

Retinoids are transported and stored mainly in the form of retinol and retinyl esters, respectively. However, RA represents the actual form of the vitamin A with the most potent biological activity.

Retinoic acid biosynthesis

RA is formed from retinol, and its biosynthesis requires of two oxidative steps: the first is the reversible oxidation of retinol to retinaldehyde, and it is generally considered to be rate-limiting (*133*, *134*). The second step is the oxidation of retinaldehyde to RA. Both steps are regulated, but it is the reversible oxidation of retinol to retinaldehyde that exhibits more control by a wide variety of enzymes, including members of the three oxidoreductases superfamilies: the microsomal SDRs, the cytosolic ADHs from MDRs and the AKRs (Fig. 1.16). The direction of the oxidoreducion reaction is determined by the availability of substrates and cofactors (*131*). AKRs are NADPH-dependent enzymes, and work in the reductive direction, whereas ADH, NAD^+-dependent enzymes, mostly work in the oxidative direction. The SDR family has examples of both specificities, allowing them to work in either direction of the pathway. The irreversible oxidation of retinaldehyde to RA involves the action of aldehyde dehydrogenases (ALDHs or RALDHs) and the cytochrome P450 (Fig. 1.16).

Our group has compared the catalytic constants with retinoids of members of the three enzyme superfamilies, determined with the same methodology (solubilitzation of retinoids with BSA and detection with HPLC) for the first time (*56*). Moreover, the specific role of AKRs has been recently reviewed by our group (*76*), comparing the different methodologies for the determination of the kinetic constants for retinoids. Briefly, the K_m value of the majority of AKR is around 1 μM, comparable to that of the members of other superfamilies, pointing that the three enzyme superfamilies are able to participate in the interconversion of retinol/retinaldehyde under physiological conditions. It is likely that these enzymes use only free retinods instead of retinoid bound to CRBP, which would have a function in retinoid storage. Considering that retinaldehyde is the immediate precursor for RA, the active hormone, and that high levels of retinaldehyde and RA can be toxic for the cell, it is not surprising that the levels of retinaldehyde are tightly controlled by a large number of enzymes that catalyze its oxidation and reduction (*56*, *131*, *135*).

Alcohol dehydrogenases

ADH1, ADH2 and ADH4 oxidise different retinoid isomers *in vitro* in the presence of NAD^+. The most active ADH with retinoids is ADH4. The spatiotemporal expression pattern of ADH1 and ADH4, and their co-localization with the onset of RA signaling in the embrionary development of mouse, suggest an active role of these enzymes in the synthesis of RA (*136*, *137*). This co-localization is also found in adult mouse tissues and in several epithelial cell populations that may require RA for differentiation, including epidermis, stomach and esophageal mucosa, adrenal cortex (*137*) and male reproductive tract (*138*). In the other hand, genetic studies with *knock-out* mice had demonstrated the participation *in vivo* of ADH1, ADH3 and ADH4 in the RA synthesis pathway (*139–141*). These works seem to demonstrate that the role of ADH1 in retinoid metabolism, specially in liver, is to provide protection against vitamin A toxicity, while ADH4 has a role in RA signaling in target tissues. Thus, in addition to the co-localization of ADH4 and the

RA synthesis mentioned above, it as been observed a decrease in the fetal survival rate in *knock-out* mice, when subjected to vitamin A deficiency during pregnancy (*142*, *143*), compared to wild-type mice.

The ADH3 form, also named glutathione-dependent formaldehyde dehydrogenase, has been also related with retinol metabolism because *knock-out* mice have a lower body weight, but it is recovered when they are supplemented with vitamin A in the diet (*140*). It has been demonstrated that the *in vitro* enzymatic activity of ADH3 is 1400-fold lower than that of ADH1 and 4000 times lower than that displayed by ADH4 with all-*trans*-retinol. However, the ubiquitous expression of ADH3 in tissues, in contrast to other ADH, could confer a special role to this enzyme in the metabolism of retinoids (*140*).

Regarding ADH2, although it is active with retinol, only represents 2% of the retinol dehydrogenase activity of the liver. Furthermore, it exhibits important kinetic differences with other species, and probably does no have an evolutionarily conserved function as a retinol dehydrogenase (*144*, *145*).

Short-chain dehydrogenases/reductases

The retinol dehydrogenases/reductases of the SDR superfamily are microsomal enzymes that are able to oxidise retinol (NAD^+-dependent forms) and reduce retinaldehyde ($NADP^+$-dependent forms). Among the first group, some human retinol dehydrogenases have been described: RoDH4 (SDR9C8) (in parenthesis the new nomenclature, gene based, is provided (*146*)), RoDH-like 3α-HSD (SDR9C4), RDH5 (SDR9C5) and RDH10 (SDR16C4), all of them with extra-ocular expression. Among the NADP(H)-dependent forms, some proteins have been described with expression restricted to the eye (prRDH (SDR28C2)), while other are expressed in multiple tissues: RDH11 (SDR71C), retSDR1 (SDR16C1) in eye and liver, and RDH12 (SDR7C2), which is the most efficient retinaldehyde reductase among the SDR and AKR enzymes. SDRs have K_m values for retinoids similar to the physiological concentrations of these compounds. However, there are some doubts about their function *in vivo* because the retinol dehydrogenases display also activity with steroids, rising the question whether they can contribute to both retinoid and steroid metabolism, and whether their contribution can be dependent on their cell-specific context (*131*). The role of these proteins in mammalian all-*trans*-RA biosynthesis and homeostasis remains to be fully investigated, but some works with cell lines point to a possible important role for some of these enzymes [11cRDH (SDR9C5), RDH12 (SDR7C2), RDHE2 (SDR16C6), and especially for RDH10 (SDR16C4)] in the RA metabolism (*134*, *147*–*150*). Mouse RDH10 (SDR16C10) is essential for RA biosynthesis in the embryonic development (*131*, *151*) and the inactivation of its gene results in embryonic lethality or severe malformations due to insufficient production of RA (*131*, *151*, *152*). RDH10 is highly conserved (99-100% amino acid sequence identity) between mouse, bovine and human, and studies in frog suggest that its ortholog is also essential for embryonic development (*150*). *In vitro* studies determined that human RDH10 recognises all-*trans*, 11-*cis* and

9-*cis*-retinol isomers as substrates and strongly prefers NAD^+ as a cofactor (*134*). These data points out that RDH10 is the major retinol dehydrogenase responsible for RA biosynthesis during embryonic development (*131*, *151*, *153*).

Aldo-keto reductases

The retinoid oxidoreductase activity was traditionally assigned to members of the MDR and SDR superfamilies. However, our group proved that members of the AKR superfamily were also active with retinoids. This activity was found for the first time in a new AKR, chicken AKR1B12, that was active towards different retinaldehyde and retinol isomers (*118*), and later in the human AKR1B1 and AKR1B10 (*13*, *44*, *56*). Regarding the AKR1C superfamily, some groups described the retinaldehyde reductase activity with the bovine enzyme prostaglandin F synthase (AKR1C7) (*154*) and rat AKR1C15 (*155*). The initial work by our group with members of the AKR1B subfamily in the metabolism and modulation of the RA pathway led us to further investigate the role of other human AKR enzymes. Thus, we characterized the kinetics of AKR1Cs (AKR1C1, 1C3 and 1C4) active with retinol and retinaldehyde and their possible contribution in this pathway (*156*). The studies showed low K_m values with both all-*trans*- and 9-*cis*-retinaldehyde, in the same range as those of AKR1Bs, SDRs and ADHs. The catalytic efficiency values were in general low, similar to those of aldose reductase (AKR1B1), with the exception of AKR1C3 with the 9-*cis* isomer of retinaldehyde, with a comparable efficiency to some SDR enzymes (*156*).

All the AKRs that display activity with retinoids have a clear preference for reduction, as it has been observed with other AKR substrates (*6*). The high efficiency of AKR1B10 to reduce retinaldehyde has been proposed as a possible mechanism involved in the development of non-small cell lung cancer (NSCLC), where AKR1B10 is found overexpressed (Figure 1.11) (*71*, *75*), and also as a protein that could act at pre-receptor level, regulating the amount of RA available for RAR and RXR receptors (Table 1.3, Figs. 1.11 and 1.16 (*8*, *13*, *69*)).

Oxidation of retinaldehyde

The irreversible NAD^+-dependent oxidation of all-*trans*-retinaldehyde to RA may occur through the action of members of two different enzymatic families: the family of the ALDHs or RALDHs and the family of the cytochrome P-450. There are different ALDHs with retinaldehyde dehydrogenase activity, but ALDH1A2 is the enzyme that displays the greatest catalytic efficiency (*157*). Cytochrome P-450A1 is the enzyme that showed the greatest *in vitro* activity in this family, but it displayed a K_m values of 12 mM with retinaldehyde, suggesting that it has a low physiological significance.

1.7.4 Retinoic acid

Once RA is formed within the cell, it is mainly bound to the cellular retinoic acid binding proteins (CRABP) and transported to the nucleus (Fig. 1.16). RA regulates gene expression mainly through

the activation of two nuclear receptor subfamilies, RARs and RXRs, both with their respective subtypes α, β and γ. Both subfamilies belong to the receptor family of the steroidal and thyroid hormones, and of the vitamin D. RARs are activated by all-*trans*- and 9-*cis*-RA, and RXRs are activated by the 9-*cis* isomer exclusively. Once the receptor has bound RA, it forms a dimer and it becomes active. Whereas RAR only can form homodimers or heterodimers with another RA receptor (RAR-RAR or RAR-RXR), RXR are able to dimerise with a variety of nuclear receptors: thyroid hormone receptors (RXR-TR), vitamin D receptors (RXR-DR) and orphan receptors. When the receptor has heterodimerized it bounds to retinoic acid response elements (RAREs or RXREs) located in the promoters of a variety of genes in the DNA. Ligand binding induces a conformational change in the RAR/RXR heterodimers which promotes gene transcription. The RA responsive genes are numerous (reported more than 500) and includes the *RAR*β gene itself. In this way, the binding of RARs or RXRs to a given RARE element as homo or heterodimers, and their complex interaction, can lead to significant differences in the expression of their target genes in various tissues (*158–160*).

A proof of the complexity and diversity of genes under the control of RA is that RA activates peroxisome proliferator-activated receptorsβ/δ (PPARβ/δ), leading to enhanced mitosis and cell proliferation in keratinocytes (*161*). Thus, RA could inhibit cell growth, as in cancer cells, by binding to RAR, and stimulate, in keratinocytes, cell proliferation with antiapoptotic actions binding through PPARβ/δ (*162*). Moreover, Tan *et al.* (*163*) found that a fatty acid binding protein (FABP5) was responsible to transport RA to the nucleus and bind PPARβ/δ. Thus, a mechanism was proposed, where RA is transported from the cytosol to the nucleus by two different mechanisms. The activation of RAR occurs when RA is delivered to RAR by cytosolic CRABP and the activation of PPARβ/δ occurs when RA is delivered to PPARβ/δ by FABP5. Therefore, the ratio between the two binding proteins determine which nuclear receptor would be activated. Cells with a high FABP5/CRABP ratio, such as keratinocytes, PPARβ/δ would be active and may lead to cell proliferation, whereas cells with high CRABP/FABP5 ratio RAR would become active and lead to growth inhibition (*162*, *164*, *165*).

The first step of the metabolic route of RA biosynthesis, the reversible oxidation of retinaldehyde to retinol, stands for the limiting step of the proces rate. Traditionally, the depicted enzymes able to perform this reaction belong to the ADH and the SDR families. The discovery by our group (*118*), that members of the AKR superfamily could act also in this metabolic step, has just reinforced the thought that this is a vital process for the cell and that it is strictly regulated (*135*). The balance between synthesis and catabolism allows a precise control of the RA levels in cells and tissues. The catabolism and inactivation of RA to more oxidised compounds like 4-hydroxy-RA or the 4-oxo-RA is performed mainly by enzymes of the CYP26 family, and it is initiated by the hydroxylation at position C4 or C18 of the β-ionone ring of RA (Fig. 1.16) (*76*, *160*, *166*).

The following chapters of this Thesis dissertation have been written as independent sections, each one with its own introduction and discussion, since they are intended to be the basis for further independent publications.

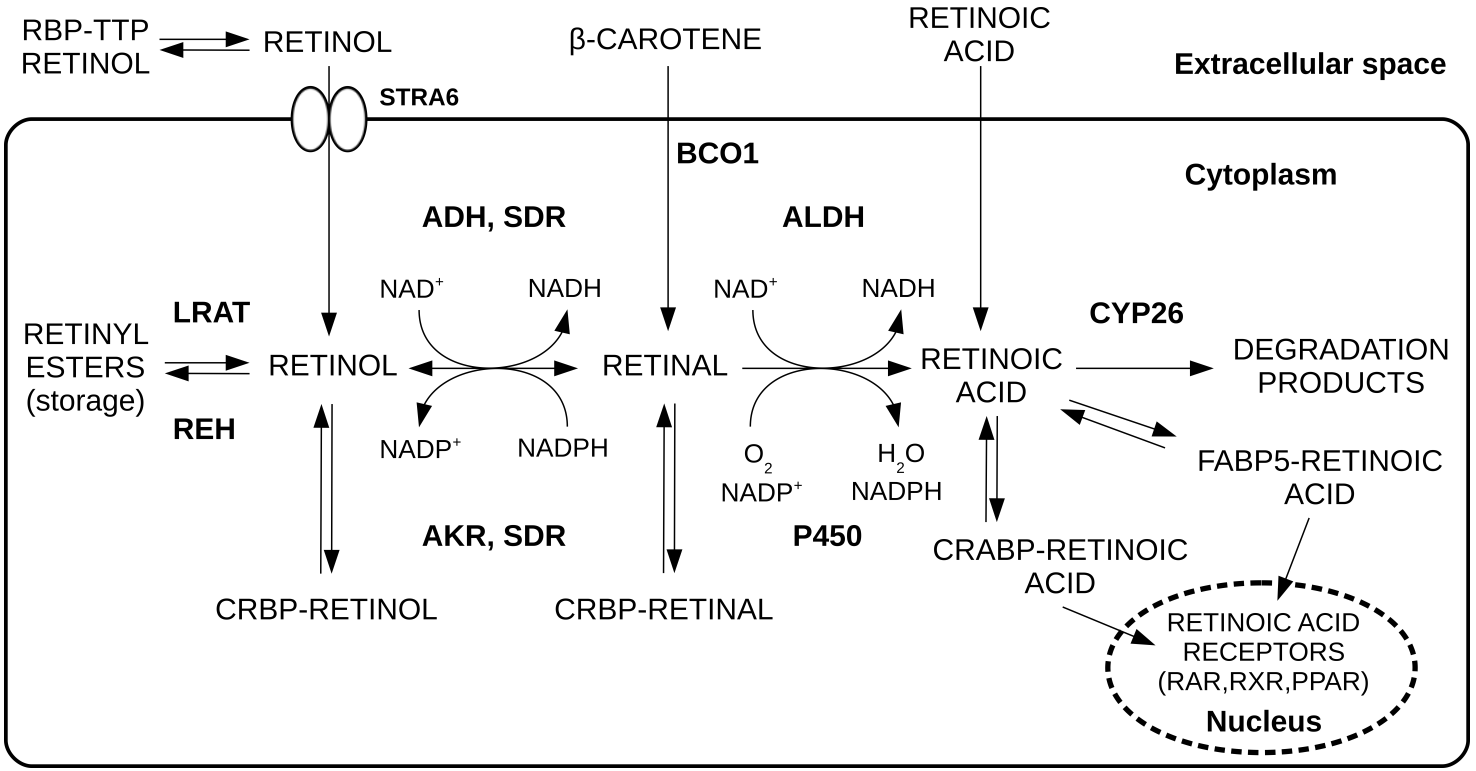

Figure 1.16: Proposed mechanism for retinoic acid synthesis and retinoid storage. Cellular uptake of retinol, carried by retinol-binding protein (RBP) complexed with thyroxine-binding protein transthyretin (TTR), of β-carotene and retinoic acid is indicated. In the target tissues, STRA6, a cell-surface receptor for RBP, facilitates retinol entry. Inside the cell, retinol or retinaldehyde may bind cellular retinol-binding protein (CRBP) and be sterified by LRAT for storage. Retinoic acid may bind cellular retinoic acid-binding protein (CRABP) or fatty acid binding protein (FABP5) in keratinocytes. The reversible interconversion of retinol and retinaldehyde, is catalyzed by members of the ADH, SDR and AKR enzyme families. The cofactor preferences of the enzymes involved are indicated. The second and irreversible step of the pathway, the oxidation of retinaldehyde to retinoic acid, is catalyzed by aldehyde dehydrogenases (ALDH) and cytochrome P450. Modified from (*167*).

Objectives

1. Functional and structural studies on AKR1B15.

In humans, at least 15 AKR members have been identified so far. The most recently described member is the aldo-keto reductase 1B15 (AKR1B15) enzyme which shares 92% amino acid sequence identity with AKR1B10. While AKR1B10 is a well characterized enzyme with high retinaldehyde reductase activity, involved in the development of several cancer types, the enzymatic activity and physiological role of AKR1B15 are still poorly known. The first objective of this thesis has been the purification of AKR1B15 and characterization of its substrate specificity, kinetics, inhibitor selectivity and structural features compared to the highly similar AKR1B10.

Partial objectives:

1. To perform the heterologous expression and purification of AKR1B15.
2. To determine of the kinetics constants of AKR1B15 for typical AKR substrates such as aldehydes and ketones.
3. To carry out the kinetic analysis of the retinaldehyde reductase activity of AKR1B15.
4. To perform the analysis of the inhibition of AKR1B15 with ARIs.
5. To compare the substrate-binding site of AKR1B15 with that of AKR1B10 and determine distinct features that could be related witht its activity and inhibition kinetics.
6. To improve the HPLC methodology to determine the levels of different retinoids in cells.
7. To determine the effect of the expression of AKR1B10 and AKR1B15 on the levels of retinoic acid in living cells.

2. AKR1B10 mutants.

AKR1B10 and AKR1B15 are clearly enzymes with different kinetic features and distinguishable structural properties. The aim of this study is to identify the amino acid residues that may explain the distinct properties, supported by site-directed mutagenesis studies.

Partial objectives:

1. To identify the main structural differences that give AKR1B10 and AKR1B15 their distinct kinetic characteristics.
2. To perform an analysis of the relevant residues of the active-site pocket and a rational design of AKR1B10 mutant enzymes resembling AKR1B15, by site-directed mutagenesis.
3. To determine the kinetic features and inhibition selectivity of the mutant enzymes to elucidate the importance of the substituted residues in the active-site pocket.

3. Characterization of AKR1B16, a new mouse AKR

Rodents are widely used models in laboratory for *in vivo* research and for understanding the physiological function of genes and proteins. However in most cases there is no direct correlation between human and murine AKR genes and proteins. A new AKR1B member was identified in mouse, AKR1B16, and the aim of this work is to characterize its functional features to understand its role in mouse, and to determine its structural and functional homology with human AKR.

Partial objectives:

1. To compare an analyse the AKR1B16 sequence, evolutionary position and structure within the AKR1B subfamily.
2. To purify and determine the kinetic characteristics of AKR1B16 with aldehydes and ketones.
3. To investigate the retinaldehyde reductase activity of AKR1B16.
4. To compare the AKR1B16 features with those of other murine and human AKR1Bs to determine its orthology.

Chapter 2

Functional and structural studies on AKR1B15

Part of these results appeared in the following publications:

Joan Giménez-Dejoz, Michal H. Kolar, Francesc X. Ruiz, Isidro Crespo, Alexandra Cousido-Siah, Alberto Podjarny, Oleg A. Barski, Jindrich Fanfrlk, Xavier Parés, Jaume Farrés and Sergio Porté. **Substrate Specificity, Inhibitor Selectivity and Structure-Function Relationships of Aldo-Keto Reductase 1B15: A Novel Human Retinaldehyde Reductase**. *PLoS ONE 10*, e0134506.

2.1 Introduction

Members of the aldo-keto reductase (AKR) superfamily share an $(\alpha/\beta)_8$ barrel fold and are mostly monomeric ($\sim$ 35 kDa) NAD(P)H-dependent enzymes catalyzing the reduction of a wide variety of endogenous carbonyl compounds such as carbohydrates, lipid aldehydes, prostaglandins, steroids and retinoids (*6*, *7*, *9*). Several AKR enzymes act in *phase-I drug metabolism* by transforming some xenobiotics, are induced by nuclear factor erythroid 2-related factor 2 (Nrf2) under oxidative stress, and are involved in cancer chemoresistance (*69*, *86*). In the human genome, fifteen AKR genes have been described which belong to three different gene families (*AKR1*, *AKR6* and *AKR7*). The *AKR1B* subfamily gene cluster, located in chromosome 7q33-35, includes the *AKR1B1, AKR1B10* and *AKR1B15* genes. A syntenic gene cluster with four loci has been described in rodent species, although gene orthologs can only be unambiguously assigned for *AKR1B1* (*11*, *168*).

The most studied enzyme of the AKR1B subfamily is AKR1B1 or aldose reductase, which reduces glucose to sorbitol under hyperglycemia and has been involved in the secondary complications of diabetic disease (*38*). Another member, AKR1B10, is normally expressed in adrenal gland and small intestine, and induced in several types of cancer, such as non-small cell lung carcinoma and hepatoma (*69*). Both enzymes have been proposed as promising oncogenic targets (*51*, *169*) and for this reason, along with the role of AKR1B1 in diabetic disease, they have been the subject of many studies in the search of selective and potent inhibitors (*52*, *84*, *93*, *170–172*). Unlike other members of the subfamily, AKR1B10 is highly active in the reduction of all-*trans*-retinaldehyde (*168*). The third gene in the *AKR1B* cluster, *AKR1B15*, has been predicted in the last decade as a result of high-throughput sequencing and annotation projects, i.e. human genome. Recently, AKR1B15 has been demonstrated to be a functional gene with low expression restricted to placenta, testes and adipose tissues. The *AKR1B15* gene undergoes alternative splicing giving rise to two protein isoforms, designated as AKR1B15.1 and AKR1B15.2. The former is a 316-amino acid protein encoded by AKR1B15-201 mRNA (Ensembl database) and showing 92% amino acid sequence identity with AKR1B10, whereas AKR1B15.2 (AKR1B15-001, Ensembl) has a longer N-terminus not homologous to other AKRs, and does not exhibit enzymatic activity or nucleotide binding (*12*). AKR1B15.1 (henceforth referred to as AKR1B15 for brevity) is localized in the mitochondrial fraction and the recombinant protein was purified and characterized, showing limited *in vitro* activity with steroids and acetoacetyl-CoA (*12*). Previously, AKR1B15 had been expressed in the insoluble fraction of mammalian cells, showing low activity with D,L-glyceraldehyde and 4-nitrobenzaldehyde (*11*). Similarly to *AKR1B10*, the *AKR1B15* gene was found to be up-regulated in the airway epithelium by smoking (*99*) and by exposure to sulforaphane, a known activator of the antioxidant response (*100*). Interest in the *AKR1B15* gene has risen lately because some allelic variants have been linked to a mitochondrial oxidative phosphorylation disease (*101*), serous ovarian carcinoma (*102*) and increased longevity (*104*).

With the aim of further characterizing the enzymatic function of AKR1B15, we have improved

the purification procedure, and have performed enzyme kinetics of the purified recombinant protein with retinaldehyde isomers and other typical carbonyl substrates of AKR1B10. We have also conducted a screening against potential inhibitors using compounds previously described for AKR1B1 or AKR1B10. Finally, based on the crystallographic structure of the AKR1B10 complex with $NADP^+$ and tolrestat, we have constructed a model of the AKR1B15 active-site pocket.

2.2 Experimental procedures

2.2.1 Bacterial strains, plasmids and reagents

E. coli BL21(DE3) strain was obtained from Novagen, while plasmids pBB540 and pBB542 (containing the chaperone-coding genes *grpE, clpB and dnaK, dnaJ, groESL*, respectively), were a kind gift from Dr. A. de Marco (*173*). The pET-28a vector containing the cDNA coding for isoform 1 of AKR1B15 (UniProt ID: C9JRZ8-2) had been described by Salabei *et al.* (*11*). pIRES-AKR1B15 was a gift from Dr. Barski. Tolrestat and sorbinil were generously provided by Prof. T.G. Flynn and Pfizer, respectively, whereas JF0064 (2,2',3,3',5,5',6,6'-octafluoro-4,4'-biphenyldiol) was obtained from Sigma-Aldrich. *Trans*-2-hexenal and 4-hydroxy-2-nonenal were commercially obtained from Cayman Chemical. All other reagents, including substrates, were purchased from Sigma-Aldrich unless otherwise indicated.

2.2.2 Protein expression and purification

E. coli BL21(DE3) strain transformed with pET-28a/AKR1B15 was grown in 1 L of 2xYT medium in the presence of 33 μg/mL kanamycin, while *E. coli* BL21(DE3) containing pBB540, pBB542 and pET-28a/AKR1B15 was grown in 6 L of M9 minimal medium supplemented with 0.4% glucose as a carbon source, in the presence of 34 μg/mL chloramphenicol, 50 μg/mL spectinomycin and 33 μg/mL kanamycin. Protein expression was then induced by the addition of 1 mM IPTG (Apollo Scientific) and cells were further incubated for 4 h at 22°C. Cells were then pelleted and resuspended in ice-cold TBI buffer (150 mM NaCl, 10 mM Tris-HCl, 5 mM imidazole, pH 8.0) containing 1% (v/v) Triton X-100. In the case of the non-chaperone-expressing *E. coli* BL21(DE3) strain, the TBI buffer also contained 1% (w/v) sarkosyl. The protein was purified using a His-Trap HP nickel-charged chelating Sepharose Fast Flow (GE Healthcare) 5 mL column using an AKTA FPLC purification system. The column was washed with TBI buffer and the enzyme was eluted stepwise with 5, 60, 100 and 500 mM imidazole in TBI buffer. The enzyme fraction eluted with 100 mM imidazole was loaded onto a PD-10 column (Millipore), which removed imidazole and changed the buffer to storage buffer (200 mM potassium phosphate, pH 7.4, 5 mM EDTA, 5 mM DTT). Finally, the protein was purified through gel filtration chromatography using a Superdex 75 10/300 GL column (GE Healthcare) equilibrated with the storage buffer. In the case of the protein expressed in the *E. coli* BL21 (DE3) strain, in the absence of chaperones, the TBI and

storage buffers contained 0.1% (w/v) sarkosyl throughout the purification procedure. AKR1B10 and AKR1B1 were expressed and purified as described previously (*13*).

2.2.3 Fluorometric and spectrophotometric assays

NADPH binding was analyzed by quenching of Trp intrinsic fluorescence of 0.5 μM protein, using a Cary Eclipse (Varian) fluorimeter, in 20 mM sodium phosphate, pH 7.0, at 25°C in a final volume of 1 mL. The excitation wavelength was 290 nm and the emission wavelength was monitored at 340 nm. AKR1B10 was used as a control. The dissociation constant (K_D) values were calculated by nonlinear fitting of experimental data, using Grafit 5.0 (Eritacus Software), to the Morrison equation:

$$\Delta F = \Delta F_{max} \cdot \frac{[E] + [NADPH] + K_D - \sqrt{([E] + [NADPH] + K_D)^2 - 4 \cdot [E] \cdot [NADPH]}}{2 \cdot [E]}$$

The activity towards aldehydes, with the exception of retinaldehydes, was analyzed spectrophotometrically using a Cary 400 Bio UV-Visible Spectrophotometer (Varian) following the decrease in the absorbance of the cofactor NADPH at 340 nm (ε_{340}=6,220 $M^{-1}\cdot cm^{-1}$) or at 365 nm in the case of cinnamaldehyde (ε_{365}=3,510 $M^{-1}\cdot cm^{-1}$)(*174*). Activities were determined in 100 mM sodium phosphate, pH 7.0, at 25°C using 0.2 mM NADPH in 0.2-cm path length cuvettes, with freshly prepared substrate solutions. One unit of activity is defined as the amount of enzyme required to transform 1 μmol of substrate per min at 25°C. Standard activities were measured before each kinetic experiment by using 10, 60 and 0.6 mM of D,L-glyceraldehyde as a substrate for AKR1B15, AKR1B10 and AKR1B1, respectively.

2.2.4 HPLC enzymatic activity assay

Activity assays with retinoids were carried out using an HPLC-based methodology (*56*). Briefly, retinaldehyde isomers were solubilized using glass tubes by a 10-min sonication at molar ratio 1:1 with fatty acid-free bovine serum albumin in 90 mM potassium phosphate, 40 mM potassium chloride, pH 7.4. The actual amount of solubilized retinoid was determined based on the corresponding molar absorption coefficient in aqueous solutions at the appropriate wavelength: (ε_{400}= 29,500 $M^{-1}\cdot cm^{-1}$ for all-*trans*-retinaldehyde and ε_{367} = 26,700 $M^{-1}\cdot cm^{-1}$ for 9-*cis*-retinaldehyde (*56*). For retinol isomers, which were used as standards of the reaction product, their concentration was determined in hexane using ε_{325} = 51,770 $M^{-1}\cdot cm^{-1}$ for all-*trans*- retinol (*175*) and ε_{325} = 43,765 $M^{-1}\cdot cm^{-1}$ for 9-*cis*-retinol (*176*). The reactions were started by the addition of cofactor and carried out for 15 min at 37°C in a final volume of 0.5 mL. With the aim to measure the steady-state enzymatic activity, the concentration of enzyme was kept from 25- to 100-fold lower than that of the substrate for all the enzymatic assays. The reactions were stopped by the addition

of 1 mL of cold methanol and after two rounds of extraction with hexane, retinoids were analyzed by HPLC (see below).

2.2.5 Determination of kinetic constants and inhibition screening

The IC_{50} activity assays were carried out based on the quantification of the NADPH consumption that takes place when the enzyme catalyzes the conversion of glyceraldehyde into glycerol. The assays were performed at 25°C in a 100 mM sodium phosphate buffer (pH 7.0), with the protein amount reaching the Vmax, and 0.2 mM NADPH. The final reaction volume was 600 μL per reaction. All compounds were dissolved in dimethyl sulfoxide, and the corresponding solution was added to the cell to be assayed in a final concentration of 2% (v/v) DMSO and incubated for 5 min at 25°C prior to the addition of the substrate. The reaction was initiated by the addition of 6 mM D,L-glyceraldehyde, and the decrease in optical density at 340 nm was monitored for at least 3 min at 25°C in a UV-visible spectrophotometer (Cary 400 Bio (Varian)). The IC_{50} value was determined as the compound concentration that inhibits the enzymatic activity by 50%. IC_{50} was calculated using the Grafit program (version 5.0; Erithacus Software) and the values were determined as the mean of three experiments ± the standard error. Standard error values were less than 20% of the mean values.

2.2.6 Homology model and conformational ensembles

The structural model of *apo*-AKR1B15 was obtained from the AKR1B10 ternary complex crystallographic structure (PDB ID: 1ZUA), used as a template for homology modeling, by running the SCWRL program (*177*). Because of the high sequence identity (92%) between the two proteins, the approach that keeps invariant the conformation of the conserved residues was adopted. The flexibility features of both AKR1B10 and AKR1B15 were studied by means of computer simulations.

The hydrogen atoms were added to the structural model of AKR1B15 as well as to the AKR1B10 crystal by the pdb2gmx tool of the GROMACS program package (*178*). The *apo* as well as *holo* forms of both structures were studied as follows: the all-atom models were energy minimized employing the Amber99sb-ildn force field (*179*, *180*) for the protein, parameters of Holmberg *et al.* (*181*) for the cofactor, and Generalized-Born implicit solvent model with parameters of Hawkins *et al.* (*182*). The minimized structures were used as the input for the tCONCOORD algorithm(*183*), which generates a set of independent conformations based on geometrical constraints (*184*). It was designed to accurately capture the protein flexibility and the validity of the resulting conformational ensembles has been proven on a variety of proteins, including also AKR1B1 (*183*). By means of tCONCOORD, we generated and analyzed the ensembles of 2500 conformations, which were subsequently used to calculate root mean square fluctuations (RMSF) of backbone atoms.

The energy minimized geometries (i.e. the starting ones for conformational sampling) were evaluated employing PROCHECK (*185*) and Verify 3D (*186*), which allow checking their stereo-

chemical quality and calculating the percentage of conformations in favored regions obtained from the Ramachandran plots.

2.2.7 AKR1B15 ternary complexes

Geometries of the ternary complexes were derived from the homology model of *holo*-AKR1B15, which was built by superimposition of the apo form and *holo*-AKR1B10 (PDB ID: 1ZUA), including the cofactor coordinates into *apo*-AKR1B15. Considering that all-*trans*-retinaldehyde and 9-*cis*-retinaldehyde are substrates, the distance between the oxygen of retinaldehyde and the catalytic residues (i.e. His111 and Tyr49) should be less than 3 Å for productive catalysis to occur. Under this assumption, the substrates were manually docked into the active site of *holo*-AKR1B15. Inhibitors were automatically docked using AutoDock 4.0 (*187*). The inhibitor JF0064 coordinates were obtained from the PDB (PDB ID 4ICC). The target geometry was extracted from the energy minimized all-*trans*-retinaldehyde complex (see below). For docking, the target was kept rigid, while all the torsional bonds in JF0064, except for the conjugated double bonds, were free to move. The docking parameters were the same as described previously (*89*).

The hydrogen atoms were added to the ternary complex and the complex was energy minimized by adopting the PM6-D3H4 method (*188*) combined with the COSMO solvent model (*189*). The residues, with at least one atom within 5 Å from any atom of the cofactor, substrate or inhibitor, were allowed to move and the rest was kept frozen but included in the Hamiltonian calculation. The PM6-D3H4 method, which has been developed to accurately describe non-covalent interactions in biomolecules, represents a well-established computational tool (*190*) and recently it has been used in the study of the inhibition of AKR1B1 (*191*). The final pdb files of *holo*-AKR1B15 and the ternary complexes were validated with the QMEAN server (*192*), with the flag "ignoring the agreement term", recommended for proteins known to have the correct fold. The volume of the active-site pocket was measured by using the POVME algorithm (*193*), whereas PyMOL (v.1.3 Schrodinger) was used for figure drawing.

2.2.8 Cell culture and transfection

HEK-293T were selected because they are well characterized in terms of retinoid metabolism (*194*, *195*). Cells were grown on 24-well plates in Dulbecco's modified Eagle's medium (DMEM) supplemented with 10% (v/v) fetal bovine serum (FBS) (Gibco BRL). Incubation was performed at 37°C in a humidified atmosphere containing 5% CO_2 / 95% air. AKR1B15 was cloned into a mammalian expression vector: pIRES-hrGFP-1α (Agilent technologies). For transfection, HEK-293T cells were plated and, after 24 h, transfected with Lipofectamine 2000 (Invitrogen) according to the manufacturer's instructions. After 4 h, fresh medium was added and cells were incubated overnight. For flow cytometry analysis, cells were trypsinized and pelled by centrifugation, and resuspended in PBS with 1% propidium iodide (Sigma), to allow the visualization of cell death.

Cells were treated for the indicated time with 10 μM all-*trans*-retinaldehyde from a stock solution in ethanol, never exceeding 0.5% (v/v) ethanol in the culture media.

2.2.9 Western-blot analysis

The cells were obtained from a confluent culture by using the standard method of trypsinization. After neutralizing trypsin, the cell pellet was washed two times in Phosphate Buffered Saline (PBS). Finally, the pellet was frozen at -20°C to facilitate cell lysis. Then, cells were thawed and broken with RIPA Buffer (Tris-HCl, pH 8.0, 1% IGEPAL CA-630, 0.5% sodium deoxycholate, 0.1% SDS, 10 mM sodium orthovanadate, 1 mM PMSF). 20 μg of cell extract and 200 ng recombinant purified AKR1B10 and AKR1B15 used and controls were loaded onto an SDS-PAGE and separation was performed at 150 V for 90 min. Then, proteins were transferred for 1 h at 100 V onto a PVDF (polyvinylidene difluoride) membrane (Millipore). Once transfer was completed, the membrane non-specific interaction sites were blocked with 5% skimmed milk solution in 0.1% Tween 20-Tris buffered saline (TTBS) for 90 min. The membrane was incubated for 90 min with rabbit primary polyclonal antibody specific against the AKR1B10 C-terminal sequence QSSHLEDYPF-DAEY kindly provided by Dr. Flynn (dilution 1:2000 in 2.5% skimmed milk solution, 0.1% TTBS). Afterwards, the membrane was incubated for 90 min with goat peroxidase-conjugated secondary polyclonal antibody against rabbit antibody constant fraction (Bio-Rad), (diluted 1:5000 in 2.5% skimmed milk solution, 0.1% TTBS). The membrane was stained by a chemiluminescent method with luminol and hydrogen peroxide. A digital camera (Bio-Rad) was used to measure band intensities. Finally, the membrane was stripped of antibody and all the process was repeated to detect β–actin, for normalization of protein loading.

2.2.10 Extraction of retinoids from cell culture

Cells were treated overnight (18 h) with 10 μM all-*trans*-retinaldehyde from a stock solution in ethanol, never exceeding 0.5% (v/v) ethanol in the culture media. After incubation, media and cells were collected separately. Media were collected in glass tubes and cells were rinsed twice with ice-cold phosphate buffer saline (PBS) and harvested by brief trypsinization and centrifugation. Cell pellets were homogenized in 0.5 mL of ice-cold PBS, transferred to glass test tubes and stored frozen at -80°C. To complete cell lysis, the thawed cell suspensions were sonicated in an ice-bath. Media aliquots (500 μL) and cell homogenates were added to a disposable glass tube. To perform retinoid extraction, 100 μL of 2.5 M ammonium acetate, pH 4, was added in order to acidify the aqueous phase and facilitate the retinoic acid recovery (*196*), then 1 mL of cold methanol was added and samples were vortex mixed. The samples were extracted twice with 4 mL of hexane. The aqueous phase was removed and hexane was evaporated under a N_2 stream.

2.2.11 HPLC analysis

Retinoids were analyzed by HPLC as previously described (*56*). Briefly, retinoids were dissolved in 200 μL hexane and injected onto a Nova Pak Silica column (4 μm, 3.9 x 150 mm) (Waters) in hexane:methyl-*tert*-butyl ether (96:4, v/v) mobile phase, at a flow rate of 2 mL/min using a Waters Alliance 2695 HPLC instrument. Elution was monitored at 370 nm for all-*trans*-retinaldehyde, 325 nm for all-*trans*-retinol and retinyl palmitate, 350 nm for all-*trans*-retinoic acid and 9,13-*cis*-retinoic acid, using a Waters 2996 photodiode array detector. Quantification of retinoids was performed by interpolating HPLC peak areas into a calibration curve. All retinoid manipulations were performed under dim or red light to prevent photoisomerization.

2.3 Results

2.3.1 Expression and purification of recombinant human AKR1B15

AKR1B15 overexpression screening

We attempted the expression and purification of recombinant AKR1B15 using different *E.coli* strains and procedures since it had been reported that AKR1B15 protein appeared to be mostly present in the insoluble fraction of cell lysates (*11*). First, with the aim to perform an optimization of the expression conditions to increase the amount of soluble protein, a small scale expression step with *E.coli* BL21 strain transformed with pET-28a(+)-AKR1B15 with different temperature and expression time conditions was tested for screening before scaling-up production. *E.coli* BL21 were incubated at 28°C until an OD600 of 0.6 had been reached, protein expression was then induced by IPTG, and cells were grown at 28°C or 22°C. To analyse the protein expression aliquots were collected at 4 hours and overnight (O/N) after the induction. The results obtained from the electrophoretic analysis of the overexpression procedure of AKR1B15 at 4 hours are shown in figure 2.1.

The presence of a major protein band in the insoluble fraction indicates that the protein had formed inclusion bodies. Only in *E.coli* grown at 22°C and 28°C in the 4 hours samples (Fig. 2.1), a little increase in the protein solubility (red mark) was detected. The electrophoretic analysis of the expression O/N did not reveal any change in the solubility of the protein (not shown). The generation of inclusion bodies is common in over-expression processes due to the saturation of the cellular protein folding machinery. We attempted the scaling up of the purification conditions seen in the overexpression screening in which AKR1B15 seemed to be present in the soluble fraction in low quantity (induction of the protein at 22°C, expression time 4h). Remarkably we were able to purify AKR1B15 from soluble fractions, although in a very low amount and with several contaminant proteins. However, these samples displayed no enzymatic activity *in vitro* using NADPH as a cofactor and typical aldo-keto reductases substrates like D,L-glyceraldehyde or p-

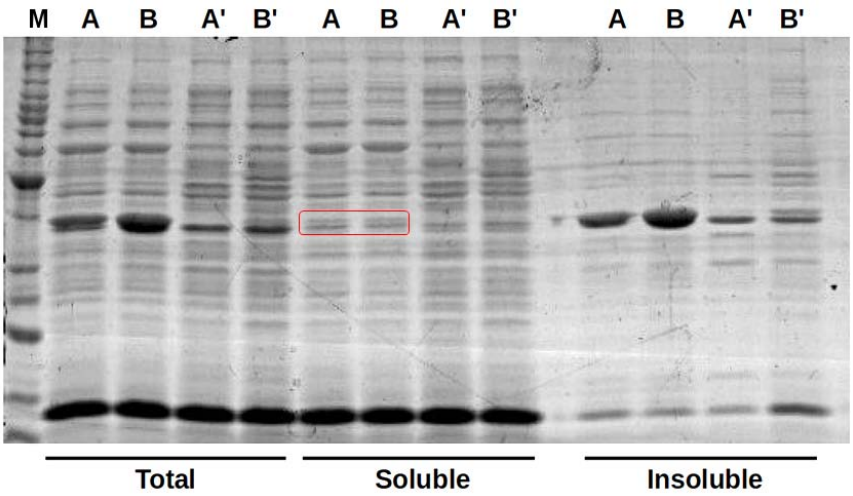

Figure 2.1: SDS-PAGE analysis of AKR1B15 expression at different temperatures in total, soluble and insoluble fractions. The gel analysis shows that AKR1B15 was predominantly associated with the insoluble fraction of BL21(DE3) cell lysates, and just a little amount is present in the soluble fraction (red mark). Lanes: A, AKR1B15 expressed at 22°C; B, protein expressed at 28°C; A', control not induced by IPTG at 22°C; B', control not induced at 28°C.

nitrobenzaldehyde. Therefore, with the aim to obtain active recombinant protein we used new purification protocols to try to purify AKR1B15 from inclusion bodies (*11*, *197*, *198*).

Purification of AKR1B15 with *N*-lauroylsarcosinate

After many unsuccessful attempts to obtain soluble AKR1B15 (i.e. using different expression plasmids, detergents and protocols), we tried the procedure based on the use of the anionic detergent sarkosyl (sodium *N*-lauroylsarcosinate) previoulsy reported by Salabei *et al.* (*11*). AKR1B15 was expressed as a recombinant protein fused to an N-terminal His tag and affinity purified from the insoluble fraction of *E.coli* lysates incubated with sarkosyl to solubilise the protein from the inclusion bodies. In our hands and in the presence of sarkosyl, the amount of soluble protein and the final yield were acceptable (see figure 2.2) and were the highest obtained of the several different purification and expression methodologies used. However, it required that a minimal concentration of sarkosyl (0.001%, w/v) was necessary to avoid protein precipitation. Sarkosyl had been described as an enzyme inhibitor (*197*). Previous data on enzymatic activity, using protein extracts from human COS7 cells transfected with AKR1B15, suggested that AKR1B15 would exhibit very weak activity towards some aldehydes (i.e. glyceraldehyde and 4-nitrobenzaldehyde) common substrates for AKR. In our analysis the AKR1B15 enzymatic activity was found to be NADPH dependent (i.e. the enzymatic activity using 0.2 mM NADH was less than 5% of that with NADPH), as it has been described for most AKR. The low K_m value of AKR1B15 for NADPH (5 μM), within the same range as those of AKR1B1 and AKR1B10 (*13*, *199*), suggested that the protein was properly folded despite the presence of detergent. Kinetic activities using a high concentration

of this enzyme (17 μM), in the presence of sarkosyl, showed that the recombinant enzyme was also active towards typical aldehyde substrates, although with extremely low activity (data not shown), precluding the determination of kinetic constants. Interestingly, AKR1B15 displayed a significant enzymatic activity towards all-*trans*-retinaldehyde, and was the only one that resembled the AKR1B10 specificity. The enzymatic activity towards retinaldehyde substrates could be determined thanks to a HPLC based method, which is more sensitive and it allowed performing enzymatic assay with less sarkosyl concentration than the spectrophotometric assay (0.001% instead of 0.033% (w/v)). It was also confirmed that sarkosyl inhibited AKR1B15 following a non-competitive model (data not shown) and also was a potent inhibitor of AKR1B10, a well characterized enzyme protein with which AKR1B15 shares a 92% of sequence identity. The IC_{50} value of sarkosyl inhibiting AKR1B10 using D,L-glyceraldehyde as substrate was 36 μM. It has to be noted that this concentration of sarkosyl was within the range of sarkosyl present in the protein samples in the purification purification procedure of AKR1B15.

Despite the high yield in protein solubilization by sarkosyl, it should be noticed that an important fraction of pure AKR1B15 was found in aggregated form, and only a small fraction of AKR1B15 was found to be in a monomeric form despite its solubilization with sarkosyl (Fig. 2.4 grey line). AKRs are mostly monomeric soluble enzymes (*6*, *7*, *9*), for this reason we thought that the very low activity found with the purified enzyme in the initial kinetic characterization was because most of AKR1B15 was in the form of inactive aggregates, not properly folded, and that only a small fraction of the protein was active as a soluble monomer. Therefore, it was necessary to perform an additional gel filtration chromatography to separate the active protein monomer from the inactive high-molecular aggregate. We were able to obtain the monomeric form of the AKR1B15 protein in a very low quantity, and kinetic studies of its activity and stability were conducted. The HPLC based methodology was used due to its high sensitivity compared to the spectrophotometric method, and all-*trans*-retinaldehyde was chosen as a substrate because it was the only with which AKR1B15 had displayed a significant activity. We found that the monomeric form of AKR1B15 was active with all-*trans*-retinaldehyde and stable over time up to 2 hours in a reaction at 37°C (Fig. 2.3).

Purification of AKR1B15 co-expressed with chaperones

To try to enhance the proportion of recombinant protein in the soluble form we used of solubility enhancer β-glycine in hyperosmothic medium. It is thought that the osmothic effect caused by sorbitol and the protective effect of glycine betaine enhanced the proper folding of proteins (*200*). However, despite of the attempts inducing of AKR1B15 protein under osmotic stress in the presence of glycine betaine and sorbitol, we did not find differences in the soluble amount of protein present in the samples compared with the controls expressed either without an hyperosmothic medium and

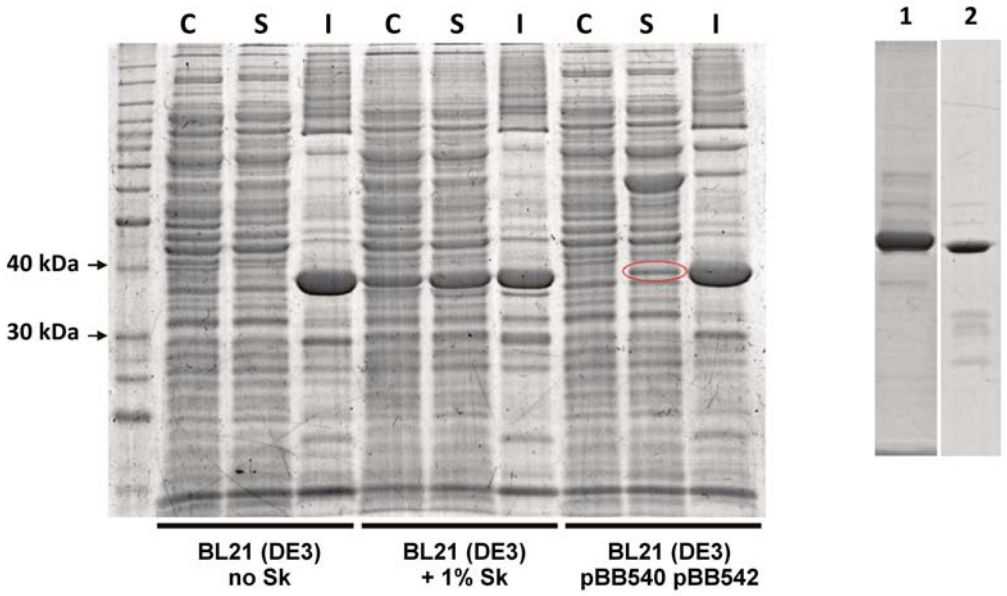

(a) (b)

Figure 2.2: Expression and purification of recombinant human AKR1B15. (a) SDS-PAGE analysis of protein expression. AKR1B15 was predominantly associated with the insoluble fraction of BL21(DE3) cell lysates. Treatment with 1% (w/v) sarkosyl (Sk) provided a much higher amount of AKR1B15 in the soluble fraction. In the case of BL21(DE3) pBB540 pBB542 cells, a protein band which is highlighted with a red oval was identified as human AKR1B15 by Peptide Mass Fingerprinting. Lanes: C, control for the soluble fraction not induced by IPTG; S, soluble fraction and I, insoluble fraction. (b) Protein purification analysis. Purification fractions eluted from the nickel affinity column chromatography using 100 mM imidazole. Lanes: 1, Protein eluted from the soluble fraction of BL21(DE3) + Sk; and 2, Protein eluted from the soluble fraction of BL21 (DE3) pBB540 pBB542.

glycine betaine. Moreover, all-*trans*-retinaldehyde activities performed by HPLC of crude extracts did not shown an increase of activity of the induced samples with the glicyne betaine, evidencing that the methodology was not helpful for increasing the soluble amount of the monomeric active form of the enzyme (data not shown). As an alternative procedure for expression, an *E.coli* BL21(DE3) strain co-expressing three chaperone systems (DnaK-DnaJ-GrpE, ClpB and GroEL-GroES) (*173*, *201*) was used.

We tried the co-expression of AKR1B15 with different combination of chaperone systems and media. The major enhance in its solubility was found when the protein was co-expressed in *E.coli* BL21(DE3) strain with three chaperone systems together and minimal medium (data not shown). Under these conditions, AKR1B15 was still found to be mainly associated with the insoluble fraction, but the amount of soluble protein recovered increased significantly (Fig. 2.1). Activities with all-*trans*-retinaldehyde carried during 1h hour, analysed by HPLC, of the soluble protein

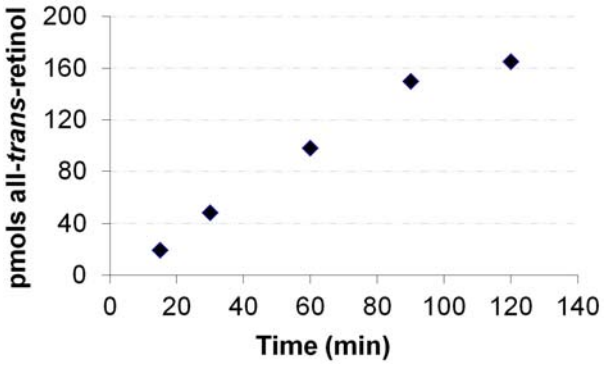

Figure 2.3: Plot of all-*trans*-retinaldehyde reductase activity of AKR1B15 (pmols of produced all-*trans*-retinol) at different reaction times using 10 μM of substrate. The progress curve was linear up to 100 min displaying that the AKR1B15 enzyme was stable at 37°C.

fraction of AKR1B15 co-expressed with chaperones, showed an increase of activity compared with controls without the chaperone systems (data not shown). Peptide mass fingerprint analysis of the isolated band from the soluble protein fraction separated by SDS-PAGE (Fig. 2.2a) identified the isolated band as being human AKR1B15. The enzyme was purified with a final yield of 1 mg protein per liter of culture, when using minimal medium. By analyzing the purified protein on SDS-PAGE (see figure 2.2b), the major band corresponded to a 37-kDa protein with minor contaminating protein bands. Analysis by gel filtration chromatography showed a molecular weight of 37 kDa for the purified protein, suggesting that AKR1B15 was obtained as a monomer (Fig. 2.4). In contrast, the soluble fraction purified with sarkosyl was in an aggregated high-molecular weight inactive form, with a major peak of 132 kDa. Fluorescence analysis of cofactor binding allowed to measure the K_D value for NADPH (113 $\pm$ 9 nM, Fig. 2.5). This value value was in the same range as that of AKR1B10 (K_D = 92 $\pm$ 35 nM).

2.3.2 Enzymatic activity and inhibition studies

AKR1B15 was active with D,L-glyceraldehyde, which was used as a substrate in the standard assay. The enzyme reduced 200 mM glucose with a much lower rate (12 mU/mg) than that exhibited by AKR1B1 (500 mU/mg), precluding the determination of kinetic constants. In contrast, AKR1B15 displayed a catalytic activity comparable or higher than that of AKR1B1 and AKR1B10 with a variety of physiological or model aldehydes and ketones of various classes. Among the compounds assayed, medium-chain (i.e. $\geq$ 6-carbon) aliphatic and aromatic carbonyl compounds were excellent substrates, with K_m values in the low micromolar range. It has to be noted that the k_{cat} values of the all substrates assayed were similar, in the same range, including the activity displayed with retinoids. Importantly, AKR1B15 was also active towards retinaldehyde isomers (Table 2), which along with acrolein, trans-2-hexenal, 4-hydroxy-2-nonenal and farnesal may constitute physiological substrates for this enzyme. The 9-*cis* isomer of retinaldehyde was the best

Table 2.1: Kinetic constants of AKR1B15, 1B10 and 1B1 with aldehydes and ketones

Substrate	**AKR1B15**			**AKR1B10**			**AKR1B1**		
	K_m (μM)	k_{cat} (min^{-1})	k_{cat}/K_m ($mM^{-1}\cdot min^{-1}$)	K_m (μM)	k_{cat} (min^{-1})	k_{cat}/K_m ($mM^{-1}\cdot min^{-1}$)	K_m (μM)	k_{cat} (min^{-1})	k_{cat}/K_m ($mM^{-1}\cdot min^{-1}$)
Carbohydrate aldehydes									
D,L-glyceraldehyde	880	10.7	12.4	6,000[a]	35[a]	6[a]	50[a]	31[a]	660[a]
Aromatic aldehydes									
pyridine-3-aldehyde	2.9	9	3,150	13[b]	150[b]	12,000[b]	10[b]	61[b]	6,100[b]
benzaldehyde	<1*	12.1	>12,100	9.7[b]	104[b]	11,000[b]	21[b]	91[b]	4,300[b]
cinnamaldehyde	<1*	13.3	>13,300	34.7	240	6,900	31	29	950
Alkanals									
hexanal	3.1	7.3	2,300	112[b]	142[b]	1,300[b]	5[b]	28[b]	5,600[b]
Alkenals									
acrolein	36	8.8	240	110[c]	116[c]	1,070[c]	884[c]	11[c]	12[c]
trans-2-hexenal	5	11.3	2,200	28[b]	49[b]	1,700[b]	9[b]	16[b]	1,800[b]
4-hydroxy-2-nonenal	2.2	5.2	2,500	31[c]	121[c]	3,900[c]	716[c]	50[c]	70[c]
citral	1.5	5.5	3,700	4.5	35	7,400	35	68	1,750
farnesal	<1*	4.8	>4,800	2.3[b]	30[b]	13,000[b]	37[b]	27[b]	700[b]
Ketones									
2-butanone	780	10.5	13.5	-	LA	-	-	LA	-
3-buten-2-one	21.3	8.2	380	-	LA	-	-	LA	-
3-nonen-2-one	1.7	6.8	4,000	-	LA	-	-	LA	-
2-cyclohexen-1-one	365	4.41	12.1	-	LA	-	-	LA	-
α-Dicarbonyls									
2,3-butanedione	<1*	10.6	>10,600	540[d]	260[d]	480[d]	110[b]	23[d]	210[d]
2,3-hexanedione	<1*	9.5	>9,500	51[b]	79[b]	1,500[b]	17[b]	49[b]	2,900[b]
β-Dicarbonyls									
2,4-pentanedione	40	2.2	55	58,900	8.6	0.15	8,100	16.7	2.2
3,5-heptanedione	1,300	5.3	3.9	>50,000	-	-	12,000	26	2.2
Cofactor									
NADPH	5.7			10			2.9[e]		

Enzymatic activity was measured spectrophotometrically. For the determination of the kinetic parameters for NADPH, 10, 60 and 0.6 mM D,L-glyceraldehyde were used for AKR1B15, AKR1B10 and AKR1B1, respectively. LA, low activity (<10 mU/mg) was detected at saturating concentration of substrate for AKR1B15. *Because of very low Km values, data are only approximate.
[a]Data from (*13*), [b](*60*), [c](*77*), [d](*202*), [e](*199*).

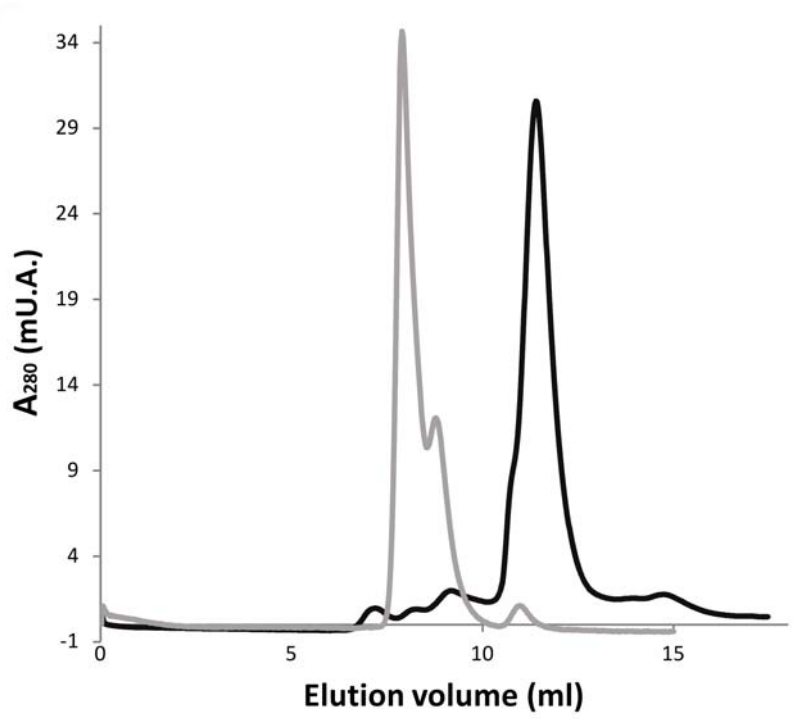

Figure 2.4: Elution profile from the Superdex 75 10/300 GL size-exclusion column chromatography. AKR1B15 purified from soluble fraction of BL21(DE3) + Sk and from soluble fraction of BL21 (DE3) pBB540 pBB542 are shown in grey and black lines, respectively. Major peaks eluting at 7.9 and 11.4 mL correspond to aggregated (132 kDa) and monomer (37 kDa) protein, respectively.

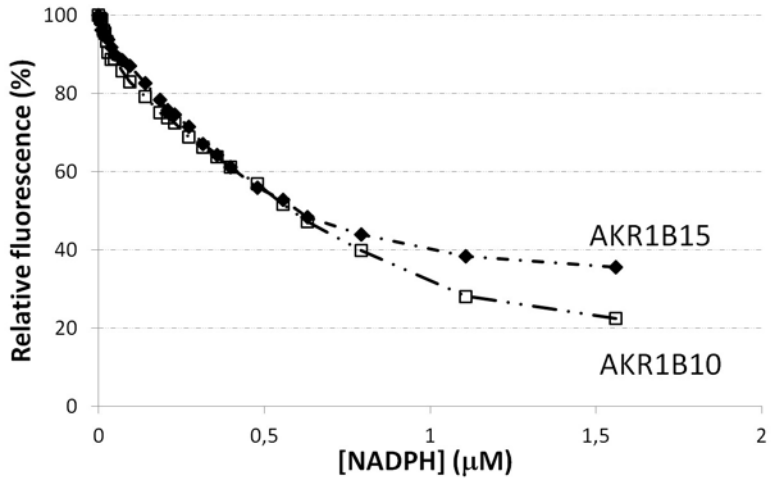

Figure 2.5: Quenching of AKR1B15 and AKR1B10 fluorescence upon binding of NADPH. Change of the protein fluorescence intensity (in percentage) upon addition of cofactor is shown. All proteins were used at a concentration of 0.5 μM in 20 mM sodium phosphate, pH 7.0, at 25°C. Graph symbols: AKR1B15 (diamonds), AKR1B10 (open squares).

substrate based on the catalytic efficiency (k_{cat}/K_m) due to a very low K_m value (160 nM) (see 2.2), which could be determined by the use of an HPLC-based method providing higher sensitivity

than the spectrophotometric assay. Regarding cofactor specificity, AKR1B15 was confirmed to be NADPH dependent (i.e. the enzymatic activity using 0.2 mM NADH was less than 5% of that with NADPH), as reported in (*12*), and described for most AKRs. The K_m value of AKR1B15 for NADPH (5 μM) is within the same range as those of AKR1B1 and AKR1B10 (table 2.1).

Table 2.2: Kinetic constants with retinaldehyde isomers

Substrate and parameter	**AKR1B15**	**AKR1B10**[a]	**AKR1B1**[a]
All-*trans*-retinaldehyde			
K_m (μM)	1 ± 0.3	0.6 ± 0.1	1.1 ± 0.1
k_{cat} (min^{-1})	5.4 ± 0.5	27 ± 1	0.9 ± 0.1
k_{cat}/K_m ($mM^{-1}\cdot min^{-1}$)	5,300 ± 1,700	45,000 ± 7,600	1,300 ± 160
9-*cis*-retinaldehyde			
K_m (μM)	0.16 ± 0.03	0.7 ± 0.1	0.4 ± 0.1
k_{cat} (min^{-1})	3.8 ± 0.2	0.9 ± 0.1	0.7 ± 0.2
k_{cat}/K_m ($mM^{-1}\cdot min^{-1}$)	25,600 ± 5,300	1,300 ± 190	1,500 ± 170

Enzymatic activity was measured by using the HPLC-based method.
[a]Data from (*13*).

Table 2.3: Inhibitory effect of different compounds on enzymatic activity.

	IC_{50} (μM)		
Inhibitor	**AKR1B15**	**AKR1B10**	**AKR1B1**
Tolrestat	>100	0.006[a]	0.01[b]
Sorbinil	>100	9.6[c]	0.55[c]
JF0064	0.034 ± 0.005	1.0[d]	0.3[d]
Epalrestat	>50	0.33[e]	0.021[e]
Oleanolic acid	>100	0.09[c]	124[c]
Sulindac	>100	2.69[e]	0.36[e]
Lithocholic acid	16.3 ± 7.6	0.12[e]	7.2[e]
UVI2008	0.85 ± 0.096	6.1[f]	>70[f]

The enzymatic activity assay was performed by using D,L-glyceraldehyde as substrate. [a]Data from (*43*), [b](*22*), [c](*92*), [d](*52*), [e](*85*), [f](*89*).

Eight AKR inhibitors were tested against AKR1B15 using D,L-glyceraldehyde as substrate (see table 2.3). Among these inhibitors, there are six of the carboxylic acid type (tolrestat, epalrestat, oleanolic acid, sulindac (a cyclooxygenases (COX) inhibitor, investigated as chemotherapeutic drug for treatment of colon and other cancers), lithocholic acid and the synthetic aromatic retinoid UVI2008, a RARβ/γ agonist (*203*)) (see Figures 2.6; 2.6a, 2.6d, 2.6e, 2.6f and 2.6g 2.6h), one of cyclic imide type (sorbinil, Figure 2.6b) and one non-classical aldose reductase inhibitor or ARI (JF0064, which has been recently described by Cousido-Siah *et al.* (*52*), see Figure 2.6c). Tolrestat, JF0064 and sulindac are potent inhibitors of AKR1B1 as well as of AKR1B10 (with IC_{50} <10 μM for both enzymes). Sorbinil and epalrestat are more selective against AKR1B1 (*88*, *98*), while

UVI2008, oleanolic and lithocholic acid are more selective against AKR1B10 (*92*). For AKR1B15, JF0064 and UVI2008 showed a significant inhibition (IC_{50} = 0.034 ± 0.005 μM for JF0064, and 0.85 ± 0.096 μM for UVI2008, Table 3), much stronger than for AKR1B1 and AKR1B10 (*52*, *89*). The steroid lithocholic acid was found to be an inhibitor of AKR1B15, in agreement with the reported observation that certain steroids are good substrates for this enzyme (*12*).

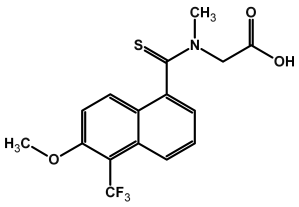

(a) Tolrestat.

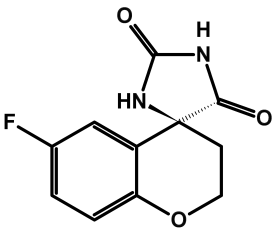

(b) Sorbinil.

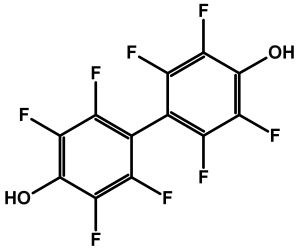

(c) JF0064.

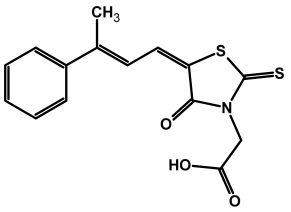

(d) Epalrestat.

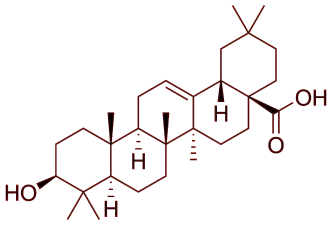

(e) Oleanolic Acid.

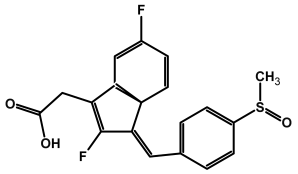

(f) Sulindac.

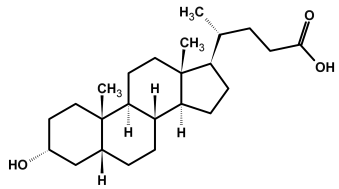

(g) Lithocolic acid.

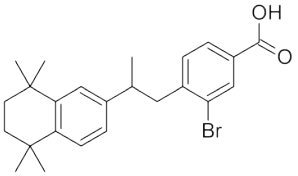

(h) UVI2008.

Figure 2.6: Molecular structure of the assayed inhibitors.

2.3.3 Structural model of AKR1B15

With the aim to compare the substrate-binding site of AKR1B15 with that of AKR1B10, and upon unsuccessful attempts of protein crystallization, a 3D homology model of AKR1B15 was built (Fig. 2.7). The SCWRL server was chosen, as it is designed specifically for predicting sidechain conformations, provided a fixed backbone usually obtained from an experimental structure. In practical terms, this is the case of AKR1B15, given its 92% sequence identity with AKR1B10. Model quality was checked by PROCHECK analyses, indicating that most residues are in the preferred regions (94.8%), whereas residues in allowed regions and outliers are 3.5 and 1.6%, respectively. The compatibility of the atomic model (3D) was checked with its own amino acid sequence (1D) using Verify 3D analysis. This analysis shows that there is no region with negative

scores, which would otherwise indicate potential problems. In addition, the analysis using the QMEAN server indicates the reliability of the model, with a QMEAN score of 0.67 out of 1, and with all the Z-scores being consistent with the good quality of the structure. Thus it may be concluded that this model is suitable for structural studies.

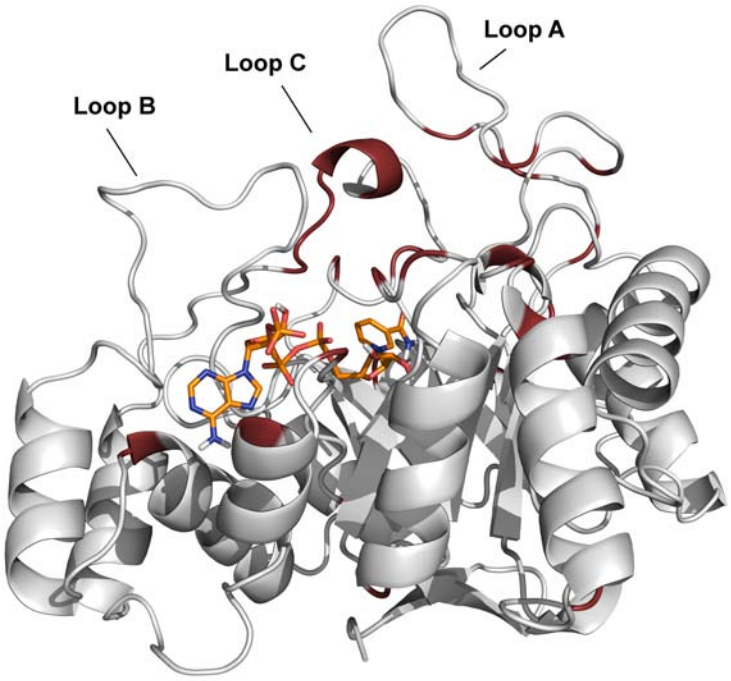

Figure 2.7: Model of AKR1B15 structure. Side view of the $(\alpha/\beta)_8$ barrel complexed the $NADP^+$. In red, the divergent residues between AKR1B15 and AKR1B10. The catalytic site is located in the center of the barrel.

2.3.4 Model analysis

Regarding the cofactor-binding site, AKR1B15 shares with AKR1B10 all residues, except for Arg22, Met265 and His269 (Fig. 2.8). The change of Lys22 in AKR1B10 to Arg in AKR1B15 may prevent its interaction with the pyrophosphate bridge of $NADP^+$ but, due to the mobility of the Arg side chain in solution, its interaction with the cofactor cannot be excluded. Met265 and His269 keep interactions with the same groups of $NADP^+$ that involve Val265 and Arg269 in AKR1B10 (i.e. a hydrogen bond between the N atom of Met265 and the 2'-phosphate group, a second hydrogen bond between the Nε of His269 and the 2'-phosphate group, and a stacking interaction of His269 with the adenine ring). Interestingly, a His residue at position 269 and its interactions have also been described in the rat AKR1B14 X-ray structure (*204*). The salt bridge between the side-chain of Asp217 and Lys263, acting as a safety belt in cofactor binding, and the stacking interaction of Tyr210 side chain with the nicotinamide ring are also conserved. This is consistent with the AKR1B15 cofactor preference for NADPH, with a low K_m value.

On the other hand, the active site displays high divergence between AKR1B15 and AKR1B10. The residue differences between the two proteins are concentrated in loops A and C which, along

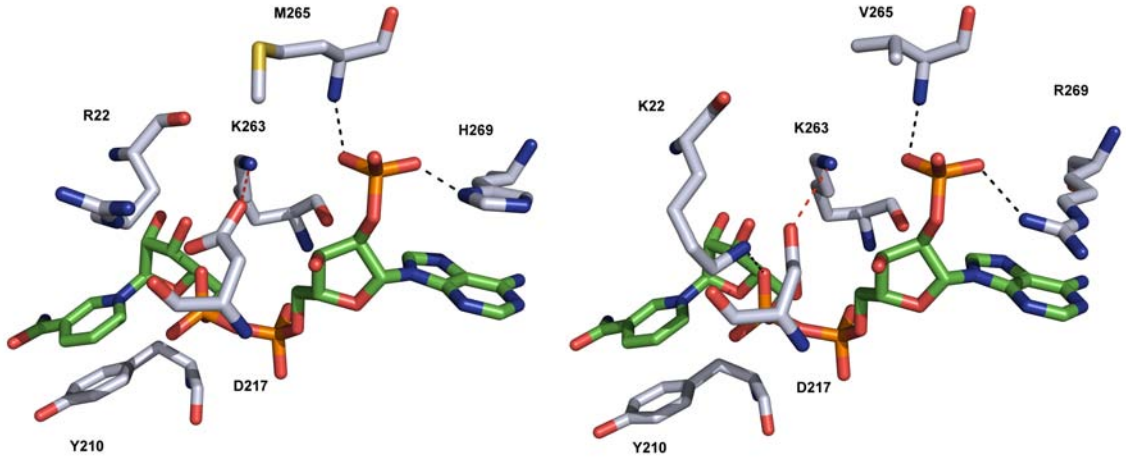

(a) (b)

Figure 2.8: Comparison of the cofactor-binding site between the AKR1B15 model (a) and the AKR1B10 crystal structure (b). Interactions of Met265 and His269 with $NADP^+$ in AKR1B15 are similar to those of Val265 and Arg269 in AKR1B10 (black dotted lines). His269 forms a π-stacking interaction with the adenine ring of the cofactor. The substitution of Lys22 by Arg in AKR1B15 prevents its interaction with the pyrophosphate bridge of $NADP^+$. The salt bridge between Asp217 and Lys263 (red dotted line), acting as a safety belt in the coenzyme binding, and the π-stacking interaction of Tyr210 with the cofactor nicotinamide ring are conserved in both AKRs. Carbon atoms of the cofactor are shown in green, whereas those of the enzyme are colored grey.

with loop B, give shape to the active-site pocket (Fig. 2.7). Thus, the catalytic residues (Asp44, Tyr49, Lys78 and His111) and those in loop B are strictly conserved. In contrast, Ser118, Leu122, Ala131, and Gly133 (in loop A), together with Cys299, Asn300, Val301, Leu302, Gln303, Ser304, and Tyr310 (in loop C) of AKR1B10 are substituted by Thr118, Phe122, Met131, Ser133, Phe299, Asp300, Phe301, Lys302, Glu303, Phe304 and Phe310, in AKR1B15. Noteworthy, residues Phe299, Phe301, Glu303 and Phe304, along with Phe48 (Val48 in AKR1B10), participate in the AKR1B15 active-site pocket, which is thus significantly smaller (60 $Å^3$ for AKR1B15 versus 279 $Å^3$ for AKR1B10) and more hydrophobic, compared to the AKR1B10 pocket (Fig. 2.9). Some of these substitutions might not only have a consequence on the shape, volume and hydrophobicity of the active site, but also on the flexibility of the polypeptide chain, which is most relevant in the loop regions. The analysis of conformational ensembles indicates that AKR1B15 would display less flexible loops A and C than AKR1B10 (Fig 2.10a). A detailed analysis of the AKR1B15 model shows van der Waals interactions between residues from these loops and residues from other protein regions (i.e. Trp21 - Phe299_*loopC*, Phe48 - Phe116_*loopA*, Phe48 - Phe123_*loopA*, Phe48 - Phe301_*loopA*, Trp112_*loopA* - Phe301_*loopC*, Phe116_*loopA* - Phe304_*loopC*, Phe123_*loopA* - Phe304_*loopC*, Met131_*loopA* - Phe304_*loopC* and Met131_*loopA* - Leu307_*loopC*). Such interactions result in a hydrophobic cluster (Fig. 2.10), which likely contributes to the lower flexibility of the AKR1B15 active site.

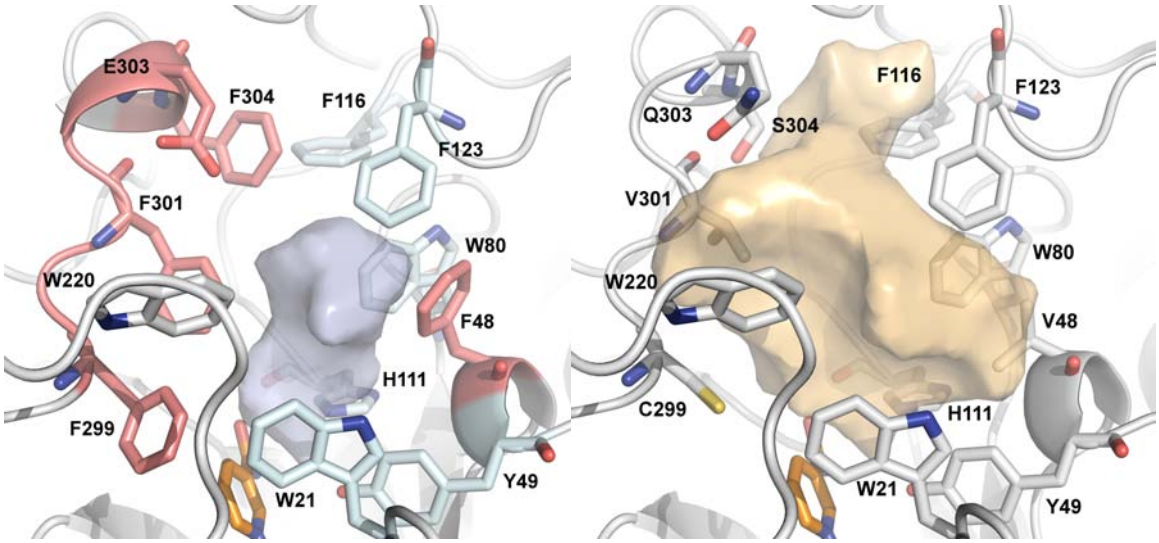

(a) AKR1B15. (b) AKR1B10.

Figure 2.9: Active site pockets of AKR1B15 (a) and AKR1B10 (b). The AKR1B15 specific residues are displayed in magenta. $NADP^+$ cofactor is colored in orange. The surface contour of pockets is shown in grey and orange for (a) AKR1B15 and (b) AKR1B10, respectively.

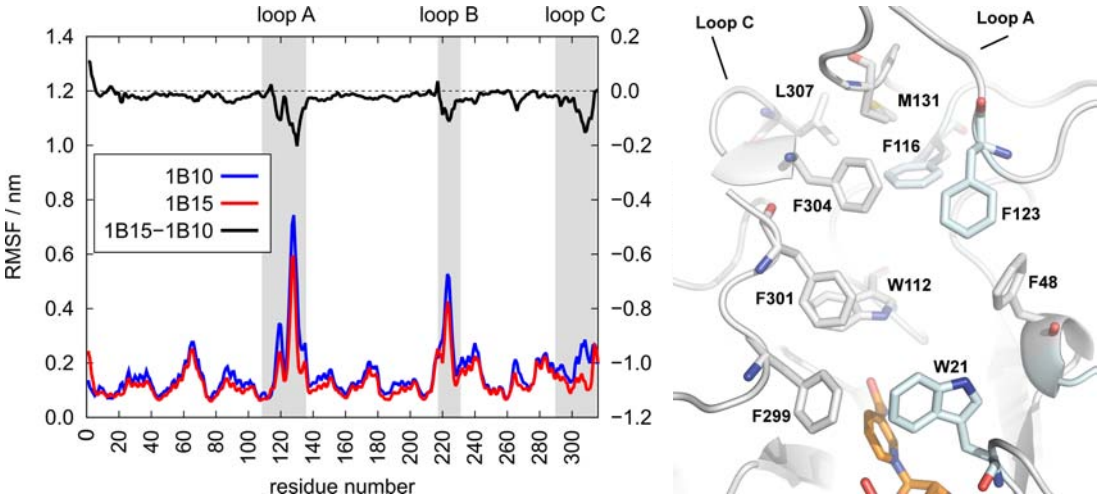

(a) RMSF. (b) AKR1B15 loops A and C.

Figure 2.10: (a) The local conformational changes in holo forms of AKR1B15 (red line) and AKR1B10 (blue line) derived from computer simulations, as indicated by root mean square fluctuations (RMSF) of backbone atoms. The residues of loops A, B and C are highlighted by grey background. The difference in RMSF between the two enzymes is displayed as a black line in the top. (b) AKR1B15 loops A and C indicating potential contacts between different residues are shown as sticks, which may explain the low flexibility of the protein in this region.

2.3.5 Docking of substrates and the inhibitor JF0064

As it has been described above, AKR1B15 is active towards retinoids, and thus the binding mode of all-*trans*- and 9-*cis*-retinaldehyde was analyzed. The obtained models were also analyzed with the QMEAN server and displayed similar scores (0.68/1 and 0.69/1, respectively) as the AKR1B15

holoenzyme model. The analysis showed that both substrates could be placed with their carbonyl groups at catalytic distance from the hydroxyl group of Tyr49, the Nε of His111, and the cofactor C4 atom (2.9, 2.9, and 3.2 Å, respectively). The two molecules would be positioned in a similar manner into a narrow and hydrophobic pocket, establishing contacts with Trp21, Phe48, Phe123, Trp220, and Phe301 (all-*trans*-retinaldehyde), and Phe48, Trp220, Phe299, and Phe301 (9-*cis*-retinaldehyde) (Fig. 2.11). A slight rearrangement of loop A and loop C (Fig 2.11) could allow the establishment of a hydrogen-bond or an electrostatic interaction between Lys125 and Glu303 (Fig. 2.12a).

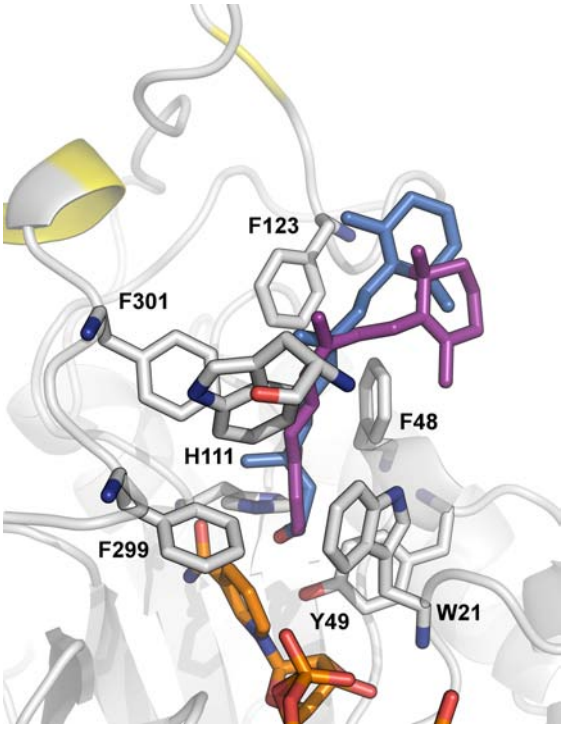

Figure 2.11: Molecular docking of retinoids to the active-site pocket of AKR1B15. Residues implicated in binding of retinoids are displayed in grey sticks. All-*trans*- and 9-*cis*-retinaldehyde are shown in blue and purple, respectively. The residues found in the most external part of all-*trans*-retinaldehyde binding channel in AKR1B10 are highlighted in yellow. NADPH is shown in orange.

The particular AKR1B15 topology brings the cyclohexene ring of all-*trans* and 9-*cis*- retinaldehyde further away from loops A and C than in AKR1B10 (Fig. 2.11, 2.12a and 2.12b). Thus these substrates do not interact with the residues that have been described as important for all-*trans*-retinaldehyde binding in AKR1B10, and which are in the most external part of the AKR1B10 pocket (*13*). Notably, some of these residues are not interacting with the retinoid substrates in AKR1B15, i.e. Lys125 and Met131 (Ala in AKR1B10) from loop A, Glu303 (Gln in AKR1B10) and Phe304 (Ser in AKR1B10) from loop C. In AKR1B10, all-*trans*- retinaldehyde binding requires a rearrangement of Lys125, not necessary for 9-*cis*-retinaldehyde, explaining the higher k_{cat} value towards the former substrate (*69*). In the case of AKR1B15, Lys125 is not involved in the

binding of either substrate, being consistent with similar k_{cat} values. The hydrophobic pocket in the external region of the active site of the enzyme, where part of the polyene chain and the cyclohexene ring of the substrate bind, corresponds to the protein region which shows more rigidity in comparison to AKR1B10 (Fig. 2.10a). Furthermore, this rigidity, likely due to the presence of the bulky Phe residues (Phe48, Phe299, Phe301 and Phe304), would make difficult the opening of the so-called "specificity pocket" (Fig. 2.12a and 2.12b), which has been described for ARI binding in AKR1B10 and AKR1B1 and which usually accommodates the hydrophobic moiety of inhibitors (*92*, *205*). This feature could have important functional consequences. For instance, it could explain the different substrate specificity and inhibitor selectivity of AKR1B15, since flexibility has been well established in connection with the active-site accessibility, and substrate and ligand binding (*206*).

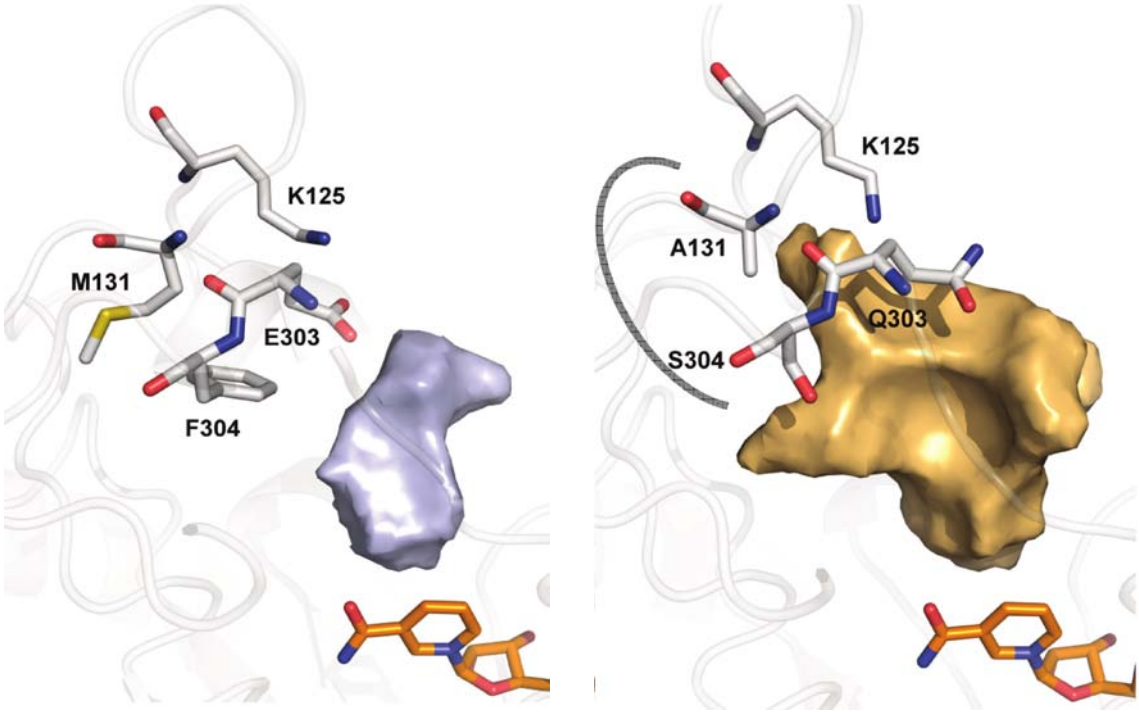

(a) AKR1B15 pocket side view.

(b) AKR1B10 pocket side view.

Figure 2.12: Side view of the surface contour of the active-site pocket, depicted in grey and orange for AKR1B15 and AKR1B10, respectively, to show the inhibitor "specificity pocket". A thick grey curved line indicates the "specificity pocket" in AKR1B10. As it is shown, this pocket may not be opened in AKR1B15, likely due to the presence of bulky Phe residues.

The compound JF0064 is the only ARI found, with the exception of UVI2008, to significantly inhibit AKR1B15, probably due to the reduced volume of the active-site cleft and to the difficulty in opening the "specificity pocket". In order to analyze JF0064 binding, a docking simulation along with energy minimization was performed. The model was again validated by using the QMEAN server and displayed a similar, though slightly better score than the rest of the AKR1B15 models (0.72/1). The Z-score (which is tending from negative digits to 0 when approximating to

experimentally determined structures) of the AKR1B15-NADP$^+$-JF0064 model (-0.92) is comparatively improved with respect to the AKR1B15 holoenzyme model (-1.64). All-*trans*- and 9-*cis*-retinaldehyde complexes show intermediate values of -1.51 and -1.35, respectively.

The conformation of the AKR1B15-NADP$^+$-JF0064 complex corresponding to the energy minimum is displayed in figure 2.13a. Binding would occur through van der Waals interactions with a large number of hydrophobic residues, and by establishing hydrogen bonds with catalytic residues (Tyr49 and His111) and Glu303. As it has been described above for substrates, the binding of the inhibitor also induced the same rearrangement of loop A and loop C, allowing for the interaction between Lys125 and Glu303. The other tested compounds did not inhibit AKR1B15 likely because of steric hindrance (e.g. Phe301 and Phe48 may clash against sorbinil, and Phe304, along with the fact that the "specificity pocket" could not be opened, may prevent tolrestat from binding) (Fig. 2.12b and 2.13b).

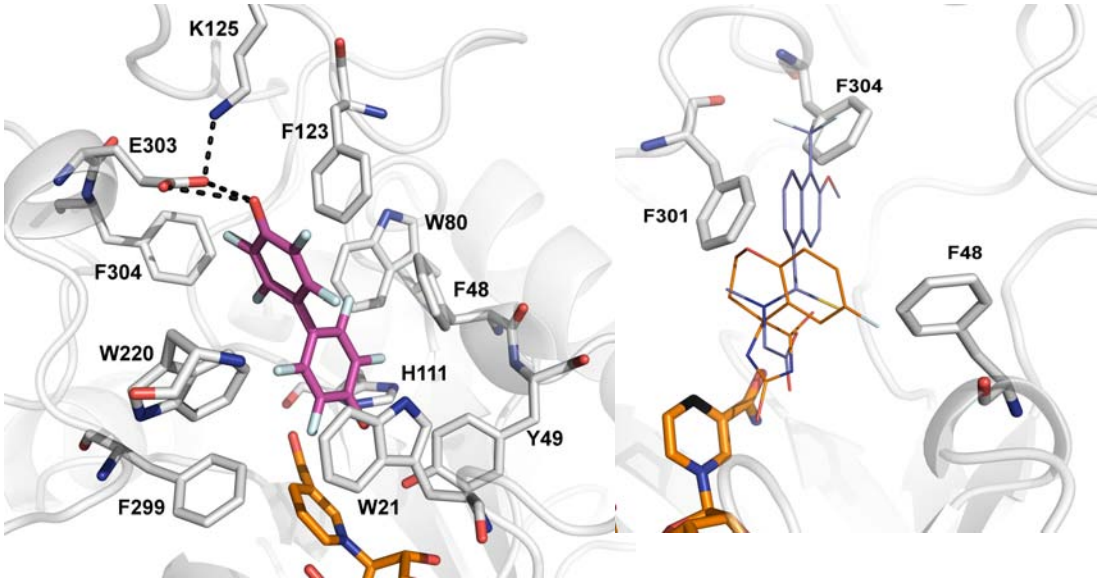

(a) JF0064 docking.

(b) Tolrestat and sorbinil docking.

Figure 2.13: Molecular docking of inhibitors to the active site pocket of AKR1B15. (a) The inhibitor JF0064 (PDB ID 4ICC) bound to AKR1B15 is displayed as sticks with C atoms in magenta, while residues interacting with the inhibitor are shown as sticks with C atoms in grey. (b) Steric hindrance preventing tolrestat (in blue) and sorbinil (in orange) from binding to the active site of AKR1B15. For this analysis, the AKR1B15 structure model was superimposed with tolrestat and sorbinil found in AKR1B10 crystallographic structures (PDB: 1ZUA and 4GA8, respectively). NADP$^+$ is colored in orange.

2.3.6 Modification of the HPLC methodology for retinoid analysis in cells

In order to understand the possible physiological role of AKR1B15, and to analyse the role of this protein in RA metabolism, we investigated whether AKR1B15 expression could decrease both retinaldehyde and RA levels *in vivo*, as we have previously demonstrated for AKR1B1, 1B10, 1C1,

1C3 and 1C4 (*69*, *156*). This would support a similar role for AKR1B15 in pre-receptor regulation of the RAR and RXR nuclear receptors. HPLC has become the method of choice for the analysis of retinoids: The characteristic UV absorption spectra of the various retinoids allow the use of diode-array detection for the identification of resolved retinoids. However, the use of HPLC in the quantification of a broad range of biologically important retinoids in a single run, within a reasonable amount of time, presents some difficulties. It is necessary an analytically robust assay which has to combine the requirements of sensitivity, specificity and resolution to separate the different isomers and analytes of retinoids endogenously present in cells (*196*, *207*). Moreover, the endogenous abundance of various retinoids is quite diverse. Thus, retinyl ester levels could be in the high micromolar range in contrast to RA levels that could be six orders of magnitude lower, in the nanomolar level (*196*, *208*, *209*). The HPLC/UV-based methodology used by our group for the analysis and characterization of enzymatic reactions of different enzymes with retinoids *in vitro* (*13*, *56*, *69*, *89*, *156*, *168*, *176*, *210*), has been extensively tested and used, showing that the extraction efficiency for both retinaldehyde and retinol is robust and excellent. However, in the cellular experiments with retinoids in which we wanted to analyse their metabolism, this methodology was not efficient enough in the extraction of all the retinoid metabolites, particularly of RA. The calculated extraction efficiency for retinoic acid was could be 15% (Fig. 2.14 lane (a)).

At this point, we tried various methodologies using different extraction solvents (hexane:dioxane:isopropanol (50:5:1) (*211*, *212*), ethyl acetate (*213*), ethanol with ammonium acetate (pH 4.5), n-hexane with ethyl acetate (9:1) (*214*), ethanol and hexane (*215*) and a two-step acid-base extraction (*196*)), to improve the efficiency of the RA extraction. From the evaluated methods, the two-step acid base extraction was the most efficient to recover multiple retinoids from cell media, with an efficiency near 100% (Fig. 2.14 lane (b)). The basification step recovers nonpolar retinoids (retinol and retinyl esters), and the acidification step with hydrochloric acid facilitates the recover of RA and other polar retinoids (*196*, *208*, *209*, *216*).

We applied this methodology for the recovery of retinoids from cells and cell media, with good results. However, after a few runs we encountered unexpected problems with the silica column, and anomalous and atypical peaks appeared. We concluded that the column became damaged and we realized that this was a result of the methodology used. The U.V. spectra of these anomalous peaks did not correspond to any retinoid standard. Moreover, the retention time of the retinoid peaks was different from its standard value, and even we observed a decrease in the absorbance of the all-*trans*-retinol peak followed by the appearance of an anomalous peak. It is known that retinoids are labile to strong acids, particularly in anhydrous conditions (*217*, *218*). In view of these results, we tried another approach based on the acidification protocol by Kane *et al.* (*216*) with minor modifications. Rather than using a strong acid like hydrochloric acid, we performed only one extraction step with a mild acidification of the media with ammonium acetate, pH 4.5 (*214*, *216*). This new methodology highly improved the RA extraction efficiency (Fig. 2.14 lane

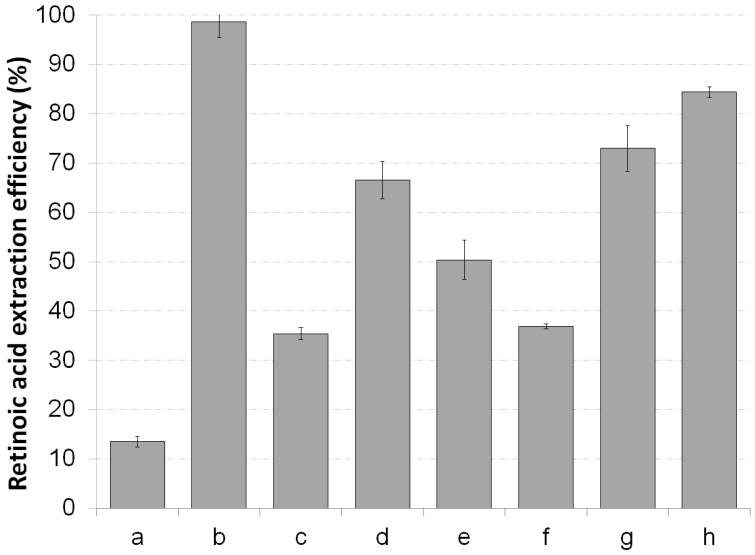

Figure 2.14: Extraction efficiency of retinoic acid from cell media using different extraction inorganic solvents. Lanes; (a), extraction with methanol + hexane, the classical method for the extraction of retinal and retinol from *in vitro* enzymatic reactions; (b), two-step acid-base extraction; (c), hexane; (d), extraction protocol used by Yamakoshi *et al.* (*214*); (e), ethanol + hexane; (f), ethyl acetate; (g) hexane:dioxane:isoprophanol (50:5:1); (h), acidification of the media with ammonium acetate (pH 4.5) + methanol + hexane.

h) without damaging the silica column neither affecting the extraction and elution of the other retinoids.

2.3.7 Analysis of AKR1B15 activity in living cells

pIRES-AKR1B15, pCMV-AKR1B10 and a control empty vector pCMV-HA were transfected into HEK293T cells and incubated with all-*trans*-retinaldehyde. Analysis of the retinoid content was carried out in triplicates for 24 h after transfection. pIRES is a dicistronic expression vector that allows the co-expression of the tag protein hrGFP in the same transcript as the gene of interest, and permits to monitor the transfection efficiency with a flow cytometer taking advantage of the hrGFP fluorescence. After screening some transfection procedures, the maximum transfection efficiency for pIRES-AKR1B15 was aproximately 48% (Fig. 2.15a). Immunoblotting using an anti-AKR1B10 antibody showed in general a lower transfection level for AKR1B15 than for AKR1B10 (Fig. 2.15b).

The levels of RA present in the culture media of cells transfected with AKR1B10 were significantly lower ($\sim$ 2 fold lower) than those of the control cells without transfection plasmid, the cells transfected with an empty plasmid and the ones overexpressing AKR1B15 (Fig. 2.16a). Moreover, the decrease of RA was accompanied by an increase in all-*trans*-retinol level in AKR1B10-transfected cells as compared with mock and AKR1B15-transfected cells. Similar results were

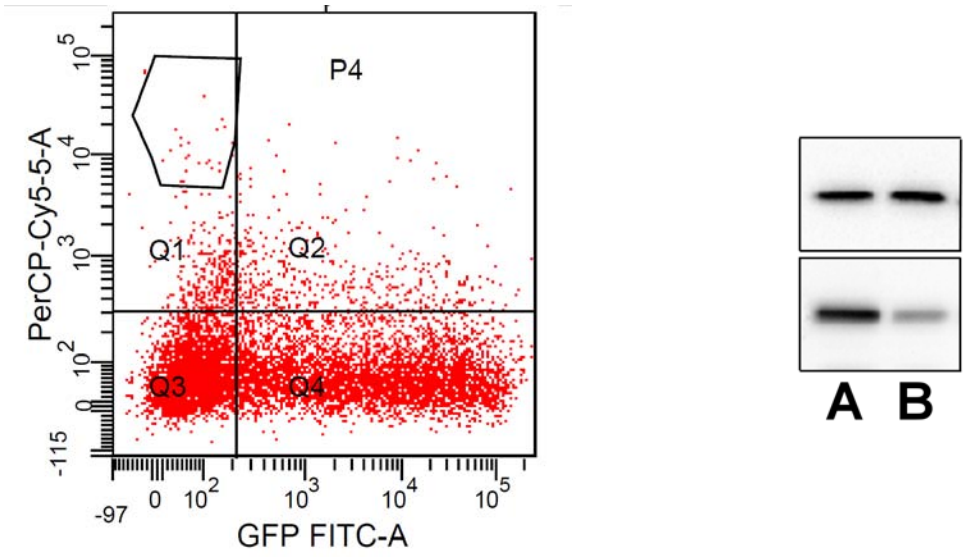

(a) (b)

Figure 2.15: Transfection of HEK293T cells with pCMV-AKR1B10 and pIRES-AKR1B15. (a), Flow cytometry analysis of transfected cells with pIRES-AKR1B15. Q1; population of dead cells (propidium iodide positive); Q2, transfected dead cells (double positive); Q3, untransfected cells; Q4, GFP-positive transfected cells. (b), Western Blot analysis of transfected cells with pCMV-AKR1B10 (lane A, bottom) and pIRES-AKR1B15 (lane B, bottom). Analysis with anti-β-actin antibody was used as a loading control, lanes A and B, top.

obtained regarding the intracellular levels of retinoids, with the AKR1B10-transfected cells showing elevated levels of retinol and retinyl esters (results no shown). However no RA could be observed in the cells and the only observable levels of all-*trans*-retinaldehyde were found in the AKR1B10-transfected cells. No difference in the retinoid content could be observed between AKR1B15-transfected and control cells.

2.4 Discussion

2.4.1 Expression and purification of recombinant human AKR1B15

We have found that AKR1B15 appears to be an enzyme with distinct and unique properties despite its high sequence identity with AKR1B10. The first of the distinct features is its high tendency to aggregation and deposition in inclusion bodies when expressed in bacterial cells. We attempted the expression and purification of recombinant AKR1B15 using different *E.coli* strains and procedures since it had been reported that AKR1B15 protein appeared to be mostly present in the insoluble fraction of cell lysates (*11*). The generation of inclusion bodies is common in over-expression processes due to the saturation of the cellular protein folding machinery. Factors that lead to recombinant protein aggregation are not only host-specific but also target protein specific, thereby no universal remedy for inclusion body formation is available, and finding the optimal conditions for every protein it is difficult and a variety of conditions had to be tested. To enhance the solubility we also studied the effects of several factors shown to improve the protein solubility:

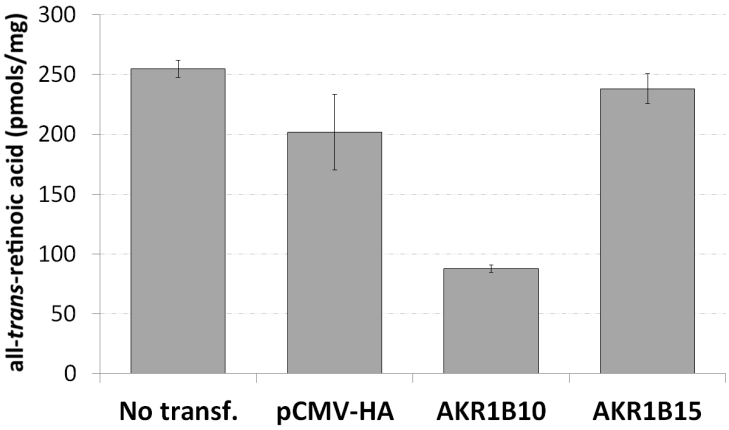

(a) Retinoic acid biosynthesis in AKR1B10-transfected cell media.

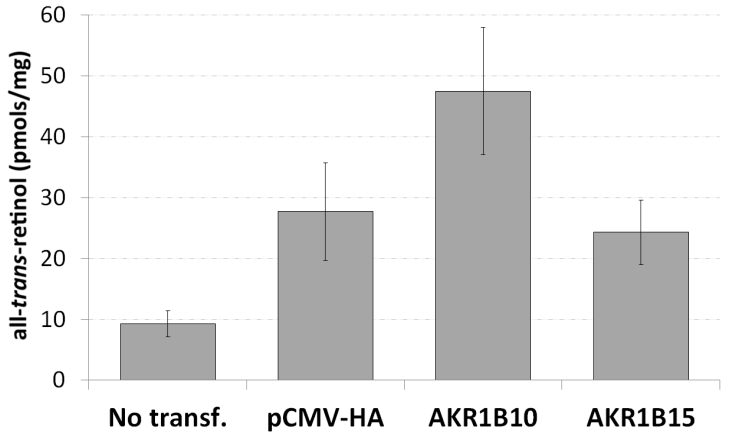

(b) Retinol levels in HEK293T cells.

Figure 2.16: Effects of AKR retinaldehyde reductase activity on the production of RA and retinol in HEK293T cells. Retinoid HEK293T cells were transfected with pCMV-HA/pCMV-AKR1B10 vector (AKR1B10) or pIRES-AKR1B15 (AKR1B15) vector and treated with 10 μM of all-*trans*-retinaldehyde for 24 h. Retinoid metabolites were analyzed by normal phase HPLC. (a), Decrease in the all-*trans*-RA production found in the culture medium of the HEK293T AKR1B10-transfected cells. (b), Increase in the level of all-*trans*-retinol in AKR1B10-transfected cells as compared with the non-transfected cells and the pCMV-HA/pIRES-AKR1B15 transfected cells.

reducing the expression level, using different bacteria strains, using various growth culture media (LB, Terrific broth, minimal medium) and expression temperatures in different combinations (*219–222*). Detailed analysis of all samples was carried out but the different conditions and combination of them did not shown differences in AKR1B15 solubility (data not shown).

The localization of AKR1B15 in a insoluble fraction of the human cell could explain the difficulties in producing recombinant protein from the soluble fraction of *E.coli*. We used an anionic detergent, as sarkosyl, to disgregate the inclusion bodies and recover the soluble protein, and the final yield of protein was acceptable. However, the detergent failed to properly solubilize AKR1B15, and mostly high molecular weight inactive aggregates were obtained, with only a small fraction in a monomeric soluble form, responsible for the low enzymatic activities observed. The majority of

AKRs are soluble monomeric enzymes (*6*, *7*, *9*) and AKR1B15, which shares a 92% of sequence identity with AKR1B10 (only 27 amino acid substitutions), a well characterized monomeric and soluble enzyme, did not present transmembrane domains in its sequence. However, Weber *et al.* (*12*) found that AKR1B15 it localized in the mitochondria and the iPSORT algorithm predicted a localization signal to mitochondria in its sequence. The use of gel filtration chromatography and the HPLC-based activities with retinoids showed that the only fraction responsible of the activity was the protein in the monomeric form (see 2.4 and 2.5).

After confirmation that only the soluble fraction showed activity, we tried to enhance the solubility of AKR1B15 with alternative procedures. Bacteria, in front a hyperosmotic stress, tend to synthetize and accumulate small organic compounds like polyols, sugars, amino acids and betaines. These osmolytes equilibrate the osmotic pressure in the salt-stressed cells. Glycine betaine is one of the most widespread osmolytes, and can be used in bacterial expression systems to increase the yield of soluble proteins, disrupt protein aggregation and promote protein refolding. Glycine betaine interacts differently with the highly exposed protein backbone that with the folded protein surface, raising the free energy of the denatured state and hence shifting the equilibrium in favor of the native state. Thus, it is thought that the osmophobic effect influences renaturation in a manner complementary to the usual forces involved in protein folding (*200*, *222–226*). However no positive effect was observed.

As an alternative procedure, the use of chaperones was attempted. Chaperones are proteins that support the folding of newly synthetised proteins to its native state and provide a control system that refolds misfolded proteins and prevents their aggregation into nonfunctional nonactive structures. It is thought that in the host bacterial cells the aggregate formation and the protein misfolding of the recombinant proteins are due to the limitations in the chaperone system capacity (*201*, *220*, *227*). It is well documented that the use of chaperone co-expression systems has a positive effect on the yield of soluble recombinant protein recovered from bacteria, but the efficiency of the chaperone combination is highly dependent of the soluble target protein and its features and interactions with chaperones while folding. Therefore, there is no universal system that can be applied as a successful approach in the use of chaperone systems. This strategy is facilitated by the possibility of employing a number of plasmid systems that encode different chaperones and co-produce the chaperones along with the heterologous protein (*227*, *228*). With this methodology we were able to purify an acceptable amount of soluble AKR1B15. Gel filtration chromatography confirmed that the protein was in a monomeric form with a molecular weight of approximately 37 kD. The analysis of the NADPH binding and the determination of its dissociation constant using fluorometric titrations for AKR1B15 and AKR1B10 supported that AKR1B15 was properly folded. It was no possible for us to determine a dissociation constant with the AKR1B15 samples previously purified with the detergent sarkosyl. Moreover, it has to be noted that, despite the results of the dissociation constant are similar to those obtained by Weber *et al.*, the maximal degree of fluorescence quenching reached by these authors was 26%, in contrast to more than 60%

in our case, very similar to the fluorescence pattern obtained with AKR1B10. This difference suggests that their protein sample was a mixture of proper monomeric active protein and inactive aggregates. These results indicate that, like other AKRs, AKR1B15 binds NADPH with high affinity.

2.4.2 AKR1B15 enzymatic activity

It has been recently reported that AKR1B15 catalyzes the reduction of acetoacetyl-CoA and the carbonyl group at C17 position of sex steroids (*12*). Additional results, obtained by using protein extracts from transfected human COS-7 cells, indicated that AKR1B15 exhibited very weak activity towards D,L-glyceraldehyde and 4-nitrobenzaldehyde (*11*), which are typical substrates of AKR enzymes. Our current analysis shows that the purified recombinant enzyme has broad substrate specificity and displays a significant enzymatic activity towards aliphatic and aromatic aldehydes and ketones (Table 2.1). The comparison between AKR1B15 and the other human AKR1B enzymes reveals some relevant distinct kinetic features. In particular, ketones and α-dicarbonyl compounds were good substrates for AKR1B15, showing higher activity and lower K_m values than AKR1B10 and AKR1B1. The β-dicarbonyl compound, 2,4-pentanedione, was also reduced by AKR1B15, consistent with the reported activity with acetoacetyl-CoA, which also has two carbonyl groups in a β-position (*12*). With other substrates, AKR1B15 exhibited lower K_m values than AKR1B10, suggesting that AKR1B15 could play a role in aldehyde detoxification and lipid peroxidation, similar to what has been suggested for other AKR1B enzymes (*37*, *229*, *230*). Among the several manifestations of oxidative damage to biological molecules, lipid peroxidation products seem to be especially harmful (*231*, *232*). They are formed when the polyunsaturated fatty acyl groups of membrane phospholipids are modified by ROS (Radical Oxygen Species), and a self-propagating chain of free radical reactions produces these electrophilic compounds, that are highly reactive (*232*). It has to be noted that mitochondria are an important source of ROS in mammalian cells. These derived products of lipid peroxidation interact with cellular nucleophiles and form covalently modified protein and DNA adducts, being cytotoxic (*233*). Documented evidence has indicated that carbonyl-derived DNA modifications result in mutagenesis, carcinogenesis and other age-related diseases (*234*, *235*). The major aldehyde products of lipid peroxidation are crotonaldehyde, malondialdehyde (MDA), acrolein and 4-hydroxy-2-nonenal (HNE)(*236*).

AKR1B15, a reportedly mitochondrial enzyme (*12*), is active towards some of these physiological substrates, i.e. acrolein and HNE, two of the most reactive and important mediators of free-radical damage, well documented in mitochondria. Moreover, cellular HNE is reported to be at a level of 0.1 to 3.0 μM range (*236*), and cellular acrolein is at 0.5 μM (*237*), concentrations in which AKR1B15 could be active, especially HNE with a 2.2 μM K_m. HNE can specifically uncouple mitochondria by interacting with uncoupling proteins (UCP1, 2 or 3). Structurally related compounds, such as trans-2-nonenal, trans-2-nonenoic acid, retinoic acid, all-*trans*-retinal and other molecules containing the reactive 2-alkenal group have the same effect (*232*, *238–240*),

suggesting that the alkenal group of these compounds reacts with protein in the mitochondria causing uncoupling. It is still unknown the physiological role of AKR1B15, but its activity towards these compounds and its mitochondrial localization could make it possible for this protein to regulate the availability of these molecules, participating in protection against the oxidative damage and aging (*232*, *238*, *239*). Interestingly, some allelic variants of AKR1B15 had been related to an increase in longevity (*104*) and to a mitochondrial oxidative phosphorilation disease (*101*).

AKR1B15 resembles AKR1B10 in having high activity with retinoids, in contrast to AKR1B1 (Table 2.2). A distinct feature of AKR1B15 is that it shows similar k_{cat} values towards all assayed substrates, including retinoids, suggesting a common rate-limiting step for all substrates. In comparison, the k_{cat} values of AKR1B1 with both retinaldehyde isomers and AKR1B10 with the 9-*cis* isomer are significantly lower than those for other substrates. This decrease in k_{cat} values had been previously interpreted as a change in the rate-limiting step (from cofactor dissociation to a slower step) of AKR1B1 and AKR1B10 reactions with these retinoids (*13*). This seems not to be the case for AKR1B15. Finally, the higher specificity of AKR1B15 for the 9-*cis* isomer is unique for the human AKR1Bs, and it matches those of AKR1C3 (*156*), which, like AKR1B15, has bulky Phe residues at positions 299 and 304 in its active site. The same residues are found in chicken AKR, also highly active with 9-*cis*-retinal (*118*).

2.4.3 AKR1B15 studies in cells

AKR1B10-transfected cells, but not AKR1B15, displayed AKR retinaldehyde reductase activity, converting all-*trans*-retinaldehyde to retinol and decreasing the levels of RA biosynthesis (Fig. 2.16). It has been postulated that AKR1B10 induction in cancer could affect cell differentiation through modulation of the RA biosynthetic pathway (*71*, *241*). Our data clearly support previous results (*69*) using and indirect reporter assay, which indicated that AKR1B10 may exert, through their retinaldehyde reductase activity, a pre-receptor regulation of RAR and RXR nuclear receptors, by changing the flow of RA biosynthesis. Similar results have been reported: *i)* monkey kidney COS-1 cells, when transiently expressing AKR1B10, doubled their capacity for all-*trans*-retinaldehyde reduction (*13*), and *ii)* the overexpression of AKR1B10 in human airway epithelial 16HBE cells treated with retinaldehyde also increased retinol production (*242*). Moreover, a recent study shows that AKR1B10 is overexpressed in keloid disease (a cutaneous tumour of unknown pathogenesis), and that its overexpression in normal skin keratinocytes affects retinoid metabolism, mimicking the retinoid expression pattern seen in the tumoral cells. Moreover, AKR1B10 overexpression in normal keratinocytes reduces RA receptor transactivation, in accordance with previous studies (*13*, *69*, *243*). Accordingly, this report confirms that overexpression of AKR1B10 influences RA biosynthesis pathway, provoking a diminution of its levels, which could lead to an increased cancer risk in target tissues.

AKR1B15 transfected cells did not display any changes in the retinoids level as compared to the control empty plasmid pCMV-HA. AKR1B15 exhibits retinaldehyde reductase activity *in vitro*,

but AKR1B10 is more efficient in reducing all-*trans*-retinaldehyde (Table 2.2). In the other hand AKR1B15 is an efficient 9-*cis*-retinaldehyde reductase, mainly for its low K_m value at nanomolar range, and with a modest k_{cat}, similar to that it has with all-*trans*-retinaldehyde. Similarly to our results with retinaldehyde, AKR1B15 was not able to reduce progesterone nor corticosteroids, and only activity with androgens and estrogens was observed when expressed in mammalian cells (*12*). Moreover, other cellular experiments indicated that AKR1B15 displayed low activity with typical AKR substrates, like D,L-glyceraldehyde and *p*-nitrobenzaldehyde (*11*), both of them active in *in vitro* assays (Table 2.1). One possibility could be that the activity of AKR1B15 is difficult to detect because of its specific localization in mitochondria, in the matrix or strongly associated with the outer membrane (*12*). Eukaryotic cell metabolism is compartmentalized in different organelles (*244*), and there is evidence that retinoid and carotenoid metabolism could be compartmentalized, avoiding competition of different enzymes for their substrates (*245*). Since AKR1B15 is a mitochondrial enzyme, its accessibility to added all-*trans*-retinaldehyde could be more limited than for the cytosolic AKR1B10. Another possibility to explain the low AKR1B15 activity in cells could be the modest transfection efficiency observed, around 50%, which together with its lower kinetic efficiency with all-*trans*-retinaldehyde, made the differences in RA quantification below the observable detection limit. Finally, it can not be discarded that even if the protein is expressed in mammalian cells, it may be in part not correctly folded or aggregated, similarly to what is observed when expressed in bacterial systems, only remaining active a minimal fraction.

2.4.4 Physiological significance

The k_{cat}/K_m value of AKR1B15 for 9-*cis*-retinaldehyde (25,600 $mM^{-1}\cdot min^{-1}$) is the highest among all the substrates checked so far, including the steroids and 3-keto-acyl-CoAs analyzed by Weber *et al.* (*12*), although these authors used different conditions for enzyme purification and kinetic studies. This is reminiscent of what has been observed for other members of the AKR superfamily, such as AKR1C3, which displays a high k_{cat}/K_m value for 9-*cis*-retinaldehyde, and it is also active with steroids, as AKR1B15 (*156*). Observations of this dual substrate specificity have been also made for SDR members (*131*). Thus, it is conceivable that AKR1B15 and some of these enzymes have a multifunctional role in the pre-receptor regulation of hormonal signaling pathways. 9-*cis*-retinoic acid does not have widespread distribution in tissues (in contrast to all-*trans*-retinoic acid) (*246*), and until date 9-*cis*-retinoic acid has only been detected by a validated LC-MS/MS methodology in pancreas, mainly localized into β-cells of the islets of Langerhans (*247*), and data indicate that it can be involved in glucose-stimulated insulin secretion acting as a pancreas-specific autacoid (local hormone) (*246*, *247*). 9-*cis*-retinoic acid has the ability to activate both RAR and RXR, with much higher affinity for RXR than all-*trans*-retinoic acid (*248*). Moreover, some studies suggest that RXR-9-*cis* retinoic acid complex induces RXRα translocation into mitochondria and increases the levels of mtDNA transcription and translation (*249*). Thus, the AKR1B15 specificity for the 9-*cis* isomer may suggest a major role in the control of RAR

and RXR mediated signaling. Regarding the reported localization of AKR1B15 in mitochondria, there is increasing evidence of retinoid metabolism in different subcellular compartments (*76*, *210*). Retinoids and their aldehyde metabolites can be generated by the asymmetric cleavage of carotenoids such xanthophylls or β-carotene by β-carotene-9',10'-dioxygenase (BCO2), which is associated with the inner mitochondrial membrane (*245*). Therefore, a putative physiological role of AKR1B15 in retinoid metabolism is compatible with its mitochondrial localization. The presence in mitochondria of other retinaldehyde reductases, such as RDH13 (*210*), gives further support to this notion. In addition, RDH10, an enzyme involved in retinoic acid synthesis, shifts between mitochondria associated membranes and lipid droplets during retinyl ester biosynthesis, similarly to cellular retinol-binding protein type 1 (*250*). Retinol has also been pinpointed as a modulator of energy homeostasis in mitochondria by regulating oxidative phosphorylation (*251*, *252*). As above suggested, an important role of AKR1B15 in metabolizing lipid peroxidation products and alkenals in mitochondria is also likely (*240*, *253*).

To summarise, despite its high sequence identity with AKR1B10, AKR1B15 appears to be an enzyme with a unique substrate specificity and narrower inhibitor selectivity. AKR1B15 displays distinct kinetic features with ketones, α-dicarbonyl compounds and is among the best 9-*cis*-retinaldehyde reductases within the AKR superfamily. Some of the most potent inhibitors of AKR1B1 and AKR1B10 did not inhibit AKR1B15. Amino acid substitutions clustered in residues located in loops A and C result in a smaller, more hydrophobic and more rigid active-site pocket of AKR1B15 as compared to that of AKR1B10. The structural model of AKR1B15 provides a powerful tool for the virtual screening of substrates and inhibitors for this enzyme. The distinct topology of the AKR1B15 fold should facilitate the design of more selective inhibitors, as it has been shown for other enzyme pairs with high sequence similarity (*254*, *255*). Finally, the finding of all-*trans*- and 9-*cis*-retinaldehyde as substrates for AKR1B15 adds further complexity to the enzymatic pathways of retinoid transformations and their cross-talk with other hormonal signaling pathways, such as that of steroids. This opens a research line to elucidate the physiological contribution of this novel human retinaldehyde reductase.

Chapter 3

AKR1B10 mutants to mimic the AKR1B15 active site

3.1 Introduction

Aldo-keto reductases (AKRs) are NAD(P)H-dependent enzymes that catalyze the reduction of carbonyl compounds, including several physiological substrates, such as lipid peroxidation products, steroids, catecholamines, prostaglandins and retinoids. Structurally, the crystallographic studies show that AKRs adopt a $(\alpha/\beta)_8$ barrel fold characterized by a deep hydrophobic active-site located within the carboxyl-terminal face of the central β-barrel, near the C-terminal end. In all characterized enzymes of the superfamily, NADP(H) binds first in a pocket generated by the C-terminal end of the β-sheet, at the base of the active-site cavity, and helps to form the site, which has a conserved catalytic tetrad (Asp44, Tyr49, Lys78 and His111; using AKR1B10 residue numbering). This site interacts with the nicotinamide ring of the cofactor through a hydrogen-bonding network. The optimal substrate positioning for a specific activity is dictated by the configuration of the residues forming the substrate-binding cavity. The distinct substrate specificity and inhibitor selectivity of AKRs are given mainly by residue differences located in the external and variable loops surrounding the active site, which have considerable plasticity (*6*, *9*, *118*, *256*, *257*).

AKR1B10 (aldose reductase-like protein) reduces a variety of aromatic and aliphatic aldehydes, dicarbonyl compounds (*57*, *59*, *60*) and cytotoxic aldehydes (acrolein and 4-hydroxy-2-nonenal) (*77*), and has high catalytic efficiency with retinals (*13*, *44*). It is up-regulated in hepatocellular carcinomas (*57*, *62*), and its elevated expression promotes proliferation of cancer cells. AKR1B10 has been also reported to be overexpressed in other tumors such as hepatocellular carcinoma (an alteration of its expression seems to occur even in pre-neoplastic conditions) and cholangiocarcinomas (*258*, *259*), pancreatic carcinoma (*66*), smokers non-small cell lung carcinomas (*68*, *260*), breast cancer (*169*), oesophageal cancer (*261*) and uterine carcinomas (*262*).

The most recently described member of the aldo-keto reductases 1B family is AKR1B15. Its gene was predicted in a *locus (tcag7.1260)* within the same gene *cluster* as human *AKR1B1* and *AKR1B10*, in chromosome 7. AKR1B15 displays 92% amino acid sequence identity with AKR1B10 (*11*). The high homology with AKR1B10 suggests that they are a result of a recent duplication event. Recent studies have demonstrated that *AKR1B15* is an active gene, which product is expressed *in vivo* and with a mitochondrial localization (*12*). Despite its high sequence identity with AKR1B10, AKR1B15 shows a unique and broad substrate specificity. Particularly, ketones are good substrates for AKR1B15 in contrast to the low activity displayed by AKR1B10. Importantly, AKR1B15 was also active towards retinaldehyde isomers, specially 9-*cis*-retinaldehyde, which is the best substrate for this enzyme (*263*), being one of the most active AKRs for this isomer. The structural model showed that its active-site pocket is smaller and more hydrophobic as compared to that of AKR1B10 (*263*). Recently, the *AKR1B15* gene was included in a list of genes linked to human oxidative phosphorylation (OXPHOS) disease (*101*). Another study points to *AKR1B15* as one of the new genes validated with a somatic missense mutations in the serous ovarian carcinoma (*102*).

Although sharing a high sequence identity, AKR1B10 and AKR1B15 are clearly enzymes with distinct kinetic features and structural properties (*12*, *263*). The sequence alignment and the structural data suggest a strong implication of residues located in loop C in the catalytic features of AKR1B15. Thus, this loop (together with loop A) are the sites where the majority of residue changes are located between AKR1B10 and AKR1B15. For that purpose we designed two mutants of AKR1B10 to substitute the most divergent residues of the active-site pocket of AKR1B10. The purpose is to mimic the binding-site pocket of AKR1B15, with lower accessible volume and more rigidity, to understand how minimal residue changes between two very similar proteins can provoke the change in their properties.

In the present work, we have investigated, by means of site-directed mutagenesis, steady-state kinetics and computer modeling, the contribution of the adjacent residues Cys299, Asn300, Val301, Leu302, Gln303, Ser304, located in the loop C of AKR1B15, to the catalytic activity and substrate specificity of the enzyme, creating a mutant enzyme from AKR1B10 (AKR1B10mut) incorporating these specific changes. In addition, we studied the participation of an additional residue change in the substrate-binding pocket (Val48 to Phe48), also involved in the reduction of volume and increased rigidity of the AKR1B15 binding pocket, by preparing the mutant enzyme AKR1B10mF48.

3.2 Experimental procedures

3.2.1 Site-directed mutagenesis

The AKR1B10 cDNA cloned into the bacterial expression vector pET-15b was used as the parental DNA for mutagenesis. Human AKR1B10 was mutated using the QuickChange Lightning Site-Directed Mutagenesis Kit (Agilent Technologies). For this purpose the following primers were used: for AKR1B10mut; mutation of segment of six consecutive residues (eight nucleotides to change six residues) AKR1B10 forward primer (5'- GAAACTGGAGGGCCTTTGACTTTAAGGAATTCTCT CATTTGGAAGAC- 3') and AKR1B10 reverse primer (5'- GTCTTCCAAATGAGAGAATTCCTT AAAGTCAAAGGCCCTCCAGTTTC- 3'). For the additional mutation of AKR1B10mut48F: forward primer (5'-CATTGACTGTGCCTATTTCTATCAGAATGAACATG-3') and reverse primer forward primer (5' -CATGTTCATTCTGATAGAAATAGGCACAGTCAATG-3'). The underlined regions correspond to the mutated nucleotides. The PCR steps were: *1)* DNA polymerase activation (95°C for 2 min), *2)* denaturing (95°C for 20 seconds), *3)* annealing (55°C for 10s) and *4)* extension (68°C for 3 min 40s). Steps 2-4 were repeated for 18 cycles. PCR product was digested with *Dpn*I restriction enzyme (provided by the manufacturer) to eliminate the parental supercoiled dsDNA. The resulting constructs (pET-15b-AKR1B10mut and pET-AKR1B10mF48) were cloned into an *E.coli* strain BL21(DE3) pLysS (Novagen) expression strain using the transformation protocol indicated by the manufacturer. Before expression, all mutated DNA were completely sequenced to ensure that unwanted mutations were absent.

3.2.2 Alignment of DNA sequences, generation of the AKR1B10 mutant models and analysis of the binding pockets

AKR1B10 and AKR1B15 sequences were gathered from UniProt data bank and analysis was performed using the ESPript 3.0 server (*264*). AKR1B10 crystallographic structure (*13*) (PDB code: 1ZUA) and the apo-structural model of AKR1B15 (*263*) were used to compare the active-site volume of AKR1B10, AKR1B15 and AKR1B10 mutants. The model structure of AKR1B10mut and AKR1B10mF48 models were generated using the Swiss-Model server. The volume of the active-site pocket was measured by using the POVME algorithm (*193*), whereas PyMOL was used for figure drawing.

3.2.3 Expression and purification of AKR1B enzymes

AKR1B10mut and AKR1B10mF48 were expressed and purified from pET-15b vector. The pET-15b constructs allow the expression of proteins with an N-terminal fused histidine tag under the control of phage T7 RNA polymerase promoter and operon lac. In the host strain used, *E.coli* BL21(DE3) pLysS, the expression of phage T7 RNA polymerase is also under the control of the operon lac promoter. Hence, the constitutive expression of the operon lac repressor (Lac I), contained in both the *E.coli* genome and the expression vector, assures the expression of the protein only in the presence of an inducer such as IPTG. For protein expression, transformed *E.coli* BL21(DE3) pLysS strains were grown in 1L of 2xYT medium in the presence of the appropriate antibiotics and was incubated at 28°C until an OD600 of 0.6 had been reached. Protein expression was then induced by the addition of 1mM IPTG and cells were grown O/N at 22°C. AKR1B10 mutant enzymes were purified as described previously for AKR1B10 (*56*). Briefly, the purification was performed by affinity chromatography on a nickel-charged chelating Sepharose Fast Flow 5-mL column (His Trap column, GE Healthcare), which specifically binds the protein due to the His tag, using an AKTA FPLC (GE Healthcare) purification system. Then, protein was eluted by applying an increasing step-wise concentration (5, 60, 100, 250 mM) of imidazole in 50 mM Tris/HCl and 0.5 M NaCl, pH 8. The imidazole present in the eluted protein fractions was removed through a PD-10 column (gel filtration-desalting column, GE Healthcare). Proteins including the His tag were stored frozen in 100 mM sodium phosphate, pH 7.

3.2.4 HPLC enzymatic activity assay

Activity assays with retinoids were carried out using an HPLC-based methodology (*56*). Briefly, retinaldehyde isomers were solubilized using glass tubes by a 10-min sonication at molar ratio 1:1 with fatty acid-free bovine serum albumin in 90 mM potassium phosphate, 40 mM potassium chloride, pH 7.4. The actual amount of solubilized retinoid was determined based on the corresponding molar absorption coefficient in aqueous solutions at the appropriate wavelength: (ε_{400} = 29,500 $M^{-1}{\cdot}cm^{-1}$ for all-*trans*-retinaldehyde and ε_{367} = 26,700 $M^{-1}{\cdot}cm^{-1}$ for 9-*cis*-retinaldehyde (*56*). For retinol isomers, which were used as standards of the reaction product, their concentration was

determined in hexane using ε_{325} = 51,770 $M^{-1}\cdot cm^{-1}$ for all-*trans*-retinol (*175*) and ε_{325} = 43,765 $M^{-1}\cdot cm^{-1}$ for 9-*cis*-retinol (*176*). The reactions were started by the addition of cofactor and carried out for 15 min at 37°C in a final volume of 0.5 mL. To measure the steady-state enzymatic activity, the concentration of enzyme was kept from 25- to 100-fold lower than that of the substrate for all the enzymatic assays. The reactions were stopped by the addition of 1 mL of cold methanol and after two rounds of extraction with hexane, retinoids were analyzed by HPLC.

3.2.5 HPLC analysis

Retinoids were analyzed by HPLC as previously described (*56*). Briefly, retinoids were dissolved in 200 μL hexane and injected onto a Nova Pak Silica column (4 μm, 3.9 x 150 mm) (Waters) in hexane:methyl-*tert*-butyl ether (96:4 v/v) mobile phase, at a flow rate of 2 mL/min using a Waters Alliance 2695 HPLC instrument. Elution was monitored at 370 nm for all-*trans*-retinaldehyde, 325 nm for all-*trans*-retinol, 350 nm for all-*trans*-retinoic acid and 9-*cis*-retinoic acid using a Waters 2996 photodiode array detector. Quantification of retinoids was performed by interpolating HPLC peak areas into a calibration curve. All retinoid manipulations were performed under dim or red light to prevent photoisomerization.

3.2.6 Spectrophotometric assays

Activity under standard conditions was measured spectrophotometrically to follow the purification procedure and to check enzyme concentration before each kinetic experiment. Standard activities were measured using 60 mM of D,L-glyceraldehyde as a substrate for AKR1B10 and AKR1B10mF48 and 100 mM for AKR1B10mut. The activity towards aldehydes, with the exception of retinaldehydes, was analyzed spectrophotometrically following the decrease in the absorbance of the cofactor NADPH at 340 nm (ε_{340} = 6,220 $M^{-1}\cdot cm^{-1}$) or at 365 nm in the case of cinnamaldehyde (ε_{365} = 3,510 $M^{-1}\cdot cm^{-1}$)(*174*). Activities were determined in 100 mM sodium phosphate, pH 7.0, at 25°C using 0.2 mM NADPH in 0.2-cm path length cuvettes, with freshly prepared substrate solutions. One unit of activity is defined as the amount of enzyme required to transform 1 μmol of substrate per min at 25°C.

3.2.7 Determination of kinetic constants and inhibition screening

All compounds tested as inhibitors were dissolved in DMSO and assayed in a final concentration of 0.1% (v/v) DMSO using D,L-glyceraldehyde as a substrate at 100mM or 60mM for AKR1B10mut and AKR1B10mF48, respectively. Kinetic constants and IC_{50} (compound concentration that inhibits enzymatic activity by 50%) values were calculated by fitting the initial rates to the appropriate equation using Grafit 5.0 (Eritacus Software) and values were given as the mean ± standard error of three experiments. Standard error values were less than 20% of the mean values.

3.3 Results

3.3.1 Comparison of the structures and catalytic pockets of AKR1B10 and AKR1B15

The small number of substitutions in the active-site of AKR1B15 as compared with AKR1B10 (mainly due to the presence of four Phe residues: Phe299, Phe301, Phe304 and Phe48) may result in a two very distinct enzymes with unique kinetic features. In order to study the effect of these residues in the catalytic properties of this enzymes, we designed two different AKR1B10 mutants, trying to mimic the AKR1B15 active-site. First, by looking at the protein alignment of AKR1B10 and AKR1B15 (Fig. 3.1), we can identify some characteristic features. The catalytic tetrad (Asp44, Tyr49, Lys78 and His111) is strictly conserved and also the majority of the residues are located in loop B. The main differences regarding the active-site pocket are found in loops A and C. Loop A includes four changes (Thr118, Phe122, Met131, Ser133, in AKR1B15, to Ser118, Leu122, Ala131, and Gly133, in AKR1B10), and loop C has seven changes (Phe299, Asp300, Phe301, Lys302, Glu303, Phe304 and Phe310, in AKR1B15, changing to Cys299, Asn300, Val301, Leu302, Gln303, Ser304, and Tyr310, in AKR1B10), which may participate in the shape and flexibility of the active site pocket. In our study, we focused on a segment of residues found at the loop C end, specifically a six consecutive residue (residues 299 to 304) segment of AKR1B15, which is located in the external part of active-site pocket.

Figure 3.1: Alignment of the amino acid sequences of AKR1B10 and AKR1B15. Amino acids of the catalytic tetrad (Asp44, Tyr49, Lys78 and His111) are highlighted in red. The proline at position 24 of AKR1B10, which has been claimed to be responsible for its cytosolic localization (*12*), is colored in blue. The serine at position 8 of AKR1B15, which is mutated in a phenotype with a mitochondrial disease (*101*), is colored in green. The mutated residues, corresponding to AKR1B15, introduced in AKR1B10 are highlighted in yellow.

Comparing the AKR1B10 crystallographic structure (PDB code 1ZUA) and the AKR1B15 computer model (*263*), together with the POVME algorithm volume analysis of the substrate-binding pockets, we noticed that the residues 299 to 304 may have a major implication in the volume differences between the two binding pockets (see Figures 2.9 and 2.13b). Therefore, to compare the substrate-binding site of the enzymes, the contour of the pocket of AKR1B10 incorporating the AKR1B15 residues of loop C (Phe299, Asp300, Phe301, Lys302, Glu303, Phe304) was calculated with the POVME algorithm. Our data showed that the volume of the active-site pocket was drastically reduced, from 279 Å^3 in AKR1B10 to 158 Å^3 in the AKR1B10mut, being more similar to the calculated volume of the AKR1B15 active site (60 Å^3). However, when superimposing the AKR1B15 and AKR1B10mut models, it can be seen that there is an additional Phe in AKR1B15 (Phe48 instead of Val48 in AKR1B10) that conforms a lateral wall of the pocket, decreasing its volume. Phe48 clashes into the calculated volume sphere, indicating that Phe48 is occupying a space in the binding site of AKR1B15, and playing a role in the volume reduction (Fig. 3.2).

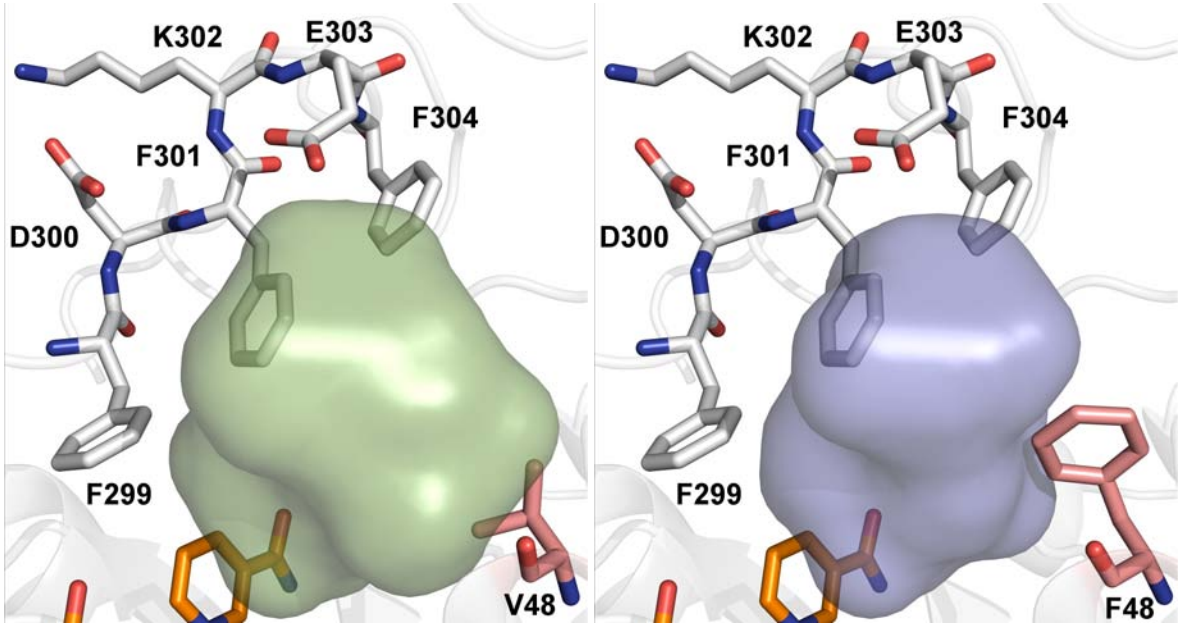

(a) AKR1B10mut model pocket volume (b) Pocket volume of AKR1B15

Figure 3.2: Comparison of the active-site pocket model of (a) AKR1B10mut with the mutated residues 299 to 304, and (b) AKR1B15. NADP$^+$ cofactor is displayed in orange. The surface contour of pockets are shown in green for the AKR1B10mut and blue for AKR1B15. The Val48 and Phe48 residues in AKR1B10mut and AKR1B15, respectively, implicated in the volume change, are displayed in magenta. The AKR1B10mut enzyme showed a reduction of the pocket volume as compared to AKR1B10 (see Fig. 2.9), but the Val48 change to Phe48 in AKR1B15 has an additional role in the reduction of the pocket volume.

3.3.2 Site-directed mutagenesis

AKR1B10 mutants were prepared to investigate the participation of the residues involved in the volume differences, in the remarkable kinetic differences between AKR1B10 and AKR1B15. First,

we mutated six consecutive residues in AKR1B10, that were replaced by their counterparts in AKR1B15: Cys299, Asn300, Val301, Leu302, Gln303 and Ser304 of AKR1B10 were substituted by Phe299, Asp300, Phe301, Lys302, Glu303 and Phe304 found in AKR1B15. This newly engineered mutant enzyme, henceforth called AKR1B10mut, was generated by mutating eight nucleotide positions in order to change the six amino acid residues, in a single mutagenesis step. In addition, we substituted the Val48 present in AKR1B10mut into a Phe48, as in the AKR1B15 pocket, with the aim of making the AKR1B10mut active-site more similar to the AKR1B15 pocket. This new enzyme, henceforth called AKR1B10mF48, incorporates the previous six mutations with the additional Phe48 change. The two mutant enzymes were purified in soluble form, by a similar procedure as that for the wild-type AKR1B10, and with an expression level of $\approx$ 10 - 15 mg/liter of culture. This argues in favor that the residues changed are not responsible for the insolubility of AKR1B15.

3.3.3 Steady-state kinetics of AKR1B10 mutant enzymes with typical AKR substrates

A kinetic characterization of the enzymes was performed using some typical AKR substrates and NADPH as a cofactor (Table 3.1). The steady-state kinetic constants of the AKR1B10mut enzyme show that all the compounds tested were substrates, with k_{cat}/K_m values similar to those previously reported for AKR1B10 and AKR1B15, displaying enzymatic activity towards aliphatic and aromatic aldehydes. However, the mutant enzyme presents both higher K_m and k_{cat} values than those for AKR1B10 and AKR1B15. The substrate with the highest catalytic efficiency for AKR1B10mut was hexanal, showing a $\sim$10-fold increase in the k_{cat}/K_m value compared to the wild-type AKR1B10 and AKR1B15 enzymes. The mutant enzyme shows the highest K_m value for D,L-glyceraldehyde among the human AKR1Bs enzymes. Importantly, the AKR1B10mut enzyme displays a significant activity with ketones, a distinct feature of AKR1B15 (*263*) in comparison with AKR1B10. This suggests that the six mutated residues (299 to 304) contribute to the specificity of AKR1B15 towards these substrates.

To explore the kinetic effect of the decrease of the accessible volume of the substrate binding pocket, produced by Phe48, we studied the kinetics of the AKR1B10mF48 mutant enzyme, which makes AKR1B10 more similar to AKR1B15. In general, AKR1B10mF48 displays similar or lower k_{cat} values for the assayed substrates as compared to AKR1B10mut. Regarding K_m values, the mutant presents in general lower values than the AKR1B10mut enzyme, making it more similar to AKR1B15 than to AKR1B10mut, but without reaching the low K_m values characteristics of the wild-type enzyme, like in the case for hexanal. However, the enzyme still exhibits higher catalytic efficiency for all the assayed substrates compared to the two wild-type enzymes. Interestingly, it has the highest catalytic efficiency with aromatic aldehydes among the human AKR1Bs enzymes, mostly because it exhibits a K_m value similar to that showed by AKR1B10, but with an increased k_{cat} value.

Interestingly, both mutated enzymes exhibit activity towards ketones, an AKR1B15 feature. However, AKR1B10mF48 K_m values with short-chain ketone substrates were more elevated than the values observed with the AKR1B10mut. Hence, in this regard, it is less similar to AKR1B15 than AKR1B10mut although AKR1B10mF48 shows a catalytic site more similar to AKR1B15. Intriguingly, AKR1B10mF48 presents an inhibition of its activity caused by high concentrations of substrate (substrate inhibition). Specifically, this phenomenon was observed with two substrates: citral and cinnamaldehyde, and it is a feature not observed either in the AKR1B10mut or in the wild-type enzymes.

3.3.4 Enzymatic activity with retinoids

AKR1B10mut displays activity with both *trans* and 9-*cis*-retinaldehyde isomers, showing for both of them higher k_{cat} and K_m values than AKR1B10 and AKR1B15 (except for the AKR1B10 k_{cat} value with all-*trans*-retinaldehyde, Table 3.2). Regarding its activity with all-*trans*-retinaldehyde, the K_m value compared to that of AKR1B10 is 10-fold higher (0.6 μM towards AKR1B10 and 6.3 μM for AKR1B10mut), and its k_{cat} value is slightly reduced. As a result of this the catalytic efficiency dropped sharply from 45,000 $mM^{-1}{\cdot}min^{-1}$ in AKR1B10 to 2,500 $mM^{-1}{\cdot}min^{-1}$ in AKR1B10mut. Moreover, the mutations could not make the mutant enzyme more efficient towards 9-*cis*-retinaldehyde, as it should be expected if the mutant were more similar to AKR1B15. This is because its K_m with this isomer increased from 0.16 μM for AKR1B15 to 5 μM for the mutant. Furthermore, although the AKR1B10mut displays activity with retinoids, its k_{cat} values are lower for retinoid substrates than those for the rest.

Similarly to what occurs with the AKR1B10mut, AKR1B10mF48 is also active toward retinoids, with high K_m and k_{cat} values. Importantly, the latter mutant enzyme displays the highest k_{cat} value for all-*trans*-retinaldehyde among all human AKRs (75.4 min^{-1}), but its elevated K_m, ~10-fold higher than that displayed for AKR1B10, results in a drop of its catalytic efficiency compared to wild-type AKR1B10 (45,000 $mM^{-1}{\cdot}min^{-1}$ *vs.* 9,180 $mM^{-1}{\cdot}min^{-1}$ for AKR1B10 and AKR1B10mF48, respectively). Regarding the activity with 9-*cis*-retinaldehyde, AKR1B10mF48 displays a higher catalytic efficiency for this substrate than AKR1B10mut and AKR1B10 wild type, therefore showing more resemblance with AKR1B15.

3.3.5 Determination of the selectivity of various inhibitors for AKR1B10 mutants

We performed a screening assay of AKR1B10mut and AKR1B10mF48 with various inhibitors belonging to different classes (Table 3.3). The selectivity of the inhibitors towards the mutants would give a estimation of the resemblances of their enzyme pockets with those of the wild-type proteins. Regarding the AKR1B10mut, all compounds except sorbinil showed an inhibitory effect, with more selectivity towards the mutant enzyme than for AKR1B15, but with less inhibition than for AKR1B10. The most potent inhibitors towards AKR1B10mut were tolrestat (a carboxylic type

Table 3.1: Kinetic constants of wild-type and mutant AKR1B10, and AKR1B15 with aldehydes and ketones.

Substrate	**AKR1B10mut**			**AKR1B10mF48**			**AKR1B15**			**AKR1B10**		
	K_m (μM)	k_{cat} (min^{-1})	k_{cat}/K_m ($mM^{-1}\cdot min^{-1}$)	K_m (μM)	k_{cat} (min^{-1})	k_{cat}/K_m ($mM^{-1}\cdot min^{-1}$)	K_m (μM)	k_{cat} (min^{-1})	k_{cat}/K_m ($mM^{-1}\cdot min^{-1}$)	K_m (μM)	k_{cat} (min^{-1})	k_{cat}/K_m ($mM^{-1}\cdot min^{-1}$)
Carbohydrate aldehydes												
D,L-glyceraldehyde	11,620	281	24	6,600	200	30.2	880	10.7	12.4	6,000[b]	35[b]	6[b]
Aromatic aldehydes												
pyridine-3-aldehyde	115	808	7,000	8.7	382.3	43,960	3	9	3,150	13[a]	150[a]	12,000[a]
benzaldehyde	286	550	1,920	24.7	348.3	14,100	<1*	12.1	>12,100	9.7[a]	104[a]	11,000[a]
cinnamaldehyde	45	700	15,575	10.8**	427.1**	39,400**	<1*	13.3	>13,300	34.7	240	6,900
Alkanals												
hexanal	25	445	17,900	20.5	320	15,500	3.1	7.3	2,300	112[a]	142[a]	1,300[a]
Alkenals												
acrolein	2,665	558	210	623	288.8	367	36	8.8	240	110[a]	116[a]	1,070[a]
trans-2-hexenal	347	147	423	27.4	77.2	2,820	5	11.3	2,200	28[a]	49[a]	1,700[a]
citral	23	97	4,200	36.2**	124.3**	3,430**	1.5	5.5	3,700	4.5[a]	35[a]	7,400[a]
farnesal	77	45	586	53.2	67.2	1,265	<1*	4.8	>4,800	2.3[a]	30[a]	13,000[a]
Ketones												
2-butanone	213	71	332	46,725	68.3	1.5	780	10.5	13.5	-	LA	-
3-buten-2-one	3,730	380	100	12,760	123.3	9.7	21.3	8.2	380	-	LA	-
3-nonen-2-one	99	80	80	22.2	36.5	1,650	1.7	6.8	4,000	-	LA	-
α-Dicarbonyls												
2,3-butanedione	94	732	790	10.5	438	41.860	<1*	10.6	>10,600	540[c]	260[c]	480[c]
β-Dicarbonyls												
2,4-pentanedione	2,310	162	70	2,490	28.7	11.5	40	2.2	55	58,900	8.6	0.15
3,5-heptanedione	NS	-	-	NS	-	-	1,300	5.3	3.9	NS	-	-
Cofactor												
NADPH	21.9			12.5			6			10		

Enzymatic activity was measured spectrophotometrically. For the determination of the kinetic parameters for NADPH, 3 and 100mM D,L-glyceraldehyde was used for AKR1B15 and AKR1B10mut, respectively, and 60mM was used for AKR1B10mF48 and AKR1B10. LA, low activity (<10 mU/mg) was detected at saturating concentration of substrate; NS, no saturation.
*Because of very low K_m value, data are only approximate. **Data fitted to substrate inhibition equation $v = \frac{Vmax\cdot[S]}{(K_m+[S]+(\frac{[S]^2}{K_i})}$ (*265*)

[a]Data from (*60*), [b](*13*) and [c](*202*).

Table 3.2: Kinetic constants with retinoids of human AKR1Bs and mutant proteins.

Substrate and Parameter	**AKR1B10mut**	**AKR1B10mutF48**	**AKR1B15**[a]	**AKR1B10**[b]	**AKR1B1**[b]
all-*trans*-retinaldehyde					
K_m (μM)	6.3 ± 1.2	8.2 ± 1	1 ± 0.3	0.6 ± 0.1	1.1 ± 0.1
k_{cat} (min^{-1})	15.6 ± 1.5	75.4 ± 3.8	5.4 ± 0.5	27± 1	0.9 ± 0.1
k_{cat}/Km (mM^{-1}·min^{-1})	2,500 ± 550	9,180 ± 1,260	5,300 ± 1,700	45,000,± 7,600	1,300 ± 160
9-*cis*-retinaldehyde					
K_m (μM)	5 ± 1	2.5 ± 0.5	0.16 ± 0.03	0.7 ± 0.1	0.4± 0.1
k_{cat} (min^{-1})	6 ± 0.5	43.0 ± 3.4	3.8 ± 0.2	0.9 ± 0.1	0.7 ± 0.2
k_{cat}/K_m (mM^{-1}·min^{-1})	1,200 ± 280	17,100 ± 3,800	25,600 ± 5,300	1,300 ± 190	1,500 ± 170

Enzymatic activity was mesured by using HPLC-based method. [a]Data taken from (*263*), [b](*13*)

inhibitor) and JF0064 (a non-classical ARI), with IC_{50} values of 0.25 and 0.75 μM, respectively. Tolrestat is one of the most potent inhibitors for AKR1B10 and JF0064 is the most potent inhibitor for AKR1B15. However, in AKR1B10mut they do not show the same inhibitory potency, being $\approx$ 100 fold less potent. The other inhibitors also have reduced potency with this mutant enzyme.

On the other hand, AKR1B10mF48 was only significantly inhibited by JF0064 (IC_{50} = 0.12 μM) and epalrestat (IC_{50} = 17.1 μM). Interestingly, only these two compounds were capable of having an inhibitory effect with AKR1B15 (*263*). All other compounds were not able to decrease the activity of the mutant enzyme (only sulindac showed a minimal inhibitory effect), while they are inhibitors of AKR1B10mut and AKR1B10. In this aspect, AKR1B10mF48 is more similar to AKR1B15 than to AKR1B10.

Table 3.3: IC_{50} values of tested inhibitors with wild-type and mutant AKR1B10 and AKR1B15.

	IC_{50} (μM)			
Inhibitor	**AKR1B10mut**	**AKR1B10mF48**	**AKR1B15**	**AKR1B10**
Tolrestat	0.25	NI	NI[a]	0.006[b]
JF0064	0.75	0.12	0.0034[a]	1.0[e]
Epalrestat	2.6	17.1	>50[a]	0.33[d]
Sorbinil	NI	NI	NI[a]	9.6[c]
Oleanolic acid	3.9	NI	NI[a]	0.09[c]
Sulindac	5.4	>50	NI[a]	0.35[d]

NI, no inhibition or IC_{50} value higher than 100 μM.

[a]Data from (*263*), [b](*43*), [c](*92*), [d](*84*), [e](*60*).

3.4 Discussion

AKR1B10 is unique within the AKR1B family in that it displays a high catalytic efficiency with all-*trans*-retinaldehyde. On the other hand, AKR1B15 showed a high k_{cat}/K_m value towards 9-*cis*-retinaldehyde, similar to that of AKR1C3 (*168*). Although AKR1B10 and AKR1B15 have a high amino acid sequence identity (92%), their active-site pocket is the most divergent part between the two proteins, as it can be seen in the sequence alignment (Figure 3.1). Interestingly, out of the 27 residue substitutions of AKR1B15, with regard to AKR1B10, six are changes to a Phe residue, a bulkier hydrophobic amino acid. Specifically, in loop C, we find that Cys299, Val301, Ser304 and Tyr310 are replaced by four Phe residues in AKR1B15, in addition to the Val48Phe and Leu122Phe changes. The introduction of these voluminous residues is crucial for the volume reduction of the catalytic-site pocket of AKR1B15 (*263*), contributing to its shape and flexibility. Due to its hydrophobicity, Phe is commonly found buried in proteins, where it can interact through its phenyl ring with other aromatic systems adding stability to the folded protein structure.

The calculated volume of the AKR1B0mut was 158 Å^3, an intermediate value between those of

AKR1B10 and AKR1B15, mainly as the result of the incorporation of three Phe residues located in loop C. It has to be noted that the volume of a binding site pocket has great pharmacological significance, because it is an important structural feature for recognising the pharmacophores and it is used in SAR (Structure-Activity Relationship) studies. For example, when the volume of a catalytic pocket site is known, potential ligands and inhibitors that are too large to fit within that volume can be eliminated in the lead-generation process, prior to virtual or high-throughput screening. Additionally, when multiple structures of the same protein are available, the variation in their binding pocket size and shape can be useful to understand the protein dynamics (*193*).

Interestingly, the k_{cat} values of AKR1B10mut and AKR1B10mF48 increased for most of the substrates as compared to wild-type enzymes. This indicates that the rate limiting, the slower step in the catalytic mechanism, presumably the release of the oxidised cofactor is faster in the mutants.

AKR1B10mut displays activity with retinoids, but its k_{cat} values are lower for retinoids than for the rest of substrates, resulting in catalytic efficiencies intermediate between the two wild-type enzymes, similar to those showed by AKR1B1. This low k_{cat} suggests a change in the limiting step of the catalyzed reaction with retinoids. Overall, the results show that the AKR1B10mut has lost the high catalytic efficiency towards all-*trans*-retinaldehyde but without gaining the specificity for the 9-*cis*-retinaldehy, a characteristic property of AKR1B15. Regarding to AKR1B10mF48 activity with retinoids, an interesting feature is that it showed similar catalytic constant values to those displayed with other substrates, indicating that possibly there is no change in the limiting step of the reaction for this mutant, similar to AKR1B15, and in contrast with what occurs in AKR1B10, AKR1B1 and AKR1B10mut. Thereby, in this feature AKR1B10mF48 mimics AKR1B15, since the enzyme has also similar turnover values for all the examined substrates, although the k_{cat} values of the mutant enzyme are much higher. In addition, the mutant has high catalytic efficiency with 9-*cis*-retinaldehyde, although with a K_m value much higher than that displayed by AKR1B15.

Overall, it can be concluded that the catalytic features are not conserved in the mutated enzymes, and that the introduced mutations may have induced a change or rearrangement of the entire structure or the loop region of the enzyme, or the active-site pocket. This results in high k_{cat} values for all substrates. Additional residue differences between AKR1B10 and AKR1B15 might be important for their distinct features. However, both mutant enzymes achieve some of the kinetic features of AKR1B15, being the activity toward ketones the most important one, but fail in reaching the high specificity observed for 9-*cis*-retinaldehyde that is distinctive of AKR1B15. AKR1B10mF48 displayed another important property of AKR1B15, which is that there is no great change in k_{cat} values between retinoids and the other substrates. This suggests that the limiting step is the same for all substrates in the two enzymes.

The inhibitor screening with both AKR1B10 mutant enzymes reported valuable information to understand the structural basis of the distinct inhibitory properties of AKR1B15. Both mutants enzymes showed very different inhibitor selectivity for some of the most potent inhibitors known

for AKR1B10. An interesting observation is the effect of DMSO on the activity and stability of the enzymes. AKR1B10, with 1% DMSO, displayed 89% activity compared with the same activity without DSMO, while the values for the remaining enzymes were AKR1B10mut ≈ 25.8%, AKR1B10mF48 ≈ 24% and AKR1B15 ≈ 23%. This shows that the wild-type AKR1B15 and the AKR1B10 mutants seem to be less stable than AKR1B10 in the presence of organic solvents, and that the substitutions performed are related for this lower stability. For this reason, the inhibition screening for these three enzymes was carried at a lower concentration of DMSO (0.1%) to avoid the inactivation of the enzyme. The AKR1B10mut was inhibited by all the tested inhibitors except by sorbinil, but in general all the inhibitors were less potent than against AKR1B10. The only inhibitor that increased its inhibitory effect for the mutant enzymes was the non-classical aldose reductase inhibitor JF0064, the only that significantly inhibits AKR1B15. The hydrophobic pocket formed by voluminous Phe residues (Phe48, Phe 299, Phe301 and Phe304) in the external region of the active site of AKR1B15, shows more rigidity in comparison to that of AKR1B10. This feature could be responsible in AKR1B15 for the difficulty in opening the specificity pocket, described for ARI binding to AKR1B10 and AKR1B1, as the region that holds the hydrophobic moiety of inhibitors, and the low inhibition profile of AKR1B15 (*92*, *205*, *263*). AKR1B10mut contains some of these bulky residues and this may explain why some compounds are not as powerful inhibitors for this enzyme as for AKR1B10.

The similarity towards AKR1B15 increased when AKR1B10mF48 was examined. With this enzyme, the only inhibitors that display an inhibitory effect were JF0064 and epalrestat (Table 3.3), and like in the case of AKR1B15, tolrestat, sorbinil, oleanolic acid and sulindac were not able to inhibit the enzyme. Additionally, JF0064 was by far the most potent inhibitor, increasing its inhibitory potency as compared to that for AKR1B10mut, inhibiting AKR1B10mutF48 at nanomolar concentration level, although with lower potency than against wild-type enzyme. This suggests that the residue 48 is important for the inhibitory effect, and it seems that the Phe at this position adds further steric hindrance for the binding of these compounds to the AKR1B10 active site.

Recently, it has been proposed that the protein function may involve multiple conformations, and flexibility may be closely linked to protein function, including enzyme catalysis (*266–268*). Most proteins, and hence enzymes, are relatively large and flexible molecules due to the non-covalent nature of their folded 3D structure (*269*). Enzyme catalysis involves binding of substrates, chemical transformation, and release of products, being a dynamic process that often involves conformational transitions (*267*). In enzymes, substrate binding can lead to the repositioning of catalytic groups, and this flexibility and dynamic process may help substrate fitting and facilitate the catalysis, reflecting the functional importance of flexible regions (*270*). Moreover, the binding and release of ligands is often accompanied by conformational changes, from subtle or minimal to important ones, and these conformational changes may be rate-limiting in the reaction scheme. Some of these changes include motions of backbone and side-chain atoms that may be required

for molecular recognition of substrate, to exclude water or for repositioning of catalytic residues, and large-scale conformational rearrangements may be required to achieve the active form of the enzyme, or in each step of the catalytic cycle. (*267–269*, *271*). Also, the enzymatic activity is known to require a precise balance between flexibility and stability (*272*). Protein dynamics is also critical for ligand or inhibitor binding, and that flexibility is key to ligand recognition. All these considerations have made some authors suggest that it is difficult to predict the ligand binding based on structural information alone, because protein flexibility may lead to unexpected ligand-binding orientations or sites (*266*, *269*). In *E.coli* dihydrofolate reductase (DHFR), for example, it has been reported that changes in the active-site volume, brought about by changing a residue of the catalytic pocket, modifies the hydride transfer donor-acceptor distance, affecting its catalytic efficiency (*268*). Similar effects of active site volume variations have been proposed for other enzymes (*273–276*). Moreover, it has also been reported that changes remote from the active-site of the HIV-1 protease are shown to alter the dynamics of the whole enzyme, and modify its substrate turnover and inhibitor binding by modulating enzyme activity (*270*). A closer and more related example is the case of AKR1D1 or steroid 5β-reductase. AKR1D1 catalyzes a crucial step in bile-acid biosynthesis to produce sterols that have emulsifying properties. There are seven point mutations associated with this disease in AKR1D1, but the mapping of these mutations to the AKR1D1 structure provides no obvious evidence as to why the enzymes have no function, since they are not located in the cofactor or the steroid binding site, or in the active site. It was pointed that these mutants were less stable (*277–279*).

Taken together, these experimental results and theoretical considerations may explain the differences observed between AKR1B10 and AKR1B15, and can also shed some light on the unexpected increase in the turnover rate (k_{cat}) value and catalytic efficiency (k_{cat}/K_m) observed in the mutant enzymes. For example, in AKR1B10, the highest mobility, as derived from the thermal B factors, corresponds to a region from Lys-125 to Ala-131 included in the loop A, which contributes to the upper lid of the active-site pocket (*13*). The six consecutive changed residues in the mutant enzyme can somewhat affect the global flexibility and dynamics of the whole enzyme, as indicated by the important effect in the AKR1B10 kinetics. The additional Phe48 mutation provokes also changes in the kinetic features of the enzyme, especially in the binding of the inhibitors, and in the rate-limiting step (all substrates had a very similar turnover rate, unlike AKR1B10 and AKR1B10mut, that display a drop in their k_{cat} values with retinoids). However, we were not fully successful in making AKR1B15 from a mutated AKR1B10, since kinetic properties were only partially reproduced. This indicates that additional residues between the two enzymes, not mutated here, 21 for AKR1B10mut and 20 for AKR1B10mF48, although not involved in the active site, may have an effect in the dynamics and flexibility of the protein, affecting the conformational changes needed for the correct substrate recognition, repositioning of catalytic groups and other dynamic features. It could not be discarded the contribution of the residue at position 122, Leu in AKR1B10 and Phe in AKR1B15. This residue is not directly involved in the binding pocket, since it is located in the

external part of the loop A, relatively exposed to solvent. However, the hydrophobic character of Phe limits its exposure to the solvent, thus it could be positioned more buried within the protein to avoid its exposure, facilitating a possible stacking interaction with Phe48. This shift would affect the flexibility and positioning of the residues of the loop, and could alter the general dynamics of the enzyme.

Chapter 4

Characterization of AKR1B16, a new mouse AKR

4.1 Introduction

There are three AKR families in mammals, AKR1, AKR6 and AKR7 (*9*). AKR6 family members are structural proteins related to the regulation of the voltage-gated potassium channels, being their β subunits (*29*). AKR1B7 are involved in the reduction of the toxin aflatoxin produced by the fungus *Aspergillus flavus* (*280*). AKR1 is the largest family of AKRs, comprising the AKR1A (aldehyde reductase), AKR1B (aldose reductase), AKR1C (hydroxysteroid reductase), AKR1D (ketosteroid reductase) and AKR1E subfamilies.

The AKR1C, 1D, and 1E subfamilies are important key enzymes in the metabolism of hormones, including androgens, estrogens, and progesterone, as well as prostaglandins (*281*). The AKR1C subfamily has been studied as drug target for its role in the detoxification of xenobiotics and its selective metabolism of steroid hormones. The AKR1B family is responsible for the reduction of toxic aldehydes generated during lipid peroxidation and steroidogenesis, and also has prostaglandine F2α synthase activity (*282*).

Rats and mice are model animals widely use in laboratory research for the study *in vivo* of numerous diseases and unravel the physiological function of genes and proteins. Some rodent gens are directly correlated to human genes, however, regarding the AKRs, this is not the case. This difference between human and rodent AKR, in general without clearly orthologous genes, impedes the use of transgenic and knockout animals as a model for the study of the physiological role of these enzymes in humans (*6*). However, although their orthology is not clear, genetic studies had grouped the human and rodent genes in the same clusters. In addition, the human and rodent AKR1B proteins differ in their kinetic constants for common carbonyl substrates and activity with prostaglandins (*60*, *282–284*). It is interesting that human AKR1B1 protein is an homologue of mouse AKR1B3, whereas AKR1B10 is not homologous to either mouse AKR1B7 or AKR1B8. A widely accepted group of ortholeg proteins is the aldose reductase cluster, with comprises AKR1B1 (human), AKR1B13 (mouse) and AKR1B4 (rat) (Fig. 4.2) (*168*).

The *AKR1B* genes in these species are clustered in a very similar way, including additional flanking genes, in different chromosomes. In human these genes are located in chromosome 7q33-35, in mouse are found in chromosome 6 and in chromosome 4 in rat. The direction of transcription is conserved for all the *AKR1B* genes although they are not located in the same chromosome, and all them comprise 10 exons. All have high sequence homology and synteny, and the physical co-localization of genetic loci and conservation of blocks indicate that the *AKR1B* genes existed before the divergence of rodents and primates, and they may have arisen from a single gene by tandem gene duplication in a recent event (*285*). There are three human genes: *AKR1B1*, *AKR1B10* and *AKR1B15*, while four genes are found in each murine species. In mouse: *Akr1b3* (aldose reductase), *Akr1b7* (previously named mouse vas deferens protein, MVDP), *Akr1b8* (previously named mouse fibroblast growth factor regulated protein (FR-1)), and the gene whose protein is studied in this Thesis, *Akr1b16*. In rat: *Akr1b4*, *Akr1b13* (previously named *Akr1b8*), *Akr1b14*

(previously *Akr1b7*) and *Akr1b17* (previously *Akr1b10*).

In the present work we aim to characterize the function of the novel mouse gene *Akr1b16*. Previous studies determined that *Akr1b16* was ubiquitously expressed in tissues, with the highest levels found in spleen, lung and heart, and lower levels in liver, kidney and brain, but no presence was found in testes (*11*). However, these studies were not able to perform an enzymatic characterization of AKR1B16, since it was found expressed in the insoluble fraction of cell lysates, although its localization was cytosolic when expressed in mammalian systems. Here we expressed an active protein and performed a kinetic characterization to investigate whether it could be the ortholog of the human AKR1B10. The finding of an AKR1B10 ortholog will enable the use of transgenic and mouse knockout technologies to study its physiological function.

4.1.1 AKR1B3, mouse aldose reductase

Akr1b3 was first isolated from a mouse kidney library from Gui and collaborators in 1995 and identified as a homologue of human aldose reductase (AKR1B1). It was found to be abundant in testis, skeletal muscle and kidney, less abundant in the ovary, vas deferens, retina and brain, and it was hardly detectable in the liver (*105*). However, a recent study determined that *Akr1b3* mRNA was 20-fold more prevalent in brain than in other tissues (*281*). The *akr1b3* gene is located in the chromosome 6, is approximately 14.2 kb in size, and the genomic organization is conserved among the human, rat and rabbit aldose reductase genes (*286*). AKR1B3 has been widely studied in *in vivo* models due to the crucial role of AKR1B1 in the development of diabetic complications. AKR1B3, being the orthologue in mouse, given the possibility to perform *in vivo* and knockout studies. In humans, the higher level of AKR1B1 expression is associated with toxicity. However, it has been noted that hyperglycemic mice are resistant to sugar-induced cataract, and levels of aldose reductase activity and sorbitol are significantly lower in mice than in rats or humans (*286*). Moreover, similar pharmacological effects of toxicity are not observed in mice unless they express a human AKR1B1 transgene. This is thought to be because mice have lower levels of AKR1B3 expression, probably insufficient to generate toxic byproducts (*287*).

Akr1b3 gene is regulated through its promoter. It has regulation by the transcription factor Nrf2 in the AP1 site located in 5'-flaking region of the gene. Nrf2 is known to be involved in the transcriptional regulation of detoxification enzymes (*40*). Another major transcriptional control element involved in the up-regulation of AKR1B1 promoter activity under hypertonic conditions is TonE (tonicity response element) (*286*). It is known that AKR1B family members (AKR1B3, AKR1B7, and AKR1B8) also possess prostaglandin $F_{2\alpha}$ synthase activity (*282*) and a recent study (*55*) has found that *Akr1b3* was expressed in preadipocytes and it has been identified as the prostaglandine $F_{2\alpha}$ synthase (PGFS) that works in adipocytes, acting in the regulation of white adipose tissue (WAT). However, it was found that the *Akr1b3* ablation in mice had no impact on adipose tissues, whereas loss of *Akr1b7* induced an expansion of fat (*55*). Moreover, it has been suggested that the prostaglandine $F_{2\alpha}$ produced by AKR1B3 suppresses adipocyte differentiation

in early stages of adipogenesis (*288*).

Enzymatically, AKR1B3 acts as an aldose reductase, showing similar K_m values for glucose (82 mM (*105*)) and catalytic efficiency for D,L-glyceraldehyde that human AKR1B1, and exhibits low activity with retinaldehyde (*168*). Another study also points to the similarity of AKR1B3 and AKR1B1 through its PGFS activity, being more selective than other AKRs such as AKR1B7, AKR1C3 and AKR5A2, and suggests that the tertiary structure of the catalytic pocket, for binding $PGF_{2\alpha}$ is similar in AKR1B3 and AKR1B1 and different from that of other members of the AKR family (*289*).

4.1.2 AKR1B7, mouse *vas deferens* protein (MVDP)

AKR1B7 was first discovered and isolated by Pailouc and collaborators from the mouse vas deferens, a part of the male reproductive system (*106*). They found that the protein was androgen dependent, the castration of the animals decreased the amount of *Akr1b7* mRNA after 30 days, and the androgen administration restores the previously observed levels of protein (*106*). Other studies have shown that Akr1b7 mRNA was highly expressed in the small intestine, with similar amounts in duodenum, jejunum, and ileum. There was also *Akr1b7* mRNA in kidney, but in much lower amount than the levels found in the small intestine (*281*) and adipose tissue (*290*). It was found *Akr1b7* mRNA in female reproductive system after stimulation by luteinizing hormone (LH) or human chorionic gonadotropin (hCG), but restricted to theca and stromal cells (*291*). Other studies point that AKR1B7 is androgen dependent in the vas deferens. No differences in its expression have been found between male and female in non-sexual tissues (*292*).

Regarding the functions of AKR1B7, it is thought to be important for metabolizing 3-keto bile acids to 3β-hydroxy bile acids, that are toxic to cultured cells, and it is also able to reduce isocaproaldehyde and 4-HNE (*18*). Thus, one of the major functions of AKR1B7 is to detoxify lipid peroxidation products. This is supported by the fact that the *Akr1b7* gene promoter has response elements to xenobiotics receptors (*293*) and farnesoid X receptors (FXR) (*284*), that activate its expression and induce AKR1B7 to detoxify lipid peroxidation products and bile acids. In addition, it is an important factor in the differentiation process leading to fully mature adipocytes, being associated with a higher ratio of preadipocytes *vs.* adipocytes. The cells that express AKR1B7 did not contain lipid droplets, and the expression level of AKR1B7 was very low in mature adipocytes (*290*). Moreover, and as said before, the ablation of this gene in mice produces an expansion of fat (*55*, *294*), having an antiadipogenic action when is overexpressed in 3T3-L1 preadipocytes (*290*). Therefore, it is thought that AKR1B7 can regulate white adipose tissue (WAT) development through two $PGF_{2\alpha}$ related mechanisms: the inhibition of adipogenesis and lipogenesis (*294*). Moreover, another work with an AKR1B7 mutant mice studied the role of AKR1B7 in the female reproductive physiology, particularly in the ovulatory process, but no differences were observed either in the reproductive function, suggesting that AKR1B7 has a dispensable role in the ovaric function, or in female fertility. The authors point that the reason could be the existance

of compensatory mechanisms such as AKR1B8 or gluthatione-S-transferases (*291*). Another study suggests that *Akr1b7* and the renin gene are coexpressed and regulated by the same factors and therefore AKR1B7 can be considered a renin marker, because allows the identification of those cells that were programmed to express renin, although its function in these cells remains unknown (*111*).

4.1.3 AKR1B8, fibroblast-dependent growth factor 1 (FR-1)

AKR1B8 was first identified by Donohue and collaborators when searching for genes inducible by fibroblast growth factor (FGF)-1 in mouse fibroblast cell culture (*107*). Tissue distribution studies reported that AKR1B8 is mainly expressed in the colon and small bowel, and in lower level in stomach, liver and brain (*108*). In another report, AKR1B8 was found expressed in equal amounts in heart, liver, spleen, colon, testis and lung, and also in brain and kidney but with lower expression (*11*). In contrast, another study found the highest mRNA levels located in testes and stomach (*281*).

Regarding its catalytic activity, AKR1B8 is capable of reducing aromatic and aliphatic aldehydes, but it has little activity with glucose, suggesting that the enzyme probably does not have a role in its metabolism *in vivo* (*109*). Futhermore, it has the ability to reduce highly reactive products produced during lipid peroxidation of polyunsatured fatty acids and phospholipid aldehydes. Compared to AKR1B7, it is more efficient in the reduction of short chain aldehydes and it seems to be the most efficient 4-HNE reductase in mouse tissues (*109*, *295*). AKR1B8 was shown to associate with the lipogenic acetyl-CoA carboxylase α (ACCA) in murine colon cancer cells. This fact and its capacity of reducing carbonyls derived from a broad range of structural classes including both aromatic and aliphatic aldehydes, have made some groups suggest that AKR1B8 is the mouse ortholog of human AKR1B10 (82.3% sequence identity), although it does not display high retinaldehyde reductase activity (*108*).

4.2 Experimental procedures

4.2.1 Expression and purification of AKR1B16

E. coli BL21(DE3) containing pBB540, pBB542 and pET-28a/Akr1b16 was grown in 4 L of M9 minimal medium supplemented with 0.4% glucose as a carbon source, in the presence of 34 μg/mL chloramphenicol, 50 μg/mL spectinomycin and 33 μg/mL kanamycin. Protein expression was then induced by the addition of 1 mM IPTG (Apollo Scientific) and cells were further incubated for 4 h at 22°C. Cells were pelleted and resuspended in ice-cold TBI buffer (150 mM NaCl, 10 mM Tris-HCl, 5 mM imidazole, pH 8.0). The protein was purified using a His-Trap HP nickel-charged chelating Sepharose Fast Flow (GE Healthcare) 5 mL column using an AKTA FPLC purification system. The column was washed with TBI buffer and the enzyme was eluted stepwise with 5, 60, 100 and 500 mM imidazole in TBI buffer. The enzyme fraction eluted with 100 mM imidazole

was loaded onto a PD-10 column (Millipore), which removed imidazole and changed the buffer to storage buffer (200 mM potassium phosphate, pH 7.4, 5 mM EDTA, 5 mM DTT).

4.2.2 Spectrophotometric assays

AKR1B16 activity under standard conditions was measured spectrophotometrically to follow the purification steps and to check enzyme concentration before each kinetic experiment. Standard activities were measured by using 10 mM D,L-glyceraldehyde as a substrate. The activity towards aldehydes, with the exception of retinaldehydes, was analyzed following the decrease in the absorbance of the cofactor NADPH at 340 nm (ε_{340} = 6,220 $M^{-1}{\cdot}cm^{-1}$) or at 365 nm in the case of cinnamaldehyde (ε_{365} = 3,510 $M^{-1}{\cdot}cm^{-1}$)(*174*). Activities were determined in 100 mM sodium phosphate, pH 7.0, at 25°C using 0.2 mM NADPH in 0.2-cm path length cuvettes, with freshly prepared substrate solutions. One unit of activity is defined as the amount of enzyme required to transform 1 μmol of substrate per min at 25°C.

4.2.3 Determination of kinetic constants and inhibition screening

All compounds tested as inhibitors were dissolved in DMSO and assayed in a final concentration of 0.1% (v/v) DMSO using 10 mM of D,L-glyceraldehyde as a substrate. Kinetic constant and IC_{50} (compound concentration that inhibits enzymatic activity by 50%) values were calculated by fitting the initial rates to the appropriate equation using Grafit 5.0 (Eritacus Software) and values were given as the mean ± standard error of three experiments. Standard error values were lower than 20% of the mean values.

4.2.4 HPLC enzymatic activity assay

Activity assays with retinoids were carried out using an HPLC-based methodology (*56*). Briefly, retinaldehyde isomers were solubilized using glass tubes by a 10-min sonication at molar ratio 1:1 with fatty acid-free bovine serum albumin in 90 mM potassium phosphate, 40 mM potassium chloride, pH 7.4. The actual amount of solubilized retinoid was determined based on the corresponding molar absorption coefficient in aqueous solutions at the appropriate wavelength: (ε_{400} = 29,500 $M^{-1}{\cdot}cm^{-1}$ for all-*trans*-retinaldehyde and ε_{367} = 26,700 $M^{-1}{\cdot}cm^{-1}$ for 9-*cis*-retinaldehyde (*56*). For retinol isomers, which were used as standards of the reaction product, their concentration was determined in hexane using ε_{325} = 51,770 $M^{-1}{\cdot}cm^{-1}$ for all-*trans*- retinol (*175*) and ε_{325} = 43,765 $M^{-1}{\cdot}cm^{-1}$ for 9-*cis*-retinol (*176*). The reactions were started by the addition of cofactor and carried out for 15 min at 37°C in a final volume of 0.5 mL. With the aim to measure the steady-state enzymatic activity, the concentration of enzyme was kept from 25- to 100-fold lower than that of the substrate for all the enzymatic assays. The reactions were stopped by the addition of 1 mL of cold methanol and after two rounds of extraction with hexane, retinoids were analyzed by HPLC.

4.2.5 HPLC analysis

Retinoids were analyzed by HPLC as previously described (*56*). Briefly, retinoids were dissolved in 200 μL of hexane and injected onto a Nova Pak Silica column (4 μm, 3.9 x 150 mm) (Waters) in hexane:methyl-*tert*-butyl ether (96:4, v/v) mobile phase, at a flow rate of 2 mL/min using a Waters Alliance 2695 HPLC instrument. Elution was monitored at 370 nm for all-*trans*-retinaldehyde and at 325 nm for all-*trans*-retinol using a Waters 2996 photodiode array detector. Quantification of retinoids was performed by interpolating HPLC peak areas into a calibration curve. All retinoid manipulations were performed under dim or red light to prevent photoisomerization.

4.2.6 Alignment of DNA sequences and generation of an AKR1B16 model

AKR1B human and murine sequences were gathered at UniProt data bank and analysis was performed using the ESPript 3.0 server (*264*). The AKR1B16 model was build using automated protein structure homology modelling server, the SWISS-MODEL (*296*, *297*). The volume of the active-site pocket was measured by using the POVME algorithm (*193*), whereas PyMOL was used for figure drawing.

4.3 Results

4.3.1 Sequence alignment

The amino acid sequences of human and murine AKR1B members are aligned in Figure 4.1, with the loops A and C, where the majority of differences of the substrate binding site are located, and loop B, which mainly determines the coenzyme binding site. The characteristic catalityc tetrade of the family (Asp44, Tyr49, Lys78 and His111) is conserved among all the proteins. As said before, it can be observed that the zone of the alignment where the majority of residue changes are located is in loop A and mainly in loop C. In the other hand, loop B is far more conserved because it is there where the residues interacting with NADP are located. The three loops have many identical residues, principally those forming the secondary structures in α-helix, β-sheet and β-turns (Fig. 4.1). Notably, a zone where a wide difference in the amino acid sequence can be found is between residues 80 to 100, which form a α-helix and a turn, close to the catalytic conserved residue Lys78. As noted by Ruiz *et al.*(*168*), all the murine proteins of similar aldose reductase type share a common Leu125 (AKR1B1, AKR1B3 and AKR1B4), while all the other enzymes (with the exception of AKR1B16 and AKR1B17 that have a threonine) share a common residue Lys125, that appeared to be an important determinant for all-*trans*-retinaldehyde specificity, at least in AKR1B10 (*13*). A similar substitution pattern also occurs with the residues Leu5, Asn9, Thr11, Leu16, Thr29, Val57, Leu63, Val67, His84, Thr114, Asp135, Thr141, Ile157, Ile170, Val182, Arg233, Pro253, Leu258, Gln275 and Lys308, in which the human and murine aldose reductase proteins (see phylogenetic tree in figure 4.2) have identical residues.

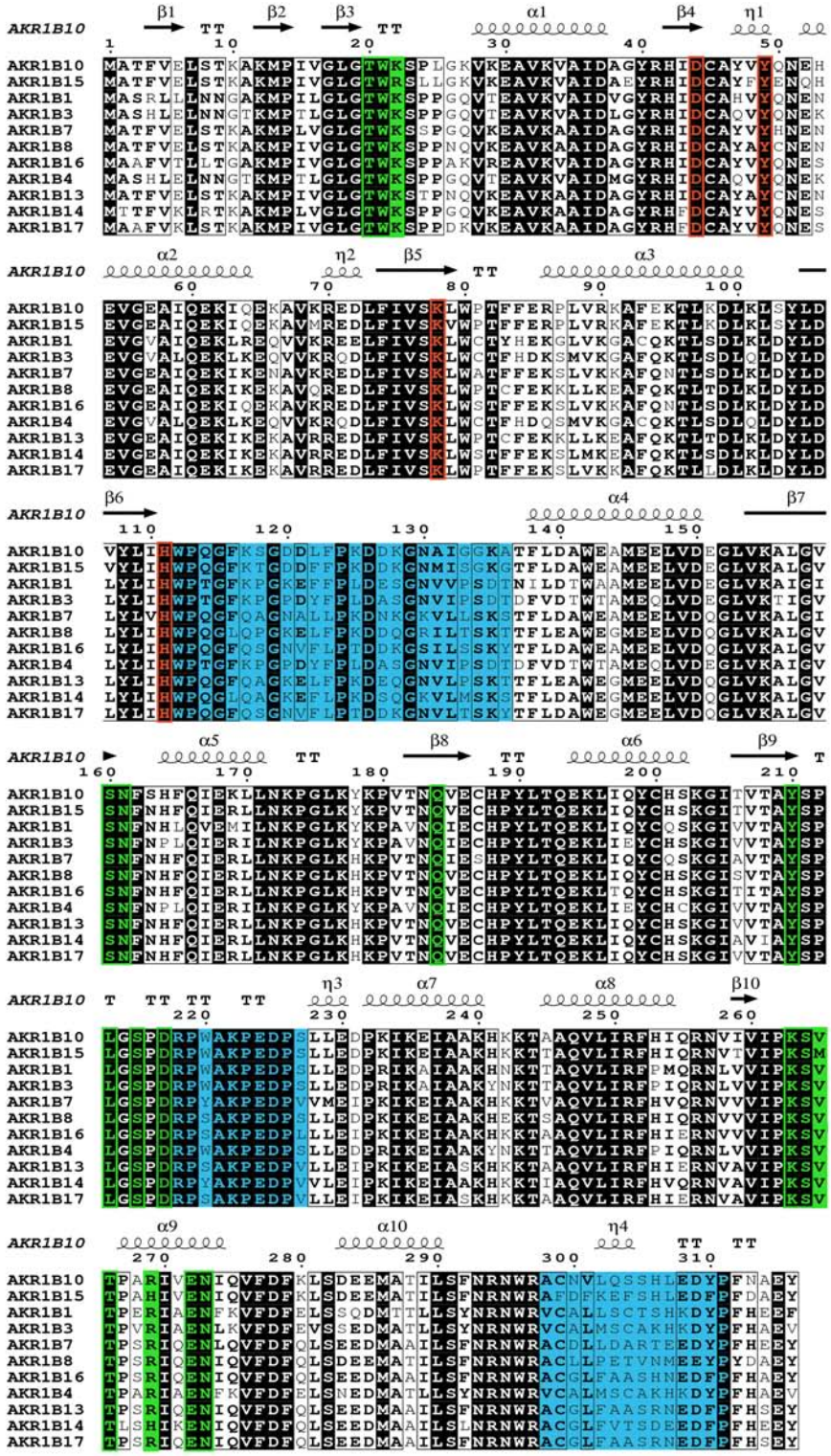

Figure 4.1: Alignment of human and murine AKR1B amino acid sequences. The conserved catalytic tetrad (Asp44, Tyr49, Lys78 and His111) is highlighted in red. Loops A, B and C are colored in blue. Important residues for the binding of cofactor are displayed in green. Secondary structure elements, obtained from AKR1B10 crystal structure (PDB 1ZUA), are shown above the sequence: α-helices are displayed as squiggles, β-strands are rendered as arrows and strict α and β turns are displayed as TT (*264*).

Table 4.1: Percentage of amino acid identity between human and murine AKR1B sequences.

AKR1B10	AKR1B15	AKR1B3	AKR1B7	AKR1B8	AKR1B16	AKR1B4	AKR1B13	AKR1B14	AKR1B17		
70.6	67.4	85.4	71.2	70.3	70.3	85.4	70.6	69.0	69.6	**AKR1B1**	Human
	91.5	70.3	79.7	82.3	82.9	70.9	81.0	78.2	82.6	**AKR1B10**	Human
		67.4	76.9	80.4	80.4	68.0	79.1	76.9	80.1	**AKR1B15**	Human
			69.3	69.0	69.6	96.8	68.7	67.4	69.0	**AKR1B3**	Mouse
				82.3	84.8	69.0	85.1	86.7	85.4	**AKR1B7**	Mouse
					82.6	69.0	90.2	83.5	84.5	**AKR1B8**	Mouse
						69.6	86.4	84.8	92.4	**AKR1B16**	Mouse
							68.7	67.4	69.0	**AKR1B4**	Rat
								87.3	92.1	**AKR1B13**	Rat
									88.3	**AKR1B14**	Rat

4.3.2 Phylogenetic tree analysis

All the mammalian and murine proteins of the AKR1B family are closely related, with sequences that show 67.4 to 96.8% of amino acid identity as shown in Table 4.1. AKR1B16 displays a high degree of identity with all the human AKR1B members, but specially with AKR1B10 (82.9%). However, the highest sequence identity between human and mice AKR1Bs is displayed by AKR1B1 and AKR1B3 with a 85.4%. It is thought that these are ortholeg proteins (*105*), with similar tissue distribution and typically enzymatic characteristics of aldose reductase. Indeed, in the phylogenetic tree they are located in the aldose reductase cluster (figure 4.2), together with AKR1B4. Remarkably, rat AKR1B4 and mouse AKR1B3 display the highest identity between members of the AKR1B subfamily, (96.8%). Interestingly, the second proteins in identity between mouse and human are AKR1B10 and the recently discovered AKR1B16 (82.9%), although they are not clustered together in the phylogenetic tree. In fact, the protein with the most resemblant sequence to mouse AKR1B16 is rat AKR1B17 (92.4%) which are very close in the cluster formed by the AKR1B7 type proteins. As pointed by Ruiz and collaborators (*168*), the AKR1B proteins can be grouped in 4 different clusters based on the phylogenetic analyses, and our results agree with this grouping. Thus the aldose reductase type proteins are clustered together (AKR1B3, AKR1B4 and AKR1B1), and they seem clearly orthologous proteins based on their enzymatic activity with glucose, although they have different expression patterns (*109*, *168*, *295*); the AKR1B8 cluster formed by rat AKR1B13, mouse 1B8 and Chinese hamster 1B9, being closely related; the AKR1B7 type cluster, where the rat proteins AKR1B7, 1B14 together with mouse 1B17 and the new mouse AKR1B16 are localised. Finally, the human AKR1B10 and AKR1B15 join together in a distinct cluster with only the rabbit AKR1B19 protein localised near them. It is interesting that both

AKR1B15 and AKR1B19 had showed significant hydroxysteroid dehydrogenase (HSD) activity, (*12*, *298*), but not AKR1B10 that only exhibits low 20α-HSD activity (*60*).

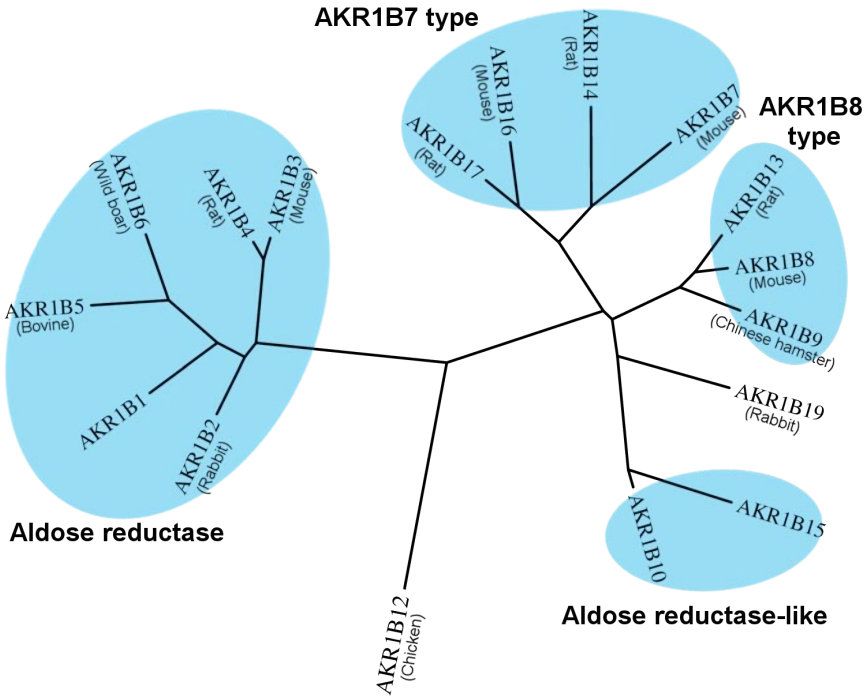

Figure 4.2: Unrooted phylogenetic tree of the all known proteins of the AKR1B family. Different clusters are indicated by shaded ovals. Non labeled proteins are human proteins. Labels; rat (*Ratus norvegicus*), mouse (*Mus musculus*), chicken (*Gallus gallus*), rabbit (*Oryctolagus cuniculus*), Chinese hamster (*Cricetulus griseus*), bovine (*Bos taurus*) and wild boar (*Sus scrofa*). Data was obtained from different databases, for multiple alignment, and TreeDyn to build a radial dendrogram, from the site (http://www.phylogeny.fr). Chicken AKR1B12 was used as an out-group. Based on (*168*)

4.3.3 Analysis of the AKR1B16 structural model

A model of the AKR1B16 protein was built with the aim to analyse the catalytic site of AKR1B16 and to compare its structure with other AKR (Fig. 4.3). The model was built using the SWISS-MODEL server, and automated system for modelling the 3D structure of a protein from its amino acid sequence using homology modelling techniques. The program gives an automated model quality estimation to select the most suitable templates, based on the QMEAN potential (*296*, *297*). For the building of the AKR1B16 model the program selected the crystallographic structure of the rat enzyme AKR1B14 (PDB 3qkz.2.A) with a sequence identity of 84.8%. Additionally, it has to be noticed that this template is an AKR1B14 mutant, in which the His269 had been mutated to Arg (H269R). In the alignment of the human and murine sequences (Fig 4.1), it can bee seen that all AKRs (with the exception of AKR1B15 and AKR1B14) have the NADPH binding site residues conserved with an arginine at position 269. Thus, the mutant AKR1B14 His269Arg is well

fitted to be used as a template for the model, because AKR1B16 also has an Arg at thus position. The global and per-residue model quality was assessed using the QMEAN scoring function. The analysis indicates the reliability of the model, with a QMEAN4 score of -0.73, and with all the Z-scores being consistent with the good quality of the structure (*297*).

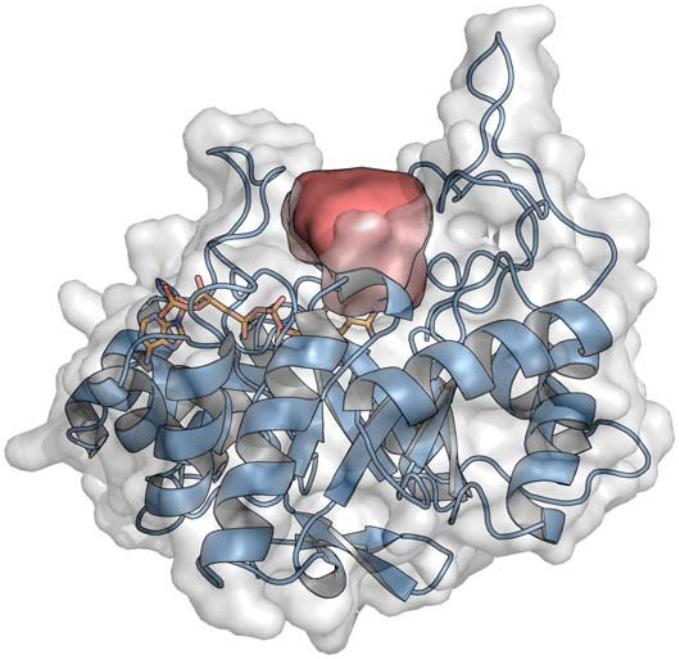

Figure 4.3: Model of AKR1B16 structure with the pocket volume representation. Cartoon side view of the $(\alpha/\beta)_8$ barrel structure of the AKR1B16 model colored in blue complexed with $NADP^+$ (depicted in orange sticks), showing the surface contour of the active-site pocket in red. The surface of the protein is represented in transparent grey.

Like other AKR1B proteins, the model displays the classical $(\alpha/\beta)_8$ barrel fold structure of the subfamily, with the least conserved residues located in three loop regions lining the active site pocket. NADPH binds to the cofactor binding site with the amino acids of loop B (together with others, see figure 4.1 colored in green) involved in the binding of the cofactor, providing positively charged residues that interact with the 2'-phosphate group and thus determining the coenzyme preference over NADH (*20*). The salt bridge between Asp217 and Lys263, that interact across the coenzyme binding cleft through a hydrogen bond, making the "safety belt"in the coenzyme binding, and the π-stacking interaction of Tyr210 with the cofactor nicotinamide ring are conserved in AKR1B16, as in AKR1B1 and AKR1B10.

Using the POVME algorithm we determined the binding site volume and shape for AKR1B16. AKR1B16 has a catalytic pocket volume slightly superior than that of AKR1B10, with 402 $Å^3$ and a more rounded shape. The binding site is limited for the global shape of the protein. Thus, AKR1B16 and 1B10 pockets have a similar depth, and their global shape varies in accordance to the more external residues located in the plastic loops that surround the active site (Fig 4.3).

4.3.4 Purification of AKR1B16 co-expressed with chaperones

Similarly as what Salabei *et al.* (*11*) previously reported, and in a similar fashion as what we observed for AKR1B15, when AKR1B16 was expressed in bacterial systems it formed inclusion bodies in the insoluble fraction of cell lysates (data not shown). Thus, we used the same successful procedure used to obtain monomeric and soluble AKR1B15 (*263*), the coexpression of AKR1B16 in *E.coli* BL21(DE3) strain together with three chaperone systems (DnaK-DnaJ-GrpE, ClpB and GroEL-GroES) (*173*, *201*, *263*). Under these conditions, AKR1B16 was still mostly expressed in the insoluble form, but the amount of soluble protein increased significantly, and the enzyme could be purified in soluble monomeric form with a final yield of $\approx$ 2 mg per liter of culture.

4.3.5 Enzymatic activity

As expected from the cofactor preference of the enzymatic family and the conserved residues in the cofactor binding site, AKR1B16 is an active protein with specificity for NADPH. No NADH dependent reductase activity was observed. The K_m value for NADPH was similar to that reported for other members of this family (K_m 0.5 μM) (*116*, *199*, *263*, *283*, *299*). We tested AKR1B16 activity with reported AKR substrates (Table 4.2). The enzyme reduced aliphatic and aromatic aldehydes, with a moderate or low activity for all the assayed compounds with k_{cat} values around 5 min^{-1}. Regarding the activity with D,L-glyceraldehyde, AKR1B16 shows K_m and k_{cat} values of 280 μM and 4.3 min^{-1}, respectively. This value is in accordance to that exhibited by other murine AKRs of the AKR1B7 cluster type (AKR1B7, 1B14 and 1B17) that display lower activity (*168*) towards this substrate than other AKRs, that show values of $\sim$ 30 min^{-1}. The best substrate for the enzyme was the aromatic pyridine-3-aldehyde, with K_m value in the low μM range. Importantly, AKR1B16 did not show reductase activity towards D-glucose, a distinct feature of aldose reductase type enzymes. The enzyme however reduced farnesal and acrolein, but did not display appreciable activity towards citral (Table 4.2). Interestingly, a good substrate for human AKR1Bs as benzaldehyde, is a poor substrate for AKR1B16, and also for other murine enzymes, with $\approx$ 10 fold difference in catalytic efficiency. The other tested compounds, such as ketones, showed low or no activity (Table 4.4).

The retinaldehyde reductase activity of AKR1B16 was analysed with the HPLC methodology used previously for other proteins of the same family (*168*). It displays low activity with both all-*trans* and 9-*cis*-retinaldehyde, resembling more to the catalytic efficiency of AKR1B1 than to AKR1B10 or AKR1B15 (Table 4.6). In fact, AKR1B16 catalytic efficiency ($\sim$ 55.5 $mM^{-1} \cdot min^{-1}$) for all-*trans*-retinaldehyde is even lower than that presented by AKR1B1 ($\sim$ 1,300 $mM^{-1} \cdot min^{-1}$) (Table 4.6). AKR1B16 has a similarly low catalytic efficiency towards all-*trans*-retinaldehyde as other murine AKR1Bs because of the low k_{cat} (<1 min^{-1}) exhibited by all members of the murine subfamily (Table 4.5).

Table 4.2: Kinetic characterization of AKR1B16 with typical AKR substrates.

Substrate	**AKR1B16**		
	K_m (μM)	k_{cat} (min^{-1})	k_{cat}/K_m ($mM^{-1}\cdot min^{-1}$)
Aromatic aldehydes			
Pyridine-3-aldehyde	3.1	5	1,630
Benzaldehyde	16.5	4.4	270
Cinnamaldehyde	16.6	4.9	293
Alkanals			
D,L-glyceraldehyde	280	4.3	15.6
Hexanal	4.9	5.5	1,100
Alkenals			
Acrolein	24.6	2.8	114.3
Trans-2-hexenal	55.2	3.9	71
Citral	-	LA	-
Farnesal	27.9	1.1	41.1
Ketones			
2-butanone	-	LA	-
3-buten-2-one	-	NA	-
3-nonen-2-one	-	LA	-
2-cyclohexen-1-one	-	LA	-
α-Dicarbonyls			
2,3-butanodione	145	5.8	40.2
2,3-Hexanedione	8	5	636
β-Dicarbonyls			
2,4-acetylacetone	-	LA	-
3,5-heptanedione	1,400	1	0.74
Cofactor			
NADPH	0.5		

Activity measured spectrophotometrically. For the kinetic parameter of NADPH, 10 mM D,L-glyceraldehyde was used. LA, low activity (<10 mU/mg); NA, no activity.

4.3.6 Inhibitor selectivity against AKR1B16

Inhibitors were assayed to obtain the IC_{50} values for D,L-glyceraldehyde reduction catalyzed by AKR1B16. Table 4.3 lists the IC_{50} values of typical ARI obtained for AKR1B16 and human AKR1B proteins. The best AKR1B16 inhibitor found was the classical ARI tolrestat, known as one of the most potent inhibitors for AKR1B10 and AKR1B1, with a potency at nanomolar level. However, it showed lower inhibition potency towards AKR1B16, with a IC_{50} value of 3 μM. The recently described non-classical ARI JF0064 also displayed less potency towards AKR1B16 than for all other human AKRs, with a IC_{50} value of 7.8 μM. The other 4 inhibitors tested, sorbinil, epalrestat, oleanolic acid and sulindac, did not display significant inhibition.

Table 4.3: AKR1B16 inhibition compared with human AKR1B enzymes

	IC_{50} (μM)			
Inhibitor	**AKR1B16**	**AKR1B10**	**AKR1B1**	**AKR1B15**
Tolrestat	2.99 ± 0.17	0.006[a]	0.01[b]	>100
Sorbinil	>100	9.6[c]	0.55[c]	>100
JF0064	7.8 ± 1.3	1.0[d]	0.3[d]	0.034
Epalrestat	NI	0.33[e]	0.021[e]	>50
Oleanolic acid	NI	0.09[c]	124[c]	>100
Sulindac	NI	0.35[e]	0.21[e]	>100

The enzymatic activity assay with inhibitors was performed by using D,L-glyceraldehyde as a substrate. NI; no inhibition. [a]Data from (*43*), [b](*22*), [c](*92*), [d](*52*) and [e](*85*).

4.4 Discussion

Recently, mouse AKR1B16 (sharing 83% and 80% amino acid sequence identity with AKR1B10 and 1B15, respectively) was expressed in the insoluble fraction of bacterial cell lysates (*11*), but no enzymatic activity could be measured. In this Thesis we have expressed and purified AKR1B16 as an active soluble protein in *E. coli* using three chaperone systems, DnaK-DnaJ-GrpE, ClpB and GroEL-GroES. A homology-based computer model of AKR1B16 was built and allowed to estimate the volume of its active-site pocket, which was much wider (402 Å^3) than those of AKR1B10 (279 Å^3) and AKR1B15 (60 Å^3). The kinetic characterization with typical AKR substrates showed that AKR1B16 is able to reduced aliphatic and aromatic carbonyl compounds, using NADPH as a cofactor, with moderate or low activity (k_{cat} values around 5 min^{-1}), being 3-pyridine-aldehyde the best susbtrate for this enzyme.

In the present study, we expressed a recombinant active form of AKR1B16 for the first time, a novel murine AKR1B protein, and characterized it in terms of its enzymatic properties and inhibition selectivity. Previous studies used the solubilization with detergents to purify this protein from the insoluble fraction when expressed in bacterial systems, but no measurable activity was reported (*11*). As possible explanation, they pointed out that AKR1B16 could have very low activity, similar to that displayed by AKR1B7, in comparison with other AKRs. Here we have purified the enzyme with the chaperone methodology obtaining enough soluble protein for a detailed kinetic analysis.

AKR1B16 and AKR1B7 are positioned together in the "AKR1B7 type"cluster and we here demonstrate that in general they have similar kinetic properties (Fig. 4.2) (*168*). Thus, both proteins present modest catalytic constants towards all the assayed substrates, between 1 and 10 min^{-1}, including all-*trans* and 9-*cis*-retinaldehyde.

The highest degree of sequence similarity of AKR1B16 is with the rat protein AKR1B17, with

Table 4.4: Kinetic constants of mouse AKR1B enzymes and rat AKR1B17.

Substrate	**AKR1B16**			**AKR1B3**			**AKR1B7**			**AKR1B8**			**AKR1B17**		
	K_m (μM)	k_{cat} (min^{-1})	k_{cat}/K_m ($mM^{-1}{\cdot}min^{-1}$)	K_m (μM)	k_{cat} (min^{-1})	k_{cat}/K_m ($mM^{-1}{\cdot}min^{-1}$)	K_m (μM)	k_{cat} (min^{-1})	k_{cat}/K_m ($mM^{-1}{\cdot}min^{-1}$)	K_m (μM)	k_{cat} (min^{-1})	k_{cat}/K_m ($mM^{-1}min^{-1}$)	K_m (μM)	k_{cat} (min^{-1})	k_{cat}/K_m ($mM^{-1}{\cdot}min^{-1}$)
Aromatic aldehydes															
Benzaldehyde	16.5	4.4	270	-	-	-	-	-	-	100[b]	17.1[b]	171[b]	9.1[f]	3.2[f]	350[f]
Alkanals															
D,L-glyceraldehyde	280	4.3	15.6	40[a]	31[a]	720[a]	8,000[a]	4.5[a]	0.6[a]	300[a]	20[a]	68[a]	220[f]	2.8[f]	13[f]
Hexanal	4.9	5.5	1,100	-	-	-	-	-	-	6[b]	12.4[b]	2,067[b]	2.1[f]	2.6[f]	1,200[f]
Glucose		NA		82,000[c]	48.5[c]	1,690[c]	2,700[d]	22.2[d]	8.2[d]		ND[b]	-		NA[f]	
Alkenals															
Acrolein	24.6	2.8	114.3	-	-	-	586[e]	16.8[e]	28.8[e]	1,290[e]	90.7[e]	70[e]	49[f]	2.9[f]	59[f]
trans-2-hexenal	55.2	3.9	71	-	-	-	ND[e]	ND[e]	2.09[e]	210[e]	40[e]	182[e]	6.1[f]	3.7[f]	600[f]
α-dicarbonyls															
2,3-butanedione	145	5.8	40.2	77[e]	56.4[e]	732[e]	70[e]	3.24[e]	46.2[e]	-	-	-	120[f]	3.9[f]	33[f]
all-*trans*-retinaldehyde	0.4	0.022	55.5	1.0[a]	0.5[a]	540[a]	0.5[a]	0.02[a]	42[a]	2.1[a]	0.05[a]	22[a]	2.6[f]	0.58[f]	220[f]

NA, no activity. ND, not detectable. Data taken from [a](*168*), [b](*109*), [c](*105*), [d](*18*), [e](*108*), and [f](*116*).

a 92.1% identity. Both proteins displayed almost identical catalytic efficiencies with substrates such as pyridine-3-aldehyde, benzaldehyde, acrolein, trans-2-hexenal, hexanal, farnesal and 2,3-butanedione. Thereby, the kinetic characterization seems to agree with the phylogenetic analysis that localised very close together both proteins. In contrast, AKR1B10 is far more active with all substrates, sometimes more than 40 fold (such as with farnesal or benzaldehyde). Importantly, AKR1B16 does not exhibit enzymatic activity in the reduction of glucose, indicating that it is not an aldose reductase type enzyme.

AKR1B16 resembles the other murine AKR1B proteins and displays low retinaldehyde reductase activity (*168*). This fact, together with the aforementioned kinetic activities, and phylogenetic analysis, seem to indicate that AKR1B10 has not a ortholeg protein neither in mouse or rat. This point out that the human AKR1B10 protein is unique in this distinct trait, the high retinaldehyde reductase catalytic efficiency. In fact, all the murine proteins display a low efficiency with this substrate, pointing that this characteristic is not evolutionary conserved in mammalian AKR1B family. The phylogenetic tree shows that AKR1B10 and AKR1B15 do not have evolutionary close proteins in other species, and form a differentiated cluster by their own, with the rabbit AKR1B19 protein being the closest one. AKR1B19 is able to reduce retinaldehyde, but with low catalytic efficiency (350 $mM^{-1} \cdot min^{-1}$)(*298*).

Murine proteins are also inhibited by ARIs, but there are few studies regarding their inhibition, and these studies differ in the methodology used and sometimes in the results reported. Among the six inhibitors tested, AKR1B16 was only inhibited by tolrestat and JF0064, and with 10-fold less potency than with human AKR1Bs. The volume pocket analysis indicates that AKR1B16 has a wider binding-site (402 $Å^3$) than AKR1B10 (279 $Å^3$) and AKR1B15 (60 $Å^3$), and with very different residues implicated in the shape of the pocket. Knowing the different cross-selectivity displayed by inhibitors towards very similar proteins such as AKR1B1, 1B10 (and 1B15) (*52*, *54*, *60*, *84–94*, *263*), it is likely that the classical ARIs would inhibit the murine AKR1Bs with different specificity, mainly because of the high plasticity and residue differences present in loops A and C. The higher volume shown by the AKR1B16 pocket may also indicate that the enzyme is able to accommodate larger inhibitors.

The mouse protein AKR1B7 is not efficiently inhibited by tolrestat, with 81% of remaining activity at 10 μM, and at 1 μM sorbinil it displayed 100% activity (*18*). This is in accordance with the results reported by Kabututu and collaborators (*282*) that found K_i values of 9.2 mM and 18 mM for tolrestat and sorbinil respectively for the inhibition of the prostaglandin $F_{2\alpha}$ synthase activity of AKR1B7. The same study found a much stronger inhibition of these compounds (K_i of 0.26 μM and 0.89 μM respectively) for AKR1B3. This is in accordance with the protein sequence identity displayed, since AKR1B16 is more similar to AKR1B17 than to AKR1B3, and it is clustered as a "AKR1B7 type"protein (Fig. 4.2), although we found some inhibition of AKR1B16 by tolrestat (Table 4.3). In the same cluster we can find the closest protein in terms of sequence identity to AKR1B16, the rat protein AKR1B17. This protein displays IC_{50} values for tolrestat

and sulindac of 7.0 and 40 μM respectively (*116*). Our data are in agreement with these values, as the AKR1B16 is not inhibited by sulindac, and point out that both are very similar proteins.

In comparison with the human enzymes, therefore unlike AKR1B10 or 1B15, which display high activity with retinaldehyde, the activity of AKR1B16 with either all-*trans* or 9-*cis*-retinaldehyde was much lower, but similar to the activities displayed by other murine AKR1Bs (*168*). In addition, AKR1B16 have different inhibitor selectivity that AKR1B10 and AKR1B1, and that it is not inhibited by some of the classical ARIs. These results, together with the phylogenetic analysis, suggest that AKR1B16 has no counterpartin the human system and therefore is not the true ortholog of AKR1B10 or 1B15.

Table 4.5: Retinaldehyde reductase activity of murine AKRs

Substrate and Parameter	**AKR1B16**	**AKR1B8**	**AKR1B3**	**AKR1B7**	**AKR1B13**	**AKR1B14**	**AKR1B17**
all-*trans*-retinaldehyde							
K_m (μM)	0.4 ± 0.066	2.1 ± 0.5 [a]	1.0 ± 0.1[a]	0.5 ± 0.1[a]			2.6[d]
k_{cat} (min^{-1})	0.022 ± 0.0005	0.05 ±0.01[a]	0.52 ±0.02[a]	0.02 ± 0.01[a]	NA[b]	LA[c]	0.58[d]
k_{cat}/K_m ($mM^{-1}{\cdot}min^{-1}$)	55.5 ± 9	22 ± 6[a]	540 ± 90[a]	42 ± 6[a]			220[a]
9-*cis*-retinaldehyde							
K_m (mM)	2.96 ± 0.6						
k_{cat} (min^{-1})	0.09 ± 0.007	ND	ND	ND	ND	ND	ND
k_{cat}/K_m ($mM^{-1}{\cdot}min^{-1}$)	29.1 ± 6						

NA, no activity. LA, low activity. ND, not determined. [a]Data from (*168*), [b](*283*), [c](*299*), [d](*116*)

Table 4.6: Retinaldehyde reductase activity of AKR1B16 compared with human AKR1B enzymes

Substrate and Parameter	**AKR1B16**	**AKR1B1**[a]	**AKR1B10**[a]	**AKR1B15**
all-*trans*-retinaldehyde				
K_m (μM)	0.4 ± 0.066	1.1 ± 0.1	0.6 ± 0.1	1 ± 0.3
k_{cat} (min^{-1})	0.022 ± 0.0005	0.9 ± 0.1	27 ± 1	5.4 ± 0.5
k_{cat}/K_m ($mM^{-1}{\cdot}min^{-1}$)	55.5 ± 8	1,300 ± 160	45,000 ± 7,600	5,300 ± 1,700
9-*cis*-retinaldehyde				
K_m (μM)	2.96 ± 0.6	0.4 ± 0.1	0.7 ± 0.1	0.16 ± 0.03
k_{cat} (min^{-1})	0.09 ± 0.007	0.7 ± 0.2	0.9 ± 0.1	3.8 ± 0.2
k_{cat}/K_m ($mM^{-1}{\cdot}min^{-1}$)	29.1 ± 6	1,500 ± 170	1,300 ± 190	25,600 ± 5,300

Enzymatic activity was measured by using the HPLC-based method. [a]Data from (*13*)

General discussion

At the start of this work, only two members of the AKR1B subfamily were known in human and three in mice. However, two novel gene *loci*, human *AKR1B15* and mouse *Akr1b16*, were predicted to exist within the *AKR1B* clusters. *AKR1B15* is localized in the same cluster as the other two *AKR1B* human genes, aldose reductase (*AKR1B1*) and *AKR1B10*. The novel gene product, AKR1B15, has a high degree of amino acid sequence identity with AKR1B10 (92%), which goes down with AKR1B1 (67%). Mouse AKR1B16 is also higly identical to AKR1B10 (83% sequence identity), and thus, they could possibly be orthologous proteins. It is assumed that *AKR1B15* has recently appeared by a gene duplication event of AKR1B10. In fact, there is a *AKR1B15*-like gene in closely related species, such as *Pan troglodytes, Pongo abelii, Pan paniscus* and *Gorilla gorilla*, with more than 96% sequence identity with the human gene. A recent study reported that these two newly predicted genes, *AKR1B15* and *Akr1b16*, were functional since they were expressed in human and mouse tissues respectively, but, when expressed in bacterial systems, both enzymes showed no activity at all and were found to precipitate into inclusion bodies (*11*). In this context, this work started with the main purpose of characterizing these two novel proteins: human AKR1B15 and mouse AKR1B16. Thus, their corresponding cDNA was transformed into different bacterial strains in order to express and purify the recombinant proteins.

The expression of the recombinant AKR1B15 was approached by applying various strategies and detergents in an attempt to avoid its precipitation into the insoluble fraction of bacterial cell lysates. Since all the conventional systems were unsuccessful, we employed a different methodology, a novel approach in the field of AKRs. It consisted of the coexpression of AKR1B15 with various chaperone systems, at low temperature, to increase the amount of protein in the soluble fraction. Molecular chaperones tipically assist newly synthesized proteins to fold into their native states, shield exposed hydrophobic patches of non-native proteins to prevent their aggregation, thus avoiding nonproductive hydrophobic interactions and helping them acquire their correct tertiary conformation (*300*). Furthermore, it has been demonstrated that their coexpression with other proteins is capable of increasing the amount of soluble target recombinant protein, which is otherwise produced mostly in inclusion bodies (*301–303*). However, the coexpression of chaperones might have some side effects by slowing bacterial growth and decreasing protein yield (*304*). This methodology was used for the first time to increase the solubility in *E. coli* of ribulose bisphosphate carboxylase (Rubisco) (*305*). Since then, many other proteins as diverse as human PP2A methyltransferase (*306*), human 11β-hydroxylase (*307*), human cytochrome P450 3A7 (CYP3A7) (*308*), *Pseudomonas putida* F61 nicotinoprotein formaldehyde dismutase (NDF) (*309*) and many other examples can be found (reviewed in (*310*)). Using this approach, we were able to obtain a sufficient amount of soluble AKR1B15 to perform a detailed characterization.

Despite being very similar to AKR1B10, an enzyme extensively studied by our group (*13*, *69*, *89*), AKR1B15 displays unique features. The kinetic characterization with aliphatic and aromatic aldehydes and ketones showed that it has a significant enzymatic activity. Remarkably, it exhibits substantial activity towards ketones (and also α-dicarbonyl compounds), a unique characteristic

within the human AKR1B proteins (Table 2.1). AKR1B15 is also active towards some other physiological substrates, such as acrolein and HNE, products of lipid peroxidation, and therefore this enzyme could play a similar role to AKR1B1 and AKR1B10 in lipid peroxidation and aldehyde detoxification in the cell (*37*). Additionally, its mitochondrial localization (*12*) could regulate the availability of molecules containing a 2-alkenal group (such as HNE), produced by ROS originated during oxidative phosphorylation, protecting against senescence (*232*, *239*, *240*).

In recent years AKRs have revealed as enzymes able to catalyze the oxidation and reduction of retinoids. This activity was well characterized in some members of the AKR1B subfamily (human AKR1B1 and 1B10 (*13*), chicken AKR1B12 (*118*), and rat (AKR1B4, AKR1B13, AKR1B14 and AKR1B17) and mouse proteins (AKR1B3, AKR1B7 and AKR1B8) (*60*, *116*, *168*, *299*)) and also in members of the AKR1C subfamily (human AKR1C1-AKR1C4 (*156*)). In this regard, two novel members of the AKR1B subfamily have been characterized here, human AKR1B15 and mouse AKR1B16.

Previous studies conducted by our group (*13*) demonstrated that AKR1B10 has a high catalytic efficiency (k_{cat}/K_m) with all-*trans*-retinaldehyde, a unique characteristic in the human AKRs, comparable to the retinaldehyde reductases of the SDR superfamily. In the present work, we examined the activity of AKR1B15 and reported that it exhibits a high catalytic efficiency for 9-*cis*-retinaldehyde isomer (25,600 $\mathrm{mM}^{-1}\cdot\mathrm{min}^{-1}$), only comparable to AKR1C3 (32,000 $\mathrm{mM}^{-1}\cdot\mathrm{min}^{-1}$). Interestingly, both enzymes share two Phe residues in the loop C, Phe299 and Phe304 (AKR1B15 numbering), being the only residues conserved within the loop. The elevated catalytic efficiency of AKR1B15 for this retinaldehyde isomer is determined mainly by its low K_m value, in the low nanomolar range. Thereby, AKR1B15 and AKR1B10 are the AKR1B enzymes with the best retinaldehyde reductase activity, but with remarkable distinct isomer specificity. AKR1B15 is the most efficient AKR with 9-*cis*-retinaldehyde, whereas AKR1B10 is the best all-*trans*-retinaldehyde reductase. However, since cellular concentration of the all-*trans* isomer is much higher than that of the 9-*cis*, both enzymes may physiologically act as all-*trans*-retinaldehyde reductases.

The different localization of AKR1B15 (mitochondria) and AKR1B10 (cytosol) would ensure that they function would not overlap. Thus, each enzyme may have a distinct role in the pre-receptor regulation of hormonal signaling pathways. In addition, there is increasing evidence that different subcellular compartments, including mitochondria, would participate in retinoid metabolism. In this regard, there are evidence of compartmentalisation in the metabolism of carotenoids (*76*). In mammals, there are two carotenoid cleavage enzymes that display different cellular localization and substrate preferences. BCO1 cleaves provitamin A carotenoids at the C15,C15' double bond in a symmetric cleavage, it localizes in cytoplasm and mutations in patients, together with knock out studies in mice, indicate that BCO1 is critical for vitamin A production and homeostasis, being the major β-carotene metabolizing enzyme in mice (*245*, *311*, *312*). In contrast, BCO2 catalyzes the asymmetric cleavage of provitamin and non provitamin A carotenoids, at C9,C10' double bond, it is associated to the mitochondrial membrane and it does

not seem to influence vitamin A dependent processes (*130*, *245*, *312*, *313*). However, it is thought that BCO2 may be important for the cleavage of asymmetric carotenoids, such as xanthophylls or β-cryptoxanthin (*312*). The products resulting from BCO2 action are aldehydes of different length, including retinaldehyde. AKR1B15 may play a role in the mitochondrial reduction of these aldehydes to retinol and other isoprenoid alcohols.

AKR1B1 is, and had been, an extensively studied enzyme as a therapeutic target, given its important participation in the metabolic hyperglycemic disequilibrium that leads to secondary complications of diabetes. The limited success in the therapeutic use of inhibitors (ARI) can be attributed to its lack of selectivity for AKR1B1, thought to be the cause of side effects of the inhibitors. Thus, there is a possible cross-inhibition of ARI with AKR1B10, that can be an unspecific target. Recently, AKR1B10 has gained relevance as a therapeutic target because it is found overexpressed in different cancer types (*51*, *64–67*) and is associated with chemoresistance, thus its selective inhibitors may be used as anti-tumor agents (*86*). AKR1B15, as being a very similar enzyme to AKR1B10 and to AKR1B1, could also be an unspecific target of the inhibitors against both enzymes. Here we showed that some classical ARIs that inhibit AKR1B1 and AKR1B10, are not capable to inhibit AKR1B15. The only tested compound able to inhibit AKR1B15 was JF0064, a non-classical ARI that can also inhibit AKR1B1 and AKR1B10 (*52*). Thus, in general, inhibitors of AKR1B10 and AKR1B1, that may be used for therapeutic purposes, could not show cross-inhibition with AKR1B15.

Despite the high sequence identity between, AKR1B10 and AKR1B15, we can say that the binding of the inhibitors to the specificity pocket of AKR1B15 exhibits different features, and this is due to subtle changes in the amino acid residues involved that influence the binding of the inhibitor by altering the size, shape and nature of the pocket. Nowadays, 17 AKR1B10 crystallographic structures, complexed with various inhibitors, have been deposited in the PDB. However, not a single AKR1B15 structure has been solved, and our attempts to crystallize the protein were unsuccessful. Thus, the construction of a molecular model, based on the 3D coordinates of AKR1B10, was useful to identify the differences in the active-site pockets between the two enzymes. Compared to AKR1B10, 1B15 has a more hydrophobic, rigid (Fig. 2.10a) and smaller pocket, mainly due to the bulky Phe residues in the AKR1B15 pocket (Phe48, Phe299, Phe301 and Phe304) (Figure 2.12). This smaller volume would make difficult to fit the inhibitors because of steric hindrance, except for JF0064. This compound may specifically interact with the AKR1B15 pocket due to its small volume and hydrophobic nature, with two symmetrical phenol rings present in its structure. Thus, it is predicted that one of the rings points towards the catalytic center of the enzyme making multiple interactions with residues of the inner part of the pocket, while the other phenol ring points towards the solvent, making hydrogen bonds with residues in loops B and C. Thus, no other tested inhibitor is small enough to fit nicely in the pocket nor is able to establish appropriate interactions with both inner residues and external loops of the AKR1B15 pocket.

Our group showed that AKR1B10 is an active retinaldehyde reductase in cells, and that its

activity can be inhibited by tolrestat. By a trans-activation assay, it was demonstrated that, when the enzyme is overexpressed in cells, it is able to decrease the synthesis of RA available for RAR and RXR receptors (*13*, *69*). The cellular experiments performed here with AKR1B15 and AKR1B10 show that AKR1B10 could alter the retinoid metabolic pathway. Applying an improved methodology for the quantification of retinoids, we observed that AKR1B10 could revert the oxidation of retinol to retinaldehyde, and consequently limiting the global flux of the pathway, reducing the level of available RA (Fig. 2.16). This result supports the hypothesis that *in vivo* AKR1B10 overexpression, as in cancer, can alter the metabolic flux of the RA synthesis pathway (*69*, *71*, *241*), and the decreased RA levels would affect processes such as cellular proliferation and differentiation. We could not demonstrate that AKR1B15 changes the RA levels in cells, although it has to be noted that this enzyme is less efficient in reducing all-*trans*-retinaldehyde than AKR1B10.

To examine how the small structural differences between AKR1B10 and AKR1B15 yield to significantly different kinetic features, we constructed mutant AKR1B10 enzymes mimicking the active site pocket of AKR1B15. A sequence alignment showed that the region of major divergence between enzymes was localized in the loop C, and contained three Phe substitutions, that greatly contributed to the volume, flexibility and shape of the pocket. A corresponding segment of six residues was substituted in AKR1B10 (AKR1B10mut). An additional mutant, with a change in the binding-pocket residue (Val48Phe) was also performed (AKR1B10mF48).

Both mutated enzymes could be purified from the soluble fraction of bacterial cells, its solubility not being affected by the mutations introduced. In this regard, Weber *et al.* (*12*) suggested that the low solubility of AKR1B15 could be explained by the different amino acid composition at the N-terminal segment of the enzyme, positions 22 and 24, that were not modified in the mutants. The mutated enzymes presented, in general, higher k_{cat} values for the substrates assayed, indicating a faster rate-limiting step, likely the release of $NADP^+$, although no residue directly implicated in the cofactor binding was changed. Importantly, the mutant enzymes acquired the catalytic activity of AKR1B15 towards ketones, demonstrating that the mutated residues in loop C are implicated in this substrate specificity.

When the mutant enzymes were examined for their activity with retinoids, both AKR1B10mut and AKR1B10mF48 had lost the high catalytic efficiency towards all-*trans*-retinaldehyde of AKR1B10 wild type. However, AKR1B10mF48 gained selectivity towards the 9-*cis*-retinaldehyde isomer and displayed a catalytic efficiency for this substrate similar to that of wild-type AKR1B15, albeit both its K_m and k_{cat} are higher. The inhibition studies also suggest that AKR1B10mF48 is more similar to AKR1B15 than the AKR1B10mut enzyme, as it presents an almost identical pattern of inhibitor selectivity. This suggests that the mutations reduced the accessible volume and increased its hydrophobicity, making the pocket of AKR1B10mF48 more similar to that of wild-type AKR1B15 than to that of AKR1B10.

In conclusion, AKR1B10mF48 resembles AKR1B15 in several features (inhibition, overall sub-

strate specificity) but other AKR1B15 characteristics (low solubility, activity with retinoids) were not attained. Although the mutated residues are important for AKR1B15 properties, other substitutions (20 residue differences between AKR1B10mF48 and AKR1B15) may also be essential to explain the remarkable differences between these two closely related enzymes.

Finally, we have also characterized a novel mouse enzyme from the AKR1B subfamily, that was predicted at the same time as AKR1B15 (*11*). Its gene is located in the same gene cluster than other mice *AKR1B* genes and displays a high degree of amino acid sequence identity with rat AKR1B17 (92.4%) (*116*), and with human AKR1B10 (82.9%). Here we performed a phylogenetic and kinetic studies, along with a structural model and inhibition selectivity screening. The results displayed that AKR1B16 belongs to the mouse AKR1B7 type proteins (*168*). The *in silico* model indicates that the novel enzyme exhibits the structure typical of the family, with conserved residues in the NADPH binding site. The volume of the catalytic pocket is larger than those of AKR1B10 and AKR1B15 (*263*). Moreover, AKR1B16 displays moderate activity with the assayed substrates, similar to AKR1B17 (*116*), and does not have significant activity with glucose. It is not related, therefore, to the aldose reductase type proteins. The retinaldehyde reductase activity of AKR1B16 is poor, very much alike to all murine AKRs. In this respect, this work has determined that AKR1B16 is not a functional orthologous protein of the highly active AKR1B10.

In summary, this Thesis has characterized two novel additions to the AKR superfamily, human AKR1B15 and mouse AKR1B16. Both proteins exhibits activity with a broad range substrates, being retinoids some of them. Despite its high sequence identity with AKR1B10, AKR1B15 presents distinct kinetic and inhibitory features resulting from a few structural changes. By site-directed mutagenesis, we have identified several residues involved in the specific AKR1B15 characteristics. The significant retinaldehyde reductase activity of AKR1B15 represents a novel addition to the multiple enzymes involved in the RA biosynthesis and signaling. Finally, with the AKR1B16 study, we complete the characterization of the mouse AKR1B subfamily, adding some evidence on the functional differences between the murine and the human AKR1B systems.

Conclusions

1. Human AKR1B15, a novel member of the aldo-keto reductase superfamily was recombinantly expressed, purified and characterized.

2. AKR1B15 was coexpressed with chaperones in order to increase the amount of protein in the soluble fraction and to obtain a monomeric active form.

3. AKR1B15 displays a unique substrate specificity and narrower inhibitor selectivity, despite the fact that shares a high sequence identity (92%) with AKR1B10.

4. AKR1B15 actively uses ketones and α-dicarbonyl compounds as substrates, showing higher k_{cat} and lower K_m values than other human AKRs.

5. AKR1B15 exhibits retinaldehyde reductase activity and it is among the best 9-*cis*-retinaldehyde reductases within the AKR superfamily.

6. AKR1B15 displays similar k_{cat} values for all the assayed substrates, including retinoids, suggesting a common rate-limiting step.

7. Most potent inhibitors of AKR1B1 and AKR1B10 fail to inhibit AKR1B15.

8. A computer model of AKR1B15 structure indicates that amino acid substitutions, clustered in residues located in loops A and C, result in a smaller, more hydrophobic and more rigid active-site pocket as compared to that of AKR1B10.

9. The finding of all-*trans*- and 9-*cis*-retinaldehyde as substrates for AKR1B15 suggests a role of the enzyme in retinoid metabolism in mitochondria, where it is located.

10. A novel HPLC-based methodology was developed that enable the separation and quantification of the major retinoids species in a single run, from cell extracts, with a good extraction efficiency.

11. The overexpression of AKR1B10, but not AKR1B15, in transfected HEK293T cells leads to a decrease of all-*trans*-retinoic acid levels and an increase of the intracellular retinol levels, thus affecting the regulation of the retinoic acid pathway at the prereceptor level.

12. Two mutants of AKR1B10 (AKR1B10mut and AKR1B10mF48) were prepared with substitutions that resemble AKR1B15 active site. They displayed generally higher K_m and k_{cat} values for all the substrates in comparison to AKR1B10, but conserving similar catalytic efficiency.

13. Both mutants resemble AKR1B15 in that they showed activity with ketones, suggesting that important residues for this activity are adjacent residues Phe299, Asp300, Phe301, Lys302, Glu303 and Phe304.

14. Inhibitors tested against the AKR1B10 mutants show lower selectivity for the mutant enzymes than for wilt-type AKR1B10. The additional Phe48 mutation produce an enzyme that displays higher similarity with AKR1B15 than AKR1B10 regarding the inhibitory selectivity.

15. The mutant enzyme AKR1B10mF48 resembles more closely AKR1B15, in important kinetic features, such as the increased catalytic efficiency for 9-*cis*-retinaldehyde, similar k_{cat} values for all the substrates assayed and comparable selectivity for different AKR inhibitors. Therefore, the residues substituted are relevant for the distinct kinetics of AKR1B15.

16. AKR1B16, a mouse protein sharing high sequence identity (83%) with AKR1B10, was recombinantly coexpressed with chaperones to increase the amount of soluble protein.

17. AKR1B16 displays similar kinetic properties as those of AKR1B7. It does not show any activity with glucose and has modest catalytic efficiency with all-*trans*- and 9-*cis*-retinaldehyde. It exhibits different inhibitor selectivity as compared to the human AKR1B enzymes, being tolrestat the most potent inhibitor.

18. The constructed molecular model of AKR1B16 structure shows a spherical and wider active-site than that of AKR1B10, where different residues conform the shape and external part of the pocket.

19. Phylogenetic, kinetic and inhibitor selectivity analyse make difficult to assign any of the human AKR1B enzymes as being the true orthologue of AKR1B16.

Bibliography

(*1*) Jez, J. M., Bennett, M. J., Schlegel, B. P., Lewis, M., and Penning, T. M. (1997). Comparative anatomy of the aldo-keto reductase superfamily. *Biochemical Journal 326*, 625–636.

(*2*) Nordling, E., Jörnvall, H., and Persson, B. (2002). Medium-chain dehydrogenases/reductases (MDR). *European Journal of Biochemistry 269*, 4267–4276.

(*3*) Persson, B., and Kallberg, Y. (2013). Classification and nomenclature of the superfamily of short-chain dehydrogenases/reductases (SDRs). *Chemico-Biological Interactions 202*, 111–115.

(*4*) Jez, J. M., and Penning, T. M. (2001). The aldo-keto reductase (AKR) superfamily: an update. *Chemico-Biological Interactions 130-132*, 499–525.

(*5*) Bohren, K. M., Bullock, B., Wermuth, B., and Gabbay, K. H. (1989). The aldo-keto reductase superfamily. cDNAs and deduced amino acid sequences of human aldehyde and aldose reductases. *Journal of Biological Chemistry 264*, 9547–9551.

(*6*) Barski, O. A., Tipparaju, S. M., and Bhatnagar, A. (2008). The aldo-keto reductase superfamily and its role in drug metabolism and detoxification. *Drug metabolism reviews 40*, 553–624.

(*7*) Jez, J. M., Flynn, T., and Penning, T. M. (1997). A new nomenclature for the aldo-keto reductase superfamily. *Biochemical Pharmacology 54*, 639–647.

(*8*) Penning, T. M., and Drury, J. E. (2007). Human aldo-keto reductases: Function, gene regulation, and single nucleotide polymorphisms. *Archives of Biochemistry and Biophysics 464*, 241–250.

(*9*) Jin, Y., and Penning, T. M. (2007). Aldo-keto reductases and bioactivation/detoxication. *Annual review of pharmacology and toxicology 47*, 263–292.

(*10*) Davidson, W., Walton, D. J., and Flynn, T. (1978). A comparative study of the tissue and species distribution of NADPH-dependent aldehyde reductase. *Comparative Biochemistry and Physiology 60*, 309–315.

(*11*) Salabei, J. K., Li, X.-P., Petrash, J. M., Bhatnagar, A., and Barski, O. A. (2011). Functional expression of novel human and murine AKR1B genes. *Chemico-biological interactions 191*, 177–184.

(*12*) Weber, S., Salabei, J. K., Möller, G., Kremmer, E., Bhatnagar, A., Adamski, J., and Barski, O. A. (2015). Aldo-Keto Reductase 1B15 (AKR1B15): a Mitochondrial Human Aldo-Keto Reductase with Activity towards Steroids and 3-Keto-acyl-CoA Conjugates. *Journal of Biological Chemistry 290*, 6531–6545.

(*13*) Gallego, O., Ruiz, F. X., Ardèvol, A., Domínguez, M., Alvarez, R., de Lera, A. R., Rovira, C., Farrés, J., Fita, I., and Parés, X. (2007). Structural basis for the high all-*trans*-retinaldehyde reductase activity of the tumor marker AKR1B10. *Proceedings of the National Academy of Sciences of the United States of America 104*, 20764–20769.

(*14*) Bennett, M. J., Schlegel, B. P., Jez, J. M. P., M., T., and Lewis, M. (1996). Structure of 3α-Hydroxysteroid/Dihydrodiol Dehydrogenase Complexed with $NADP^+$. *Biochemistry 35*, 10702–10711.

(*15*) Ma, H., Ratnam, K., and Penning, T. M. (2000). Mutation of Nicotinamide Pocket Residues in Rat Liver 3α-Hydroxysteroid Dehydrogenase Reveals Different Modes of Cofactor Binding. *Biochemistry 39*, 102–109.

(*16*) Liu, S.-Q., Jin, H., Zacarias, A., Srivastava, S., and Bhatnagar, A. (2001). Binding of pyridine coenzymes to the β-subunit of the voltage sensitive potassium channels. *Chemico-Biological Interactions 130-132*, 955–962.

(*17*) Ikeda, S., Okuda-Ashitaka, E., Masu, Y., Suzuki, T., Watanabe, K., Nakao, M., Shingu, K., and Ito, S. (1999). Cloning and characterization of two novel aldo-keto reductases (AKR1C12 and AKR1C13) from mouse stomach. *FEBS Letters 459*, 433–437.

(*18*) Lefrançois-Martinez, A.-M., Tournaire, C., Martinez, A., Berger, M., Daoudal, S., Tritsch, D., Veyssière, G., and Jean, C. (1999). Product of Side-chain Cleavage of Cholesterol, Isocaproaldehyde, Is an Endogenous Specific Substrate of Mouse Vas Deferens Protein, an Aldose Reductase-like Protein in Adrenocortical Cells. *Journal of Biological Chemistry 274*, 32875–32880.

(*19*) Ratnam, K., Ma, H., and Penning, T. M. (1999). The Arginine 276 Anchor for NADP(H) Dictates Fluorescence Kinetic Transients in 3α-Hydroxysteroid Dehydrogenase, a Representative Aldo-Keto Reductase. *Biochemistry 38*, 7856–7864.

(*20*) Wilson, D., Bohren, K., Gabbay, K., and Quiocho, F. (1992). An unlikely sugar substrate site in the 1.65 Å structure of the human aldose reductase holoenzyme implicated in diabetic complications. *Science 257*, 81–84.

(*21*) Barski, O. A., Gabbay, K., Grimshaw, C., and Bohren, K. (1995). Mechanism of human aldehyde reductase: characterization of the active site pocket. *Biochemistry 35*, 11264–11275.

(*22*) Ehrig, T., Bohren, K. M., Prendergast, F. G., and Gabbay, K. H. (1994). Mechanism of aldose reductase inhibition: binding of $NADP^+$/NADPH and alrestatin-like inhibitors. *Biochemistry 33*, 7157–7165.

(*23*) Jin, Y., and Penning, T. M. (2006). Multiple Steps Determine the Overall Rate of the Reduction of 5α-Dihydrotestosterone Catalyzed by Human Type 3 3α-Hydroxysteroid Dehydrogenase: Implications for the Elimination of Androgens. *Biochemistry 45*, 13054–13063.

(*24*) Tipparaju, S. M., Liu, S.-Q., Barski, O. A., and Bhatnagar, A. (2007). NADPH binding to β-subunit regulates inactivation of voltage-gated K^+ channels. *Biochemical and Biophysical Research Communications 359*, 269–276.

(*25*) Pollak, N., Niere, M., and Ziegler, M. (2007). NAD Kinase Levels Control the NADPH Concentration in Human Cells. *Journal of Biological Chemistry 282*, 33562–33571.

(*26*) El-Kabbani, O., and Podjarny, A. (2007). Selectivity determinants of the aldose and aldehyde reductase inhibitor-binding sites. *Cellular and Molecular Life Sciences 64*, 1970–1978.

(*27*) Fujii, Y., Watanabe, K., Hayashi, H., Urade, Y., Kuramitsu, S., Kagamiyama, H., and Hayaishi, O. (1990). Purification and characterization of ρ-crystallin from Japanese common bullfrog lens. *Journal of Biological Chemistry 265*, 9914–9923.

(*28*) Weng, J., Cao, Y., Moss, N., and Zhou, M. (2006). Modulation of Voltage-dependent Shaker Family Potassium Channels by an Aldo-Keto Reductase. *Journal of Biological Chemistry 281*, 15194–15200.

(*29*) Xie, Z., Barski, O. A., Cai, J., Bhatnagar, A., and Tipparaju, S. M. (2011). Catalytic reduction of carbonyl groups in oxidized PAPC by Kvβ2 (AKR6). *Chemico-Biological Interactions 191*, 255–260.

(*30*) Ma, J., Yan, R., Zu, X., Cheng, J.-M., Rao, K., Liao, D.-F., and Cao, D. (2008). Aldo-keto Reductase Family 1B10 Affects Fatty Acid Synthesis by Regulating the Stability of Acetyl-CoA Carboxylase-α in Breast Cancer Cells. *Journal of Biological Chemistry 283*, 3418–3423.

(*31*) Wang, C., Yan, R., Luo, D., Watabe, K., Liao, D.-F., and Cao, D. (2009). Aldo-keto Reductase Family 1 Member B10 Promotes Cell Survival by Regulating Lipid Synthesis and Eliminating Carbonyls. *Journal of Biological Chemistry 284*, 26742–26748.

(*32*) Pawlowski, J. E., and Penning, T. M. (1994). Overexpression and mutagenesis of the cDNA for rat liver 3α-hydroxysteroid/dihydrodiol dehydrogenase. Role of cysteines and tyrosines in catalysis. *Journal of Biological Chemistry 269*, 13502–13510.

(*33*) Schlegel, B. P., Ratnam, K., and Penning, T. M. (1998). Retention of NADPH-Linked Quinone Reductase Activity in an Aldo-Keto Reductase Following Mutation of the Catalytic Tyrosine. *Biochemistry 37*, 11003–11011.

(*34*) Liu, S. Q., Bhatnagar, A., and Srivastava, S. K. (1993). Bovine lens aldose reductase. pH-dependence of steady-state kinetic parameters and nucleotide binding. *Journal of Biological Chemistry 268*, 25494–25499.

(*35*) Bohren, K. M., Grimshaw, C. E., Lai, C. J., Harrison, D. H., Ringe, D., Petsko, G. A., and Gabbay, K. H. (1994). Tyrosine-48 Is the Proton Donor and Histidine-110 Directs Substrate Stereochemical Selectivity in the Reduction Reaction of Human Aldose Reductase: Enzyme Kinetics and Crystal Structure of the Y48H Mutant Enzyme. *Biochemistry 33*, 2021–2032.

(*36*) Schlegel, B. P., Jez, J. M., and Penning, T. M. (1998). Mutagenesis of 3α-Hydroxysteroid Dehydrogenase Reveals a "Push-Pull" Mechanism for Proton Transfer in Aldo-Keto Reductases. *Biochemistry 37*, 3538–3548.

(*37*) Martin, H. J., and Maser, E. (2009). Role of human aldo-keto-reductase AKR1B10 in the protection against toxic aldehydes. *Chemico-Biological Interactions 178*, 145–150.

(*38*) Oates, P. J. (2008). Aldose reductase, still a compelling target for diabetic neuropathy. *Current drug targets 9*, 14–36.

(*39*) Petrash, J. M. (2004). All in the family: aldose reductase and closely related aldo-keto reductases. *Cellular Molecular Life Science 7*, 737–749.

(*40*) Nishinaka, T., and Yabe-Nishimura, C. (2001). EGF receptor-ERK pathway is the major signaling pathway that mediates upregulation of aldose reductase expression under oxidative stress. *Free Radical Biology and Medicine 31*, 205–216.

(*41*) Nakamura, N., Obayashi, H., Fujii, M., Fukui, M., Yoshimori, K., Ogata, M., Hasegawa, G., Shigeta, H., Kitagawa, Y., Yoshikawa, T., Kondo, M., Ohta, M., Nishimura, M., Nishinaka, T., and Nishimura, C. (2000). Induction of aldose reductase in cultured human microvascular endothelial cells by advanced glycation end products. *Free Radical Biology and Medicine 29*, 17–25.

(*42*) Alkayyali, S., and Lyssenko, V. (2014). Genetics of diabetes complications. *Mammalian Genome 25*, 384–400.

(*43*) Ruiz Figueras, F. X. Aldo-ceto reductases humanes de les subfamílies AKR1B i AKR1C: activitat amb retinoides i cerca d'inhibidors., Ph.D. Thesis, Universtitat Autònoma de Barcelona, 2010.

(*44*) Crosas, B., Hyndman, D. J., Gallego, O., Martras, S., Parés, X., Flynn, T. G., and Farrés, J. (2003). Human aldose reductase and human small intestine aldose reductase are efficient retinal reductases: consequences for retinoid metabolism. *Biochemical Journal 373*, 1973–1979.

(*45*) Srivastava, S. K., Ramana, K. V., and Bhatnagar, A. (2005). Role of Aldose Reductase and Oxidative Damage in Diabetes and the Consequent Potential for Therapeutic Options. *Endocrine Reviews 26*, 380–392.

(*46*) Ramana, K. V., Chandra, D., Srivastava, S., Bhatnagar, A., Aggarwal, B. B., and Srivastava, S. K. (2002). Aldose Reductase Mediates Mitogenic Signaling in Vascular Smooth Muscle Cells. *Journal of Biological Chemistry 277*, 32063–32070.

(*47*) Tammali, R., Ramana, K. V., Singhal, S. S., Awasthi, S., and Srivastava, S. K. (2006). Aldose Reductase Regulates Growth Factor-Induced Cyclooxygenase-2 Expression and Prostaglandin E2 Production in Human Colon Cancer Cells. *Cancer Research 66*, 9705–9713.

(*48*) Jin, J., Krishack, P., and Cao, D. (2006). Role of aldo-keto reductases in development of prostate and breast cancer. *Frontiers in Bioscience 11*, 2767–2773.

(*49*) Kaiserova, K., Tang, X.-L., Srivastava, S., and Bhatnagar, A. (2008). Role of Nitric Oxide in Regulating Aldose Reductase Activation in the Ischemic Heart. *Journal of Biological Chemistry 283*, 9101–9112.

(*50*) Thiagarajan, D., Ananthakrishnan, R., Zhang, J., O'Shea, K. M., Quadri, N., Li, Q., Sas, K., Jing, X., Rosario, R., Pennathur, S., Schmidt, A. M., and Ramasamy, R. (2016). Aldose Reductase Acts as a Selective Derepressor of PPARγ and the Retinoic Acid Receptor. *Cell Reports 15*, 181–196.

(*51*) Tammali, R., Reddy, A. B. M., Saxena, A., Rychahou, P. G., Evers, B. M., Qiu, S., Awasthi, S., Ramana, K. V., and Srivastava, S. K. (2011). Inhibition of aldose reductase prevents colon cancer metastasis. *Carcinogenesis 32*, 1259–1267.

(*52*) Cousido-Siah, A., Ruiz, F. X., Mitschler, A., Porté, S., de Lera, A. R., Martín, M. J., Manzanaro, S., de la Fuente, J. A., Terwesten, F., Betz, M., Klebe, G., Farrés, J., Parés, X., and Podjarny, A. (2014). Identification of a novel polyfluorinated compound as a lead to inhibit the human enzymes aldose reductase and AKR1B10: structure determination of both ternary complexes and implications for drug design. *Acta Crystallographica Section D 70*, 889–903.

(*53*) Foppiano, M., and Lombardo, G. (1997). Worldwide pharmacovigilance systems and tolrestat withdrawal. *The Lancet 349*, 399–400.

(*54*) Liu, J., Wen, G., and Cao, D. (2009). Aldo-Keto Reductase Family 1 Member B1 Inhibitors: Old Drugs with New Perspectives. *Recent Patents on Anti-Cancer Drug Discovery 4*, 246–253.

(*55*) Pastel, E., Pointud, J.-C., Loubeau, G., Dani, C., Slim, K., Martin, G., Volat, F., Sahut-Barnola, I., Val, P., Martinez, A., and Lefrançois-Martinez, A.-M. (2015). Aldose Reductases Influence Prostaglandin $F_{2\alpha}$ Levels and Adipocyte Differentiation in Male Mouse and Human Species. *Endocrinology 156*, 1671–1684.

(*56*) Gallego, O., Belyaeva, O. V., Porté, S., Ruiz, F. X., Stetsenko, A. V., Shabrova, E. V., Kostereva, N. V., Farrés, J., Parés, X., and Kedishvili, N. Y. (2006). Comparative functional analysis of human medium-chain dehydrogenases, short-chain dehydrogenases/reductases and aldo-keto reductases with retinoids. *The Biochemical journal 399*, 101–109.

(*57*) Cao, D., Fan, S. T., and Chung, S. S. (1998). Identification and Characterization of a Novel Human Aldose Reductase-like Gene. *The Journal of Biological Chemistry 273*, 11429–11435.

(*58*) Hyndman, D. J., and Flynn, T. (1998). Sequence and expression levels in human tissues of a new member of the aldo-keto reductase family 1. *Biochimica et Biophysica Acta 1399*, 198–202.

(*59*) Martin, H.-J. M., Breyer-Pfaff, U., Wsol, V., Venz, S., Block, S., and Maser, E. (2009). Purification and characterization of AKR1B10 from human liver: role in carbonyl reduction of xenobiotics. *Drug Metabolism and Disposition 34*, 464–470.

(*60*) Endo, S., Matsunaga, T., Mamiya, H., Ohta, C., Soda, M., Kitade, Y., Tajima, K., Zhao, H.-T., El-Kabbani, O., and Hara, A. (2009). Kinetic studies of AKR1B10, human aldose reductase-like protein: endogenous substrates and inhibition by steroids. *Archives of biochemistry and biophysics 487*, 1–9.

(*61*) Scuric, Z., Stain, S. C., Anderson, W. F., and Hwang, J.-J. (1998). New member of aldose reductase family proteins overexpressed in human hepatocellular carcinoma. *Hepatology 27*, 943–950.

(*62*) Zeindl-Eberhart, E., Haraida, S., Liebmann, S., Jungblut, P., Lamer, S., Mayer, D., Jäger, G., Chung, S., and Rabes, H. (2004). Detection and Identification of Tumor-Associated Protein Variants in Human Hepatocellular Carcinomas. *Hepatology 39*, 540–549.

(*63*) Mori, M. et al. (2016). Aldo-keto reductase family 1 member B10 is associated with hepatitis B virus-related hepatocellular carcinoma risk. (accepted for publication). *Hepatology Research*, doi: 10.1111/hepr.12725.

(*64*) Laffin, B., and Petrash, M. (2012). Expression of the Aldo-Keto Reductases AKR1B1 and AKR1B10 in Human Cancers. *Frontiers in Pharmacology 3*.

(*65*) Abedin, Z., Sen, S., and Field, J. (2012). Aldo-Keto Reductases Protect Lung Adenocarcinoma Cells from the Acute Toxicity of B[a]P-7,8-*trans*-Dihydrodiol. *Chemical Research in Toxicology 25*, 113–121.

(*66*) Chung, Y. T., Matkowskyj, K. A., Li, H., Bai, H., Zhang, W., Tsao, M.-S., Liao, J., and Yang, G.-Y. (2012). Overexpression and oncogenic function of aldo-keto reductase family 1B10 (AKR1B10) in pancreatic carcinoma. *Modern Pathology 25*, 758–766.

(*67*) Li, H., Yang, A. L., Chung, Y. T., Zhang, W., Liao, J., and Yang, G.-Y. (2013). Sulindac inhibits pancreatic carcinogenesis in LSL KrasG12D-LSL Trp53R172H-Pdx-1 Cre mice via suppressing aldo-keto reductase family 1B10 (AKR1B10). *Carcinogenesis 34*, 2090–2098.

(*68*) Fukumoto, S.-i. et al. (2005). Overexpression of the Aldo-Keto Reductase Family Protein AKR1B10 Is Highly Correlated with Smokers' Non–Small Cell Lung Carcinomas. *Clinical Cancer Research 11*, 1776–1785.

(*69*) Ruiz, F. X., Gallego, O., Ardèvol, A., Moro, A., Domínguez, M., Alvarez, S., Alvarez, R., de Lera, A. R., Rovira, C., Fita, I., Parés, X., and Farrés, J. (2009). Aldo-keto reductases from the AKR1B subfamily: retinoid specificity and control of cellular retinoic acid levels. *Chemico-biological interactions 178*, 171–177.

(*70*) Yi, J., *Aldo-keto reductases and role in human disease*; Frontiers Research Topic Ebook; Frontiers E-books: 2013.

(*71*) Penning, T. M. (2005). AKR1B10: a new diagnostic marker of non-small cell lung carcinoma in smokers. *Clinical Cance Research 5*, 80–83.

(*72*) Burchiel, S. W., Thompson, T. A., Lauer, F. T., and Oprea, T. I. (2007). Activation of dioxin response element (DRE)-associated genes by benzo(a)pyrene 3,6-quinone and benzo(a)pyrene 1,6-quinone in MCF-10A human mammary epithelial cells. *Toxicology and Applied Pharmacology 221*, 203–214.

(*73*) Liu, Z., Zhong, L., Krishack, P. A., Robbins, S., Cao, J. X., Zhao, Y., Chung, S., and Cao, D. (2009). Structure and promoter characterization of aldo-keto reductase family 1B10 gene. *Gene 437*, 39–44.

(*74*) Yan, R., Zu, X., Ma, J., Liu, Z., Adeyanju, M., and Cao, D. (2007). Aldo-keto reductase family 1 B10 gene silencing results in growth inhibition of colorectal cancer cells: Implication for cancer intervention. *International Journal of Cancer 121*, 2301–2306.

(*75*) Quinn, A. M., Harvey, R. G., and Penning, T. M. (2008). Oxidation of PAH trans-Dihydrodiols by Human Aldo-Keto Reductase AKR1B10. *Chemical Research in Toxicology 21*, 2207–2215.

(*76*) Ruiz, F. X., Porté, S., Parés, X., and Farrés, J. (2012). Biological role of aldo-keto reductases in retinoic Acid biosynthesis and signaling. *Frontiers in pharmacology 3*, 58.

(*77*) Shen, Y., Zhong, L., Johnson, S., and Cao, D. (2011). Human aldo-keto reductases 1B1 and 1B10: a comparative study on their enzyme activity toward electrophilic carbonyl compounds. *Chemico-biological interactions 191*, 192–198.

(*78*) Bacolod, M. D., Lin, S. M., Johnson, S. P., Bullock, N., Colvin, M., Bigner, D. D., and Friedman, H. S. (2008). The Gene Expression Profiles of Medulloblastoma Cell Lines Resistant to Preactivated Cyclophosphamide. *Current Cancer Drug Targets 8*, 172–179.

(*79*) Noh, E. J., Jang, E. R., Jeong, G., Lee, Y. M., Min, C. K., and Lee, J.-S. (2005). Methyl CpG–Binding Domain Protein 3 Mediates Cancer-Selective Cytotoxicity by Histone Deacetylase Inhibitors via Differential Transcriptional Reprogramming in Lung Cancer Cells. *Cancer Research 65*, 11400–11410.

(*80*) Selga, E., Noé, V., and Ciudad, C. J. (2008). Transcriptional regulation of aldo-keto reductase 1C1 in HT29 human colon cancer cells resistant to methotrexate: Role in the cell cycle and apoptosis. *Biochemical Pharmacology 75*, 414–426.

(*81*) Yang, X., Tang, D., Wang, J., and Cao, D. (2003). Screening of the drug resistance-associated gene in HepG2 cell line transfected with aldose reductase like gene-1 (ARL-1). *Ai Zheng 22*, 1289–1295.

(*82*) Zhong, L., Shen, H., Huang, C., Jing, H., and Cao, D. (2011). AKR1B10 induces cell resistance to daunorubicin and idarubicin by reducing C13 ketonic group. *Toxicology and Applied Pharmacology 255*, 40–47.

(*83*) Heibein, A. D., Guo, B., Sprowl, J. A., MacLean, D. A., and Parissenti, A. M. (2012). Role of aldo-keto reductases and other doxorubicin pharmacokinetic genes in doxorubicin resistance, DNA binding, and subcellular localization. *BMC Cancer 12*, 1–14.

(*84*) Endo, S., Matsunaga, T., Kuwata, K., Zhao, H.-T., El-Kabbani, O., Kitade, Y., and Hara, A. (2010). Chromene-3-carboxamide derivatives discovered from virtual screening as potent inhibitors of the tumour maker, AKR1B10. *Bioorganic & medicinal chemistry 18*, 2485–2490.

(*85*) Endo, S., Matsunaga, T., Soda, M., Tajima, K., Zhao, H.-T., El-Kabbani, O., and Hara, A. (2010). Selective inhibition of the tumor marker AKR1B10 by antiinflammatory N-phenylanthranilic acids and glycyrrhetic acid. *Biological & pharmaceutical bulletin 33*, 886–890.

(*86*) Matsunaga, T., Wada, Y., Endo, S., Soda, M., El-Kabbani, O., and Hara, A. (2012). Aldo-Keto Reductase 1B10 and Its Role in Proliferation Capacity of Drug-Resistant Cancers. *Frontiers in pharmacology 3*.

(*87*) Matsunaga, T., Endo, S., Soda, M., Zhao, H.-T., El-Kabbani, O., Tajima, K., and Akira, H. (2009). Potent and selective inhibition of the tumor marker AKR1B10 by bis-demethoxy curcumin: Probing the active site of the enzyme with molecular modeling and site-directed mutagenesis. *Biochemical and Biophysical Research Communications 389*, 128–132.

(*88*) Ruiz, F. X., Cousido-Siah, A., Mitschler, A., Farrés, J., Parés, X., and Podjarny, A. (2013). X-ray structure of the V301L aldo-keto reductase 1B10 complexed with $NADP^+$ and the potent aldose reductase inhibitor fidarestat: Implications for inhibitor binding and selectivity. *Chemico-Biological Interactions 202*, 178–185.

(*89*) Porté, S., Ruiz, F. X., Giménez, J., Molist, I., Alvarez, S., Domínguez, M., Alvarez, R., de Lera, A. R., Parés, X., and Farrés, J. (2013). Aldo-keto reductases in retinoid metabolism: search for substrate specificity and inhibitor selectivity. *Chemico-biological interactions 202*, 186–194.

(*90*) Cousido-Siah, A., Ruiz, F. X., Crespo, I., Porté, S., Mitschler, A., Parés, X., Podjarny, A., and Farrés, J. (2015). Structural analysis of sulindac as an inhibitor of aldose reductase and AKR1B10. *Chemico-Biological Interactions 234*, 290–296.

(*91*) Ruiz, F. X., Cousido-Siah, A., Porté, S., Domínguez, M., Crespo, I., Rechlin, C., Mitschler, A., de Lera, Á. R., Martín, M. J., de la Fuente, J. Á., Klebe, G., Parés, X., Farrés, J., and Podjarny, A. (2015). Structural Determinants of the Selectivity of 3-Benzyluracil-1-acetic Acids toward Human Enzymes Aldose Reductase and AKR1B10. *ChemMedChem 10*, 1989–2003.

(*92*) Zhang, L., Zhang, H., Zhao, Y., Li, Z., Chen, S., Zhai, J., Chen, Y., Xie, W., Wang, Z., Li, Q., Zheng, X., and Hu, X. (2013). Inhibitor selectivity between aldo-keto reductase superfamily members AKR1B10 and AKR1B1: Role of Trp112 (Trp111). *FEBS Letters 587*, 3681–3686.

(*93*) Soda, M., Hu, D., Endo, S., Takemura, M., Li, J., Wada, R., Ifuku, S., Zhao, H.-T., El-Kabbani, O., Ohta, S., Yamamura, K., Toyooka, N., Hara, A., and Matsunaga, T. (2012). Design, synthesis and evaluation of caffeic acid phenethyl ester-based inhibitors targeting a selectivity pocket in the active site of human aldo-keto reductase 1B10. *European journal of medicinal chemistry 48*, 321–329.

(*94*) Takemura, M., Endo, S., Matsunaga, T., Soda, M., Zhao, H.-T., El-Kabbani, O., Tajima, K., Iinuma, M., and Hara, A. (2011). Selective Inhibition of the Tumor Marker Aldo-keto Reductase Family Member 1B10 by Oleanolic Acid. *Journal of Natural Products 74*, 1201–1206.

(*95*) Song, D.-G., Lee, J. Y., Lee, E. H., Jung, S. H., Nho, C. W., Cha, K. H., Koo, S. Y., and Pan, C.-H. (2010). Inhibitory effects of polyphenols isolated from *Rhus verniciflua* on Aldo-keto reductase family 1B10. *BMB reports 4*, 268–272.

(*96*) Zhao, H.-T., Soda, M., Endo, S., Hara, A., and El-Kabbani, O. (2010). Selectivity determinants of inhibitor binding to the tumour marker human aldose reductase-like protein (AKR1B10) discovered from molecular docking and database screening. *European Journal of Medicinal Chemistry 45*, 4354–4357.

(*97*) Hara, A., Matsuura, K., Tamada, Y., Sato, K., Miyabe, Y., Deyashiki, Y., and Ishida, N. (1996). Relationship of human liver dihydrodiol dehydrogenases to hepatic bile acid binding protein and an oxidoreductase of human colon cells. *Biochemical Journal 313 (pt2)*, 373–376.

(*98*) Verma, M., Martin, H.-J., Haq, W., O'Connor, T. R., Maser, E., and Balendiran, G. K. (2008). Inhibiting wild-type and C299S mutant AKR1B10; a homologue of aldose reductase upregulated in cancers. *European Journal of Pharmacology 584*, 213–221.

(*99*) Hackett, N. R., Butler, M. W., Shaykhiev, R., Salit, J., Omberg, L., Rodriguez-Flores, J. L., Mezey, J. G., Strulovici-Barel, Y., Wang, G., Didon, L., and Crystal, R. G. (2012). RNA-Seq quantification of the human small airway epithelium transcriptome. *BMC genomics 13*, 82.

(*100*) Constantinescu, S., Hecht, K., Sobotzki, N., Erzinger, M. M., Bovet, C., Shay, J. W., Wollscheid, B., Sturla, S. J., Marra, G., and Beerenwinkel, N. (2014). Transcriptomic responses of cancerous and noncancerous human colon cells to sulforaphane and selenium. *Chemical research in toxicology 27*, 377–386.

(*101*) Calvo, S. E. et al. (2012). Molecular diagnosis of infantile mitochondrial disease with targeted next-generation sequencing. *Science translational medicine 4*, 118ra10.

(*102*) Reumers, J., De Rijk, P., Zhao, H., Liekens, A., Smeets, D., Cleary, J., Van Loo, P., Van Den Bossche, M., Catthoor, K., Sabbe, B., Despierre, E., Vergote, I., Hilbush, B., Lambrechts, D., and Del-Favero, J. (2012). Optimized filtering reduces the error rate in detecting genomic variants by short-read sequencing. *Nature biotechnology 30*, 61–68.

(*103*) Tanowitz, H. B., Mukhopadhyay, A., Ashton, A. W., Lisanti, M. P., Machado, F. S., Weiss, L. M., and Mukherjee, S. (2011). Microarray analysis of the mammalian thromboxane receptor *Trypanosoma cruzi* interaction. *Cell Cycle 10*, 1132–1143.

(*104*) Yashin, A. I., Wu, D., Arbeev, K. G., and Ukraintseva, S. V. (2010). Joint influence of small-effect genetic variants on human longevity. *Aging 2*, 612–620.

(*105*) Gui, T., Tanimoto, T., Kokai, Y., and Nishimura, C. (1995). Presence of a Closely Related Subgroup in the Aldo-ketoreductase Family of the Mouse. *European Journal of Biochemistry 227*, 448–453.

(*106*) Pailhoux, E. A., Martinez, A., Veyssiere, G. M., and Jean, C. G. (1990). Androgen-dependent protein from mouse vas deferens. cDNA cloning and protein homology with the aldo-keto reductase superfamily. *Journal of Biological Chemistry 265*, 19932–19936.

(*107*) Donohue, P. J., Alberts, G. F., Hampton, B. S., and Winkles, J. A. (1994). A delayed-early gene activated by fibroblast growth factor-1 encodes a protein related to aldose reductase. *Journal of Biological Chemistry 269*, 8604–8609.

(*108*) Joshi, A., Rajput, S., Wang, C., Ma, J., and Cao, D. (2010). Murine aldo-keto reductase family 1 subfamily B: identification of AKR1B8 as an ortholog of human AKR1B10. *Biological Chemistry 391*, 1371–1378.

(*109*) Srivastava, S., Harter, T. M., Chandra, A., Bhatnagar, A., Srivastava, S. K., and Mark, P. J. (1998). Kinetic Studies of FR-1, a Growth Factor-Inducible Aldo-Keto Reductase. *Biochemistry 37*, 12909–12917.

(*110*) Machura, K., Iankilevitch, E., Neubauer, B., Theuring, F., and Kurtz, A. (2013). The aldo-keto reductase AKR1B7 coexpresses with renin without influencing renin production and secretion. *Renal Physiology 304*, 578–584.

(*111*) Lin, E. E., Pentz, E. S., Sequeira-Lopez, M. L. S., and Gomez, R. A. (2015). Aldo-keto reductase 1b7, a novel marker for renin cells, is regulated by cyclic AMP signaling. *American Journal of Physiology - Regulatory, Integrative and Comparative Physiology 309*, 576–584.

(*112*) Jagoe, W. N., Howe, K., O'Brien, S. C., and Carroll, J. (2013). Identification of a role for a mouse sperm surface aldo-keto reductase (AKR1B7) and its human analogue in the detoxification of the reactive aldehyde, acrolein. *Andrologia 45*, 326–331.

(*113*) Zeindl-Eberhart, E., Klugbauer, S., Dimitrijevic, N., Jungblut, P. R., Lamer, S., and Rabes, H. M. (2001). Proteome analysis of rat hepatomas: Carcinogen-dependent tumor-associated protein variants. *ELECTROPHORESIS 22*, 3009–3018.

(*114*) Old, S. E., Sato, S., Kador, P. F., and Carper, D. A. (1990). In vitro expression of rat lens aldose reductase in *Escherichia coli*. *Proceedings of the National Academy of Sciences of the United States of America 87*, 4942–4945.

(*115*) Martinez, A., Aigueperse, C., Val, P., Dussault, M.-H., Tournaire, C., Berger, M., Veyssière, G., Jean, C., and Lefrançois Martinez, A.-M. (2001). Physiological functions and hormonal regulation of mouse vas deferens protein (AKR1B7) in steroidogenic tissues. *Chemico-Biological Interactions 130-132*, 903–917.

(*116*) Endo, S., Matsunaga, T., Kuragano, T., Ohno, S., Kitade, Y., Tajima, K., El-Kabbani, O., and Hara, A. (2010). Properties and tissue distribution of a novel aldo–keto reductase encoding in a rat gene (Akr1b10). *Archives of Biochemistry and Biophysics 503*, 230–237.

(*117*) Hyndman, D. J., Takenoshita, R., Vera, N. L., Pang, S. C., and Flynn, T. G. (1997). Cloning, Sequencing, and Enzymatic Activity of an Inducible Aldo-Keto Reductase from Chinese Hamster Ovary Cells. *Journal of Biological Chemistry 272*, 13286–13291.

(*118*) Crosas, B., Cederlund, E., Torres, D., Jornvall, H., Farrés, J., and Parés, X. (2001). A vertebrate aldo-keto reductase active with retinoids and ethanol. *The Journal of biological chemistry 276*, 19132–19140.

(*119*) Ho, H. T. B., Chung, S. K., Law, J. W. S., Ko, B. C. B., Tam, S. C. F., Brooks, H. L., Knepper, M. A., and Chung, S. S. M. (2000). Aldose Reductase-Deficient Mice Develop Nephrogenic Diabetes Insipidus. *Molecular and Cellular Biology 20*, 5840–5846.

(*120*) Ye, Q., Hyndman, D., Li, X., Flynn, T. G., and Jia, Z. (2000). Crystal structure of CHO reductase, a member of the aldo-keto reductase superfamily. *Proteins: Structure, Function, and Bioinformatics 38*, 41–48.

(*121*) Blomhoff, R., and Blomhoff, H. K. (2006). Overview of retinoid metabolism and function. *Journal of Neurobiology 66*, 606–630.

(*122*) Martras, S., Álvarez, R., Gallego, O., Domínguez, M., de Lera, Á. R., Farrés, J., and Parés, X. (2004). Kinetics of human alcohol dehydrogenase with ring-oxidized retinoids: effect of Tween 80. *Archives of Biochemistry and Biophysics 430*, 210–217.

(*123*) Kakkad, B. P., and Ong, D. E. (1988). Reduction of retinaldehyde bound to cellular retinol-binding protein (type II) by microsomes from rat small intestine. *Journal of Biological Chemistry 263*, 12916–12919.

(*124*) Kelly, M., and von Lintig, J. (2015). STRA6: role in cellular retinol uptake and efflux. *Hepatobiliary Surgery and Nutrition 4*, 229–242.

(*125*) Kawaguchi, R., Zhong, M., Kassai, M., Ter-Stepanian, M., and Sun, H. (2015). Vitamin A Transport Mechanism of the Multitransmembrane Cell-Surface Receptor STRA6. *5*, 425.

(*126*) Kawaguchi, R., Yu, J., Ter-Stepanian, M., Zong, M., Cheng, G., Yuan, Q., Jin, M., Travis, G. H., Ong, D., and Sun, H. (2011). Receptor-Mediated Cellular Uptake Mechanism That Couples to Intracellular Storage. *ACS Chemical Biology 6*, 1041–1051.

(*127*) Kawaguchi, R., Yu, J., Honda, J., Hu, J., Whitelegge, J., Ping, P., Wiita, P., Bok, D., and Sun, H. (2007). A Membrane Receptor for Retinol Binding Protein Mediates Cellular Uptake of Vitamin A. *Science 315*, 820–825.

(*128*) Isken, A., Golczak, M., Oberhauser, V., Hunzelmann, S., Driever, W., Imanishi, Y., Palczewski, K., and Palczewski, J. P. (2008). RBP4 Disrupts Vitamin A Uptake Homeostasis in a STRA6-Deficient Animal Model for Matthew-Wood Syndrome. *Cell Metabolism 7*, 258–268.

(*129*) O'Byrne, S. M., and Blaner, W. S. (2013). Retinol and retinyl esters: biochemistry and physiology. *Journal of Lipid Research 54*, 1731–1743.

(*130*) Eroglu, A., and Harrison, E. H. (2013). Carotenoid metabolism in mammals, including man: formation, occurrence, and function of apocarotenoids. *Journal of Lipid Research 54*, 1719–1730.

(*131*) Kedishvili, N. Y. (2013). Enzymology of retinoic acid biosynthesis and degradation. *Journal of lipid research 54*, 1744–1760.

(*132*) Harrison, E. H. (2012). Mechanisms involved in the intestinal absorption of dietary vitamin A and provitamin A carotenoids. *Biochimica et Biophysica Acta 1821*, 70–77.

(*133*) Napoli, J. L. (1999). Interactions of retinoid binding proteins and enzymes in retinoid metabolism. *Biochimica et Biophysica Acta 1440*, 139–162.

(*134*) Belyaeva, O. V., Johnson, M. P., and Kedishvili, N. Y. (2008). Kinetic Analysis of Human Enzyme RDH10 Defines the Characteristics of a Physiologically Relevant Retinol Dehydrogenase. *Journal of Biological Chemistry 283*, 20299–20308.

(*135*) Parés, X., Farrés, J., Kedishvili, N., and Duester, G. (2008). Medium- and short-chain dehydrogenase/reductase gene and protein families. *Cellular and Molecular Life Sciences 65*, 3936–3949.

(*136*) Ang, H. L., Deltour, L., Hayamizu, T. F., Zgombic-Knight, M., and Duester, G. (1996). Retinoic Acid Synthesis in Mouse Embryos during Gastrulation and Craniofacial Development Linked to Class IV Alcohol Dehydrogenase Gene Expression. *Journal of Biological Chemistry 271*, 9526–9534.

(*137*) Haselbeck, R. J., Ang, H. L., and Duester, G. (1997). Class IV alcohol/retinol dehydrogenase localization in epidermal basal layer: Potential site of retinoic acid synthesis during skin development. *Developmental Dynamics 208*, 447–453.

(*138*) Deltour, L., Haselbeck, R. J., Ang, H. L., and Duester, G. (1997). Localization of class I and class IV alcohol dehydrogenases in mouse testis and epididymis: potential retinol dehydrogenases for endogenous retinoic acid synthesis. *Biology of Reproduction 56*, 102–109.

(*139*) Deltour, L., Foglio, M. H., and Duester, G. (1999). Metabolic Deficiencies in Alcohol Dehydrogenase Adh1, Adh3 and Adh4 Null Mutant Mice: overlapping roles of ADH1 and ADH4 in ethanol clearance and metabolism of retinol to retinoic acid. *Journal of Biological Chemistry 274*, 16796–16801.

(*140*) Molotkov, A., Fan, X., Deltour, L., Foglio, M. H., Martras, S., Farrés, J., Parés, X., and Duester, G. (2002). Stimulation of retinoic acid production and growth by ubiquitously expressed alcohol dehydrogenase Adh3. *Proceedings of the National Academy of Sciences of the United States of America 99*, 5337–5342.

(*141*) Molotkov, A., Ghyselinck, N. B., Chambon, P., and Duester, G. (2004). Opposing actions of cellular retinol-binding protein and alcohol dehydrogenase control the balance between retinol storage and degradation. *Biochemical Journal 383*, 295–302.

(*142*) Deltour, L., Foglio, M. H., and Duester, G. (1999). Impaired retinol utilization in Adh4 alcohol dehydrogenase mutant mice. *Developmental Genetics 25*, 1–10.

(*143*) Molotkov, A., Deltour, L., Foglio, M. H., Cuenca, A. E., and Duester, G. (2002). Distinct Retinoid Metabolic Functions for Alcohol Dehydrogenase Genes Adh1 and Adh4 in Protection against Vitamin A Toxicity or Deficiency Revealed in Double Null Mutant Mice. *Journal of Biological Chemistry 277*, 13804–13811.

(*144*) Svensson, S., Some, M., Lundsjö, A., Helander, A., Cronholm, T., and Höög, J.-O. (1999). Activities of human alcohol dehydrogenases in the metabolic pathways of ethanol and serotonin. *European Journal of Biochemistry 262*, 324–329.

(*145*) Yang, Z.-N., Davis, G. J., Hurley, T. D., Stone, C. L., Li, T.-K., and Bosron, W. F. (1994). Catalytic Efficiency of Human Alcohol Dehydrogenases for Retinol Oxidation and Retinal Reduction. *Alcoholism: Clinical and Experimental Research 18*, 587–591.

(*146*) Persson, B. et al. (2009). The SDR (short-chain dehydrogenase/reductase and related enzymes) nomenclature initiative. *Chemico-Biological Interactions 178*, 94–98.

(*147*) Lee, S.-A., Belyaeva, O. V., and Kedishvili, N. Y. (2008). Effect of lipid peroxidation products on the activity of human retinol dehydrogenase 12 (RDH12) and retinoid metabolism. *Biochimica et Biophysica Acta 1782*, 421–425.

(*148*) Lee, S.-A., Belyaeva, O. V., and Kedishvili, N. Y. (2010). Disease-associated variants of microsomal retinol dehydrogenase 12 (RDH12) are degraded at mutant-specific rates. *FEBS Letters 584*, 507–510.

(*149*) Lee, S.-A., Belyaeva, O. V., Wu, L., and Kedishvili, N. Y. (2011). Retinol Dehydrogenase 10 but Not Retinol/Sterol Dehydrogenase(s) Regulates the Expression of Retinoic Acid-responsive Genes in Human Transgenic Skin Raft Culture. *Journal of Biological Chemistry 286*, 13550–13560.

(*150*) Belyaeva, O. V., Lee, S.-A., Adams, M. K., Chang, C., and Kedishvili, N. Y. (2012). Short Chain Dehydrogenase/Reductase Rdhe2 Is a Novel Retinol Dehydrogenase Essential for Frog Embryonic Development. *Journal of Biological Chemistry 287*, 9061–9071.

(*151*) Sandell, L. L., Sanderson, B. W., Moiseyev, G., Johnson, T., Mushegian, A., Young, K., Rey, J.-P., Ma, J.-X., Staehling-Hampton, K., and Trainor, P. A. (2007). RDH10 is essential for synthesis of embryonic retinoic acid and is required for limb, craniofacial, and organ development. *Genes & Development 21*, 1113–1124.

(*152*) Rhinn, M., Schuhbaur, B., Niederreither, K., and Dollé, P. (2011). Involvement of retinol dehydrogenase 10 in embryonic patterning and rescue of its loss of function by maternal retinaldehyde treatment. *Proceedings of the National Academy of Sciences 108*, 16687–16692.

(*153*) Lee, S.-A., Belyaeva, O. V., and Kedishvili, N. Y. (2009). Biochemical characterization of human epidermal retinol dehydrogenase 2. *Chemico-Biological Interactions 178*, 182–187.

(*154*) Endo, K., Fukui, M., Mishima, M., and Watanabe, K. (2001). Metabolism of Vitamin A Affected by Prostaglandin F Synthase in Contractile Interstitial Cells of Bovine Lung. *Biochemical and Biophysical Research Communications 287*, 956–961.

(*155*) Endo, S., Matsunaga, T., Horie, K., Tajima, K., Bunai, Y., Carbone, V., El-Kabbani, O., and Hara, A. (2007). Enzymatic characteristics of an aldo-keto reductase family protein (AKR1C15) and its localization in rat tissues. *Archives of Biochemistry and Biophysics 465*, 136–147.

(*156*) Ruiz, F. X., Porté, S., Gallego, O., Moro, A., Ardèvol, A., Del Río-Espinola, A., Rovira, C., Farrés, J., and Parés, X. (2011). Retinaldehyde is a substrate for human aldo-keto reductases of the 1C subfamily. *The Biochemical journal 440*, 335–344.

(*157*) Duester, G. (2000). Families of retinoid dehydrogenases regulating vitamin A function. *European Journal of Biochemistry 267*, 4315–4324.

(*158*) Poulain, S., Evenou, F., Carré, M.-C., Corbel, S., Vignaud, J.-M., and Martinet, N. (2009). Vitamin A/retinoids signalling in the human lung. *Lung Cancer 66*, 1–7.

(*159*) Zhang, R., Wang, Y., Li, R., and Chen, G. (2015). Transcriptional Factors Mediating Retinoic Acid Signals in the Control of Energy Metabolism. *16*, 14210–14244.

(*160*) Tang, X.-H., and Gudas, L. J. (2011). Retinoids, Retinoic Acid Receptors, and Cancer. *Annual Review of Pathology: Mechanisms of Disease 6*, 345–364.

(*161*) Shaw, N., Elholm, M., and Noy, N. (2003). Retinoic Acid Is a High Affinity Selective Ligand for the Peroxisome Proliferator-activated Receptor β/δ. *Journal of Biological Chemistry 278*, 41589–41592.

(*162*) Wolf, G. (2008). Retinoic acid as cause of cell proliferation or cell growth inhibition depending on activation of one of two different nuclear receptors. *Nutrition Reviews 66*, 55–59.

(*163*) Tan, N.-S., Shaw, N. S., Vinckenbosch, N., Liu, P., Yasmin, R., Desvergne, B., Wahli, W., and Noy, N. (2002). Selective Cooperation between Fatty Acid Binding Proteins and Peroxisome Proliferator-Activated Receptors in Regulating Transcription. *Molecular and Cellular Biology 22*, 5114–5127.

(*164*) Schug, T. T., Berry, D. C., Shaw, N. S., Travis, S. N., and Noy, N. (2007). Opposing Effects of Retinoic Acid on Cell Growth Result from Alternate Activation of Two Different Nuclear Receptors. *Cell 129*, 723–733.

(*165*) Schug, T. T., Berry, D. C., Toshkov, I. A., Cheng, L., Nikitin, A. Y., and Noy, N. (2008). Overcoming retinoic acid-resistance of mammary carcinomas by diverting retinoic acid from PPARβ/δ to RAR. *Proceedings of the National Academy of Sciences 105*, 7546–7551.

(*166*) Kumar, S., Sandell, L. L., Trainor, P. A., Koentgen, F., and Duester, G. (2012). Alcohol and aldehyde dehydrogenases: Retinoid metabolic effects in mouse knockout models. *Biochimica et Biophysica Acta 1821*, 198–205.

(*167*) Duester, G. (1996). Involvement of Alcohol Dehydrogenase, Short-Chain Dehydrogenase / Reductase, Aldehyde Dehydrogenase, and Cytochrome P450 in the Control of Retinoid Signaling by Activation of Retinoic Acid Synthesis. *Biochemistry 35*, 12221–12227.

(*168*) Ruiz, F. X., Moro, A., Gallego, O., Ardèvol, A., Rovira, C., Petrash, J. M., Parés, X., and Farrés, J. (2011). Human and rodent aldo-keto reductases from the AKR1B subfamily and their specificity with retinaldehyde. *Chemico-biological interactions 191*, 199–205.

(*169*) Ma, J., Luo, D.-X., Huang, C., Shen, Y., Bu, Y., Markwell, S., Gao, J., Liu, J., Zu, X., Cao, Z., Gao, Z., Lu, F., Liao, D.-F., and Cao, D. (2012). AKR1B10 overexpression in breast cancer: association with tumor size, lymph node metastasis and patient survival and its potential as a novel serum marker. *International Journal of Cancer 131*, 862–871.

(*170*) Chatzopoulou, M., Alexiou, P., Kotsampasakou, E., and Demopoulos, V. J. (2012). Novel aldose reductase inhibitors: a patent survey (2006–present). *Expert opinion on therapeutic patents 22*, 1303–1323.

(*171*) Pathania, S., Randhawa, V., and Bagler, G. (2013). Prospecting for novel plant-derived molecules of *Rauvolfia serpentina* as inhibitors of Aldose Reductase, a potent drug target for diabetes and its complications. *PloS ONE 8*, e61327.

(*172*) Zhang, L., Zhang, H., Zheng, X., Zhao, Y., Chen, S., Chen, Y., Zhang, R., Li, Q., and Hu, X. (2014). Structural basis for the inhibition of AKR1B10 by caffeic acid phenethyl ester (CAPE). *ChemMedChem 9*, 706–709.

(*173*) de Marco, A., Deuerling, E., Mogk, A., Tomoyasu, T., and Bukau, B. (2007). Chaperone-based procedure to increase yields of soluble recombinant proteins produced in *E. coli*. *BMC biotechnology 7*, 32.

(*174*) Larroy, C., Parés, X., and Biosca, J. A. (2002). Characterization of a *Saccharomyces cerevisiae* NADP(H)-dependent alcohol dehydrogenase (ADHVII), a member of the cinnamyl alcohol dehydrogenase family. *European Journal of Biochemistry 269*, 5738–5745.

(*175*) Kuksa, V., Imanishi, Y., Batten, M., Palczewski, K., and Moise, A. R. (2003). Retinoid cycle in the vertebrate retina: experimental approaches and mechanisms of isomerization. *Vision research 43*, 2959–2981.

(*176*) Belyaeva, O. V., Korkina, O. V., Stetsenko, A. V., Kim, T., Nelson, P. S., and Kedishvili, N. Y. (2005). Biochemical properties of purified human retinol dehydrogenase 12 (RDH12): catalytic efficiency toward retinoids and C9 aldehydes and effects of cellular retinol-binding protein type I (CRBPI) and cellular retinaldehyde-binding protein (CRALBP) on the oxidation and reduction of retinoids. *Biochemistry 44*, 7035–7047.

(*177*) Canutescu, A. A., Shelenkov, A. A., and Dunbrack, R. L. (2003). A graph-theory algorithm for rapid protein side-chain prediction. *Protein science 12*, 2001–2014.

(*178*) Pronk, S., Páll, S., Schulz, R., Larsson, P., Bjelkmar, P., Apostolov, R., Shirts, M. R., Smith, J. C., Kasson, P. M., van der Spoel, D., Hess, B., and Lindahl, E. (2013). GROMACS 4.5: a high-throughput and highly parallel open source molecular simulation toolkit. *Bioinformatics 29*, 845–854.

(*179*) Hornak, V., Abel, R., Okur, A., Strockbine, B., Roitberg, A., and Simmerling, C. (2006). Comparison of multiple Amber force fields and development of improved protein backbone parameters. *Proteins 65*, 712–725.

(*180*) Lindorff-Larsen, K., Piana, S., Palmo, K., Maragakis, P., Klepeis, J. L., Dror, R. O., and Shaw, D. E. (2010). Improved side-chain torsion potentials for the Amber ff99SB protein force field. *Proteins 78*, 1950–1958.

(*181*) Holmberg, N., Ryde, U., and Bülow, L. (1999). Redesign of the coenzyme specificity in L-lactate dehydrogenase from *Bacillus stearothermophilus* using site-directed mutagenesis and media engineering. *Protein engineering 12*, 851–856.

(*182*) Hawkins, G. D., Cramer, C. J., and Truhlan, D. G. (1996). Parametrized Models of Aqueous Free Energies of Solvation Based on Pairwise Descreening of Solute Atomic Charges from a Dielectric Medium. *Journal of Physical Chemistry 100*, 19824–19839.

(*183*) Seeliger, D., Haas, J., and de Groot, B. L. (2007). Geometry-based sampling of conformational transitions in proteins. *Structure 15*, 1482–1492.

(*184*) de Groot, B. L., van Aalten, D. M., Scheek, R. M., Amadei, A., Vriend, G., and Berendsen, H. J. (1997). Prediction of protein conformational freedom from distance constraints. *Proteins 29*, 240–251.

(*185*) Laskowski, R. A., MacArthur, M. W., Moss, D. S., and Thornton, J. M. (1993). PROCHECK: a program to check the stereochemical quality of protein structures. *Journal of Applied Crystallography 26*, 283–291.

(*186*) Eisenberg, D., Luthy, R., and Bowie, J. U. (1997). VERIFY3D: assessment of protein models with three-dimensional profiles. *Methods in enzymology 277*, 396–404.

(*187*) Goodsell, D. S., Morris, G. M., and Olson, A. J. Automated docking of flexible ligands: applications of AutoDock. *Journal of molecular recognition 9*, 1–5.

(*188*) Řezáč, J., Fanfrlík, J., Salahub, D., and Hobza, P. (2009). Semiempirical Quantum Chemical PM6 Method Augmented by Dispersion and H-Bonding Correction Terms Reliably Describes Various Types of Noncovalent Complexes. *Journal of Chemical Theory and Computation 5*, 1749–1760.

(*189*) Klamt, A., and Schüürmann, G. (1993). COSMO: a new approach to dielectric screening in solvents with explicit expressions for the screening energy and its gradient. *Journal of the Chemical Society 2*, 799–805.

(*190*) Lepšík, M., Řezáč, J., Kolář, M., Pecina, A., Hobza, P., and Fanfrlík, J. (2013). The Semiempirical Quantum Mechanical Scoring Function for *In Silico* Drug Design. *ChemPlusChem 78*, 921–931.

(*191*) Fanfrlík, J., Kolář, M., Kamlar, M., Hurný, D., Ruiz, F. X., Cousido-Siah, A., Mitschler, A., Rezáč, J., Munusamy, E., Lepšík, M., Matějíček, P., Veselý, J., Podjarny, A., and Hobza, P. (2013). Modulation of aldose reductase inhibition by halogen bond tuning. *ACS chemical biology 8*, 2484–2492.

(*192*) Benkert, P., Tosatto, S. C. E., and Schomburg, D. (2008). QMEAN: A comprehensive scoring function for model quality assessment. *Proteins 71*, 261–277.

(*193*) Durrant, J. D., de Oliveira, C. A. F., and McCammon, J. A. (2011). POVME: an algorithm for measuring binding-pocket volumes. *Journal of molecular graphics & modelling 29*, 773–776.

(*194*) Chen, Y., Ma, J.-x., and Crouch, R. K. (2003). Down-regulation of RPE65 protein expression and promoter activity by retinoic acid. *Molecular Vision*, 345–354.

(*195*) Chen, Y., Moiseyev, G., Wu, B. X., Ma, J.-x., and Crouch, R. K. (2003). Visual cycle retinoid processing proteins are present in HEK293S cells. *Vision Research 43*, 3037–3044.

(*196*) Kane, M. A., Chen, N., Sparks, S., and Napoli, J. L. (2005). Quantification of endogenous retinoic acid in limited biological samples by LC/MS/MS. *Biochemical Journal 388*, 363–369.

(*197*) Tao, H., Liu, W., Simmons, B. N., Harris, H. K., Cox, T. C., and Massiah, M. A. (2010). Purifying natively folded proteins from inclusion bodies using sarkosyl, Triton X-100, and CHAPS. *BioTechniques 48*, 61–64.

(*198*) Tsumoto, K., Ejima, D., Kumagai, I., and Arakawa, T. (2003). Practical considerations in refolding proteins from inclusion bodies. *Protein Expression and Purification 28*, 1–8.

(*199*) Kubiseski, T. J., and Flynn, T. G. (1995). Studies on human aldose reductase. Probing the role of arginine 268 by site-directed mutagenesis. *The Journal of biological chemistry 270*, 16911–16917.

(*200*) Maloney, P. C., and Ambudkar, S. V. (1989). Functional reconstitution of prokaryote and eukaryote membrane proteins. *Archives of Biochemistry and Biophysics 269*, 1–10.

(*201*) de Marco, A. (2007). Protocol for preparing proteins with improved solubility by co-expressing with molecular chaperones in *Escherichia coli*. *Nature Protocols 2*, 2632–2639.

(*202*) Calam, E., Porté, S., Fernàndez, M. R., Farrés, J., Parés, X., and Biosca, J. A. (2013). Biocatalytic production of alpha-hydroxy ketones and vicinal diols by yeast and human aldo-keto reductases. *Chemico-biological interactions 202*, 195–203.

(*203*) Germain, P., Kammerer, S., Pérez, E., Peluso-Iltis, C., Tortolani, D., Zusi, F. C., Starrett, J., Lapointe, P., Daris, J.-P., Marinier, A., de Lera, A. R., Rochel, N., and Gronemeyer, H. (2004). Rational design of RAR-selective ligands revealed by RARβ crystal stucture. *EMBO reports 5*, 877–882.

(*204*) Sundaram, K., Endo, S., Matsunaga, T., Tanaka, N., Hara, A., and El-Kabbani, O. (2012). Structure of the His269Arg mutant of the rat aldose reductase-like protein AKR1B14 complexed with NADPH. *Acta Crystallographica Section F 68*, 400–403.

(*205*) Urzhumtsev, A., Tête-Favier, F., Mitschler, A., Barbanton, J., Barth, P., Urzhumtseva, L., Biellmann, J. F., Podjarny, A., and Moras, D. (1997). A 'specificity' pocket inferred from the crystal structures of the complexes of aldose reductase with the pharmaceutically important inhibitors tolrestat and sorbinil. *Structure 5*, 601–612.

(*206*) Kokkinidis, M., Glykos, N., Fadouloglou, V., Christov, C., Karabencheva-Christova, T., Kokkinidis, M., Glykos, N., and Fadouloglou, V. In *Advances in Protein Chemistry and Structural Biology*, 2012; Vol. 87, pp 181–218.

(*207*) Barua, B. A., and Olson, J. A. (1998). Reversed-phase gradient high-performance liquid chromatographic procedure for simultaneous analysis of very polar to nonpolar retinoids, carotenoids and tocopherols in animal and plant samples. *Journal of Chromatography B: Biomedical Sciences and Applications 707*, 69–79.

(*208*) Kane, M. A., Folias, A. E., Wang, C., and Napoli, J. L. (2008). Quantitative Profiling of Endogenous Retinoic Acid in Vivo and in Vitro by Tandem Mass Spectrometry. *Analytical Chemistry 80*, 1702–1708.

(*209*) Kane, M. A., Folias, A. E., and Napoli, J. L. (2008). HPLC/UV quantitation of retinal, retinol, and retinyl esters in serum and tissues. *Analytical Biochemistry 378*, 71–79.

(*210*) Belyaeva, O. V., Korkina, O. V., Stetsenko, A. V., and Kedishvili, N. Y. (2008). Human retinol dehydrogenase 13 (RDH13) is a mitochondrial short-chain dehydrogenase/reductase with a retinaldehyde reductase activity. *The FEBS journal 275*.

(*211*) McCaffery, P., Evans, J., Koul, O., Volpert, A., Reid, K., and Ullman, D. M. (2002). Retinoid quantification by HPLC/MS^n. *Journal of Lipid Research 43*, 1143–1149.

(*212*) Evans, J. E., and McCaffery, P. In *Retinoids. Methods and protocols*, Sun, H., and Travis, G. H., Eds.; Methods in Molecular Biology, Vol. 652; Humana Press: 2010; Chapter 8, pp 149–162.

(*213*) Ramadan, A., Benito, C., Gerhard, D., Walter, E. H., Christel, H.-M., and Jürgen, B. (2012). Quantification of retinoid concentrations in human serum and brain tumor tissues. *Analytica Chimica Acta 725*, 57–66.

(*214*) Yamakoshi, Y., Fukasawa, H., Yamauchi, T., Waki, H., Kadowaki, T., Shudo, K., and Kagechika, H. (2002). Determination of Endogenous Levels of Retinoic Acid Isomers in Type II Diabetes Mellitus Patients. Possible Correlation with HbA1c Values. *Biological and Pharmaceutical Bulletin 25*, 1268–1271.

(*215*) Kim, Y.-K., and Quadro, L. In *Retinoids. Methods and protocols*, Sun, H., and Travis, G. H., Eds.; Methods in Molecular Biology, Vol. 652; Humana Press: 2010; Chapter 15, pp 263–275.

(*216*) Kane, M. A., and Napoli, J. L. In *Retinoids. Methods and protocols*, Sun, H., and Travis, G. H., Eds.; Methods in Molecular Biology, Vol. 652; Humana Press: 2010; Chapter 1, pp 1–54.

(*217*) Johnson, K. J., *The Retinoids: Biology, Chemistry, and Medicine*; Biochemical Education; Headington Hill Hall: 1994.

(*218*) Wyss, R., and Bucheli, F. (1996). Quantitative analysis of retinoids in biological fluids by high-performance liquid chromatography using column swithching. I. Determination of isotretinoin and tretinoin and their 4-oxo metabolites in plasma. *Journal of Chromatography 2*, 303–314.

(*219*) Weickert, M. J., Doherty, D. H., Best, E. A., and Olins, P. O. (1996). Optimization of heterologous protein production in Escherichia coli. *Current Opinion in Biotechnology 7*, 494–499.

(*220*) Hannig, G., and Makrides, S. C. (1998). Strategies for optimizing heterologous protein expression in Escherichia coli. *Trends in Biotechnology 16*, 54–60.

(*221*) Schein, C. H., and Noteborn, M. H. M. (1988). Formation of Soluble Recombinant Proteins in Escherichia Coli is Favored by Lower Growth Temperature. *Nature Biotechnology 3*, 291–294.

(*222*) Hartinger, D., Heinl, S., Schwartz, E. H., Grabherr, R., Schatzmayr, G., Haltrich, D., and Moll, W.-D. (10). Enhancement of solubility in Escherichia coli and purification of an aminotransferase from Sphingopyxis sp. MTA144 for deamination of hydrolyzed fumonisin B1. *Microbial Cell Factories 9*, 1–14.

(*223*) Blackwell, J. R., and Horgan, R. (1991). A novel strategy for production of a highly expressed recombinant protein in an active form. *FEBS Letters 295*, 10–12.

(*224*) Picaud, S., Olsson, M. E., and Brodelius, P. E. (2007). Improved conditions for production of recombinant plant sesquiterpene synthases in Escherichia coli. *Protein Expression and Purification 51*, 71–79.

(*225*) Bolen, D., and Baskakov, I. V. (2001). The osmophobic effect: natural selection of a thermodynamic force in protein folding. *Journal of Molecular Biology 310*, 955–963.

(*226*) Felitsky, D. J., Cannon, J. G., Capp, M. W., Hong, J., Van Wynsberghe, A. W., Anderson, C. F., and Record Jr., M. T. (2004). The Exclusion of Glycine Betaine from Anionic Biopolymer Surface: Why Glycine Betaine Is an Effective Osmoprotectant but Also a Compatible Solute. *Biochemistry 43*, 14732–14743.

(*227*) de Marco, A., and Marco, V. D. (2004). Bacteria co-transformed with recombinant proteins and chaperones cloned in independent plasmids are suitable for expression tuning. *Journal of Biotechnology 109*, 45–52.

(*228*) Schlapschy, M., Grimm, S., and Skerra, A. (2006). A system for concomitant overexpression of four periplasmic folding catalysts to improve secretory protein production in *Escherichia coli*. *Protein Engineering Design and Selection 19*, 385–390.

(*229*) Pastel, E., Pointud, J.-C., Volat, F., Martinez, A., and Lefrançois-Martinez, A.-M. (2012). Aldo-Keto Reductases 1B in Endocrinology and Metabolism. *Frontiers in pharmacology 3*, 148.

(*230*) Yadav, U. C., Ramana, K., and Srivastava, S. K. (2013). Aldose reductase regulates acrolein-induced cytotoxicity in human small airway epithelial cell. *Free Radical Biology and Medicine 65*, 15–25.

(*231*) Estebauer, H., Schaur, R. J., and Zollner, H. (1991). Chemistry and biochemistry of 4-hydroxynonenal, malonaldehyde and related aldehydes. *Free Radical Biology and Medicine 11*, 81–128.

(*232*) Echtay, K. S., Esteves, T. C., Pakay, J. L., Jekabsons, M. B., Lambert, A. J., Portero-Otín, M., Pamplona, R., Vidal-Puig, A. J., Wang, S., Roebuck, S. J., and Brand, M. D. (2003). A signalling role for 4-hydroxy-2-nonenal in regulation of mitochondrial uncoupling. *The EMBO Journal 22*, 4103–4110.

(*233*) Hashimoto, M., Sibata, T., Wasada, H., Toyokuni, S., and Uchida, K. (2003). Structural Basis of Protein-bound Endogenous Aldehydes: Chemical and immunochemical characterizations of configurational isomers of a 4-hydroxy-2-nonenal-histidine adduct. *Journal of Biological Chemistry 278*, 5044–5051.

(*234*) Eder, E., Scheckenbach, S., Deininger, C., and Huffman, C. (1993). The possible role of α, β-unsaturated carbonyl compounds in mutagenesis and carcinogenesis. *Toxicology letters 67*, 87–103.

(*235*) Esterbauer, H., Eckl, P., and Ortner, A. (1990). Possible mutagens derived from lipids and lipid precursors. *Mutation Research/Reviews in Genetic Toxicology 238*, 223–233.

(*236*) De Bont, R., and van Larebeke, N. (2004). Endogenous DNA damage in humans: a review of quantitative data. *Mutagenesis 19*, 169–185.

(*237*) Kato, S., Post, G. C., Bierbaum, V. M., and Koch, T. H. (2002). Chemical Ionization Mass Spectrometric Determination of Acrolein in Human Breast Cancer Cells. *Analytical Biochemistry 305*, 251–259.

(*238*) Rousset, S., Alves-Guerra, M.-C., Mozo, J., Miroux, B., Cassard-Doulcier, A.-M., Bouillaud, F., and Ricquier, D. (2004). The Biology of Mitochondrial Uncoupling Proteins. *Diabetes 53*, S130–S135.

(*239*) Echtay, K. S., Pakay, J. L., and Esteves, M. D., Telma C. Brand (2005). Hydroxynonenal and uncoupling proteins: A model for protection against oxidative damage. *BioFactors 24*, 119–130.

(*240*) Echtay, K. S., and Brand, M. D. (2007). 4-hydroxy-2-nonenal and uncoupling proteins: an approach for regulation of mitochondrial ROS production. *Redox report : communications in free radical research 12*, 26–29.

(*241*) Penning, T. M., and Lerman, C. (2008). Genomics of smoking exposure and cessation: lessons for cancer prevention and treatment. *Cancer Prevenion Research 2*, 80–83.

(*242*) Wang, R., Wang, G., Ricard, M. J., Ferris, B., Strulovici-Barel, Y., Salit, J., Hackett, N. R. H., Gudas, L. J., and Crystal, R. G. (2010). Smoking-Induced Upregulation of AKR1B10 Expression in the Airway Epithelium of Healthy Individuals. *Chest 138*, 1402–1410.

(*243*) Jumper, N., Hodgkinson, T., Arscott, G., Har-Shai, Y., Paus, R., and Bayat, A. (2016). The aldo-keto reductase AKR1B10 is upregulated in keloid epidermis, implicating retinoic acid pathway dysregulation in the pathogenesis of keloid disease. *The Journal of Investigative Dermatology*, Accepted manuscript.

(*244*) Lewis, C. A., Parker, S. J., Fiske, B. P., McCloskey, D., Gui, D. Y., Green, C. R., Vokes, N. I., Feist, A. M., Vander Heiden, M. G., and Metallo, C. M. (2014). Tracing Compartmentalized NADPH Metabolism in the Cytosol and Mitochondria of Mammalian Cells. *Molecular Cell 55*, 253–263.

(*245*) Palczewski, G., Amengual, J., Hoppel, C. L., and von Lintig, J. (2014). Evidence for compartmentalization of mammalian carotenoid metabolism. *FASEB journal : official publication of the Federation of American Societies for Experimental Biology*, 1–13.

(*246*) Kane, M. A. (2011). Analysis, occurrence, and function of 9-cis-retinoic acid. *Biochimica et Biophysica Acta (BBA) - Molecular and Cell Biology of Lipids 1821*, 10–20.

(*247*) Kane, M. A., Folias, A. E., Pingitore, A., Perri, M., Obrochta, K. M., Krois, C. R., Cione, E., Ryu, J. Y., and Napoli, J. L. (2010). Identification of 9-cis-retinoic acid as a pancreas-specific autacoid that attenuates glucose-stimulated insulin secretion. *Proceedings of the National Academy of Sciences 107*, 21884–21889.

(*248*) Heyman, R. A., Mangelsdorf, D. J., Dyck, J. A., Stein, R. B., Eichele, G., Evans, R. M., and Thaller, C. (1992). 9-cis retinoic acid is a high affinity ligand for the retinoid X receptor. *Cell 68*, 397–406.

(*249*) Lin, Y.-W., Lien, L.-M., Yeh, T.-S., Wu, H.-M., Liu, Y.-L., and Hsieh, R.-H. (2008). 9-cis retinoic acid induces retinoid X receptor localized to the mitochondria for mediation of mitochondrial transcription. *Biochemical and Biophysical Research Communications 377*, 351–354.

(*250*) Jiang, W., and Napoli, J. L. (2013). The retinol dehydrogenase Rdh10 localizes to lipid droplets during acyl ester biosynthesis. *Journal of Biological Chemistry 288*, 589–597.

(*251*) Acin-Perez, R., Hoyos, B., Zhao, F., Vinogradov, V., Fischman, D., Harris, R., Leitges, M., Wongsiriroj, N., Blaner, W., Manfredi, G., and Hammerling, U. (2010). Control of oxidative phosphorylation by vitamin A illuminates a fundamental role in mitochondrial energy homoeostasis. *The FASEB journal: official publication of the Federation of American Societies for Experimental Biology 24*.

(*252*) Hoyos, B., Acin-Perez, R., Fischman, D. A., Manfredi, G., and Hammerling, U. (2012). Hiding in plain sight: Uncovering a new function of vitamin A in redox signaling. *Biochimica et Biophysica Acta - Molecular and Cell Biology of Lipids 1821*, 241–247.

(*253*) Zhong, H., and Yin, H. (2015). Role of lipid peroxidation derived 4-hydroxynonenal (4-HNE) in cancer: Focusing on mitochondria. *Redox Biology 4*, 193–199.

(*254*) Luong, C., Miller, A., Barnett, J., Chow, J., Ramesha, C., and Browner, M. F. (1996). Flexibility of the NSAID binding site in the structure of human cyclooxygenase-2. *Nature structural biology 3*, 927–933.

(*255*) Kimble-Hill, A. C., Parajuli, B., Chen, C.-H., Mochly-Rosen, D., and Hurley, T. D. (2014). Development of selective inhibitors for aldehyde dehydrogenases based on substituted indole-2,3-diones. *Journal of medicinal chemistry 57*, 714–722.

(*256*) Sanli, G., Dudley, J. I., and Blaber, M. (2003). Structural biology of the aldo-keto reductase family of enzymes. *Cell Biochemistry and Biophysics 38*, 79–101.

(*257*) Endo, S., Matsunaga, T., Ikari, A., El-Kabbani, O., Hara, A., and Kitade, Y. (2015). Identification of a determinant for strict NADP(H)-specificity and high sensitivity to mixed-type steroid inhibitor of rabbit aldo–keto reductase 1C33 by site-directed mutagenesis. *Archives of Biochemistry and Biophysics 569*, 19–25.

(*258*) Heringlake, S., Hofdmann, M., Fiebeler, A., Manns, M. P., Schmiegel, W., and Tannapfel, A. (2010). Identification and expression analysis of the aldo–keto reductase 1B10 gene in primary malignant liver tumours. *Journal og Hepatologhy 52*, 220–227.

(*259*) Tsuzura, H., Genda, T., Sato, S., Murata, A., Kanemitsu, Y., Narita, Y., Ishikawa, S., Kikuchi, T., Mori, M., Hirano, K., Iijima, K., Wada, R., and Ichida, T. (2014). Expression of Aldo-Keto Reductase Family 1 Member B10 in the Early Stages of Human Hepatocarcinogenesis. *International Journal of Molecular Sciences 15*, 6556–6558.

(*260*) Kang, M.-W., Lee, E.-S., Yoon, S., Jo, J., Lee, J., Kim, H., Choi, Y., Kim, K., Shim, Y., Kim, J., and Kim, H. (2011). AKR1B10 is Associated with Smoking and Smoking-Related Non-Small-Cell Lung Cancer. *Journal of International Medical Research 39*, 78–85.

(*261*) Breton, J., Gage, M. C., Hay, A. W., Keen, J. N., Wild, C. P., Donnellan, C., Findlay, J. B., and Hardie, L. J. (2008). Proteomic screening of a cell line model of esophageal carcinogenesis identifies cathepsin D and aldo-keto reductase 1C2 and 1B10 dysregulation in barrett's esophagus and esophageal adenocarcinoma. *Journal of Proteome Research 7*, 1953–1962.

(*262*) Yoshitake, H., E, Takahashi, M., Ishikawa, H., Nojima, M., Iwanari, H., Watanabe, A., Aburatani, H., Yoshida, K., Ishi, K., Takamori, K., Ogawa, H., Hamakubo, T., Kodama, T., and Araki, Y. (2007). Aldo-keto reductase family 1, member B10 in uterine carcinomas: a potential risk factor of recurrence after surgical therapy in cervical cancer. *International Journal of Gynecological Cancer 17*, 1300–1306.

(*263*) Giménez-Dejoz, J., Kolář, M. H., Ruiz, F. X., Crespo, I., Cousido-Siah, A., Podjarny, A., Barski, O. A., Fanfrlík, J., Parés, X., Farrés, J., and Porté, S. (2015). Substrate Specificity, Inhibitor Selectivity and Structure-Function Relationships of Aldo-Keto Reductase 1B15: A Novel Human Retinaldehyde Reductase. *PLoS ONE 10*, e0134506.

(*264*) Robert, X., and Gouet, P. (2014). Deciphering key features in protein structures with the new ENDscript server. *Nucleic Acids Research 42*, W320–W324.

(*265*) Cleland, W. W. (1979). Substrate inhibition. *Methods in Enzymology 63*, 500–13.

(*266*) Ramanathan, A., and Agarwal, P. K. (2006). Evolutionarily Conserved Linkage between Enzyme Fold, Flexibility, and Catalysis. *PLoS Biology 11*, e1001193.

(*267*) Boehr, D. D., Dyson, H. J., and Wright, P. E. (2006). An NMR Perspective on Enzyme Dynamics. *Chemical Reviews 106*, 3055–3079.

(*268*) Luk, L. Y. P., Loveridge, E. J., and Allemann, R. K. (2015). Protein motions and dynamic effects in enzyme catalysis. *Physical Chemistry Chemical Physics 17*, 30817–30827.

(*269*) Gutteridge, A., and Thornton, J. (2005). Conformational Changes Observed in Enzyme Crystal Structures upon Substrate Binding. *Journal of Molecular Biology 346*, 21–28.

(*270*) Mittal, S., Cai, Y., N. L. Nalam, M., Bolon, D. N. A., and Schiffer, C. A. (2012). Hydrophobic Core Flexibility Modulates Enzyme Activity in HIV-1 Protease. *Journal of the American Chemical Society 134*, 4163–4168.

(*271*) Karshikoff, A., Nilsson, L., and Ladenstein, R. (2015). Rigidity versus flexibility: the dilemma of understanding protein thermal stability. *FEBS Journal 282*, 3899–3917.

(*272*) Henzler-Wildman, K. A., Lei, M., Thai, V., Kerns, S. J., Martin, K., and Kern, D. (2007). A hierarchy of timescales in protein dynamics is linked to enzyme catalysis. *Nature 450*, 913–916.

(*273*) Pudney, C. R., Johannissen, L. O., Sutcliffe, M. J., Hay, S., and Scrutton, N. S. (2010). Direct Analysis of Donor-Acceptor Distance and Relationship to Isotope Effects and the Force Constant for Barrier Compression in Enzymatic H-Tunneling Reactions. *Journal of the American Chemical Society 132*, 11329–11335.

(*274*) Knapp, M. J., Rickert, K., and Klinman, J. P. (2002). Temperature-Dependent Isotope Effects in Soybean Lipoxygenase-1: Correlating Hydrogen Tunneling with Protein Dynamics. *Journal of the American Chemical Society 124*, 3865–3874.

(*275*) Hu, S., Sharma, S. C., Scouras, A. D., Soudackov, A. V., Marcus Carr, C. A., Hammes-Schiffer, S., Alber, T., and Klinman, J. P. (2014). Extremely Elevated Room-Temperature Kinetic Isotope Effects Quantify the Critical Role of Barrier Width in Enzymatic C-H Activation. *Journal of the American Chemical Society 136*, 8157–8160.

(*276*) Bahnson, B. J., Colby, T. D., Chin, J. K., Goldstein, B. M., and Klinman, J. P. (1997). A link between protein structure and enzyme catalyzed hydrogen tunneling. *Proceedings of the National Academy of Sciences of the United States of America 94*, 12797–12802.

(*277*) Penning, T. M. (2015). The aldo-keto reductases (AKRs): Overview. *Chemico-Biological Interactions 234*, 236–246.

(*278*) Gonzales, E., Cresteil, D., Baussan, C., Dabadie, A., Gerhardt, M.-F., and Jacquemin, E. (2004). SRD5B1 (AKR1D1) gene analysis in 4-3-oxosteroid 5β-reductase deficiency: evidence for primary genetic defect. *Journal of Hepatology 40*, 716–718.

(*279*) Drury, J. E., Mindnich, R., and Penning, T. M. (2010). Characterization of Disease-related 5β-Reductase (AKR1D1) Mutations Reveals Their Potential to Cause Bile Acid Deficiency. *Journal of Biological Chemistry 285*, 24529–24537.

(*280*) Guengerich, F. P., and Johnson, W. W. (1999). Kinetics of hydrolysis and reaction of aflatoxin B1 exo-8,9-epoxide and relevance to toxicity and detoxication. *Drug Metabolism Reviews 31*, 141–158.

(*281*) Pratt-Hyatt, M., Lickteig, A. J., and Klaassen, C. D. (2013). Tissue Distribution, Ontogeny, and Chemical Induction of Aldo-Keto Reductases in Mice. *Drug Metabolism and Disposition 41*, 1480–1487.

(*282*) Kabututu, Z., Manin, M., Pointud, J.-C., Maruyama, T., Nagata, N., Lambert, S., Lefrançois-Martinez, A.-M., Martinez, A., and Urade, Y. (2009). Prostaglandin F2α Synthase Activities of Aldo-Keto Reductase 1B1, 1B3 and 1B7. *Journal of Biochemistry 145*, 161–168.

(*283*) Endo, S., Matsunaga, T., Mamiya, H., Hara, A., Kitade, Y., Tajima, K., and El-Kabbani, O. (2009). Characterization of a rat NADPH-dependent aldo-keto reductase (AKR1B13) induced by oxidative stress. *Chemico-Biological Interactions 178*, 151–157.

(*284*) Schmidt, D. R., Schmidt, S., Holmstrom, S. R., Makishima, M., Yu, R. T., Cummins, C. L., Mangelsdorf, D. J., and Kliewer, S. A. (2011). AKR1B7 Is Induced by the Farnesoid X Receptor and Metabolizes Bile Acids. *Journal of Biological Chemistry 286*, 2425–2432.

(*285*) Ho, H. T. B., Jenkins, N. A., Copeland, N. G., Gilbert, D. J., Winkles, J. A., Louie, H. W. Y., Lee, F. K., Chung, S. S. M., and Chung, S. K. (1999). Comparisons of genomic structures and chromosomal locations of the mouse aldose reductase and aldose reductase-like genes. *European Journal of Biochemistry 259*, 726–730.

(*286*) McGowan, M. H., Iwata, T., and Carper, D. A. (1998). Characterization of the Mouse Aldose Reductase Gene and Promoter in a Lens Epithelial Cell Line. *Molecullar Vision 2*.

(*287*) Ramasamy, R., and Goldberg, I. J. (2010). Aldose Reductase and Cardiovascular Diseases, Creating Human-Like Diabetic Complications in an Experimental Model. *Circulation Research 106*, 1449–1458.

(*288*) Fujimori, K., Ueno, T., Nagata, N., Kashiwagi, K., Aritake, K., Amano, F., and Urade, Y. (2010). Suppression of Adipocyte Differentiation by Aldo-keto Reductase 1B3 Acting as Prostaglandin F2α Synthase. *Journal of Biological Chemistry 285*, 8880–8886.

(*289*) Nagata, N., Kusakari, Y., Fukunishi, Y., Inoue, T., and Urade, Y. (2011). Catalytic mechanism of the primary human prostaglandin $F_{2\alpha}$ synthase, aldo-keto reductase 1B1 prostaglandin D_2 synthase activity in the absence of NADP(H). *FEBS Journal 278*, 1288–1298.

(*290*) Tirard, J., Gout, J., Lefrançois-Martinez, A. M., Martinez, A., Begeot, M., and Naville, D. (2007). A Novel Inhibitory Protein in Adipose Tissue, the Aldo-Keto Reductase AKR1B7: Its Role in Adipogenesis. *Endocrinology 148*, 1996–2005.

(*291*) Baumann, C., Davies, B., Peters, M., Kaufmann-Reiche, U., Lessl, M., and Theuring, F. (2007). AKR1B7 (mouse vas deferens protein) is dispensable for mouse development and reproductive success. *Reproduction 134*, 97–109.

(*292*) Lau, E. T., Cao, D., Lin, C., Chung, S. K., and Chung, S. S. (1995). Tissue-specific expression of two aldose reductase-like genes in mice: abundant expression of mouse vas deferens protein and fibroblast growth factor-regulated protein in the drenal gland. *Biochemical Journal 312*, 609–615.

(*293*) Liu, M.-J., Takahashi, Y., Wada, T., He, J., Gao, J., Tian, Y., Li, S., and Xie, W. (2009). The Aldo-Keto Reductase Akr1b7 Gene Is a Common Transcriptional Target of Xenobiotic Receptors Pregnane X Receptor and Constitutive Androstane Receptor. *Molecular Pharmacology 76*, 604–611.

(*294*) Volat, F. E., Pointud, J.-C., Pastel, E., Morio, B., Sion, B., Hamard, G., Guichardant, M., Colas, R., Lefrançois-Martinez, A.-M., and Martinez, A. (2012). Depressed Levels of Prostaglandin $F_{2\alpha}$ in Mice Lacking Akr1b7 Increase Basal Adiposity and Predispose to Diet-Induced Obesity. *Diabetes 61*, 2796–2806.

(*295*) Spite, M., Baba, S., Ahmed, Y., Barski, O., Nijhawan, K., Petrash, J. M., Bhatnagar, A., and Srivastava, S. (2007). Substrate specificity and catalytic efficiency of aldo-keto reductases with phospholipid aldehydes. *Biochemical Journal 405*, 95–105.

(*296*) Biasini, M., Bienert, S., Waterhouse, A., Arnold, K., Studer, G., Schmidt, T., Kiefer, F., Cassarino, T. G., Bertoni, M., Bordoli, L., and Schwede, T. (2014). SWISS-MODEL: modelling protein tertiary and quaternary structure using evolutionary information. *Nucleic Acids Research 42*, W252–W258.

(*297*) Benkert, P., Biasini, M., and Schwede, T. (2011). Toward the estimation of the absolute quality of individual protein structure models. *Bioinformatics 27*, 343–350.

(*298*) Endo, S., Matsunaga, T., Kumada, S., Fujimoto, A., Ohno, S., El-Kabbani, O., Hu, D., Toyooka, N., Mano, J., Tajima, K., and Hara, A. (2012). Characterization of rabbit aldose reductase-like protein with 3β-hydroxysteroid dehydrogenase activity. *Archives of Biochemistry and Biophysics 527*, 23–30.

(*299*) Endo, S., Matsunaga, T., Fujita, A., Tajima, K., El-Kabbani, O., and Hara, A. (2011). Rat Aldose Reductase-Like Protein (AKR1B14) Efficiently Reduces the Lipid Peroxidation Product 4-Oxo-2-nonenal. *Biological and Pharmaceutical Bulletin 33*, 1886–1890.

(*300*) Hartl, F. U., and Hayer-Hartl, M. (2002). Molecular Chaperones in the Cytosol: from Nascent Chain to Folded Protein. *Science 295*, 1852–1858.

(*301*) Lu, Q., and Aon, J. C. (2014). Co-expression for intracellular processing in microbial protein production. *Biotechnology Letters 36*, 427–441.

(*302*) Chuang, C.-k., Su, Y.-S., Fan, C.-T., Lee, W.-C., and Chen, M.-Y. (2009). A dual-functional E. coli vector for expressing recombinant protein with high solubility and antigen presentation ability. *Protein Expression and Purification 65*, 51–56.

(*303*) Kyratsous, C. A., Silverstein, S. J., DeLong, C. R., and Panagiotidis, C. A. (2009). Chaperone-fusion expression plasmid vectors for improved solubility of recombinant proteins in Escherichia coli. *Gene 440*, 9–15.

(*304*) Martínez-Alonso, M., García-Fruitós, E., Ferrer-Miralles, N., Rinas, U., and Villaverde, A. (2010). Side effects of chaperone gene co-expression in recombinant protein production. *Microbial Cell Factories 9*, 1–6.

(*305*) Goloubinoff, P., Gatenby, A. A., and Lorimer, G. H. (1989). GroE heat-shock proteins promote assembly of foreign prokaryotic ribulose bisphosphate carboxylase oligomers in Escherichia coli. *Nature 337*, 44–47.

(*306*) George, R. R., Harris, R., Nunn, C. M., Cramer, R., and Djordjevic, S. (2002). Chaperonin assisted overexpression, purification, and characterisation of human PP2A methyltransferase. *Protein Expression and Purification 26*, 266–274.

(*307*) Zollner, A., Kagawa, N., Waterman, M. R., Nonaka, Y., Takio, K., Shiro, Y., Hannemann, F., and Bernhardt, R. (2008). Purification and functional characterization of human 11β hydroxylase expressed in Escherichia coli. *FEBS Journal 275*, 799–810.

(*308*) Inoue, E., Takahashi, Y., Imai, Y., and Kamataki, T. (2000). Development of Bacterial Expression System with High Yield of CYP3A7, a Human Fetus-Specific Form of Cytochrome P450. *Biochemical and Biophysical Research Communications 269*, 623–627.

(*309*) Yanase, H., Moriya, K., Mukai, N., Kawata, Y., Okamoto, K., and Kato, N. (2002). Effects of GroESL Coexpression on the Folding of Nicotinoprotein Formaldehyde Dismutase from Pseudomonas putida F61. *Bioscience, Biotechnology, and Biochemistry 66*, 85–91.

(*310*) Kolaj, O., Spada, S., Robin, S., and Wall, J. G. (2009). Use of folding modulators to improve heterologous protein production in Escherichia coli. *Microbial Cell Factories 8*, 1–17.

(*311*) Mein, J. R., Dolnikowski, G. G., Ernst, H., Russell, R. M., and Wang, X.-D. (2011). Enzymatic formation of apo-carotenoids from the xanthophyll carotenoids lutein, zeaxanthin and β-cryptoxanthin by ferret carotene-9',10'-monooxygenase. *Archives of Biochemistry and Biophysics 506*, 109–121.

(*312*) Amengual, J., Widjaja-Adhi, M. A. K., Rodriguez-Santiago, S., Hessel, S., Golczak, M., Palczewski, K., and von Lintig, J. (2013). Two Carotenoid Oxygenases Contribute to Mammalian Provitamin A Metabolism. *Journal of Biological Chemistry 288*, 34081–34096.

(*313*) Amengual, J., Lobo, G. P., Golczak, M., Li, H. N. M., Klimova, T., Hoppel, C. L., Wyss, A., Palczewski, K., and von Lintig, J. (2011). A mitochondrial enzyme degrades carotenoids and protects against oxidative stress. *The FASEB Journal 25*, 948–959.

Appendix

PLOS | ONE

RESEARCH ARTICLE

Substrate Specificity, Inhibitor Selectivity and Structure-Function Relationships of Aldo-Keto Reductase 1B15: A Novel Human Retinaldehyde Reductase

Joan Giménez-Dejoz[1], Michal H. Kolář[2,3], Francesc X. Ruiz[4], Isidro Crespo[1], Alexandra Cousido-Siah[4], Alberto Podjarny[4], Oleg A. Barski[5], Jindřich Fanfrlík[2], Xavier Parés[1], Jaume Farrés[1]*, Sergio Porté[1]*

1 Department of Biochemistry and Molecular Biology, Faculty of Biosciences, Universitat Autònoma de Barcelona, Bellaterra, Barcelona, Spain, **2** Institute of Organic Chemistry and Biochemistry, Academy of Sciences of the Czech Republic, Prague, Czech Republic, **3** Institute of Neuroscience and Medicine (INM-9) and Institute for Advanced Simulation (IAS-5), Forschungszentrum Jülich GmbH, Jülich, Germany, **4** Department of Integrative Structural Biology, Institut de Génétique et de Biologie Moléculaire et Cellulaire-Centre de Biologie Intégrative, CNRS, INSERM, UdS, Illkirch CEDEX, France, **5** Diabetes and Obesity Center, School of Medicine, University of Louisville, Louisville, Kentucky, United States of America

* jaume.farres@uab.cat (JF); sergio.porte@gmail.com (SP)

OPEN ACCESS

Citation: Giménez-Dejoz J, Kolář MH, Ruiz FX, Crespo I, Cousido-Siah A, Podjarny A, et al. (2015) Substrate Specificity, Inhibitor Selectivity and Structure-Function Relationships of Aldo-Keto Reductase 1B15: A Novel Human Retinaldehyde Reductase. PLoS ONE 10(7): e0134506. doi:10.1371/journal.pone.0134506

Editor: Fernando Rodrigues-Lima, University Paris Diderot-Paris 7, FRANCE

Received: March 31, 2015

Accepted: July 9, 2015

Published: July 29, 2015

Data Availability Statement: All relevant data are within the paper.

Funding: JGD, IC, XP, JF and SP received support from Spanish Ministerio de Economía y Competitividad [BFU2011-24176] (http://www.mineco.gob.es) and Generalitat de Catalunya [2009 SGR 795] (http://www.gencat.cat/agaur). FXR, ACS and AP received support from Centre National de la Récherche Scientifique (http://www.cnrs.fr); Institut National de la Santé et de la Recherche Médicale (http://www.inserm.fr); Université de Strasbourg

Abstract

Human aldo-keto reductase 1B15 (AKR1B15) is a newly discovered enzyme which shares 92% amino acid sequence identity with AKR1B10. While AKR1B10 is a well characterized enzyme with high retinaldehyde reductase activity, involved in the development of several cancer types, the enzymatic activity and physiological role of AKR1B15 are still poorly known. Here, the purified recombinant enzyme has been subjected to substrate specificity characterization, kinetic analysis and inhibitor screening, combined with structural modeling. AKR1B15 is active towards a variety of carbonyl substrates, including retinoids, with lower k_{cat} and K_m values than AKR1B10. In contrast to AKR1B10, which strongly prefers all-*trans*-retinaldehyde, AKR1B15 exhibits superior catalytic efficiency with 9-*cis*-retinaldehyde, the best substrate found for this enzyme. With ketone and dicarbonyl substrates, AKR1B15 also shows higher catalytic activity than AKR1B10. Several typical AKR inhibitors do not significantly affect AKR1B15 activity. Amino acid substitutions clustered in loops A and C result in a smaller, more hydrophobic and more rigid active site in AKR1B15 compared with the AKR1B10 pocket, consistent with distinct substrate specificity and narrower inhibitor selectivity for AKR1B15.

Introduction

Members of the aldo-keto reductase (AKR) superfamily share an $(\alpha/\beta)_8$ barrel fold and are mostly monomeric (~35 kDa) NAD(P)H-dependent enzymes catalyzing the reduction of a

(https://www.unistra.fr); Région Alsace (http://www.region.alsace); Hôpital Civil de Strasbourg (http://www.chru-strasbourg.fr/Hopital-civi);I Instruct (part of the European Strategy Forum of Research Infrastructures; ESFRI) (https://www.structuralbiology.eu); and French Infrastructure for Integrated Structural Biology (FRISBI) [ANR-10-INSB-05-01] (http://frisbi.eu). FXR received support from Fondation pour la Recherche Médicale [SPF20121226275] (http://www.frm.org). The funders had no role in study design, data collection and analysis, decision to publish, or preparation of the manuscript.

Competing Interests: The authors have declared that no competing interests exist.

wide variety of endogenous carbonyl compounds such as carbohydrates, lipid aldehydes, prostaglandins, steroids and retinoids [1,2]. Several AKR enzymes act in phase-I drug metabolism by transforming some xenobiotics, are induced by nuclear factor erythroid 2-related factor 2 (Nrf2) under oxidative stress, and are involved in cancer chemoresistance [3,4]. In the human genome, fifteen *AKR* genes have been described which belong to three different gene families (*AKR1*, *AKR6* and *AKR7*). The *AKR1B* subfamily gene cluster, located in chromosome 7q33-35, includes the *AKR1B1*, *AKR1B10* and *AKR1B15* genes. A syntenic gene cluster with four *loci* has been described in rodent species, although gene orthologs can only be unambiguously assigned for *AKR1B1* [5,6].

The most studied enzyme of the AKR1B subfamily is AKR1B1 or aldose reductase, which reduces glucose to sorbitol under hyperglycemia and has been involved in the secondary complications of diabetic disease [7]. Another member, AKR1B10, is normally expressed in adrenal gland and small intestine, and induced in several types of cancer, such as non-small cell lung carcinoma and hepatoma [3]. Both enzymes have been proposed as promising oncogenic targets [8,9] and for this reason, along with the role of AKR1B1 in diabetic disease, they have been the subject of many studies in the search of selective and potent inhibitors [10–15]. Unlike other members of the subfamily, AKR1B10 is highly active in the reduction of all-*trans*-retinaldehyde [5]. The third gene in the *AKR1B* cluster, *AKR1B15*, has been predicted in the last decade as a result of high-throughput sequencing and annotation projects, i.e. human genome. Recently, *AKR1B15* has been demonstrated to be a functional gene with low expression restricted to placenta, testes and adipose tissues. The *AKR1B15* gene undergoes alternative splicing giving rise to two protein isoforms, designated as AKR1B15.1 and AKR1B15.2. The former is a 316-amino acid protein encoded by *AKR1B15-201 mRNA* (Ensembl database) and showing 92% amino acid sequence identity with AKR1B10, whereas AKR1B15.2 (*AKR1B15-001*, Ensembl) has a longer N-terminus not homologous to other AKRs, and does not exhibit enzymatic activity or nucleotide binding [16]. AKR1B15.1 (henceforth referred to in this manuscript as AKR1B15 for brevity) is localized in the mitochondrial fraction and the recombinant protein was purified and characterized, showing limited *in vitro* activity with steroids and acetoacetyl-CoA [16]. Previously, AKR1B15.1 had been expressed in the insoluble fraction of mammalian cells, showing low activity with D,L-glyceraldehyde and 4-nitrobenzaldehyde [6]. Similarly to *AKR1B10*, the *AKR1B15* gene was found to be up-regulated in the airway epithelium by smoking [17] and by exposure to sulforaphane, a known activator of the antioxidant response [18]. Interest in the *AKR1B15* gene has risen lately because some allelic variants have been linked to a mitochondrial oxidative phosphorylation disease [19], serous ovarian carcinoma [20] and increased longevity [21].

With the aim of further characterizing the enzymatic function of AKR1B15, we have performed enzyme kinetics of the purified recombinant protein with retinaldehyde isomers and other typical carbonyl substrates of AKR1B10. We have also conducted a screening against potential inhibitors using compounds previously described for AKR1B1 or AKR1B10. Finally, based on the crystallographic structure of the AKR1B10 complex with $NADP^+$ and tolrestat, we have constructed a model of the AKR1B15 active-site pocket.

Materials and Methods

Bacterial strains, plasmids and reagents

E. coli BL21(DE3) strain was obtained from Novagen, while plasmids pBB540 and pBB542 (containing the chaperone-coding genes *grpE*, *clpB* and *dnaK*, *dnaJ*, *groESL*, respectively), were a kind gift from Dr. A. de Marco [22]. The pET-28a vector containing the cDNA coding for isoform 2 of AKR1B15 (**UniProt ID: C9JRZ8-2**) had been described by Salabei *et al.* [6].

Tolrestat and sorbinil were generously provided by Prof. T.G. Flynn and Pfizer, respectively, whereas JF0064 (2,2',3,3',5,5',6,6'-octafluoro-4,4'-biphenyldiol) was obtained from Sigma-Aldrich. *Trans*-2-hexenal and 4-hydroxy-2-nonenal were commercially obtained from Cayman Chemical. All other reagents, including substrates, were purchased from Sigma-Aldrich unless otherwise indicated.

Protein expression and purification

E. coli BL21(DE3) strain transformed with pET-28a/AKR1B15 was grown in 1 L of 2xYT medium in the presence of 33 μg/mL kanamycin, while *E. coli* BL21(DE3) containing pBB540, pBB542 and pET-28a/AKR1B15 was grown in 6 L of M9 minimal medium supplemented with 20% glucose as a carbon source, in the presence of 34 μg/mL chloramphenicol, 50 μg/mL spectinomycin and 33 μg/mL kanamycin. Protein expression was then induced by the addition of 1 mM IPTG (Apollo Scientific) and cells were further incubated for 4 h at 22°C. Cells were then pelleted and resuspended in ice-cold TBI buffer (150 mM NaCl, 10 mM Tris-HCl, 5 mM imidazole, pH 8.0) containing 1% (v/v) Triton X-100. In the case of the non-chaperone-expressing *E. coli* BL21(DE3) strain, the TBI buffer also contained 1% (w/v) sarkosyl. The protein was purified using a His-Trap HP nickel-charged chelating Sepharose Fast Flow (GE Healthcare) 5-mL column using an AKTA FPLC purification system. The column was washed with TBI buffer and the enzyme was eluted stepwise with 5, 60, 100 and 500 mM imidazole in TBI buffer. The enzyme fraction eluted with 100 mM imidazole was loaded onto a PD-10 column (Millipore), which removed imidazole and changed the buffer to storage buffer (200 mM potassium phosphate, pH 7.4, 5 mM EDTA, 5 mM DTT). Finally, the protein monomer was purified through gel filtration chromatography using a Superdex 75 10/300 GL column (GE Healthcare) equilibrated with the storage buffer. In the case of the protein expressed in the *E. coli* BL21 (DE3) strain, in the absence of chaperones, the TBI and storage buffers contained 0.1% (w/v) sarkosyl throughout the purification procedure. AKR1B10 and AKR1B1 were expressed and purified as described previously [23].

Fluorimetric and spectrophotometric assays

NADPH binding was analyzed by quenching of Trp intrinsic fluorescence of 0.5 μM protein, using a Cary Eclipse (Varian) fluorimeter, in 20 mM sodium phosphate, pH 7.0, at 25°C in a final volume of 1 mL. The excitation wavelength was 290 nm and the emission wavelength was monitored at 340 nm. AKR1B10 was used as a control. The dissociation constant (K_D) values were calculated by nonlinear fitting of experimental data, using Grafit 5.0 (Eritacus Software), to the Morrison equation:

$$\Delta F = \Delta F_{max} \cdot \frac{[E] + [NADPH] + K_D - \sqrt{([E] + [NADPH] + K_D)^2 - 4 \cdot [E] \cdot [NADPH]}}{2 \cdot [E]}$$

The activity towards aldehydes, with the exception of retinaldehydes, was analyzed spectrophotometrically following the decrease in the absorbance of the cofactor NADPH at 340 nm (ε_{340} = 6,220 $M^{-1} \cdot cm^{-1}$) or at 365 nm in the case of cinnamaldehyde (ε_{365} = 3,510 $M^{-1} \cdot cm^{-1}$) [24]. Activities were determined in 100 mM sodium phosphate, pH 7.0, at 25°C, using 0.2 mM NADPH in 0.2-cm path length cuvettes, with freshly prepared substrate solutions. One unit of activity is defined as the amount of enzyme required to transform 1 μmol of substrate per min at 25°C.

HPLC enzymatic activity assay

Activity assays with retinoids were carried out using an HPLC-based methodology [25]. Briefly, retinaldehyde isomers were solubilized using glass tubes by a 10-min sonication at molar ratio 1:1 with fatty acid-free bovine serum albumin in 90 mM potassium phosphate, 40 mM potassium chloride, pH 7.4. The actual amount of solubilized retinoid was determined based on the corresponding molar absorption coefficient in aqueous solutions at the appropriate wavelength: ε_{400} = 29,500 $M^{-1}{\cdot}cm^{-1}$ for all-*trans*-retinaldehyde and ε_{367} = 26,700 $M^{-1}{\cdot}cm^{-1}$ for 9-*cis*-retinaldehyde [25]. For retinol isomers, which were used as standards of the reaction product, their concentration was determined in hexane using ε_{325} = 51,770 $M^{-1}{\cdot}cm^{-1}$ for all-*trans*-retinol [26] and ε_{325} = 43,765 $M^{-1}{\cdot}cm^{-1}$ for 9-*cis*-retinol [27]. The reactions were started by the addition of cofactor and carried out for 15 min at 37°C in a final volume of 0.5 mL. With the aim to measure the steady-state enzymatic activity, the concentration of enzyme was kept from 25- to 100-fold lower than that of the substrate for all the enzymatic assays. The reactions were stopped by the addition of 1 mL of cold methanol and after two rounds of extraction with hexane, retinoids were analyzed by HPLC as previously described [25]. All retinoid manipulations were performed under dim light.

Determination of kinetic constants and inhibition screening

All compounds tested as inhibitors were dissolved in DMSO and assayed in a final concentration of 0.1% (v/v) DMSO using 6 mM D,L-glyceraldehyde as a substrate. Kinetic constant and IC_{50} (compound concentration that inhibits enzymatic activity by 50%) values were calculated by fitting the initial rates to the appropriate equation using Grafit 5.0 (Eritacus Software) and values were given as the mean ± standard error of three experiments. Standard error values were less than 20% of the mean values.

Homology model and conformational ensembles

The structural model of *apo*-AKR1B15 was obtained from the AKR1B10 ternary complex crystallographic structure (**PDB ID: 1ZUA**), used as a template for homology modeling, by running the SCWRL program [28]. Because of the high sequence identity (92%) between the two proteins, the approach that keeps invariant the conformation of the conserved residues was adopted. The flexibility features of both AKR1B10 and AKR1B15 were studied by means of computer simulations.

The hydrogen atoms were added to the structural model of AKR1B15 as well as to the AKR1B10 crystal by the pdb2gmx tool of the GROMACS program package [29]. The *apo* as well as *holo* forms of both structures were studied as follows: the all-atom models were energy minimized employing the Amber99sb-ildn force field [30,31] for the protein, parameters of Holmberg *et al.* [32] for the cofactor, and Generalized-Born implicit solvent model with parameters of Hawkins *et al.* [33]. The minimized structures were used as the input for the tCONCOORD algorithm [34], which generates a set of independent conformations based on geometrical constraints [35]. It was designed to accurately capture the protein flexibility and the validity of the resulting conformational ensembles has been proven on a variety of proteins, including also AKR1B1 [34]. By means of tCONCOORD, we generated and analyzed the ensembles of 2500 conformations, which were subsequently used to calculate root mean square fluctuations (RMSF) of backbone atoms.

The energy minimized geometries (i.e. the starting ones for conformational sampling) were evaluated employing PROCHECK [36] and Verify 3D [37], which allow checking their stereochemical quality and calculating the percentage of conformations in favored regions obtained from the Ramachandran plots.

AKR1B15 ternary complexes

Geometries of the ternary complexes were derived from the homology model of *holo*-AKR1B15, which was built by superimposition of the *apo* form and *holo*-AKR1B10 (**PDB ID: 1ZUA**), including the cofactor coordinates into *apo*-AKR1B15. Considering that all-*trans*-retinaldehyde and 9-*cis*-retinaldehyde are substrates, the distance between the oxygen of retinaldehyde and the catalytic residues (i.e. His111 and Tyr49) should be less than 3 Å for productive catalysis to occur. Under this assumption, the substrates were manually docked into the active site of *holo*-AKR1B15. Inhibitors were automatically docked using AutoDock 4.0 [38]. The inhibitor JF0064 coordinates were obtained from the PDB (**PDB ID 4ICC**). The target geometry was extracted from the energy minimized all-*trans*-retinaldehyde complex (see below). For docking, the target was kept rigid, while all the torsional bonds in JF0064, except for the conjugated double bonds, were free to move. The docking parameters were the same as described previously [39].

The hydrogen atoms were added to the ternary complex and the complex was energy minimized by adopting the PM6-D3H4 method [40] combined with the COSMO solvent model [41]. The residues, with at least one atom within 5 Å from any atom of the cofactor, substrate or inhibitor, were allowed to move and the rest was kept frozen but included in the Hamiltonian calculation. The PM6-D3H4 method, which has been developed to accurately describe non-covalent interactions in biomolecules, represents a well-established computational tool [42] and recently it has been used in the study of the inhibition of AKR1B1 [43]. The final pdb files of *holo*-AKR1B15 and the ternary complexes were validated with the QMEAN server [44], with the flag "ignoring the agreement terms", recommended for proteins known to have the correct fold. The volume of the active-site pocket was measured by using the POVME algorithm [45], whereas PyMOL (v.1.3; Schrödinger) was used for figure drawing.

Results and Discussion

Expression and purification of recombinant human AKR1B15

We attempted the expression and purification of recombinant AKR1B15 using different *E. coli* strains and procedures. In all cases, the protein appeared to be mostly present in the insoluble fraction of cell lysates. Previously, Salabei *et al.* [6] had described a successful procedure based on the use of the anionic detergent sarkosyl (sodium *N*-lauroylsarcosinate). In our hands and in the presence of sarkosyl, the amount of soluble protein and the final yield were acceptable (Fig 1A and 1B). However, AKR1B15 was mainly associated with higher molecular weight aggregates (Fig 1C), which were found to be enzymatically inactive. Only a small fraction of AKR1B15 was found to be in an active monomeric form. A minimal concentration of sarkosyl (0.001%, w/v) was necessary to avoid protein precipitation. Sarkosyl had been described as an enzyme inhibitor [46], and was confirmed that it inhibited AKR1B15 following a non-competitive model (data not shown). As an alternative procedure for expression, an *E. coli* BL21(DE3) strain co-expressing three chaperone systems (DnaK-DnaJ-GrpE, ClpB and GroEL-GroES) [22] was used. Under these conditions, AKR1B15 was still found to be mainly associated with the insoluble fraction, but the amount of soluble protein recovered increased significantly (Fig 1A). Peptide mass fingerprint analysis of the soluble protein fraction separated by SDS-PAGE identified the isolated band as being human AKR1B15 (data not shown). The enzyme was purified with a final yield of 1 mg protein per liter of culture, when using minimal medium. Analysis by gel filtration chromatography showed a molecular weight of 37 kDa for the purified protein, suggesting that AKR1B15 was obtained as a monomer (Fig 1C). By analyzing the purified protein on SDS-PAGE (Fig 1B, lane 2), the major band corresponded to the 37-kDa

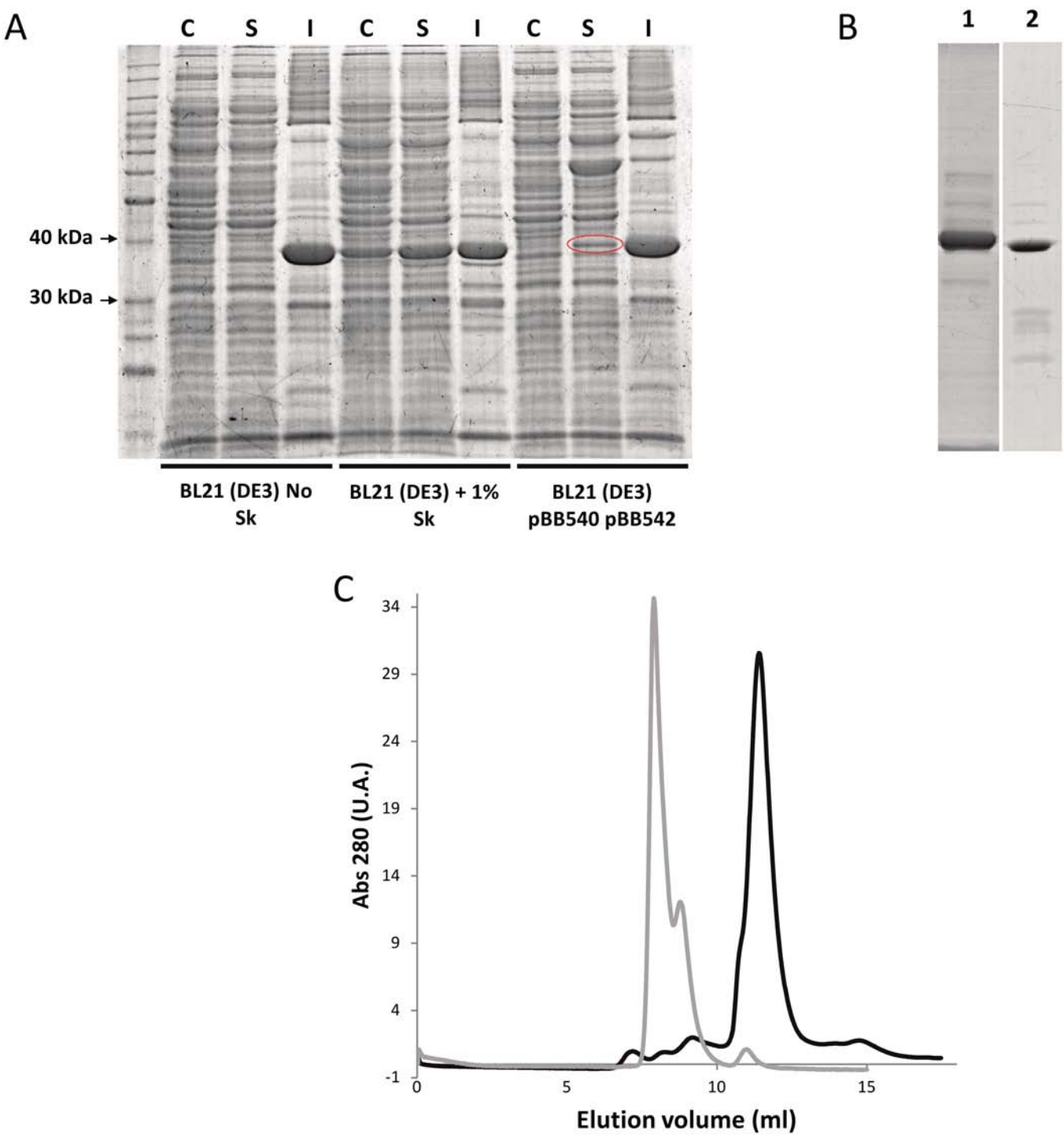

Fig 1. Expression and purification of recombinant human AKR1B15. (*A*) SDS-PAGE analysis of protein expression, showing that AKR1B15 was predominantly associated with the insoluble fraction of BL21(DE3) cell lysates. Treatment with 1% (w/v) sarkosyl (Sk) provided a much higher amount of AKR1B15 in the soluble fraction. In the case of BL21(DE3) pBB540 pBB542 cells, a protein band which is highlighted with a red oval was identified as human AKR1B15 by Peptide Mass Fingerprinting. Lanes: C, control for the soluble fraction not induced by IPTG; S, soluble fraction; and I, insoluble fraction. *(B)* SDS-PAGE analysis of protein purification, showing fractions eluted from the nickel affinity column chromatography using 100 mM imidazole. Lanes: 1, Protein eluted from the soluble fraction of BL21(DE3) + Sk; and 2, Protein eluted from the soluble fraction of BL21 (DE3) pBB540 pBB542. *(C)* Elution profile from the Superdex 75 10/300 GL column chromatography. AKR1B15 purified from soluble fraction of BL21(DE3) + Sk and from soluble fraction of BL21 (DE3) pBB540 pBB542 are shown in grey and black lines, respectively. Major peaks eluting at 7.9 and 11.4 mL correspond to aggregated (132 kDa) and monomer (37 kDa) protein, respectively.

doi:10.1371/journal.pone.0134506.g001

enzyme, with some minor contaminating protein bands. Fluorescence analysis of cofactor binding allowed us to determine the K_D value for NADPH (113 ± 9 nM, Fig 2). The determined K_D value was in the same range with that of AKR1B10 (K_D = 92 ± 35 nM).

Enzymatic activity and inhibition studies

It has been recently reported that AKR1B15 catalyzes the reduction of acetoacetyl-CoA and the carbonyl group at C17 position of sex steroids [16]. Additional results, obtained by using protein extracts from transfected human COS-7 cells, indicated that AKR1B15 exhibited very weak activity towards D,L-glyceraldehyde and 4-nitrobenzaldehyde [6], which are typical substrates of AKR enzymes. Our current analysis shows that the purified recombinant enzyme has broad substrate specificity and displays a significant enzymatic activity towards aliphatic and aromatic aldehydes and ketones (Table 1). AKR1B15 was active with D,L-glyceraldehyde, which was used as a substrate in the standard assay. The enzyme reduced 200 mM glucose with a much lower rate (12 mU/mg) than that exhibited by AKR1B1 (500 mU/mg), precluding the determination of kinetic constants. In contrast, AKR1B15 displayed a catalytic activity comparable or higher than that of AKR1B1 and AKR1B10 with a variety of physiological or model aldehydes and ketones of various classes. Among the compounds assayed, medium-chain (i.e. $\geq$ 6-carbon) aliphatic and aromatic carbonyl compounds were excellent substrates, with K_m values in the low micromolar range. Importantly, AKR1B15 was also active towards retinaldehyde isomers (Table 2), which along with acrolein, *trans*-2-hexenal, 4-hydroxy-2-nonenal and farnesal may constitute physiological substrates for this enzyme. The 9-*cis* isomer of retinaldehyde was the best substrate based on the catalytic efficiency (k_{cat}/K_m) due to a very low K_m value (160 nM) (Table 2), which could be determined by the use of an HPLC-based method providing higher sensitivity than the spectrophotometric assay. Regarding cofactor specificity, AKR1B15 was confirmed to be NADPH dependent (i.e. the enzymatic activity using 0.2 mM NADH was less than 5% of that with NADPH), as reported in [16], and described for most AKRs. The K_m value of AKR1B15 for NADPH (5 μM) is within the same range as those of AKR1B1 and AKR1B10 (Table 1).

The comparison between AKR1B15 and the other human AKR1B enzymes reveals some relevant distinct kinetic features (Table 1). In particular, ketones and α-dicarbonyl compounds were good substrates for AKR1B15, showing higher activity and lower K_m values than AKR1B10 and AKR1B1. The β-dicarbonyl compound, 2,4-pentanedione, was also reduced by AKR1B15, consistent with the reported activity with acetoacetyl-CoA, which also has two carbonyl groups in a β-position [16]. For other substrates, AKR1B15 exhibited lower K_m values than AKR1B10, suggesting that AKR1B15 could play a role in aldehyde detoxification, similar to what has been suggested for other AKR1B enzymes [47]. AKR1B15 resembles AKR1B10 in having high activity with retinoids, in contrast to AKR1B1 (Table 2). A distinct feature of AKR1B15 is that it keeps similar k_{cat} values towards all assayed substrates, including retinoids, suggesting a common rate-limiting step. In comparison, the k_{cat} values of AKR1B1 with both retinaldehyde isomers and AKR1B10 with the 9-*cis* isomer are significantly lower than those for other substrates. This decrease in k_{cat} values had been interpreted before as a change in the rate-limiting step (from cofactor dissociation to a slower step) of AKR1B1 and AKR1B10 reactions with these retinoids [23]. This seems not to be the case for AKR1B15. Finally, the higher specificity of AKR1B15 for the 9-*cis* isomer is unique for the human AKR1Bs, and it matches those of AKR1C3 [48], which like AKR1B15 also has bulky Phe residues at positions 299 and 304 in its active site, and chicken AKR [49].

Seven AKR inhibitors were tested against AKR1B15 using D,L-glyceraldehyde as substrate (Table 3). Among these inhibitors, there are five of the carboxylic acid type (tolrestat,

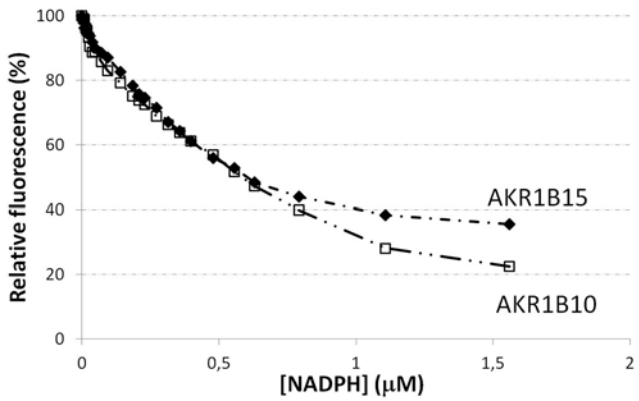

Fig 2. Quenching of AKR1B15 and AKR1B10 fluorescence upon binding of NADPH. Change of the protein fluorescence intensity (in percentage) upon addition of cofactor is shown. All proteins were used at a concentration of 0.5 μM in 20 mM sodium phosphate, pH 7.0, at 25°C. Graph symbols: AKR1B15 (diamonds), AKR1B10 (open squares).

doi:10.1371/journal.pone.0134506.g002

epalrestat, oleanolic acid, sulindac and lithocholic acid), one of cyclic imide type (sorbinil) and one non-classical aldose reductase inhibitor or ARI (JF0064, which has been recently described by Cousido-Siah *et al* [15], Fig 3). Tolrestat, JF0064 and sulindac are potent inhibitors of AKR1B1 as well as of AKR1B10 (with IC_{50}<10 μM for both enzymes). Sorbinil and epalrestat are more selective against AKR1B1 [50,51], while oleanolic and lithocholic acid are more selective against AKR1B10 [52]. For AKR1B15, only JF0064 showed a significant inhibition (IC_{50} = 0.034 ± 0.005 μM, Table 3), much stronger than for AKR1B1 and AKR1B10 [15]. The steroid lithocholic acid was found to be an inhibitor of AKR1B15, in agreement with the reported observation that certain steroids are good substrates for this enzyme [16].

Structural model of AKR1B15

With the aim to compare the substrate-binding site of AKR1B15 with that of AKR1B10, and upon unsuccessful attempts of protein crystallization, a 3D homology model of AKR1B15 was built (Fig 4A). The SCWRL server was chosen, as it is designed specifically for predicting side-chain conformations, provided a fixed backbone usually obtained from an experimental structure. In practical terms, this is the case of AKR1B15, given its 92% sequence identity with AKR1B10. Model quality was checked by PROCHECK analyses, indicating that most residues are in the preferred regions (94.8%), whereas residues in allowed regions and outliers are 3.5 and 1.6%, respectively. The compatibility of the atomic model (3D) was checked with its own amino acid sequence (1D) using Verify 3D analysis. This analysis shows that there is no region with negative scores, which would otherwise indicate potential problems. In addition, the analysis using the QMEAN server indicates the reliability of the model, with a QMEAN score of 0.67 out of 1, and with all the Z-scores being consistent with the good quality of the structure. Thus it may be concluded that this model is suitable for structural studies.

Model analysis

Regarding the cofactor-binding site, AKR1B15 shares with AKR1B10 all residues, except for Arg22, Met265 and His269 (Fig 5). The change of Lys22 in AKR1B10 to Arg in AKR1B15 may prevent its interaction with the pyrophosphate bridge of $NADP^+$ but, due to the mobility of the Arg side chain in solution, its interaction with the cofactor cannot be excluded. Met265 and His269 keep interactions with the same groups of $NADP^+$ that involve Val265 and Arg269 in

Table 1. Kinetic constants of AKR1B15, AKR1B10 and AKR1B1 with aldehydes and ketones.

Substrate	AKR1B15			AKR1B10			AKR1B1		
	K_m (μM)	k_{cat} (min^{-1})	k_{cat}/K_m ($mM^{-1}·min^{-1}$)	K_m (μM)	k_{cat} (min^{-1})	k_{cat}/K_m ($mM^{-1}·min^{-1}$)	K_m (μM)	k_{cat} (min^{-1})	k_{cat}/K_m ($mM^{-1}·min^{-1}$)
Carbohydrate aldehydes									
D,L-glyceraldehyde	880	10.7	12.4	6,000[a]	35[a]	6[a]	50[a]	31[a]	660[a]
Aromatic aldehydes									
pyridine-3-aldehyde	2.9	9	3,150	13[b]	150[b]	12,000[b]	10[b]	61[b]	6,100[b]
benzaldehyde	<1*	12.1	>12,100	9.7[b]	104[b]	11,000[b]	21[b]	91[b]	4,300[b]
cinnamaldehyde	<1*	13.3	>13,300	34.7	240	6,900	31	29	950
Alkanals									
hexanal	3.1	7.3	2,300	112[b]	142[b]	1,300[b]	5[b]	28[b]	5,600[b]
Alkenals									
acrolein	36	8.8	240	110[c]	116[c]	1,070[c]	884[c]	11[c]	12[c]
trans-2-hexenal	5	11.3	2,200	28[b]	49[b]	1,700[b]	9[b]	16[b]	1,800[b]
4-hydroxy-2-nonenal	2.2	5.2	2,500	31[c]	121[c]	3,900[c]	716[c]	50[c]	70[c]
citral	1.5	5.5	3,700	4.5	35	7,400	35	68	1,750
farnesal	<1*	4.8	>4,800	2.3[b]	30[b]	13,000[b]	37[b]	27[b]	700[b]
Ketones									
2-butanone	780	10.5	13.5		LA			LA	
3-buten-2-one	21.3	8.2	380		LA			LA	
3-nonen-2-one	1.7	6.76	4,000		LA			LA	
2-cyclohexen-1-one	365	4.41	12.1		LA			LA	
α-Dicarbonyls									
2,3-butanedione	<1*	10.6	>10,600	540[d]	260[d]	480[d]	110[d]	23[d]	210[d]
2,3-hexanedione	<1*	9.5	>9,500	51[b]	79[b]	1,500[b]	17[b]	49[b]	2,900[b]
β-Dicarbonyls									
2,4-pentanedione	40	2.2	55	58,900	8.6	0.15	8,100	16.7	2.2
3,5-heptanedione	1,300	5.3	3.9	>50,000	-	-	12,000	26	2.2
Cofactor									
NADPH	5.7			10			2.9[e]		

Enzymatic activity was measured spectrophotometrically. For the determination of the kinetic parameters for NADPH, 3 and 60 mM D,L-glyceraldehyde was used with AKR1B15 and AKR1B10, respectively. LA, low activity (≤ 10 mU/mg) was detected at saturating concentration of substrate for AKR1B15; ND, not determined.

*Because of very low K_m value, data are only approximate.

[a]Data from [23].

[b]Data from [66].

[c]Data from [67].

[d]Data from [68].

[e]Data from [69].

doi:10.1371/journal.pone.0134506.t001

AKR1B10 (i.e. a hydrogen bond between the N atom of Met265 and the 2′-phosphate group, a second hydrogen bond between the Nε of His269 and the 2′-phosphate group, and a stacking interaction of His269 with the adenine ring). Interestingly, a His residue at position 269 and its interactions have also been described in the rat AKR1B14 X-ray structure [53]. The salt bridge between the side-chain of Asp217 and Lys263, acting as a safety belt in cofactor binding, and the stacking interaction of Tyr210 side chain with the nicotinamide ring are also conserved.

Table 2. Kinetic constants with retinaldehyde isomers.

Substrate and parameter	AKR1B15	AKR1B10[a]	AKR1B1[a]
All-*trans*-retinaldehyde			
K_m (μM)	1 ± 0.3	0.6 ± 0.1	1.1 ± 0.1
k_{cat} (min^{-1})	5.4 ± 0.5	27 ± 1	0.9 ± 0.1
k_{cat}/K_m ($mM^{-1}\cdot min^{-1}$)	5,300 ± 1,700	45,000 ± 7,600	1,300 ± 160
9-*cis*-retinaldehyde			
K_m (μM)	0.16 ± 0.03	0.7 ± 0.1	0.4 ± 0.1
k_{cat} (min^{-1})	3.8 ± 0.2	0.9 ± 0.1	0.7 ± 0.2
k_{cat}/K_m ($mM^{-1}\cdot min^{-1}$)	25,600 ± 5,300	1,300 ± 190	1,500 ± 170

Enzymatic activity was measured by using the HPLC-based method.

[a]Data from [23]

doi:10.1371/journal.pone.0134506.t002

This is consistent with the AKR1B15 cofactor preference for NADP(H) and the low K_m value of AKR1B15 for NADPH.

On the other hand, the active site displays high divergence between AKR1B15 and AKR1B10. The residue differences between the two proteins are concentrated in loops A and C which, along with loop B, give shape to the active-site pocket (Fig 4A). Thus, the catalytic residues (Asp44, Tyr49, Lys78 and His111) and those in loop B are strictly conserved. In contrast, Ser118, Leu122, Ala131, and Gly133 (in loop A), together with Cys299, Asn300, Val301, Leu302, Gln303, Ser304, and Tyr310 (in loop C) of AKR1B10 are substituted by Thr118, Phe122, Met131, Ser133, Phe299, Asp300, Phe301, Lys302, Glu303, Phe304 and Phe310, in AKR1B15. Noteworthy, residues Phe299, Phe301, Glu303 and Phe304, along with Phe48 (Val48 in AKR1B10), participate in the AKR1B15 active-site pocket, which is thus significantly smaller (60 $Å^3$ for AKR1B15 *versus* 279 $Å^3$ for AKR1B10) and more hydrophobic, compared to the AKR1B10 pocket (Fig 4B and 4C). Some of these substitutions might not only have a consequence on the shape, volume and hydrophobicity of the active site, but also on the flexibility of the polypeptide chain, which is most relevant in the loop regions. The analysis of

Table 3. Inhibitory effect of different compounds on enzymatic activity.

	IC_{50} (μM)		
Inhibitor	**AKR1B15**	**AKR1B10**	**AKR1B1**
Tolrestat	> 100	0.006	0.01[a]
Sorbinil	> 100	9.6[b]	0.55[b]
JF0064	0.034 ± 0.005	1.0[d]	0.3[d]
Epalrestat	> 50	0.33[c]	0.021[c]
Oleanolic acid	> 100	0.09[b]	124[b]
Sulindac	>100	0.35[c]	0.21[c]
Lithocholic acid	16.3 ± 7.6	0.12[d]	7.2[d]

The enzymatic activity assay with inhibitors was performed by using D,L-glyceraldehyde as a substrate. JF0064: 2,2',3,3',5,5',6,6'-octafluoro-4,4'-biphenyldiol

[a]Data from [70].

[b]Data from [52].

[c]Data from [71].

[d]Data from [66]

doi:10.1371/journal.pone.0134506.t003

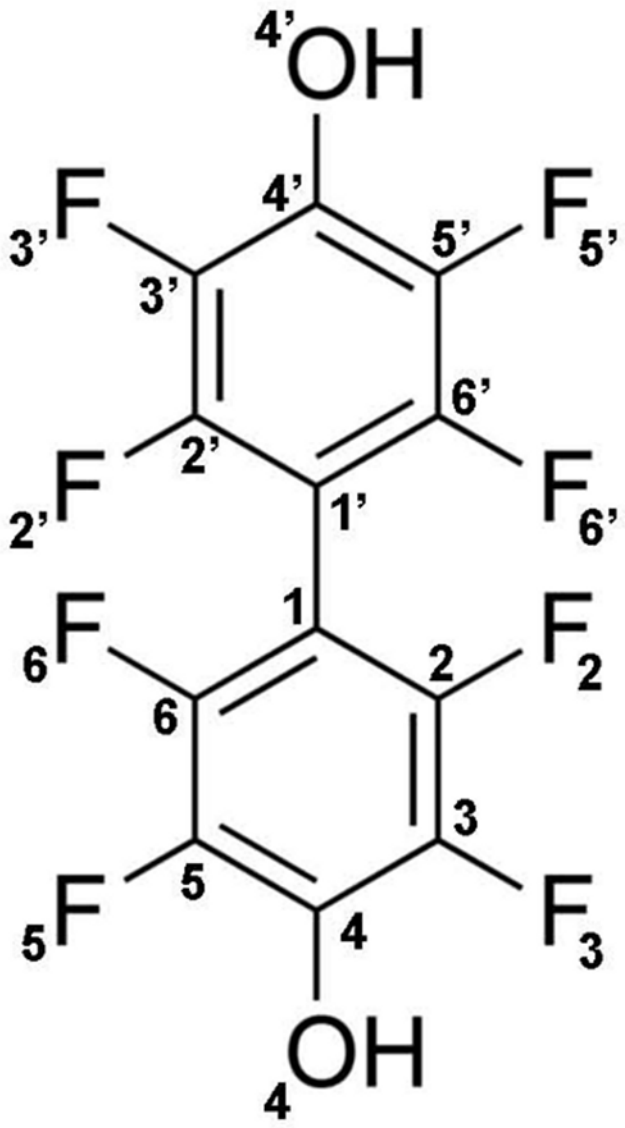

Fig 3. Molecular structure of compound JF0064, 2,2',3,3',5,5',6,6'-octafluoro-4,4'-biphenyldiol.

doi:10.1371/journal.pone.0134506.g003

conformational ensembles indicates that AKR1B15 would display less flexible loops A and C than AKR1B10 (Fig 4D). A detailed analysis of the AKR1B15 model shows van der Waals interactions between residues from these loops and residues from other protein regions (i.e. Trp21-Phe299_*loopC*, Phe48-Phe116_*loopA*, Phe48-Phe123_*loopA*, Phe48-Phe301_*loopA*, Trp112_*loopA*-Phe301_*loopC*, Phe116_*loopA*-Phe304_*loopC*, Phe123_*loopA*-Phe304_*loopC*, Met131_*loopA*-Phe304_*loopC* and Met131_*loopA*-Leu307_*loopC*). Such interactions result in a hydrophobic cluster (Fig 4E), which likely contributes to the lower flexibility of the AKR1B15 active site.

Docking of substrates and the inhibitor JF0064

As it has been described above, AKR1B15 is active towards retinoids, and thus the binding mode of all-*trans*- and 9-*cis*-retinaldehyde was analyzed. The obtained models were also

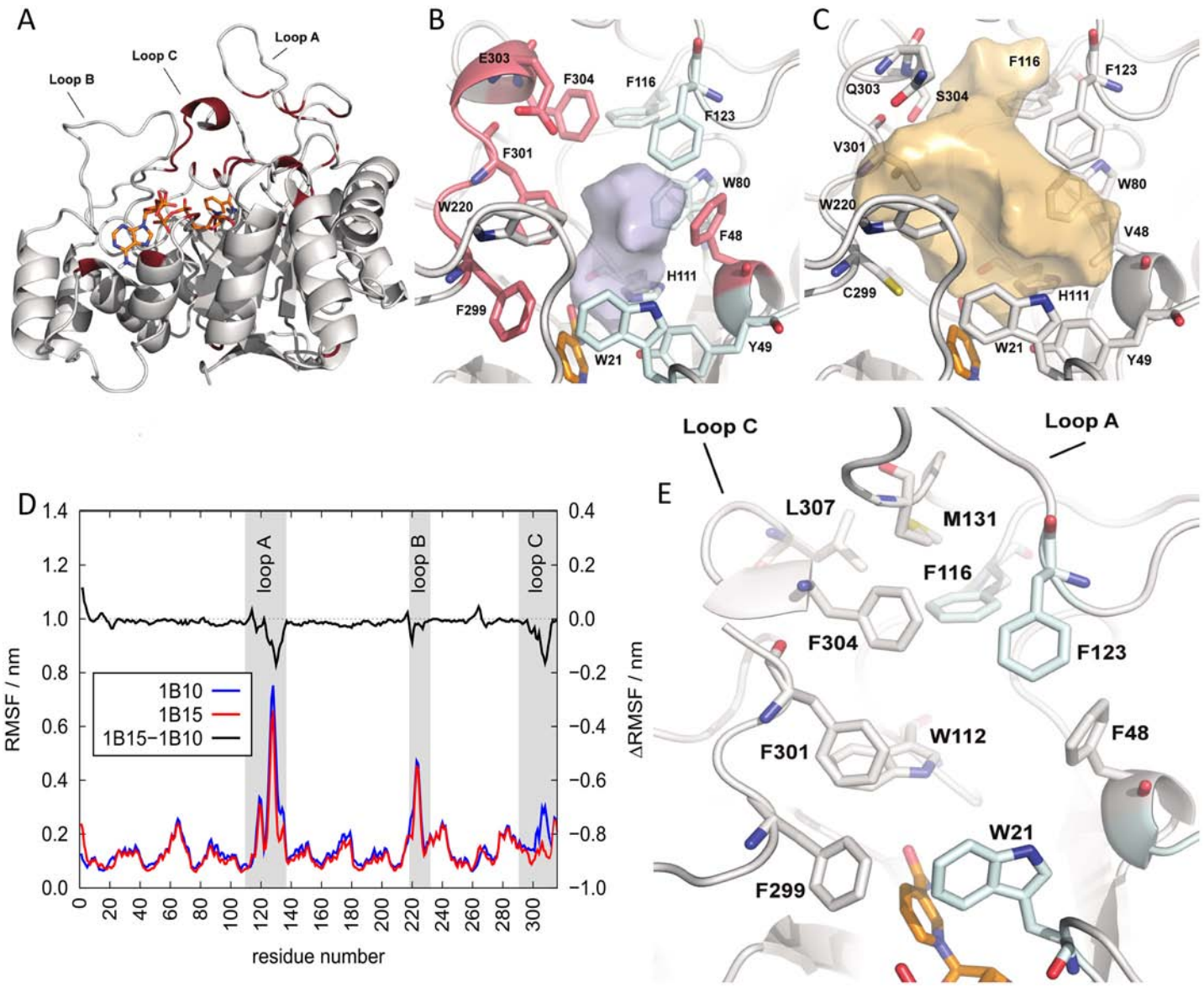

Fig 4. Model of AKR1B15 structure. (*A*) Side view of the $(\alpha/\beta)_8$ barrel. In red, the divergent residues between AKR1B15 and AKR1B10. (*B*) and (*C*) Active-site pockets of AKR1B15 and AKR1B10, respectively. The AKR1B15-specific residues are displayed in magenta. $NADP^+$ cofactor is colored in orange. The surface contour of pockets is shown in grey and orange for AKR1B15 and AKR1B10, respectively. (*D*) The local conformational changes in *holo* forms of AKR1B15 (red line) and AKR1B10 (blue line) derived from computer simulations, as indicated by root mean square fluctuations (RMSF) of backbone atoms. The residues of loops A, B and C are highlighted by grey background. The difference in RMSF between the two enzymes is displayed as a black line in the top. *(E)* AKR1B15 loops A and C indicating potential contacts between different residues are shown as sticks, which may explain the low flexibility of the protein in this region. Figures have been drawn using PyMOL.

doi:10.1371/journal.pone.0134506.g004

analyzed with the QMEAN server and displayed similar scores (0.68/1 and 0.69/1, respectively) as the AKR1B15 holoenzyme model. The analysis showed that both substrates could be placed with their carbonyl groups at catalytic distance from the hydroxyl group of Tyr49, the Nε of His111, and the cofactor C4 atom (2.9, 2.9, and 3.2 Å, respectively). The two molecules would be positioned in a similar manner into a narrow and hydrophobic pocket, establishing contacts with Trp21, Phe48, Phe123, Trp220, and Phe301 (all-*trans*-retinaldehyde), and Phe48, Trp220, Phe299, and Phe301 (9-*cis*-retinaldehyde) (Fig 6A). A slight rearrangement of loop A and loop

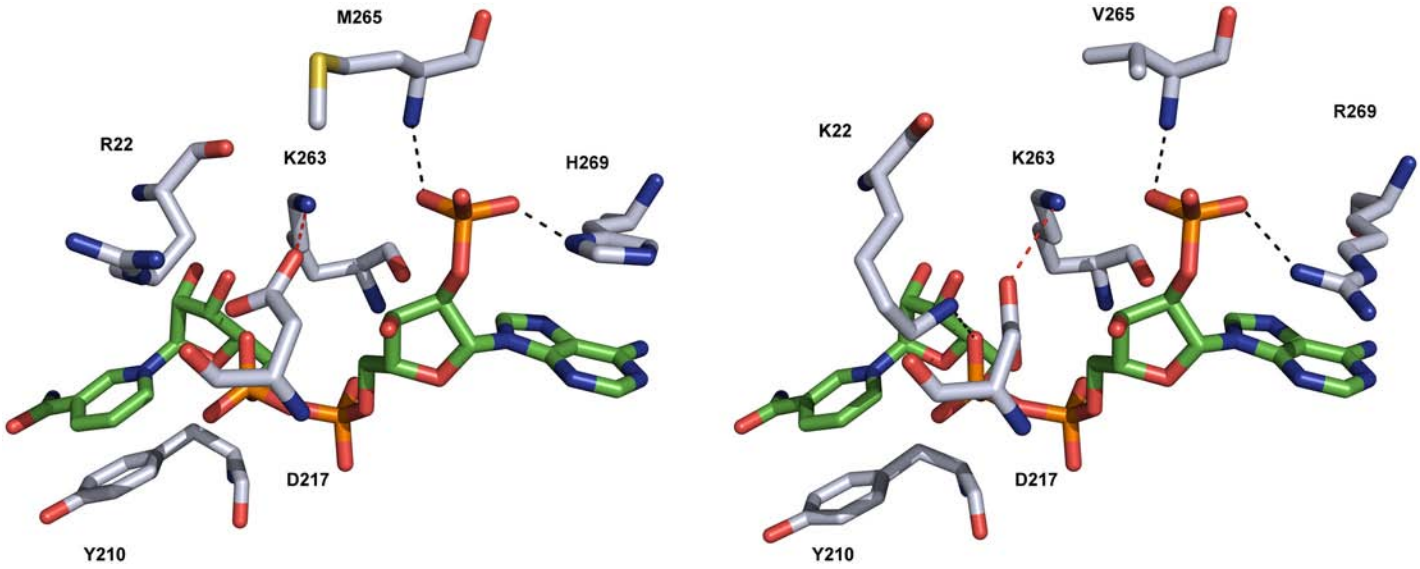

Fig 5. Comparison of the cofactor-binding site between the AKR1B15 model (*A*) and the AKR1B10 crystal structure (*B*). Interactions of Met265 and His269 with $NADP^+$ in AKR1B15 are similar to those of Val265 and Arg269 in AKR1B10 (black dotted lines). His269 forms a π-stacking interaction with the adenine ring of the cofactor. The substitution of Lys22 by Arg in AKR1B15 prevents its interaction with the pyrophosphate bridge of $NADP^+$. The salt bridge between Asp217 and Lys263 (red dotted line), acting as a safety belt in the coenzyme binding, and the π-stacking interaction of Tyr210 with the cofactor nicotinamide ring are conserved between the two AKRs. Carbon atoms of the cofactor are shown in green, whereas those of the enzyme are colored grey. Figures have been drawn using PyMOL.

doi:10.1371/journal.pone.0134506.g005

C (Fig 6A) could allow the establishment of a hydrogen-bond or an electrostatic interaction between Lys125 and Glu303 (Fig 6B).

The particular AKR1B15 topology brings the cyclohexene ring of all-*trans* and 9-*cis*-retinaldehyde further away from loops A and C than in AKR1B10 (Fig 6A, 6B and 6C). Thus these substrates do not interact with the residues that have been described as important for all-*trans*-retinaldehyde binding in AKR1B10, and which are in the most external part of the AKR1B10 pocket [23]. Notably, some of these residues are not interacting with the retinoid substrates in AKR1B15, i.e. Lys125 and Met131 (Ala in AKR1B10) from loop A, Glu303 (Gln in AKR1B10) and Phe304 (Ser in AKR1B10) from loop C. In AKR1B10, all-*trans*-retinaldehyde binding requires a rearrangement of Lys125, not necessary for 9-*cis*-retinaldehyde, explaining the higher k_{cat} value towards the former substrate [3]. In the case of AKR1B15, Lys125 is not involved in the binding of either substrate, being consistent with similar k_{cat} values. The hydrophobic pocket in the external region of the active site of the enzyme, where part of the polyene chain and the cyclohexene ring of the substrate bind, corresponds to the protein region which shows more rigidity in comparison to AKR1B10 (Fig 4D). Furthermore, this rigidity, likely due to the presence of the bulky Phe residues (Phe48, Phe299, Phe301 and Phe304), would make difficult the opening of the so-called "specificity pocket" (Fig 6B and 6C), which has been described for ARI binding in AKR1B10 and AKR1B1 and which usually accommodates the hydrophobic moiety of inhibitors [52,54]. This feature could have important functional consequences. For instance, it could explain the different substrate specificity and inhibitor selectivity of AKR1B15, since flexibility has been well established in connection with the active-site accessibility, and substrate and ligand binding [55].

The compound JF0064 is the only ARI found to significantly inhibit AKR1B15, probably due to the reduced volume of the active-site cleft and to the difficulty in opening the "specificity pocket". In order to analyze JF0064 binding, a docking simulation along with energy

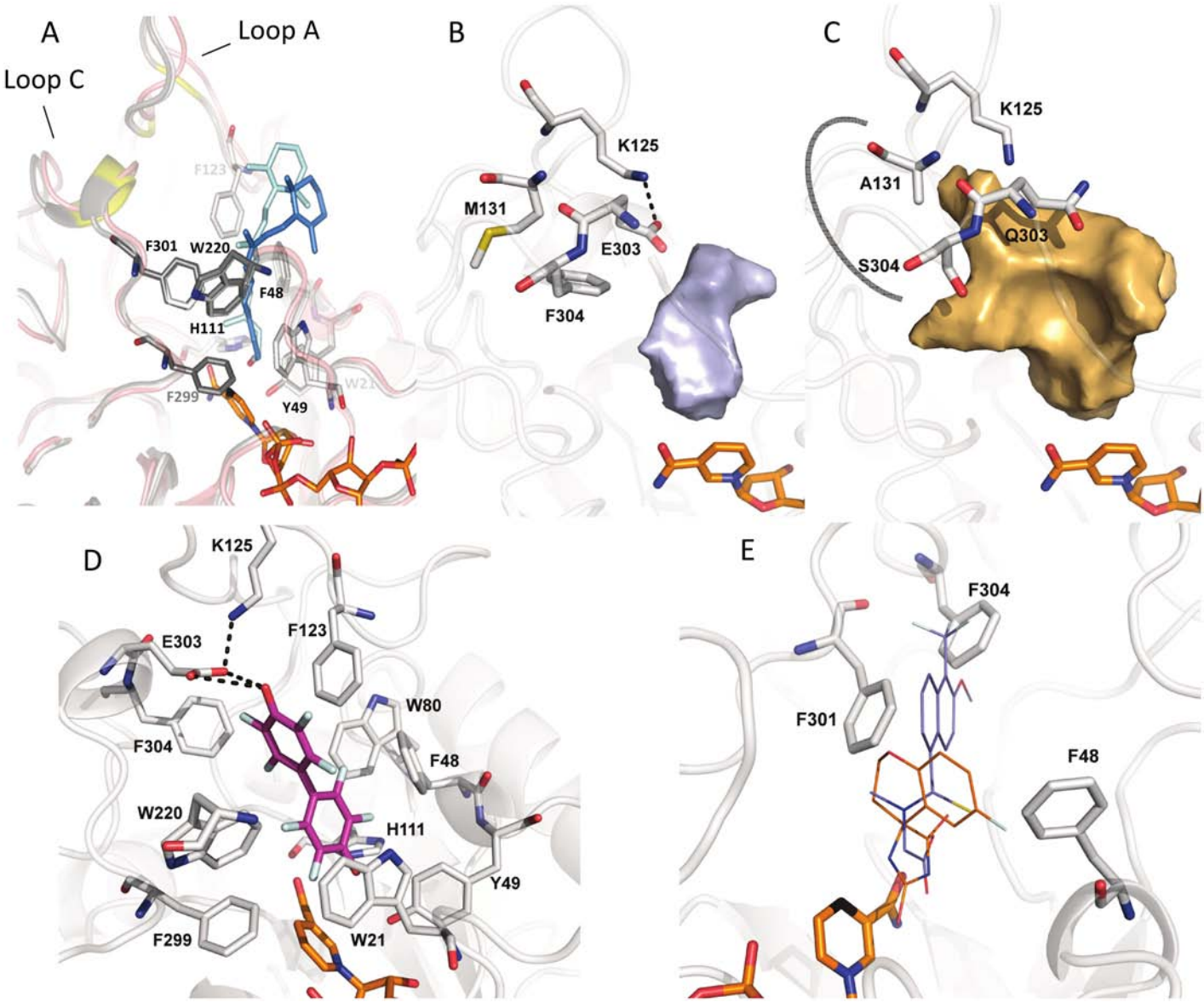

Fig 6. Molecular docking of substrates or inhibitors to the active-site pocket of AKR1B15. (*A*) Residues implicated in binding all-*trans*- and 9-*cis*-retinaldehyde are displayed in light and dark grey sticks; while the substrates are shown in light and dark blue, respectively. The residues found in the most external part of all-*trans*-retinaldehyde binding channel in AKR1B10 are highlighted in yellow. The energy minimized *apo*-conformation is displayed in magenta cartoon. (*B*) and (*C*) Side view of the surface contour of the active-site pocket, depicted in grey and orange for AKR1B15 and AKR1B10, respectively, to show the inhibitor "specificity pocket". A thick grey curved line indicates the "specificity pocket" in AKR1B10. As it is shown, this pocket may not be opened in AKR1B15, likely due to the presence of bulky Phe residues. (*D*) The inhibitor JF0064 (PDB ID 4ICC) bound to AKR1B15 is displayed as sticks with C atoms in magenta, while residues interacting with the inhibitor are shown as sticks with C atoms in grey. (*E*) Steric hindrance preventing tolrestat (in blue) and sorbinil (in orange) from binding to the active site of AKR1B15. For this analysis, the AKR1B15 structure model was superimposed with the AKR1B10 crystallographic structures with tolrestat (PDB ID 1ZUA) and sorbinil (PDB ID 4GA8). $NADP^+$ is colored in orange. Figures have been drawn using PyMOL.

doi:10.1371/journal.pone.0134506.g006

minimization was performed. The model was again validated by using the QMEAN server and displayed a similar, though slightly better score than the rest of the AKR1B15 models (0.72/1). The Z-score (which is tending from negative digits to 0 when approximating to experimentally determined structures) of the AKR1B15-$NADP^+$-JF0064 model (−0.92) is comparatively

improved with respect to the AKR1B15 holoenzyme model (−1.64). All-*trans*- and 9-*cis*-retinaldehyde complexes show intermediate values of −1.51 and −1.35, respectively.

The conformation of the AKR1B15-$NADP^+$-JF0064 complex corresponding to the energy minimum is displayed in Fig 6D. Binding would occur through van der Waals interactions with a large number of hydrophobic residues, and by establishing hydrogen bonds with catalytic residues (Tyr49 and His111) and Glu303. As it has been described above for substrates, the binding of the inhibitor also induced the same rearrangement of loop A and loop C, allowing for the interaction between Lys125 and Glu303. The other tested compounds did not inhibit AKR1B15 likely because of steric hindrance (e.g. Phe301 and Phe48 may clash against sorbinil, and Phe304, along with the fact that the "specificity pocket" could not be opened, may prevent tolrestat from binding) (Fig 6C and 6E).

Physiological significance

The kcat/Km value of AKR1B15 for 9-*cis*-retinaldehyde (25,600 $mM^{-1}\cdot min^{-1}$) is the highest among all the substrates checked so far, including the steroids and 3-keto-acyl-CoAs analyzed by Weber *et al*. [16], although these authors used different conditions for enzyme purification and kinetic studies. This is reminiscent of what has been observed for other members of the AKR superfamily, such as AKR1C3, which displays a high kcat/Km value for 9-*cis*-retinaldehyde but it is also active against steroids and prostaglandins [48]. Observations of dual substrate specificity have also been made for members of the short-chain dehydrogenase/reductase superfamily [56]. Thus, it is conceivable that AKR1B15 and some of these enzymes have a multifunctional role in the pre-receptor regulation of hormonal signaling pathways. The AKR1B15 specificity for the 9-*cis* isomer may suggest a major role in the control of RAR and RXR mediated signaling, but we cannot exclude other physiological functions. Regarding the reported localization of AKR1B15 in mitochondria, there is increasing evidence that retinoid metabolism takes place in different subcellular compartments [57,58], mitochondria being one of them. Carotenoids and their aldehyde metabolites can be generated by the asymmetric cleavage of β-carotene by β-carotene-9',10'-oxygenase (BCO2), which is associated with the inner mitochondrial membrane [59]. Therefore, a putative physiological role of AKR1B15 in retinoid metabolism is compatible with its mitochondrial localization. The presence in mitochondria of other retinaldehyde reductases, such as RDH13 [57], gives further support to this notion. In addition, RDH10, an enzyme involved in retinoic acid synthesis, shifts between mitochondria associated membranes and lipid droplets during retinyl ester biosynthesis, similarly to cellular retinol-binding protein type 1 [60]. Retinol has also been pinpointed as a modulator of energy homeostasis in mitochondria by regulating oxidative phosphorylation [61]. An additional role of AKR1B15 in metabolizing lipid peroxidation products and alkenals in mitochondria cannot be ruled out [62,63].

Conclusions

Despite its high sequence identity with AKR1B10, AKR1B15 appears to be an enzyme with a unique substrate specificity and narrower inhibitor selectivity. AKR1B15 displays distinct kinetic features with ketones, α-dicarbonyl compounds and is among the best 9-*cis*-retinaldehyde reductases within the AKR superfamily. Some of the most potent inhibitors of AKR1B1 and AKR1B10 did not inhibit AKR1B15. Amino acid substitutions clustered in residues located in loops A and C result in a smaller, more hydrophobic and more rigid active-site pocket of AKR1B15 as compared to that of AKR1B10. The structural model of AKR1B15 provides a powerful tool for the virtual screening of substrates and inhibitors for this enzyme. The distinct topology of the AKR1B15 fold should facilitate the design of more selective inhibitors, as it has

been shown for other enzyme pairs with high sequence similarity [64,65]. Finally, the finding of all-*trans*- and 9-*cis*-retinaldehyde as substrates for AKR1B15 adds further complexity to the enzymatic pathways of retinoid transformations and their cross-talk with other hormonal signaling pathways, such as that of steroids. This opens a research line to elucidate the physiological contribution of this novel human retinaldehyde reductase.

Acknowledgments

We thank Dr. A. de Marco for kindly providing chaperone-encoding plasmids pBB540 and pBB545.

Author Contributions

Conceived and designed the experiments: JGD XP J. Farrés SP. Performed the experiments: JGD MHK FXR ACS AP J. Fanfrlík IC SP. Analyzed the data: JGD MHK FXR ACS J. Fanfrlík IC XP J. Farrés SP. Contributed reagents/materials/analysis tools: MHK FXR OAB. Wrote the paper: JGD MHK FXR ACS J. Fanfrlík IC XP J. Farrés SP.

References

1. Jin Y, Penning TM. Aldo-keto reductases and bioactivation/detoxication. Annu Rev Pharmacol Toxicol. 2007; 47: 263–292. PMID: 16970545
2. Barski OA, Tipparaju SM, Bhatnagar A. The aldo-keto reductase superfamily and its role in drug metabolism and detoxification. Drug Metab Rev. 2008; 40: 553–624. PMID: 18949601
3. Ruiz FX, Gallego O, Ardèvol A, Moro A, Domínguez M, Alvarez S, et al. Aldo-keto reductases from the AKR1B subfamily: retinoid specificity and control of cellular retinoic acid levels. Chem Biol Interact. 2009; 178: 171–177. doi: 10.1016/j.cbi.2008.10.027 PMID: 19014918
4. Matsunaga T, Wada Y, Endo S, Soda M, El-Kabbani O, Hara A. Aldo-Keto Reductase 1B10 and Its Role in Proliferation Capacity of Drug-Resistant Cancers. Front Pharmacol. 2012; 3: 5. doi: 10.3389/fphar.2012.00005 PMID: 22319498
5. Ruiz FX, Moro A, Gallego O, Ardèvol A, Rovira C, Petrash JM, et al. Human and rodent aldo-keto reductases from the AKR1B subfamily and their specificity with retinaldehyde. Chem Biol Interact. 2011; 191: 199–205. doi: 10.1016/j.cbi.2011.02.007 PMID: 21329680
6. Salabei JK, Li X-P, Petrash JM, Bhatnagar A, Barski OA. Functional expression of novel human and murine AKR1B genes. Chem Biol Interact. 2011; 191: 177–184. doi: 10.1016/j.cbi.2011.01.020 PMID: 21276782
7. Oates PJ. Aldose reductase, still a compelling target for diabetic neuropathy. Curr Drug Targets. 2008; 9: 14–36. PMID: 18220710
8. Ma J, Luo DX, Huang C, Shen Y, Bu Y, Markwell S, et al. AKR1B10 overexpression in breast cancer: association with tumor size, lymph node metastasis and patient survival and its potential as a novel serum marker. Int J Cancer. 2012; 131: 862–871.
9. Tammali R, Reddy ABM, Saxena A, Rychahou PG, Evers BM, Qiu S, et al. Inhibition of aldose reductase prevents colon cancer metastasis. Carcinogenesis. 2011; 32: 1259–1267. doi: 10.1093/carcin/bgr102 PMID: 21642355
10. Endo S, Matsunaga T, Kuwata K, Zhao H-T, El-Kabbani O, Kitade Y, et al. Chromene-3-carboxamide derivatives discovered from virtual screening as potent inhibitors of the tumour maker, AKR1B10. Bioorg Med Chem. 2010; 18: 2485–2490. doi: 10.1016/j.bmc.2010.02.050 PMID: 20304656
11. Chatzopoulou M, Alexiou P, Kotsampasakou E, Demopoulos VJ. Novel aldose reductase inhibitors: a patent survey (2006—present). Expert Opin Ther Pat. 2012; 22: 1303–1323. doi: 10.1517/13543776.2012.726615 PMID: 22998509
12. Pathania S, Randhawa V, Bagler G. Prospecting for novel plant-derived molecules of Rauvolfia serpentina as inhibitors of Aldose Reductase, a potent drug target for diabetes and its complications. PLoS One. 2013; 8: e61327. doi: 10.1371/journal.pone.0061327 PMID: 23613832
13. Soda M, Hu D, Endo S, Takemura M, Li J, Wada R, et al. Design, synthesis and evaluation of caffeic acid phenethyl ester-based inhibitors targeting a selectivity pocket in the active site of human aldo-keto reductase 1B10. Eur J Med Chem. 2012; 48: 321–329. doi: 10.1016/j.ejmech.2011.12.034 PMID: 22236472

14. Zhang L, Zhang H, Zheng X, Zhao Y, Chen S, Chen Y, et al. Structural basis for the inhibition of AKR1B10 by caffeic acid phenethyl ester (CAPE). ChemMedChem. 2014; 9: 706–709. doi: 10.1002/cmdc.201300455 PMID: 24436249

15. Cousido-Siah A, Ruiz FX, Mitschler A, Porté S, de Lera AR, Martín MJ, et al. Identification of a novel polyfluorinated compound as a lead to inhibit the human enzymes aldose reductase and AKR1B10: structure determination of both ternary complexes and implications for drug design. Acta Crystallogr D Biol Crystallogr. 2014; 70: 889–903. doi: 10.1107/S1399004713033452 PMID: 24598757

16. Weber S, Salabei JK, Möller G, Kremmer E, Bhatnagar A, Adamski J, et al. Aldo-Keto Reductase 1B15 (AKR1B15): a Mitochondrial Human Aldo-Keto Reductase with Activity towards Steroids and 3-Keto-acyl-CoA Conjugates. J Biol Chem. 2015; 209: 6531–6545

17. Hackett NR, Butler MW, Shaykhiev R, Salit J, Omberg L, Rodriguez-Flores JL, et al. RNA-Seq quantification of the human small airway epithelium transcriptome. BMC Genomics. 2012; 13: 82. doi: 10.1186/1471-2164-13-82 PMID: 22375630

18. Constantinescu S, Hecht K, Sobotzki N, Erzinger MM, Bovet C, Shay JW, et al. Transcriptomic responses of cancerous and noncancerous human colon cells to sulforaphane and selenium. Chem Res Toxicol. 2014; 27: 377–386. doi: 10.1021/tx400427t PMID: 24383545

19. Calvo SE, Compton AG, Hershman SG, Lim SC, Lieber DS, Tucker EJ, et al. Molecular diagnosis of infantile mitochondrial disease with targeted next-generation sequencing. Sci Transl Med. 2012; 4: 118ra10. doi: 10.1126/scitranslmed.3003310 PMID: 22277967

20. Reumers J, De Rijk P, Zhao H, Liekens A, Smeets D, Cleary J, et al. Optimized filtering reduces the error rate in detecting genomic variants by short-read sequencing. Nat Biotechnol. 2012; 30: 61–8.

21. Yashin AI, Wu D, Arbeev KG, Ukraintseva SV. Joint influence of small-effect genetic variants on human longevity. Aging. 2010; 2: 612–620. PMID: 20834067

22. De Marco A, Deuerling E, Mogk A, Tomoyasu T, Bukau B. Chaperone-based procedure to increase yields of soluble recombinant proteins produced in *E. coli*. BMC Biotechnol. 2007; 7: 32. PMID: 17565681

23. Gallego O, Ruiz FX, Ardèvol A, Domínguez M, Alvarez R, de Lera AR, et al. Structural basis for the high all-trans-retinaldehyde reductase activity of the tumor marker AKR1B10. Proc Natl Acad Sci USA. 2007; 104: 20764–20769. PMID: 18087047

24. Larroy C, Fernandez MR, Gonzalez E, Parés X, Biosca JA. Characterization of the Saccharomyces cerevisiae YMR318C (ADH6) gene product as a broad specificity NADPH-dependent alcohol dehydrogenase: relevance in aldehyde reduction. Biochem J. 2002; 172: 163–172.

25. Gallego O, Belyaeva OV, Porté S, Ruiz FX, Stetsenko AV, Shabrova EV, et al. Comparative functional analysis of human medium-chain dehydrogenases, short-chain dehydrogenases/reductases and aldo-keto reductases with retinoids. Biochem J. 2006; 399: 101–109. PMID: 16787387

26. Kuksa V, Imanishi Y, Batten M, Palczewski K, Moise AR. Retinoid cycle in the vertebrate retina: experimental approaches and mechanisms of isomerization. Vision Res. 2003; 43: 2959–2981. PMID: 14611933

27. Belyaeva OV, Korkina OV, Stetsenko AV, Kim T, Nelson PS, Kedishvili NY. Biochemical properties of purified human retinol dehydrogenase 12 (RDH12): catalytic efficiency toward retinoids and C9 aldehydes and effects of cellular retinol-binding protein type I (CRBPI) and cellular retinaldehyde-binding protein (CRALBP) on the oxidation and reduction of retinoids. Biochemistry. 2005; 44: 7035–7047. PMID: 15865448

28. Canutescu AA, Shelenkov AA, Dunbrack RL. A graph-theory algorithm for rapid protein side-chain prediction. Protein Sci. 2003; 12: 2001–2014. PMID: 12930999

29. Pronk S, Páll S, Schulz R, Larsson P, Bjelkmar P, Apostolov R, et al. GROMACS 4.5: a high-throughput and highly parallel open source molecular simulation toolkit. Bioinformatics. 2013; 29: 845–854. doi: 10.1093/bioinformatics/btt055 PMID: 23407358

30. Hornak V, Abel R, Okur A, Strockbine B, Roitberg A, Simmerling C. Comparison of multiple Amber force fields and development of improved protein backbone parameters. Proteins. 2006; 65: 712–725. PMID: 16981200

31. Lindorff-Larsen K, Piana S, Palmo K, Maragakis P, Klepeis JL, Dror RO, et al. Improved side-chain torsion potentials for the Amber ff99SB protein force field. Proteins. 2010; 78: 1950–1958. doi: 10.1002/prot.22711 PMID: 20408171

32. Holmberg N, Ryde U, Bülow L. Redesign of the coenzyme specificity in L-lactate dehydrogenase from bacillus stearothermophilus using site-directed mutagenesis and media engineering. Protein Eng. 1999; 12: 851–856. PMID: 10556245

33. Hawkins GD, Cramer CJ, Truhlan DG. Parametrized Models of Aqueous Free Energies of Solvation Based on Pairwise Descreening of Solute Atomic Charges from a Dielectric Medium. J Phys Chem. 1996; 100: 19824–19839.

34. Seeliger D, Haas J, de Groot BL. Geometry-based sampling of conformational transitions in proteins. Structure. 2007; 15: 1482–1492. PMID: 17997973

35. De Groot BL, van Aalten DM, Scheek RM, Amadei A, Vriend G, Berendsen HJ. Prediction of protein conformational freedom from distance constraints. Proteins. 1997; 29: 240–251. PMID: 9329088

36. Laskowski RA, MacArthur MW, Moss DS, Thornton JM. PROCHECK: a program to check the stereochemical quality of protein structures. J Appl Crystallogr. International Union of Crystallography; 1993; 26: 283–291.

37. Eisenberg D, Lüthy R, Bowie JU. VERIFY3D: assessment of protein models with three-dimensional profiles. Methods Enzymol. 1997; 277: 396–404. PMID: 9379925

38. Goodsell DS, Morris GM, Olson AJ. Automated docking of flexible ligands: applications of AutoDock. J Mol Recognit. 9: 1–5. PMID: 8723313

39. Porté S, Ruiz FX, Giménez J, Molist I, Alvarez S, Domínguez M, et al. Aldo-keto reductases in retinoid metabolism: search for substrate specificity and inhibitor selectivity. Chem Biol Interact. 2013; 202: 186–194. doi: 10.1016/j.cbi.2012.11.014 PMID: 23220004

40. ezáč J, Fanfrlík J, Salahub D, Hobza P. Semiempirical Quantum Chemical PM6 Method Augmented by Dispersion and H-Bonding Correction Terms Reliably Describes Various Types of Noncovalent Complexes. J Chem Theory Comput. 2009; 5: 1749–1760.

41. Klamt A, Schüürmann G. COSMO: a new approach to dielectric screening in solvents with explicit expressions for the screening energy and its gradient. J Chem Soc. 1993; 2: 799–805.

42. Lepšík M, ezáč J, Kolář M, Pecina A, Hobza P, Fanfrlík J. The Semiempirical Quantum Mechanical Scoring Function for In Silico Drug Design. Chempluschem. 2013; 78: 921–931.

43. Fanfrlík J, Kolář M, Kamlar M, Hurný D, Ruiz FX, Cousido-Siah A, et al. Modulation of aldose reductase inhibition by halogen bond tuning. ACS Chem Biol. 2013; 8: 2484–2492. doi: 10.1021/cb400526n PMID: 23988122

44. Benkert P, Tosatto SCE, Schomburg D. QMEAN: A comprehensive scoring function for model quality assessment. Proteins. 2008; 71: 261–277. PMID: 17932912

45. Durrant JD, de Oliveira CAF, McCammon JA. POVME: an algorithm for measuring binding-pocket volumes. J Mol Graph Model. 2011; 29: 773–776. doi: 10.1016/j.jmgm.2010.10.007 PMID: 21147010

46. Tao H, Liu W, Simmons BN, Harris HK, Cox TC, Massiah M a. Purifying natively folded proteins from inclusion bodies using sarkosyl, Triton X-100, and CHAPS. Biotechniques. 2010; 48: 61–64. doi: 10.2144/000113304 PMID: 20078429

47. Pastel E, Pointud J-C, Volat F, Martinez A, Lefrançois-Martinez A-M. Aldo-Keto Reductases 1B in Endocrinology and Metabolism. Front Pharmacol. 2012; 3: 148. doi: 10.3389/fphar.2012.00148 PMID: 22876234

48. Ruiz FX, Porté S, Gallego O, Moro A, Ardèvol A, Del Río-Espínola A, et al. Retinaldehyde is a substrate for human aldo-keto reductases of the 1C subfamily. Biochem J. 2011; 440: 335–344. doi: 10.1042/BJ20111286 PMID: 21851338

49. Crosas B, Cederlund E, Torres D, Jornvall H, Farrés J, Parés X. A vertebrate aldo-keto reductase active with retinoids and ethanol. J Biol Chem. 2001; 276: 19132–19140. PMID: 11278684

50. Verma M, Martin HJ, Haq W, O'Connor TR, Maser E, Balendiran GK. Inhibiting wild-type and C299S mutant AKR1B10; a homologue of aldose reductase upregulated in cancers. Eur J Pharmacol. 2008; 584: 213–221. doi: 10.1016/j.ejphar.2008.01.036 PMID: 18325492

51. Ruiz FX, Cousido-Siah A, Mitschler A, Farrés J, Parés X, Podjarny A. X-ray structure of the V301L aldo—keto reductase 1B10 complexed with NADP+ and the potent aldose reductase inhibitor fidarestat: Implications for inhibitor binding and selectivity. Chem Biol Interact. 2013; 202: 178–185. doi: 10.1016/j.cbi.2012.12.013 PMID: 23295227

52. Zhang L, Zhang H, Zhao Y, Li Z, Chen S, Zhai J, et al. Inhibitor selectivity between aldo-keto reductase superfamily members AKR1B10 and AKR1B1: role of Trp112 (Trp111). FEBS Lett. 2013; 587: 3681–3686. doi: 10.1016/j.febslet.2013.09.031 PMID: 24100137

53. Sundaram K, Dhagat U, Endo S, Chung R, Matsunaga T, Hara A, et al. Structure of rat aldose reductase-like protein AKR1B14 holoenzyme: Probing the role of His269 in coenzyme binding by site-directed mutagenesis. Bioorg Med Chem Lett. 2011; 21: 801–804. doi: 10.1016/j.bmcl.2010.11.086 PMID: 21168333

54. Urzhumtsev A, Tête-Favier F, Mitschler A, Barbanton J, Barth P, Urzhumtseva L, et al. A "specificity" pocket inferred from the crystal structures of the complexes of aldose reductase with the pharmaceutically important inhibitors tolrestat and sorbinil. Structure. 1997; 5: 601–612. PMID: 9195881

55. Kokkinidis M, Glykos NM, Fadouloglou VE. Protein Flexibility and Enzymatic Catalysis. Adv Protein Chem Struct Biol. 2012. pp. 181–218. doi: 10.1016/B978-0-12-398312-1.00007-X PMID: 22607756

56. Kedishvili NY. Enzymology of retinoic acid biosynthesis and degradation. J Lipid Res. 2013; 54: 1744–1760. doi: 10.1194/jlr.R037028 PMID: 23630397

57. Belyaeva OV, Korkina OV, Stetsenko AV, Kedishvili NY. Human retinol dehydrogenase 13 (RDH13) is a mitochondrial short-chain dehydrogenase/reductase with a retinaldehyde reductase activity. FEBS J. 2008; 275: 138–147. PMID: 18039331

58. Ruiz FX, Porté S, Parés X, Farrés J. Biological role of aldo-keto reductases in retinoic Acid biosynthesis and signaling. Front Pharmacol. 2012; 3: 58. doi: 10.3389/fphar.2012.00058 PMID: 22529810

59. Palczewski G, Amengual J, Hoppel CL, von Lintig J. Evidence for compartmentalization of mammalian carotenoid metabolism. FASEB J. 2014; 1–13. doi: 10.1096/fj.14-0101LTE

60. Jiang W, Napoli JL. The retinol dehydrogenase Rdh10 localizes to lipid droplets during acyl ester biosynthesis. J Biol Chem. 2013; 288: 589–597. doi: 10.1074/jbc.M112.402883 PMID: 23155051

61. Acin-Perez R, Hoyos B, Zhao F, Vinogradov V, Fischman D a, Harris R a, et al. Control of oxidative phosphorylation by vitamin A illuminates a fundamental role in mitochondrial energy homoeostasis. FASEB J. 2010; 24: 627–636. doi: 10.1096/fj.09-142281 PMID: 19812372

62. Echtay KS, Brand MD. 4-hydroxy-2-nonenal and uncoupling proteins: an approach for regulation of mitochondrial ROS production. Redox Rep. 2007; 12: 26–29. PMID: 17263904

63. Zhong H, Yin H. Role of lipid peroxidation derived 4-hydroxynonenal (4-HNE) in cancer: Focusing on mitochondria. Redox Biol. 2015; 4: 193–199. doi: 10.1016/j.redox.2014.12.011 PMID: 25598486

64. Luong C, Miller A, Barnett J, Chow J, Ramesha C, Browner MF. Flexibility of the NSAID binding site in the structure of human cyclooxygenase-2. Nat Struct Biol. 1996; 3: 927–933. PMID: 8901870

65. Kimble-Hill AC, Parajuli B, Chen CH, Mochly-Rosen D, Hurley TD. Development of selective inhibitors for aldehyde dehydrogenases based on substituted indole-2,3-diones. J Med Chem. 2014; 57: 714–722. doi: 10.1021/jm401377v PMID: 24444054

66. Endo S, Matsunaga T, Mamiya H, Ohta C, Soda M, Kitade Y, et al. Kinetic studies of AKR1B10, human aldose reductase-like protein: endogenous substrates and inhibition by steroids. Arch Biochem Biophys. 2009; 487: 1–9. doi: 10.1016/j.abb.2009.05.009 PMID: 19464995

67. Shen Y, Zhong L, Johnson S, Cao D. Human aldo-keto reductases 1B1 and 1B10: a comparative study on their enzyme activity toward electrophilic carbonyl compounds. Chem Biol Interact. 2011; 191: 192–198. doi: 10.1016/j.cbi.2011.02.004 PMID: 21329684

68. Calam E, Porté S, Fernández MR, Farrés J, Parés X, Biosca JA. Biocatalytic production of alpha-hydroxy ketones and vicinal diols by yeast and human aldo-keto reductases. Chem Biol Interact. 2013; 202: 195–203. doi: 10.1016/j.cbi.2012.12.006 PMID: 23295224

69. Kubiseski TJ, Flynn TG. Studies on human aldose reductase. Probing the role of arginine 268 by site-directed mutagenesis. J Biol Chem. 1995; 270: 16911–16917. PMID: 7622508

70. Ehrig T, Bohren KM, Prendergast FG, Gabbay KH. Mechanism of aldose reductase inhibition: binding of NADP+/NADPH and alrestatin-like inhibitors. Biochemistry. 1994; 33: 7157–7165. PMID: 8003482

71. Endo S, Matsunaga T, Soda M, Tajima K, Zhao H-T, El-Kabbani O, et al. Selective inhibition of the tumor marker AKR1B10 by antiinflammatory N-phenylanthranilic acids and glycyrrhetic acid. Biol Pharm Bull. 2010; 33: 886–890. PMID: 20460771